

Precision Top-Quark Physics with Leptonic Final States

Von der Fakultät für Mathematik, Informatik und Naturwissenschaften
der RWTH Aachen University zur Erlangung des akademischen Grades
eines Doktors der Naturwissenschaften genehmigte Dissertation

vorgelegt von

Master of Science
Rene Poncelet

aus Uslar/Schönhagen

Berichter: Universitätsprofessor Dr. rer. nat. Michal Czakon
Universitätsprofessor Dr. rer. nat. Robert Harlander

Tag der mündlichen Prüfung: 24.09.2018

Diese Dissertation ist auf den Internetseiten der Universitätsbibliothek verfügbar.

Abstract

Since their discovery in high energy collisions at the Tevatron collider, more than twenty years ago, top-quarks constitute an important pillar of modern particle physics. As the heaviest particles of the Standard Model of particle physics (SM), they play a crucial role in many phenomenological applications. Their large mass relates them tightly to various other components of the SM. Examples of importance are parameters of the electroweak sector which are influenced through corrections originating from top-quark loops. This enables important consistency checks of the SM itself. For such checks, precisely known parameters estimated from measurements at colliders like the LHC are crucial. By carefully comparing data and theoretical predictions, parameters of the theory, e.g. the top-quark mass, can be extracted. To do so accurate predictions are necessary. Quantum Field Theory (QFT) is the theoretical framework the SM is build upon, and it can be systematically approximated in perturbation theory. Quantum Chromo Dynamics (QCD) describe the strong interaction between colored particles and most of the dynamics of top-quarks produced in high energy collisions of hadronic bound states. State of the art calculations evaluate the partonic cross section at next-to-next-to-leading order (NNLO). Thus, perturbative QCD is used to obtain predictions of fully inclusive or differential cross sections of top-quarks which show very good agreement with the measurements, while small uncertainties on the theoretical as well as the experimental side allow for precise parameter extractions. These measurements rely on well understood modeling of the top-quarks in hard scattering processes.

A remarkable feature of top-quarks is their very short lifetime which is below even the typical hadronization time of colored particles. Top-quark decays thus presents a unique opportunity for studying a bare quark. Inclusion of the decay in the evaluation of top-quark pair production through NNLO in QCD is the central goal of this work. The Narrow-Width-Approximation (NWA) is employed to reduce the computational burden by factorizing production and decay. It is possible to keep information about the polarization state of the top-quarks which affects the decay. To do so at NNLO, two-loop polarized matrix elements for top-quark pair production are required. The evaluation of two-loop amplitudes is demanding and their calculation is an important part of this thesis.

Another technical component needed for such a calculation is an efficient method to handle contributions from real radiation. While automatized frameworks exist at NLO, the NNLO case is much more involved. A fully general method of handling this kind of calculation is given by the Sector-improved residue subtraction scheme (STRIPPER) which is discussed in this work. Also, modifications to improve the efficiency of this scheme are presented. In combination, this allows to present the first calculation of top-quark pair production including decays in NWA at NNLO in QCD. First results compared to LHC data show remarkable agreement. The calculation is fully differential and allows for a broad band of future phenomenological studies. The extraction of the top-quark mass from differential distributions or the investigation of top-quark spin-properties at high precision are examples for phenomenological applications for these original calculations.

Zusammenfassung

Top-Quarks sind seit ihrer Entdeckung in Hochenergiekollisionen am Tevatron-Beschleuniger vor über zwanzig Jahren ein wichtiger Bestandteil moderner Teilchenphysik. Als schwerste Teilchen des Standardmodells der Teilchenphysik (SM) spielen sie eine entscheidende Rolle in vielen phänomenologischen Anwendungen. Ihre große Masse verbindet sie eng mit verschiedenen anderen Komponenten des SM. Ein wichtiges Beispiel für solch eine Verbindung sind elektroschwache Parameter, die über Schleifenkorrekturen von der Top-Quark-Masse abhängen. Der Vergleich der so berechneten Werte mit den experimentell bestimmten Werten für die elektroschwachen Parameter erlaubt somit wichtige Konsistenzprüfungen des SM. Von besonderer Wichtigkeit sind daher präzise Messungen dieser Parameter an Beschleunigern wie dem Large-Hadron-Collider (LHC). Die Messung von Parametern wie der Top-Quark-Masse erfolgt durch sorgfältigen Vergleich von Messungen und theoretischen Vorhersagen von Wirkungsquerschnitten. Die Quantenchromodynamik (QCD) beschreibt die starke Wechselwirkung zwischen Teilchen mit Farbladung und somit einen wesentlichen Anteil der Dynamik von Top-Quarks, die bei Hochenergiekollisionen von Hadronen entstehen. Berechnungen des partonischen Wirkungsquerschnitts auf Grundlage der Störungstheorie zweiter Ordnung (next-to-next-to-leading order: NNLO) sind der aktuelle Stand der Forschung und zeigen eine bemerkenswerte Übereinstimmung mit bisherigen Messungen. Die extrem geringen Unsicherheiten sowohl auf theoretischer als auch auf experimenteller Seite erlauben hoch präzise Messungen von Parametern des SM.

Eine charakteristische Eigenschaft der Top-Quarks ist ihre sehr kurze Lebensdauer, welche kürzer ist als die typische Hadronisierungszeit. Top-Quark-Zerfälle bieten so eine einzigartige Gelegenheit, freie Quarks zu studieren. Die Berücksichtigung dieses Zerfalls bei der Berechnung der Top-Quark-Paar-Produktion in der QCD mit Störungstheorie der zweiten Ordnung ist das zentrale Ziel dieser Arbeit. Eine Näherung für kleine Zerfallsbreiten (Narrow-Width-Approximation: NWA) wird verwendet, um den Rechenaufwand zu reduzieren. Es ist möglich, Information über den Polarisationszustand der Top-Quarks bei der Berechnung zu berücksichtigen, welche den Zerfall beeinflusst. Dazu sind auf NNLO polarisierte Matrixelemente mit zwei Schleifen für die Top-Quark-Paar-Produktion erforderlich, und deren Berechnung ist ein substantieller Teil dieser Arbeit.

Eine weitere technische Komponente, die für solche Berechnungen nötig ist, ist eine effiziente Methode, um Beiträge aus reeler Strahlung zu berücksichtigen. Während für die Störungstheorie erster Ordnung automatisierte Verfahren existieren, ist der Fall zweiter Ordnung komplizierter und Gegenstand momentaner Forschung. In dieser Arbeit kommt zur Behandlung derartiger Beiträge das sog. STRIPPER-Verfahren (sector-improved residue subtraction scheme) zum Einsatz. Neben dem Verfahren werden auch Modifikationen zur Verbesserung der Effizienz desselben vorgestellt. Dies ermöglicht erstmals eine Berechnung der Top-Quark-Paar-Produktion inklusive Zerfall unter den oben genannten Annahmen. Der Vergleich erster Ergebnisse mit LHC-Daten zeigt hervorragende Übereinstimmungen für totale und differentielle Wirkungsquerschnitte. Die in dieser Arbeit vorgestellte Rechnung ermöglicht eine breite Palette zukünftiger phänomenologischer Studien, etwa die Messung der Top-Quark-Masse aus differentiellen Verteilungen oder die Untersuchung von Top-Quark-Spin-Eigenschaften.

List of publication

This thesis is based on the author's research conducted at the Institute for Theoretical Particle Physics and Cosmology of the RWTH Aachen University. The research resulted in the following publication:

- L. Chen, et al., “Polarized double-virtual amplitudes for heavy-quark pair production”, JHEP **03** (2018) 085, arXiv:1712.08075 [hep-ph]

Contents

1. Top-Quark physics at Hadron Colliders	1
1.1. Discovery at TeVatron	1
1.2. Top-Quark Physics at the LHC	2
1.3. Top-quark properties	6
2. The Top-Quark in Theory	13
2.1. Factorization in production and decay	13
2.1.1. Collinear Factorization	14
2.1.2. Renormalization of virtual amplitudes	16
2.1.3. Matrix element factorization	19
2.1.4. Narrow-Width-Approximation	23
2.1.5. Spinor-Helicity method	25
2.2. Production and Decay	27
2.2.1. Stable top-quark production	28
2.2.2. Top-quark decay	30
2.2.3. Unstable top-quarks	33
3. Polarized Double Virtual Top-Quark Pair Production	35
3.1. Decomposition of Amplitudes	35
3.1.1. Spin and Color structures	35
3.1.2. Projection method	40
3.2. Evaluation of Feynman Integrals	40
3.2.1. Canonicalization	41
3.2.2. Evaluation of master integrals	42
3.3. Renormalization	44
3.4. Finite-remainder functions	46
3.5. Spin-Density Matrix	49
3.5.1. Threshold expansions	52
3.6. Spin structures and correlation matrices	54
3.6.1. Spin-structures	54
3.6.2. Helicity correlation matrices	55
4. Real radiation contribution	57
4.1. Subtraction Schemes at NNLO	58
4.1.1. Slicing methods	58
4.1.2. Subtraction methods	60
4.2. Sector-improved Residue Subtraction Scheme	62
4.2.1. General setup	62
4.3. Phase Space Parameterization	64
4.3.1. Original phase space parameterization	64
4.3.2. New phase space parameterization	65

Contents

4.4.	Subtraction terms	78
4.4.1.	Generation of subtraction terms	78
4.4.2.	Subtraction kinematics	79
4.4.3.	Azimuthal averaging	82
4.5.	Four-Dimensional Formulation	82
4.5.1.	Separately finite contributions	83
4.6.	't Hooft-Veltman Corrections	88
4.6.1.	Measurement function based approach	89
4.6.2.	Calculation of 't Hooft-Veltman corrections	93
5.	Top-pair production and decay at NNLO in QCD	101
5.1.	Treatment of top-quark width in perturbation theory	101
5.2.	Dipole subtraction for decay corrections	103
5.3.	Results for LHC	105
5.3.1.	Fiducial cross sections	106
5.3.2.	Differential distributions	107
6.	Summary and Conclusions	111
A.	General Notation and conventions	113
A.1.	Notation	113
A.2.	Spherical coordinates in d dimensions	114
A.3.	Definitions of contributions	116
B.	Renormalization Constants	119
B.1.	UV renormalization constants	119
B.2.	Supplements for IR renormalization	120
C.	Factorization Formula	123
C.1.	Infrared limits of tree-level amplitudes	123
C.1.1.	Collinear limits	123
C.1.2.	Soft limits	127
C.2.	Infrared limits of one-loop matrix elements	128
C.2.1.	Collinear limit	128
C.2.2.	Soft limit	129
C.2.3.	Limits of matrix elements of $Z^{(1)}$	133
C.2.4.	Limits of the finite remainder	134
C.3.	Splitting functions	135
D.	$t\bar{t}$ amplitude supplements	139
D.1.	Projectors	139

1. Top-Quark physics at Hadron Colliders

1.1. Discovery at TeVatron

More than twenty years ago, the top-quark was confirmed to be observed in proton-anti-proton collisions at the Tevatron collider by the CDF [2] and D0 [3] experiments separately. Its discovery was a huge success of the Standard Model of Particle Physics (SM). The existence of the top-quark was predicted already two decades before this great achievement, as a third generation of quarks was proposed by Kobayashi and Masakawa [4] as answer to the CP problem in the weak sector. The first evidence for a third generation of particles was the discovery of the τ - lepton [5], two years later. It was Harrari who introduced the naming of the "bottom" or "beauty" quark together with the name of the partner the "top" or "truth" quark [6] of the yet hypothetical particles. Only few years later the observation of a resonance structure in muon pair spectra [7] marked the first measurement of the bottom quark. The search for the new presumably heavy partner of the bottom quark was unsuccessful for almost twenty years. However, due to consistency constraints within the Standard Model the mass of the new particle could quite well be constrained, for instance by the Large Electron Positron (LEP) collider at CERN [8]. In 1995 finally, the experiments located at the TeVatron accelerator operating at a center-of-mass energy of 1.96 TeV, the most powerful machine at that time, announced the discovery of a heavy particle with right properties in the expected mass window. The properties of the top-quark are quite remarkable and opened up a rich field of particle physics. The investigation of physics related to top-quarks is still one of the main interests of the particle physics community.

With a pole mass of roughly 173 GeV, the top-quark is the heaviest elementary particle observed so far. Its large mass implies the special role of the top-quark within the SM and beyond. The top-quark mass is naively a free input parameter but relates through quantum corrections to a broad band of parameters and observables, such that it provides a strong test of internal consistency of the model. Or provides the possibility for indirect evidence of new physics beyond the Standard Model (BSM).

Another remarkable property is the short life time of the top-quark. The life time is about 10^{-25} seconds and thus shorter than the hadronization time which is of order 10^{-24} . It allows for the unique opportunity to study a bare quark and its quantum numbers absent of hadronization effects polluting the measurements. As mentioned, the relation of the top-quark mass to other parameters allows for precision tests of the Standard Model. One important example is the relation between the masses of the W/Z - and Higgs-boson and the top-quark. They are related through top-quark and Higgs-boson loops in higher order corrections to the propagator of the W and Z bosons. This relation can be used to predict masses from measurements of a subset of those. The comparison with direct measurements of the predicted mass results in consistency checks of the Standard Model [9, 10]. In this way it was possible to constrain the mass of the top-quark to a quite narrow window prior to its discovery. The strong constraints between top and vector boson masses inherit from the fact that the relation is quadratic in the top mass. For the Higgs boson,

1. Top-Quark physics at Hadron Colliders

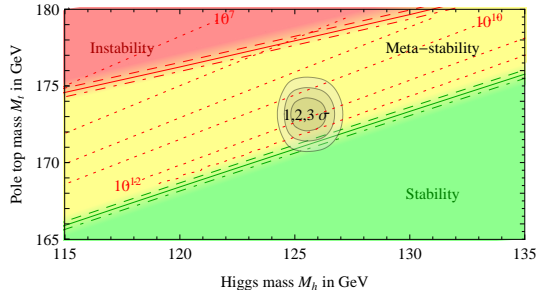


Figure 1.1.: Stability landscape for different configurations of Higgs and top-quark masses and uncertainty bands of current mass measurements. [11] .

for instance, the dependence is only logarithmic and thus constraints are much weaker.

Another peculiar influence of the top-quark mass on the Standard Model is given through the running of Yukawa couplings. In lowest order perturbation theory the Higgs potential has the famous "Mexican hat" shape, which describes a stable electroweak vacuum. The quartic coupling is an input parameter of the theory and thus gets modified through quantum corrections. The influence of the top-quark mass is such that for certain values another minimum at higher Higgs field values appears. Thus it might be possible that our 'false' vacuum decays into the actual vacuum at some point. For current values of the top-quark and Higgs masses the Standard Model seems to be in a meta-stable phase as depicted in figure 1.1, where the life time of the 'false vacuum' is near the age of the universe [11].

The crucial ingredients for this kind of analyses are precise measurements of the parameter entering the Lagrangian and thus the Standard Model. Precision physics requires well understood experiments and theory descriptions. Usually lepton colliders provide a clean and precise environment to perform parameter estimations at high accuracy. The most powerful lepton machine was LEP, it provided excellent results for masses of the electroweak bosons and couplings as well the strong coupling [8]. However, the center of mass energy of the colliding beams was not high enough to produce top-quarks and Higgs-bosons on their mass shell. Up to now only hadron colliders like the Tevatron or the LHC provide energies which are high enough to produce those frequently enough to measure them. The physics at these colliders is dominated by strong interactions between the color charged constituents of the hadron. The collision cover and probe a broad band of energy scales. Combined with large interaction rates they provide therefore a huge discovery potential. Their precision on the other hand is limited by the hadronic physics that arises naturally. Even though hadron machines are regarded as 'discovery' rather than 'precision' machines, the era of precision physics at Hadron colliders has begun.

1.2. Top-Quark Physics at the LHC

The LHC physics programme followed the Tevatron and started operation in 2009. Since then it provides large amount of data from the proton-proton collisions at 7,8 and 13 TeV center of mass energy. In figure 1.2 the collected amount of data so far of the LHC experiments is visualised [12, 13].

The integrated luminosity recorded by the two main experiments from the 13 TeV run

1.2. Top-Quark Physics at the LHC

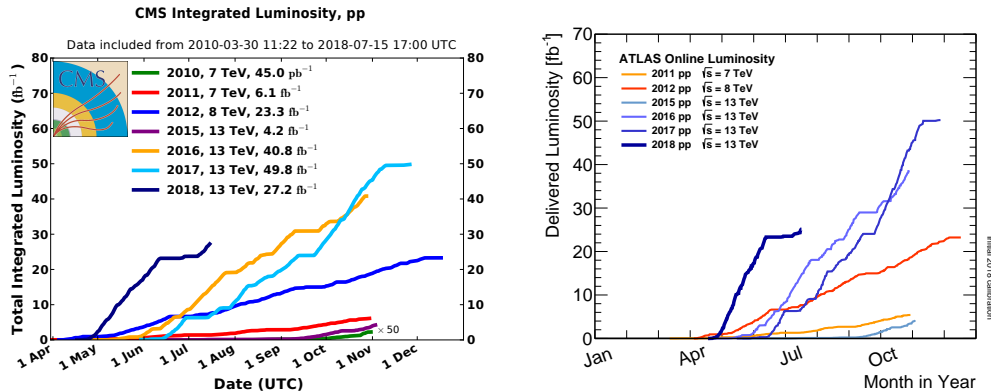


Figure 1.2.: Integrated luminosity of the two main experiments at LHC, CMS [14] and ATLAS [15], respectively.

up to now is

$$\text{ATLAS} = 111\text{fb}^{-1}, \text{CMS} = 109\text{fb}^{-1}. \quad (1.1)$$

There is a vast landscape of processes that have been observed and measured in the past eight years. The figure 1.3 summarizes the results of cross section measurements for many Standard Model process. They are compared to the Standard Model theory predictions and show a remarkable agreement. This shows the validity of the Standard Model over many orders of magnitude in the production cross section. The experimental uncertainties on these measurements are for various processes at a compatible order to the uncertainty estimate of the theory prediction.

The theoretical description of the physics at hadron colliders is governed by Quantum Chromo Dynamics (QCD). QCD is a $SU(3)$ gauge theory [16] modeling the strong interactions of quarks and gluons. These partons are the constituents of hadronic bound states like the proton. At low energies the strong coupling constant α_s becomes large and give rise to confinement. At high energies, on the other hand, QCD is asymptotically free such that α_s becomes small and a perturbative treatment becomes feasible. The low energy physics of the incoming hadron can be separated from high energy collision of the constituents with the help of factorization theorem. Hadronic states are described by the parton model. The abundance of quarks and gluons with a given momentum fraction inside a hadron is parameterized with the help of parton distribution functions (PDFs). The hadronic cross section of a given process then factorizes into a convolution of a partonic cross section and the PDFs. The partonic cross section can be treated in perturbation theory. The PDFs on the other hand need to be inferred from experiment since it is not possible (yet) to derive them from first-principles. There are different sources of uncertainties in the theoretical description. There are uncertainties related to the free parameter of the theory, for example free parameters of the Lagrangian or the PDFs themselves. Those can be conceptually extracted in independent measurements to allow for new predictions. The perturbative expansion of partonic cross section yields another source of uncertainty. The expansions are truncated and the influence of higher orders needs to be estimated to give a reliable theory description. Next-to-leading order QCD calculations are state of the art for all processes of interest.

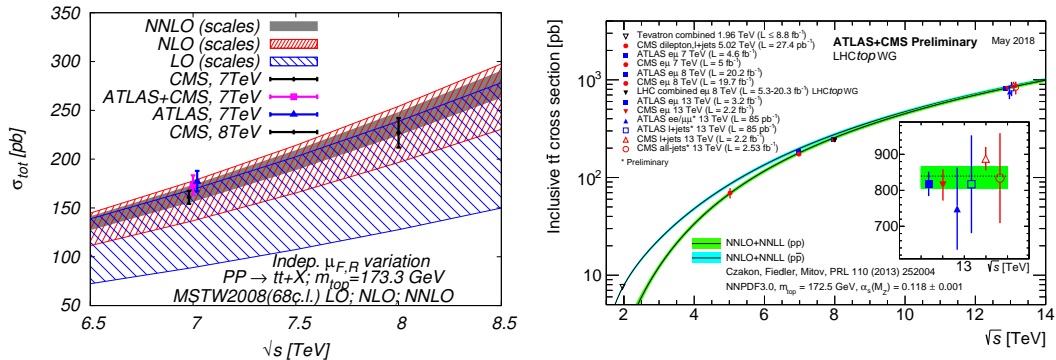


Figure 1.4.: Theory predictions of the total inclusive cross section of $t\bar{t}$ production compared to ATLAS and CMS measurements. The left figure shows the scale dependence of the theory prediction at LO, NLO and NNLO [32]. The right figure has been taken from [33].

The automatization of tree-level and one-loop matrix-elements [18–21] as well as the handling of real radiation contributions with the help of subtraction schemes [22–24] are the foundations of the “NLO-revolution” in past ten years. Monte Carlo frameworks such as MADGRAPH[18], SHERPA [25], HELACNLO [26] and others provide all necessary ingredients to perform full-fledged next-to-leading order calculation for virtually all Standard Model processes and beyond. Additionally the inclusion of parton shower algorithms, like [24, 27–29] on top of leading and next-to-leading order calculations allow for a more realistic event modelling. Moving to next-to-next-to-leading order in QCD the situation looks quite different. On one hand the handling of real radiation is still a difficult problem due to the much more complicated infrared singularity structure. A detailed discussion of real radiation in NNLO calculations is given in chapter 4. On the other hand the availability of two loop amplitudes is limited to $2 \rightarrow 2$ processes up to now. In some cases of comparable importance are NLO electroweak calculations and more or less recently their inclusion became reality, for example see [20, 21, 30, 31].

The top-quark plays an essential role in the physics program of the LHC. After its discovery at the Tevatron, the focus is on precise as possible measurements of top-quark properties to either improve the Standard Model with better input values or to unveil inconsistencies and signs of new physics. The production of a top-quark pair is an extensively studied process at LHC, for examples see Refs [34–37]. The production is mediated dominantly by QCD, while electroweak production modes play only a negligible role. While at Tevatron the quark anti-quark annihilation channels was most important production channel (85%) at the LHC the gluon initiated production dominates ($\sim 85\%$). The theoretical description of this process has quite some history. The first dedicated next-to-leading order calculation was performed in late 80’s [38, 39] and [40]. The next-to-leading order correction have been found sizeable and were later refined by NLL resummations [41–43]. The resummation program was extended to NNLL [44–48], over the years before the first NNLO calculation for the inclusive cross section was presented [49–52] including the aforementioned NNLL soft gluon resummation. Only a short time later the calculation was performed also on differential level [53–58]. So far for on-shell stable top-quarks. Since top-quarks decay immediately, a more realistic treatment takes also decays into account and also there progress

1. Top-Quark physics at Hadron Colliders

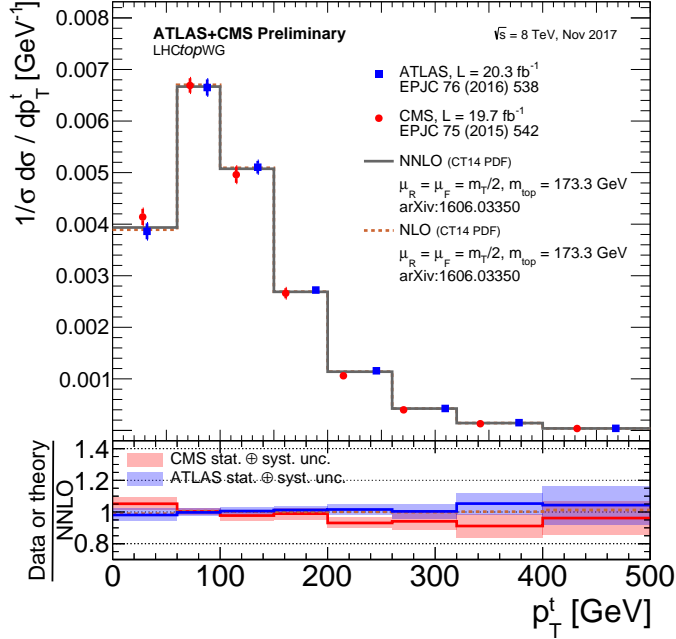


Figure 1.5.: Differential cross section for $t\bar{t}$ production, measured in the di-lepton channel and compared to SM theory [33].

was made in different directions. Within the Narrow-Width-Approximation, which allows to keep the top-quarks on-shell but keeps spin information, motivated by the small width of the top-quark first calculations were presented in Refs [59, 60]. Even more realistic are full off-shell calculations which consider the complete production of the decay final state [61–66]. The NLO calculations were also refined with parton showers, with and without the inclusion of the decay [67–69].

The total cross section is good example for well converging perturbative series. The left figure in Fig 1.4 shows the theory predictions for the total cross section of $t\bar{t}$ production for different orders in perturbation theory together with an error estimate from scale variations. Each subsequent higher order prediction lies within the estimated uncertainty which signals a good convergence. In the right figure is a comparison between the predicted cross section and measurements performed by the ATLAS and CMS collaborations. They agree remarkably well within the errors. The cross section can also be studied in a more exclusive way. An example is given in figure 1.5 which shows a differential distribution with respect to the transverse momentum of the top-quark. Also here remarkable agreement between measurements and Standard Model is found.

1.3. Top-quark properties

The top-quark mass Besides the production cross section the mass is an important property of the top-quark. As a free parameter of the Lagrangian, it needs to be determined by experiment. However, the treatment within the theoretical description of the mass plays a crucial role. All free parameters of the Lagrangian are subject to renormalization. The renormalization procedure is not unique and the very details of the chosen renormalization

1.3. Top-quark properties

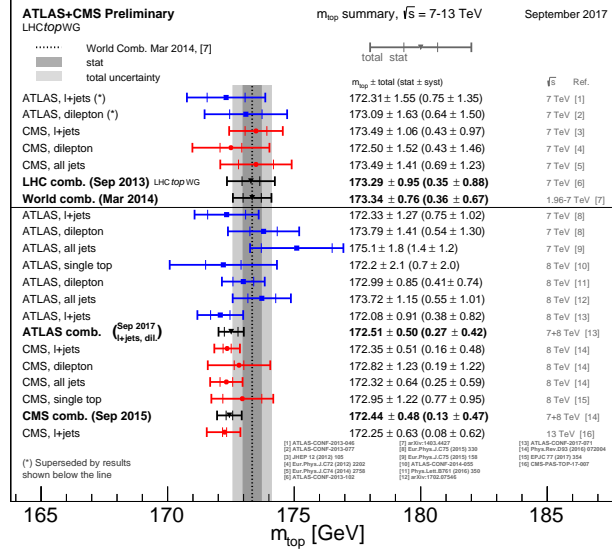


Figure 1.6.: Summary of various top-quark mass measurements. Published by the Top working group [33], details of the different measurements can be found in references given in the figure.

scheme has impact on the interpretation of the mass.

The pole mass m_t is probably the most intuitive definition. It can be defined by considering top-quarks as asymptotic free states in perturbative QCD. It is then given by real part of the top-quark propagator pole at $m_t + i\Gamma_t$ with the width Γ_t . In this treatment it relates to the peak of the invariant mass distribution of top-quark decay products. However, even though this is well defined in perturbative QCD, top-quarks are not free particles since they are color charged and thus subject to confinement. This non perturbative effects lead to absence of the pole in the full propagator. This leads to an ambiguity of the pole mass definition, which is naively expected to be of $\mathcal{O}(\Lambda_{QCD})$, thus of order of separation between low and high energy scales in QCD. In a recent study of this so-called renormalon ambiguity [70–72] it has been shown that the effect is about 70 MeV [73]. There are also studies which suggest that the inclusion of parton-showers correspond to a different renormalization scheme [74] and previous works. This ambiguity propagates to the all observables that depend on the top-quark mass m_t and thus limits conceptually the precision of pole mass measurements. This mass has been measured by experiment and the current experimental status is summarized in figure 1.6.

The $\overline{\text{MS}}$ mass $\bar{m}_t(\mu)$ is obtained when using the $\overline{\text{MS}}$ renormalization scheme for the mass parameter. This introduces an explicit dependence on the renormalization scale μ which governed by the renormalization group equation (RGE)

$$\mu^2 \frac{\partial \bar{m}_t(\mu)}{\partial \mu^2} = \bar{m}_t(\mu) \gamma_m \quad (1.2)$$

with the mass anomalous dimension γ_m . This equation follows directly from the fact that the bare mass does not depend on the renormalization scale and is known up to five loops [75]. With this equation \bar{m}_t can be evaluated at any scale by fixing its value at a specific scale. This can be done by relating this mass definition to the pole mass and using its

1. Top-Quark physics at Hadron Colliders

measured value as input. The relation reads to next to leading order

$$m_t = \bar{m}_t \left[1 + \frac{\alpha_s}{\pi} C_F \left(1 - \frac{3}{4} \ln(\bar{m}_t^2/\mu^2) \right) \right] \quad (1.3)$$

but is known up to four loops [76, 77]. This relation introduces the renormalon ambiguity also to this short distance mass. A pole mass of approximately 173 GeV translates to $\bar{m}_t(\bar{m}_t) \approx 163$ GeV.

Another way to define the top-quark mass is through its production threshold. Predominately relevant for lepton-colliders, the study of the threshold gives a clean and theoretically well controlled opportunity to measure the mass. However, the details of the description of top-quark production at the threshold give rise to various definitions, for example the 1S mass [78] or the potential subtracted (PS) mass [79].

The precise extraction of the top-quark mass parameter from measurements at colliders is an experimental and theoretical challenge. Many different methods of varying precision and model dependence are employed to perform this task. A common method is the usage of theory input to prepare predictions for different input parameters. These templates are compared after simulating the transition to observable events and detector effects to measured data. By finding the best match the input parameter are fitted to the data. The effectiveness of this method strongly depends on the observable investigated. An example is the extraction of the top-quark mass with the help of the total cross section [36, 80, 81]. The value extracted from 7 TeV data by the CMS collaboration is for instance $173.8_{-1.8}^{+1.7}$ GeV [82]. Also more exclusive observables are used, a review can be found in [83–86]. A more recent example is the ρ_s observable defined through the invariant mass of a reconstructed $t\bar{t}$ pair and accompanying jet [87, 88]

$$\rho_s = \frac{2m_0}{\sqrt{m_{t\bar{t}j}^2}} \quad \text{with} \quad m_0 = 170 \text{ GeV} \quad (1.4)$$

The shape of the normalized differential cross section with respect to ρ_s

$$\mathcal{R} = \frac{1}{\sigma} \frac{\partial \sigma}{\partial \rho_s} \quad (1.5)$$

has quite strong dependence on the top-quark mass parameter. Additionally, due to the normalization, the theoretical and systematic errors are quite well under control. The extraction using this parameter was performed by the ATLAS [89] and CMS [90] collaboration. In figure 1.7 is a comparison of theory predictions for different top masses and the measured distribution. The extracted mass with this method in case of ATLAS is

$$m_t = 173.7 \pm 1.5(\text{stat}) \pm 1.4(\text{syst.})_{-0.5}^{+1.0}(\text{theory})\text{GeV} \quad (1.6)$$

which is quite competitive with the extraction of the top mass from the total cross section. A quite similar method is the extraction from kinematic endpoints. An example is given in [91]. There the transverse mass of the top-quark is reconstructed. For onshell top-quarks this mass has a maximum value which depends on the top-quark mass itself. By measuring this edge in the distribution of the transverse mass implicitly the top-quark mass is measured. The results from the various methods result in the world average from

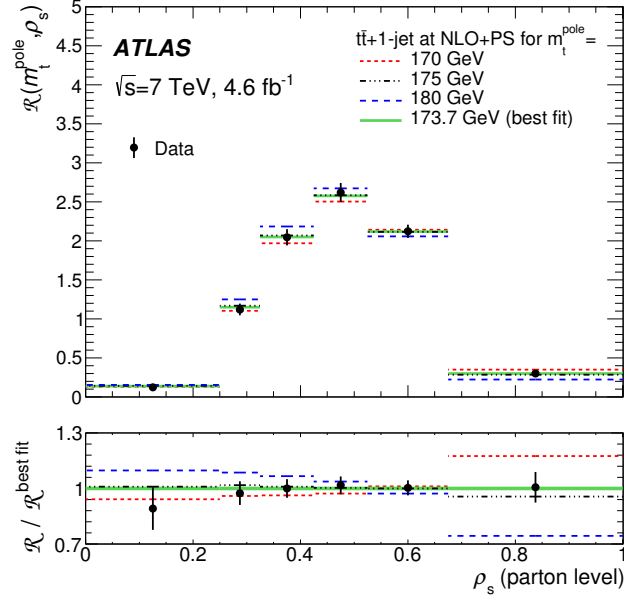


Figure 1.7.: Measurement of the differential distribution of the ρ_s observable, together with predictions for varied top mass and best fit result [89].

2014

$$m_t = 173.34 \pm 0.74 \text{ GeV} \quad (1.7)$$

for the pole mass.

Top-quark decays and spin As mentioned already in various contexts, the top-quark is not stable and decays imitatively after it is produced. The short life time $\tau \approx 10^{-25}\text{s}$, or the small decay width $\Gamma_t \sim \mathcal{O}(1) \text{ GeV}$, is the reason that the top-quark decays before hadronization effects can wash out the properties of the bare quark. This allows to study the quantum numbers like spin, charge of a quark and its couplings to electroweak bosons in a clean environment.

The decay of the top-quark is mediated by the weak interaction and can be described by the three processes

$$t \rightarrow bW^+, \quad t \rightarrow sW^+ \quad \text{and} \quad t \rightarrow dW^+. \quad (1.8)$$

The decay rate in the three channels are proportional to V_{tb}, V_{ts} and V_{td} , where V_{ij} are entries of the CKM matrix. Due to the strong hierarchy of the CKM matrix the decay rates into s and d quarks are negligible and thus the total width of the top-quark is well approximated by

$$\Gamma_t \equiv \Gamma_t(t \rightarrow W^+b). \quad (1.9)$$

The decay width is not a free parameter of the theory but can rather be expressed through masses and couplings. In lowest order in perturbation theory the total width can be

1. Top-Quark physics at Hadron Colliders

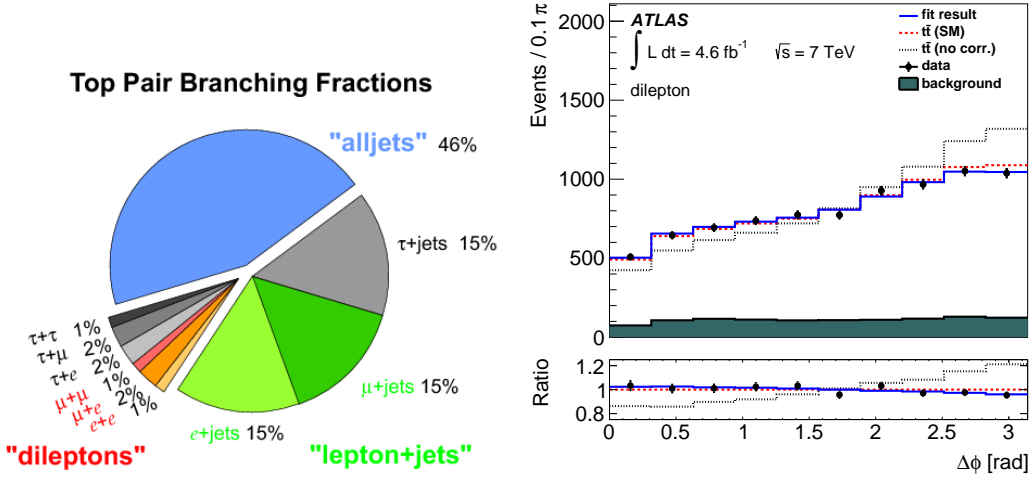


Figure 1.8.: (left) Visualization of top branching fractions[98]. (right) Shown is the differential distribution with respect to the azimuthal angular difference $\Delta\phi$ [99].

evaluated to

$$\Gamma_t^{(0)} = \frac{G_F m_t^3}{8\pi\sqrt{2}} (1 - r^2)^2 (1 + 2r^2) \quad \text{with} \quad r^2 = \frac{m_W^2}{m_t^2} \quad (1.10)$$

which corresponds to a numerical value

$$\Gamma_t(m_t = 173.3 \text{ GeV}) = 1.5048 \text{ GeV} \quad (1.11)$$

For the anti top-quark the same holds (the processes are charged conjugated) due to CPT invariance. The next-to-leading order QCD contribution was already calculated some time ago [92], also including effects from the light quark mass and off-shell W s. The next-to-leading order EW corrections are also known and presented in [93]. A little bit more recent are the NNLO corrections in [94–96] and [97], which are discussed in more detail later. The higher order QCD corrections of $\mathcal{O}(10\%)$, and thus quite sizeable.

In the case of top-quark pair production the decay of the top-quarks and the subsequent decay of the W -bosons results in variety of different decay channels. They are summarized in figure 1.8. Top-quark pair events are usually identified through two reconstructed b -jets and the decay products of the W -bosons. The b -jets can be distinguished experimentally from other jets to unusual long life-time of the b quarks since their decay is CKM suppressed. The long life time results in displaced vertices different from the interaction point of the hard scattering event. Sophisticated analysis techniques and precise particle tracking allows for high tagging efficiencies. The decay into quark final states, which are identified as accumulated jets in experiments, has the largest branching fraction. Thus the statistics of observed events in this channel is quite high. However, this channel suffers from the large combinatoric possibilities to assign the various jets to the two top-quarks and large QCD background. The fully leptonic channel where both W decay into charged leptons and neutrinos has the advantages that it is easy to detect. The leptons (not necessary the τ lepton) provide a clean signature. But it has two drawbacks: low statistics due to the small branching fraction and lost information due to the neutrinos which leave the

detector unnoticed. The only information about the neutrinos is the missing transverse energy. The lepton plus jet channel is the middle ground, larger statistics but still quite easy identifiable final state signature. Also the neutrino momentum is better constraint by the missing transverse energy and can be reconstructed up to two-fold ambiguity [100].

The top-quarks are in general produced unpolarized [101], however the coupling to the W is a left-handed coupling. The decay products carry therefore information over the polarization of the decayed top-quark. The polarization of the top-quark has for instance impact on angular distributions. Taking into account both top-quarks, the correlation between the decay products reveals information over the spin properties of the top-quarks. An example is the azimuthal angular distance of the two final state leptons in the di-lepton channel $\Delta\phi$. In figure 1.8 a corresponding measurement together with theory predictions is shown. For comparison also predictions which neglected the spin information is given. Evidently, the spin correlation of the top-quarks has important impact on the shape of the distribution.

This work is structured as follows: After a general introduction in top-quark physics at hadron colliders presented in this chapter, the modelling and description of top-quark processes within Quantum Field theory is outlined in chapter 2. Crucial ideas from factorization and renormalization are reviewed and aligned in context suitable for this work. Additionally, the state of the art of phenomenological calculations for top-quark pair production and decays in context of LHC are discussed, since they build the foundations of the project presented in this thesis. Working towards top-quark pair production and decay within the Narrow-Width-Approximation, the calculation of polarized double virtual amplitudes needed for polarized top-quark pairs through NNLO in QCD is presented in chapter 3. In chapter 4 a short overview over the various competing techniques is given, followed by a detailed description of the Sector-improved residue subtraction scheme. The scheme is slightly modified from its original formulation with the aim to improve convergence and elegance. This scheme is used in chapter 5 to perform a fully differential calculation of top quark pair production and decay in the Narrow-Width-Approximation through NNLO in QCD. Results are compared to lower orders and with published data from the ATLAS and CMS working groups. This work is concluded with a summary and final discussion of the results in chapter 6.

2. The Top-Quark in Theory

This chapter gives an overview over concepts that appear in the modelling of top-quark pair production and its decay at hadron colliders. A special focus is put on the role of factorization, separating perturbative from non-perturbative physics. Also, some general methods that facilitate higher order calculations are discussed. After the introduction of various ingredients, a review of the current status of top-quark theory predictions is given. In the Standard Model all fermions acquire mass due to their Yukawa coupling to the Higgs-field. Considering high energy interactions at colliders like the LHC, the mass of the light quarks $\{u, d, c, s, b\}$ is comparatively small and they are treated as massless in the following discussion. The top-quark, however, with a mass of $m_t \approx 173$ GeV has to be treated as a massive particle.

2.1. Factorization in production and decay

The theoretical modelling of top-quark pair production at hadron colliders relies on factorization [102], as basically all other production processes do. The factorization theorems allow to separate physics on long and short distances scale, or equivalently, physics at small and high energies. The very nature of the colliding particles at the LHC does not allow for a direct description of production processes within perturbative QFT. The proton is a hadronic bound state whose dynamics, to our understanding, are governed by low energy interactions, i.e. the non-perturbative regime of Quantum Chromo Dynamics (QCD). Even though non-perturbative QCD builds up a huge and rich field of physics, it is not yet possible to describe this kind of bound states with the required precision from first principles. Factorization allows to separate the low-energy dynamics from high energy scattering processes of the proton's constituents and parameterize it in terms of parton distribution functions (PDFs) [103–106]. These PDFs, denoted by $\phi_a(x)$, are universal features of the proton and, following the parton model, describe the probability to encounter a specific parton a with a momentum fraction x . The PDFs may be determined in different experiments and at various energies by carefully comparing measured cross sections with predictions of well established processes. The PDFs depend on the energy scale μ_F at which they are measured, such that $\phi_a(x) \equiv \phi_a(x, \mu_F)$. The energy scale is usually given by the typical scale of the process under consideration, for instance the partonic collision energy. However, PDFs at different energy scales are not unrelated to each other, but rather are connected by differential equations in μ_F , the PDF evolution equations or DGLAP equations. Since the measurement of the PDFs is tightly connected to the value and running of $\alpha_s(\mu_F)$, together they provide a predictive set of equations:

$$\mu_F^2 \frac{df_i(x, \mu_F)}{d\mu_F^2} = (P_{ij} \otimes f_j)(x, \mu_F) \quad (2.1)$$

$$\mu_F^2 \frac{d\alpha_s(\mu_F)}{d\mu_F^2} = \beta(\alpha_s(\mu_F)). \quad (2.2)$$

2. The Top-Quark in Theory

The symbol \otimes denotes a convolution as defined in A.35. These equations allow to predict the PDFs and α_s at any energy scale μ_F as soon as the boundary conditions are fixed at some energy scale. From the converse perspective, these equations allow for including measurements at different energy scales to determine the common boundary condition. On the right-hand side of the evolution equations appear the Altarelli-Parisi splitting functions as well as the β -function. They can be determined from perturbative QCD as a series in $\alpha_s(\mu_F)$, thus from first principles. Different orders in this expansion will lead to different PDFs $\phi_a(x, \mu_F)$, or, the other way around, to different boundaries. Consequently there are different existing PDF sets (LO, NLO, NNLO, ...) depending on the expansion depth of the evolution equations. The depth is usually matched to the perturbative order of the partonic prediction used for extracting the PDFs. This is necessary to consistently treat the logarithms of the renormalization and factorization scale appearing in various contributions.

Coming back to top-quark pair production, the hadronic cross section may be written in a factorized form,

$$\sigma_{h_1 h_2}(P_1, P_2) = \sum_{ab} \int \int_0^1 dx_1 dx_2 \phi_{a/h_1}(x_1, \mu_F^2) \phi_{b/h_2}(x_2, \mu_F^2) \tilde{\sigma}_{ab}(x_1 P_1, x_2 P_2, \alpha_s(\mu_R^2), \mu_R^2, \mu_F^2), \quad (2.3)$$

with the partonic cross-section $\tilde{\sigma}_{ab}$. The renormalization scale μ_R enters the partonic cross section through the running of α_s and higher order contributions. The partonic cross section then may be expanded in a series of α_s whose coefficients can be calculated in perturbation theory. The higher order terms contain contributions from additional radiation, and thus from higher multiplicity processes, as well as additional virtual quantum loops and, at high enough order, combinations of both. In virtual contributions divergences arise from infinitely large momenta flowing through loops. They can be regularized and removed by renormalization. There are different regularization schemes that can be employed. However, throughout this work dimensional regularization in $d = 4 - 2\epsilon$ spacetime dimensions is used. The removal of this type of divergences can be achieved through absorption into unobservable quantities of the underlying Lagrangian. Additionally, infrared divergences remain in the virtual contributions due to soft and collinear loop momenta. They also arise in the real radiation contribution due to the unresolved emissions. The handling of UV and IR divergences in loop amplitudes is discussed in more detail in section 2.1.2. Usually, the KLN theorem [107, 108] ensures that all divergences cancel and a finite result is obtained when combining the different contribution suitably in terms of infrared safe observables. This is not true in the presence of hadronic objects in the initial state. The reason for this are collinear emissions to initial state particles which, in contrast to final state collinear emission, are not averaged over. Collinear renormalization is necessary to absorb these singularities within the PDFs themselves.

2.1.1. Collinear Factorization

To cancel all divergencies in hadronic cross-sections it is necessary to remove divergences arising from initial state collinear radiation. Similar to UV renormalization, it is possible to perform a redefinition of parameters that enter the theory. Since this is a phenomenon which enters through the initial state only, it is not feasible to perform the renormaliza-

2.1. Factorization in production and decay

tion at Lagrangian level. The PDFs appearing in the cross-section formula (2.3) are the only parameters left. Assuming that the PDFs appearing in that equation are the bare quantities, collinear counter terms Z_{ij} are introduced in the following way

$$\phi_i^0(x) = Z_{ij} \otimes \phi_j = \int_x^1 \frac{dz}{z} Z_{ij} \left(\frac{x}{z}, \mu_F \right) f_j(z, \mu_F) \quad (2.4)$$

where the f_j are the observable renormalized PDFs. The renormalization constant matrix Z_{ij} can be expressed through the Altarezi-Parisi splitting functions, but beyond the divergences it is scheme dependent. In the $\overline{\text{MS}}$ scheme they read up to NNLO

$$\begin{aligned} Z_{ij}(x, \mu_F) &= Z_{ij}^{(0)}(x, \mu_F) + Z_{ij}^{(1)}(x, \mu_F) + Z_{ij}^{(2)}(x, \mu_F) + \mathcal{O}(\alpha_s^3) \\ &= \delta_{ij} \delta(1-x) + \frac{\alpha_s(\mu_F)}{2\pi} \frac{P_{ij}^{(0)}(x)}{\epsilon} + \left(\frac{\alpha_s(\mu_F)}{2\pi} \right)^2 \\ &\cdot \left[\frac{P_{ij}^{(1)}(x)}{2\epsilon} + \frac{1}{2\epsilon^2} \left((P_{ik}^{(0)} \otimes P_{kj}^{(0)})(x) - \frac{\beta_0}{2} P_{ij}^{(0)}(x) \right) \right] + \mathcal{O}(\alpha_s^3(\mu_F)), \end{aligned} \quad (2.5)$$

where $P_{ij}^{(n)}(x)$ and β_0 are given by the perturbative expansions

$$P_{ij}(x, \mu_F) = \sum_{n=0} \left(\frac{\alpha_s(\mu_F)}{2\pi} \right)^{n+1} P_{ij}^{(n)}(x) \quad (2.6)$$

$$\beta(\alpha_s(\mu_F)) = -4\pi \sum_{n=0} \left(\frac{\alpha_s(\mu_F)}{2\pi} \right)^{n+1} \beta_n \quad (2.7)$$

of the splitting and β function, respectively. Applying this to the hadronic cross section formula and expanding everything up to NNLO, the finite total cross section reads

$$\begin{aligned} \sigma_{h_1 h_2}(P_1, P_2) &= \\ &\sum_{ab} \int \int_0^1 dx_1 dx_2 \phi_{a/h_1}(x_1, \mu_F^2) \phi_{b/h_2}(x_2, \mu_F^2) \left(\hat{\sigma}_{ab}^{(0)} + \hat{\sigma}_{ab}^{(1)} + \hat{\sigma}_{ab}^{(2)} \right) + \mathcal{O}(\alpha_s^3) \end{aligned} \quad (2.8)$$

with

$$\hat{\sigma}_{ab}^{(0)} = \tilde{\sigma}_{ab}^{(0)} \quad (2.9)$$

$$\hat{\sigma}_{ab}^{(1)} = \tilde{\sigma}_{ab}^{(1)} + \left[Z_{ka}^{(1)} \otimes \tilde{\sigma}_{kb}^{(0)} + Z_{kb}^{(1)} \otimes \tilde{\sigma}_{ak}^{(0)} \right] \quad (2.10)$$

$$\begin{aligned} \hat{\sigma}_{ab}^{(2)} &= \tilde{\sigma}_{ab}^{(2)} + \left[Z_{ka}^{(2)} \otimes \tilde{\sigma}_{kb}^{(0)} + Z_{kb}^{(2)} \otimes \tilde{\sigma}_{ak}^{(0)} + Z_{ka}^{(1)} \otimes \tilde{\sigma}_{kb}^{(1)} \right. \\ &\quad \left. + Z_{kb}^{(1)} \otimes \tilde{\sigma}_{ak}^{(1)} + Z_{ka}^{(1)} \otimes Z_{lb}^{(1)} \otimes \tilde{\sigma}_{kl}^{(0)} \right] \end{aligned} \quad (2.11)$$

The expansion in α_s is meant to be on top of the order α_s needed for the lowest order contribution. In the case of $t\bar{t}$, the lowest order is of order α_s^2 .

2. The Top-Quark in Theory

2.1.2. Renormalization of virtual amplitudes

In the partonic cross sections $\tilde{\sigma}_{ab}$ and $\hat{\sigma}_{ab}$ virtual amplitudes contribute beyond the leading order in perturbation theory. It is well known that there are divergences related to large loop momenta within transition amplitudes (UV divergences) and, due to the appearance of massless particles, soft and collinear divergences (IR divergences). In a renormalizable theory like QCD, the UV divergences can be absorbed in the free (bare) parameters of the underlying Lagrangian after a suitable regularization has been applied. Different regularization schemes were developed in history of higher order QFT. Conventional dimensional regularization (CDR) [109–112] is one of the most used ones and also employed throughout this thesis. A detailed discussion of the definitions and assumptions entering this regularization scheme is given for example in [113]. Calculations in this scheme are done consistently in $d = 4 - 2\epsilon$ space time dimensions, by analytical continuation. Remarkably, gauge symmetries are not affected by this extension, which is a great advantage of this scheme. There are variants of this scheme like the four dimensional helicity scheme (FDH) or 't Hooft-Veltman scheme (HV) which differ by the treatment of the spin-degrees of freedom of external and virtual particles. There are also conceptual different regularization schemes like Pauli-Villars (only for UV divergencies) or mass regularization. One important result of renormalization theory is the independence of physical results on the regularization scheme as well as renormalization scheme.

UV renormalization

Considering top-quark pair production in QCD, the theory contains two free parameters, α_s and m_t . All UV divergences can be absorbed in the bare parameters and the normalization of the fields, since they are independent of the kinematics of UV divergent quantities. This can be achieved by multiplicative renormalization constants that relate the renormalized with the bare quantities

$$\text{coupling:} \quad \alpha_s^0 = \left(\frac{e^{\gamma_E} \mu_R^2}{4\pi} \right)^\epsilon Z_{\alpha_s}^{(n_f)}(\mu_R) \alpha_s^{(n_f)}(\mu_R) \quad (2.12)$$

$$\text{mass:} \quad m_t^0 = Z_m m_t \quad (2.13)$$

$$\text{fields:} \quad \Psi_q^0 = Z_q^{\frac{1}{2}} \Psi_q, \quad \Psi_Q^0 = Z_Q^{\frac{1}{2}} \Psi_Q, \quad A_\mu^0 = Z_3^{\frac{1}{2}} A_\mu \quad (2.14)$$

with $q \in \{d, u, s, c, b\}$ and $Q \in \{t\}$. The number of active quarks flavors n_f that contributes to the running of α_s is the sum of the number of massless quarks n_l and heavy quarks n_h . This introduces a mismatch to the number of active flavors present in evolution of the PDFs, see equation (2.2). In the factorization formula (2.3) it was assumed that the top-quarks are too heavy to be produced highly relativistically, such that one could neglect the mass, for the given hadronic center energy. Therefore there is no top-quark PDF and the number of active flavors is given by n_l . To obtain a consistent treatment of α_s in the partonic cross section one has to decouple the top-quark from the running of α_s . This can be achieved by introducing the decoupling constant ζ_{α_s}

$$\alpha_s^{(n_f)} = \zeta_{\alpha_s} \alpha_s^{(n_l)}. \quad (2.15)$$

With this replacement all expressions can be expanded consistently in $\alpha_s^{(n_l)}$, which will be denoted as α_s for brevity. The actual form of the constants Z_i (ζ_{α_s}) depends on

2.1. Factorization in production and decay

the regularization and the renormalization scheme used. While the UV poles are fixed through the theory, the finite part of the constants is ambiguous and gives rise to various renormalization schemes. Two schemes are employed in all calculations presented in this thesis. The on-shell scheme is used for all fields and the mass, and the $\overline{\text{MS}}$ scheme used for the coupling constant. The renormalization constants can be treated in perturbation theory

$$Z = 1 + \sum_{n=1} \left(\frac{\alpha_s^{(n_f)}}{2\pi} \right)^n Z^{(n)} \quad (2.16)$$

and up to NNLO all necessary constants are given in appendix B.

One essential type of quantities that require renormalization are partonic scattering amplitudes which describe the partonic production of a top-quark pair, plus possibly additional radiation of massless particles. The renormalized amplitude written in terms of bare quantities is given by

$$|\mathcal{M}_{i_1, i_2, \dots, i_n}(\alpha_s, m_t, \mu_R, \epsilon)\rangle = \left(\frac{e^{\gamma_E} \mu_R^2}{4\pi} \right)^{-\frac{n}{2}\epsilon} \prod_{i=1}^N \sqrt{Z_i} |\mathcal{M}_{i_1, i_2, \dots, i_n}^0(\alpha_s^0, m_t^0, \epsilon)\rangle. \quad (2.17)$$

Expansion of both sides in α_s yields the renormalized amplitudes entering the partonic cross section $\tilde{\sigma}_{ab}$ in equation (2.8). All constants act multiplicatively and, besides the bare amplitude, the expansion yields counter terms on the right-hand side. Special care has to be taken in case of the mass renormalization constant. It enters the amplitude through the top-quark propagator

$$\frac{i}{\not{p} - m_t^0 + i\eta} = \frac{i}{\not{p} - Z_m m_t + i\eta}, \quad (2.18)$$

but it can be rewritten in a convenient way, by making use of an inverse Dyson resummation

$$\begin{aligned} \frac{i}{\not{p} - Z_m m_t + i\eta} &= \frac{i}{\not{p} - m_t + i\eta} \frac{1}{1 - \frac{Z_m - 1}{\not{p} - m_t + i\eta}} \\ &= \frac{i}{\not{p} - m_t + i\eta} \sum_{k=0} \left(\frac{Z_m - 1}{\not{p} - m_t + i\eta} \right)^k \\ &= \frac{i}{\not{p} - m_t + i\eta} + \left(\frac{\alpha_s^{(n_f)}}{2\pi} \right) \frac{i Z_m^{(1)} m_t}{(\not{p} - m_t + i\eta)^2} \\ &\quad + \left(\frac{\alpha_s^{(n_f)}}{2\pi} \right)^2 \left(\frac{i Z_m^{(2)} m_t}{(\not{p} - m_t + i\eta)^2} + \frac{i (Z_m^{(1)} m_t)^2}{(\not{p} - m_t + i\eta)^3} \right) + \mathcal{O}(\alpha_s^3) \end{aligned} \quad (2.19)$$

which can be employed in a straight forward way, in the evaluation of the expansion of (2.17) on the right-hand side.

IR renormalization

After removing UV divergences from the theory, virtual amplitudes still contain infrared divergences. They originate from internal massless particles becoming collinear to external

2. The Top-Quark in Theory

particles or becoming soft. Fortunately, these infrared limits can be investigated in a systematic way. The infrared structure of QCD amplitudes is completely known up to the two-loop level [114–119] and can be expressed through lower order amplitudes. The factorization of the divergences can be written in terms of the operator $\mathbf{Z} = \mathbf{1} + \mathbf{Z}^{(1)} + \mathbf{Z}^{(2)} + \mathcal{O}(\alpha_s^3)$ which acts on color space:

$$|\mathcal{M}^{(0)}\rangle = |\mathcal{F}^{(0)}\rangle, \quad (2.20)$$

$$|\mathcal{M}^{(1)}\rangle = \mathbf{Z}^{(1)} |\mathcal{M}^{(0)}\rangle + |\mathcal{F}^{(1)}\rangle, \quad (2.21)$$

$$|\mathcal{M}^{(2)}\rangle = \mathbf{Z}^{(2)} |\mathcal{M}^{(0)}\rangle + \mathbf{Z}^{(1)} |\mathcal{F}^{(1)}\rangle + |\mathcal{F}^{(2)}\rangle \quad (2.22)$$

$$= (\mathbf{Z}^{(2)} - \mathbf{Z}^{(1)} \mathbf{Z}^{(1)}) |\mathcal{M}^{(0)}\rangle + \mathbf{Z}^{(1)} |\mathcal{M}^{(1)}\rangle + |\mathcal{F}^{(2)}\rangle. \quad (2.23)$$

The \mathbf{Z} operator can be determined by the anomalous dimension matrix $\mathbf{\Gamma}$ through the renormalization group equation

$$\frac{d}{d \ln \mu_R} \mathbf{Z}(\epsilon, \{p_i\}, \{m_i\}, \mu_R) = -\mathbf{\Gamma}(\{p_i\}, \{m_i\}, \mu_R) \mathbf{Z}(\epsilon, \{p_i\}, \{m_i\}, \mu_R). \quad (2.24)$$

The matrix $\mathbf{\Gamma}$ was calculated within the aforementioned references. The matrix depends on the exact process under consideration. With the summation convention given in the appendix A the matrix reads

$$\begin{aligned} \mathbf{\Gamma}(\{\underline{p}\}, \{\underline{m}\}, \mu) &= \sum_{(i,j)} \frac{\mathbf{T}_i \cdot \mathbf{T}_j}{2} \gamma_{\text{cusp}}(\alpha_s^{(n_i)}) \ln \frac{\mu^2}{-s_{ij}} + \sum_i \gamma^i(\alpha_s^{(n_i)}) \\ &- \sum_{(I,J)} \frac{\mathbf{T}_I \cdot \mathbf{T}_J}{2} \gamma_{\text{cusp}}(\beta_{IJ}, \alpha_s^{(n_i)}) + \sum_I \gamma^I(\alpha_s^{(n_i)}) + \sum_{I,j} \mathbf{T}_I \cdot \mathbf{T}_j \gamma_{\text{cusp}}(\alpha_s^{(n_i)}) \ln \frac{m_I \mu}{-s_{Ij}} \\ &+ \sum_{(I,J,K)} i f^{abc} \mathbf{T}_I^a \mathbf{T}_J^b \mathbf{T}_K^c F_1(\beta_{IJ}, \beta_{JK}, \beta_{KI}) \\ &+ \sum_{(I,J)} \sum_k i f^{abc} \mathbf{T}_I^a \mathbf{T}_J^b \mathbf{T}_k^c f_2\left(\beta_{IJ}, \ln \frac{-\sigma_{Jk} v_J \cdot p_k}{-\sigma_{Ik} v_I \cdot p_k}\right). \end{aligned} \quad (2.25)$$

The equation can be solved by an ansatz for the α_s expansion of $\mathbf{\Gamma}$, as demonstrated in [120]. The first two non/trivial terms of the expansion of \mathbf{Z} can be written in terms of the α_s expansion of the anomalous dimension matrix

$$\mathbf{\Gamma} = \sum_{n=0}^{\infty} \mathbf{\Gamma}_n \left(\frac{\alpha_s}{4\pi}\right)^{n+1} \quad (2.26)$$

and its derivative

$$\mathbf{\Gamma}' = \frac{\partial \mathbf{\Gamma}}{\partial \ln \mu_R}, \quad \mathbf{\Gamma}' = \sum_{n=0}^{\infty} \mathbf{\Gamma}'_n \left(\frac{\alpha_s}{4\pi}\right)^{n+1} \quad (2.27)$$

and reads [121]

$$\mathbf{Z}^{(1)} = \frac{\alpha_s}{4\pi} \left(\frac{\Gamma'_0}{4\epsilon^2} + \frac{\mathbf{\Gamma}_0}{2\epsilon} \right) \quad (2.28)$$

$$\mathbf{Z}^{(2)} = \left(\frac{\alpha_s}{4\pi} \right)^2 \left[\frac{(\Gamma'_0)^2}{32\epsilon^4} + \frac{\Gamma'_0}{8\epsilon^3} \left(\mathbf{\Gamma}_0 - \frac{3}{2}\beta_0 \right) + \frac{\mathbf{\Gamma}_0}{8\epsilon^2} (\mathbf{\Gamma}_0 - 2\beta_0) + \frac{\mathbf{\Gamma}'_1}{16\epsilon^2} + \frac{\mathbf{\Gamma}_1}{4\epsilon} \right]. \quad (2.29)$$

The expressions for the anomalous dimensions and functions F_1 and f_2 is given in the appendix B. These IR “counterterms” are intrinsically different from UV counterterms. In particular they depend on the kinematics of the external particles and the divergences are supposed to cancel against unresolved radiation integrated over their phase space from higher multiplicity matrix elements.

2.1.3. Matrix element factorization

Besides purely virtual radiative corrections, higher order partonic cross-sections contain contributions from additional radiation. How to deal with these real radiation contributions is discussed in detail in chapter 4. The central problem which has to be faced, are divergences generated by soft and/or collinear emissions that need to be integrated over. There are many different competing approaches to this problem, some of them discussed in more detail in section 4.1. However, all of them rely in one way or another on factorization of matrix elements in these critical limits. Factorization in this context means that in a soft or collinear limit the matrix element is factorized into a universal process-independent function and a lower multiplicity matrix element. Even though the two limits, i.e. soft and collinear, are quite different, both limits commute, a feature known as *color coherence* which is manifest in the factorization formula itself. The discussion of processes at NNLO requires not only limits of single particles becoming soft or collinear, but also double/soft and triple-collinear limits. All necessary functions, as long as tree-level amplitudes are concerned, have been evaluated in [122].

Soft limits

The single soft limit only concerns gluons due to flavor conservation. If one gluon with momentum q becomes soft, i.e. $q \rightarrow 0$, amplitudes factorize by the well known formula

$$\left| \mathcal{M}_{g,a_1,\dots,a_n}^{(0)}(q, p_1, \dots) \right\rangle = g\mu^\epsilon \mathbf{J}^\mu(q) \left| \mathcal{M}_{a_1,\dots,a_n}^{(0)}(p_1, \dots) \right\rangle \quad (2.30)$$

with the eikonal current

$$\mathbf{J}^\mu(q) = \sum_{i=1}^n \mathbf{T}^i \frac{p_i^\mu}{p_i \cdot q}. \quad (2.31)$$

For squared matrix elements the factorization can be obtained from the above formula,

$$\begin{aligned} & \left| \mathcal{M}_{g,a_1,\dots}^{(0)}(q, p_1, \dots) \right|^2 \simeq \\ & -4\pi\alpha_s \sum_{ij} \mathcal{S}_{ij}(q) \left\langle \mathcal{M}_{a_1,\dots}^{(0)}(p_1, \dots) \left| \mathbf{T}_i \cdot \mathbf{T}_j \right| \mathcal{M}_{a_1,\dots}^{(0)}(p_1, \dots) \right\rangle \end{aligned} \quad (2.32)$$

2. The Top-Quark in Theory

with

$$\mathcal{S}_{ij}(q) = \frac{p_i \cdot p_j}{(p_i \cdot q)(p_j \cdot q)}. \quad (2.33)$$

The fact that the color correlators of all particles contribute, represents the long-range nature of the soft limit. In case of two partons becoming soft, two different situations have to be distinguished. Consistent with flavor conservation, a pair of quarks can become soft together. This is reflected in the fact that the double soft limit is defined through two momenta q_1 and q_2 becoming soft in a correlated uniform way

$$q_1 \rightarrow \lambda q_1, \quad q_2 \rightarrow \lambda q_2, \quad \lambda \rightarrow 0. \quad (2.34)$$

For a $q\bar{q}$ pair this results in

$$|\mathcal{M}_{q,\bar{q},a_1,\dots}^{(0)}(q_1, q_2, p_1, \dots)|^2 \simeq (4\pi\alpha_s)^2 T_F \sum_{ij} \mathcal{I}_{ij} \left\langle \mathcal{M}_{a_1,\dots}^{(0)}(p_1, \dots) \left| \mathbf{T}_i \cdot \mathbf{T}_j \right| \mathcal{M}_{a_1,\dots}^{(0)}(p_1, \dots) \right\rangle \quad (2.35)$$

where the function \mathcal{I}_{ij} is defined in the Appendix C. For two gluons in the same limit, the following is found

$$\begin{aligned} |\mathcal{M}_{g,g,a_1,\dots}^{(0)}(q_1, q_2, p_1, \dots)|^2 &\simeq -4\pi\alpha_s \\ &\left[\frac{1}{2} \sum_{ij} \mathcal{S}_{ij}(q_1) \mathcal{S}_{kl}(q_2) \left\langle \mathcal{M}_{a_1,\dots}^{(0)}(p_1, \dots) \left| \{\mathbf{T}_i \cdot \mathbf{T}_j, \mathbf{T}_k \cdot \mathbf{T}_l\} \right| \mathcal{M}_{a_1,\dots}^{(0)}(p_1, \dots) \right\rangle \right. \\ &\quad \left. - C_A \sum_{ij} \mathcal{S}_{ij}(q_1, q_2) \left\langle \mathcal{M}_{a_1,\dots}^{(0)}(p_1, \dots) \left| \mathbf{T}_i \cdot \mathbf{T}_j \right| \mathcal{M}_{a_1,\dots}^{(0)}(p_1, \dots) \right\rangle \right] \quad (2.36) \end{aligned}$$

where again the function \mathcal{I}_{ij} is defined in Appendix C.

Collinear limits

The limit where two partons of flavor a_1 and a_2 with the momenta p_1 and p_2 become close in phase space can be described by the Sudakov parameterization

$$p_1^\mu = zp^\mu + k_\perp^\mu - \frac{k_\perp^2}{z} \frac{n^\mu}{2p \cdot n}, \quad p_2^\mu = (1-z)p^\mu - k_\perp^\mu - \frac{k_\perp^2}{1-z} \frac{n^\mu}{2p \cdot n}, \quad (2.37)$$

where the three momenta k_\perp, p and n have been introduced. They fulfill the following relations

$$p^2 = n^2 = p \cdot k_\perp = n \cdot k_\perp = 0. \quad (2.38)$$

In the limit $k_\perp^\mu \rightarrow 0$ the matrix elements factorize in the following way

$$|\mathcal{M}_{a_1,a_2,\dots}^{(0)}(p_1, p_2, \dots)|^2 \simeq 4\pi\alpha_s \frac{2}{s_{12}} \left\langle \mathcal{M}_{a,\dots}^{(0)}(p, \dots) \left| \hat{\mathbf{P}}_{a_1 a_2}^{(0)}(z, k_\perp; \epsilon) \right| \mathcal{M}_{a,\dots}^{(0)}(p, \dots) \right\rangle \quad (2.39)$$

2.1. Factorization in production and decay

where $s_{12} = (p_1 + p_2)^2$. The flavour a is determined from the flavour combination a_1 and a_2 through flavour conservation. If at least one of the two is a gluon a is given by the other flavor and if a_1 and a_2 are a quark-anti-quark pair or two gluons, a is a gluon. The operator $\hat{\mathbf{P}}_{a_1 a_2}^{(0)}(z, k_\perp; \epsilon)$ acts on spin space of parton a

$$\langle s | \hat{\mathbf{P}}_{a_1 a_2}^{(0)}(z, k_\perp; \epsilon) | s' \rangle = \hat{P}_{a_1 a_2}^{(0), ss'}. \quad (2.40)$$

The form of the splitting function depends on which combination of quarks and gluons the collinear pair is build of. The various functions are given in appendix C. At next-to-next-to-leading order the triple collinear limit also needs to be investigated. For that purpose the momenta p_i of partons with flavour a_i with $i \in \{1, 2, 3\}$, are parameterized in the following way

$$p_i^\mu = x_i p^\mu + k_{\perp i}^\mu - \frac{k_{\perp i}^2}{x_i} \frac{n^\mu}{2p \cdot n} \quad (2.41)$$

where the introduced momenta have similar properties as in the single collinear case above

$$p^2 = n^2 = p \cdot k_{\perp i} = n \cdot k_{\perp i} = 0. \quad (2.42)$$

In the triple collinear limit $k_{\perp i} \rightarrow 0$ matrix elements factorize as

$$|\mathcal{M}_{a_1, a_2, a_3, \dots}^{(0)}(p_1, p_2, p_3, \dots)|^2 \simeq \left(\frac{8\pi\alpha_s}{s_{123}} \right)^2 \left\langle \mathcal{M}_{a, \dots}^{(0)}(xp, \dots) \left| \hat{\mathbf{P}}_{a_1 a_2 a_3}^{(0)}(z_i, k_{\perp i}; \epsilon) \right| \mathcal{M}_{a, \dots}^{(0)}(xp, \dots) \right\rangle \quad (2.43)$$

where

$$z_i = \frac{x_i}{x}, \quad \text{with} \quad x = \sum_i x_i. \quad (2.44)$$

The various formulae for the splitting functions are collected in the appendix C as well.

Soft-Collinear limits

Soft-collinear limits, where a parton becomes soft and collinear can most easily be obtained from the corresponding collinear limit by additionally taking $z \rightarrow 0$ or 1 (depending on momentum routing). In case of two unresolved partons, there are limits where one parton becomes collinear and the other soft. Most of them are obtained from iterative application of the above formula. One special case emerges when the partons become collinear to each other and become soft together. This case is governed by the factorization formula

$$|\mathcal{M}_{a_1, a_2, a_3, \dots}^{(0)}(q_1, q_2, p, \dots)|^2 \simeq (4\pi\alpha_s)^2 \frac{2}{s_{12}} \hat{P}_{a_1 a_2}^{(0), \mu\nu}(z_{12}, k_\perp; \epsilon) \left\langle \mathcal{M}_{a_3, \dots}^{(0)}(p, \dots) \left| \mathbf{J}_\mu(q_1 + q_2) \mathbf{J}_\nu(q_1 + q_2) \right| \mathcal{M}_{a_3, \dots}^{(0)}(p, \dots) \right\rangle. \quad (2.45)$$

2. The Top-Quark in Theory

Soft and collinear limits beyond tree-level

At next-to-next-to-leading order, single soft and/or collinear limits of one-loop amplitudes appear in addition to the discussed limits of tree-level amplitudes. Their limits are special with respect to their scaling behavior since the limits decompose into two different components. For the collinear limit, for instance, there is one part which is a tree-level splitting function times a lower multiplicity one-loop matrix-element. The other part is a one-loop splitting function times tree-level matrix element. A similar decomposition occurs in the soft limit. Due to the integration over the loop-momentum in the one-loop factorization formula (done in CDR), this part contains terms like

$$s_{12}^{-\epsilon}, \quad \left(\frac{z}{1-z} \right)^\epsilon \quad \text{or} \quad (\mathcal{S}_{ij})^\epsilon \quad (2.46)$$

where s_{12} and z defined as in equation 2.37. These terms modify the scaling behaviour in the corresponding infrared limits. To be more precise, the soft limit of a one-loop matrix element reads

$$\begin{aligned} & 2 \operatorname{Re} \left\langle \mathcal{M}_{g,a_1,\dots}^{(0)}(q, p_1, \dots) \left| \mathcal{M}_{g,a_1,\dots}^{(1)}(q, p_1, \dots) \right. \right\rangle \simeq -4\pi\alpha_s \\ & \left\{ \sum_{(i,j)} (\mathcal{S}_{ij}(q) - \mathcal{S}_{ii}(q)) 2 \operatorname{Re} \left\langle \mathcal{M}_{a_1,\dots}^{(0)}(p_1, \dots) \left| \mathbf{T}_i \cdot \mathbf{T}_j \left| \mathcal{M}_{a_1,\dots}^{(1)}(p_1, \dots) \right. \right. \right\rangle \right. \\ & + \frac{\alpha_s}{4\pi} \left[\sum_{(i,j)} (\mathcal{S}_{ij}(q) - \mathcal{S}_{ii}(q)) R_{ij} \left\langle \mathcal{M}_{a_1,\dots}^{(0)}(p_1, \dots) \left| \mathbf{T}_i \cdot \mathbf{T}_j \left| \mathcal{M}_{a_1,\dots}^{(0)}(p_1, \dots) \right. \right. \right\rangle \right. \\ & \left. \left. - 4\pi \sum_{(i,j,k)} \mathcal{S}_{ik}(q) I_{ij} \left\langle \mathcal{M}_{a_1,\dots}^{(0)}(p_1, \dots) \left| f^{abc} T_i^a T_j^b T_k^c \left| \mathcal{M}_{a_1,\dots}^{(0)}(p_1, \dots) \right. \right. \right\rangle \right] \right\}, \quad (2.47) \end{aligned}$$

where the formulae for the R_{ij} and I_{ij} functions are given in the appendix C. In both functions a factor $\mathcal{S}_{ij}^\epsilon \sim \lambda^{2-2\epsilon} \left(\mathcal{S}_{ij}^{\text{reg}} \right)^\epsilon$ appears besides renormalization contributions which is the origin of altered scaling in the soft case. The functions $\mathcal{S}_{ij}^{\text{reg}}$ are finite in the soft limit. Schematically the matrix element (abbreviated by f) scales as

$$f \xrightarrow{\lambda \rightarrow 0} \frac{1}{\lambda^2} (f^0 + \lambda^{-2\epsilon} f^\epsilon) \quad (2.48)$$

The collinear limit, parameterized in same way as the normal single collinear limit, reads

$$\begin{aligned} & 2 \operatorname{Re} \left\langle \mathcal{M}_{a_1,a_2,\dots}^{(0)}(p_1, p_2, \dots) \left| \mathcal{M}_{a_1,a_2,\dots}^{(1)}(p_1, p_2, \dots) \right. \right\rangle \\ & \simeq 4\pi\alpha_s \frac{2}{s_{12}} \left[2 \operatorname{Re} \left\langle \mathcal{M}_{a,\dots}^{(0)}(p, \dots) \left| \hat{\mathbf{P}}_{a_1 a_2}^{(0)}(z, k_\perp; \epsilon) \left| \mathcal{M}_{a,\dots}^{(1)}(p, \dots) \right. \right. \right\rangle \right. \\ & \left. + \frac{\alpha_s}{4\pi} \left\langle \mathcal{M}_{a,\dots}^{(0)}(p, \dots) \left| \hat{\mathbf{P}}_{a_1 a_2}^{(1)}(z, k_\perp; \epsilon) \left| \mathcal{M}_{a,\dots}^{(0)}(p, \dots) \right. \right. \right\rangle \right] \quad (2.49) \end{aligned}$$

with the one-loop splitting functions $\hat{\mathbf{P}}_{a_1 a_2}^{(1)}$ which are given in full form in appendix C.

Here, the factor $s_{12}^{-\epsilon}$ changes the scaling in the collinear limit. Expressing this invariant

2.1. Factorization in production and decay

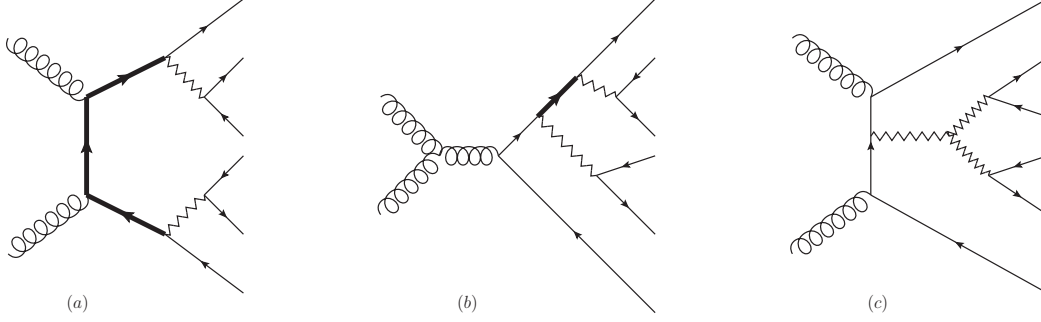


Figure 2.1.: Examples of Feynman diagrams contributing to the full $pp \rightarrow \bar{b}b\ell^+\ell'^-\nu_\ell\bar{\nu}_{\ell'}$ process. (a) double resonant, (b) single resonant and (c) non resonant.

through the Sudakov parameterization

$$s_{12} = -\frac{k_\perp^2}{z(1-z)} \quad (2.50)$$

the matrix element scales like

$$f \rightarrow \frac{1}{-k_\perp^2} (f^0 + (-k_\perp^2)^\epsilon f^\epsilon) . \quad (2.51)$$

Considering the soft-collinear limit, the factor $(z/(1-z))^\epsilon$ additionally plays a role. The transverse component scales here like $k_\perp = \lambda k_\perp$, while either $z = \lambda z_{reg}$ or $1-z = \lambda z_{Reg}$, with a regular function z_{reg} . For the one-loop matrix element the following scaling behaviour is found

$$f \rightarrow \frac{1}{-k_\perp^2 \lambda^2} (f^0 + (-k_\perp^2 \lambda^2)^\epsilon f^\epsilon) . \quad (2.52)$$

2.1.4. Narrow-Width-Approximation

Due to limitations set by the availability of high multiplicity two-loop matrix elements, it is not possible to calculate the full process $pp \rightarrow \bar{b}b\ell^+\ell'^-\nu_\ell\bar{\nu}_{\ell'}$ at next-to-next-to-leading order. However, the two-loop matrix elements for the production of a (polarized) top-quark pair (see chapter 3) as well as for the top-quark decay (see section 2.2.2), are available. To achieve a separation between the production process $pp \rightarrow t\bar{t}$ and the leptonic decays, $t \rightarrow b\ell^+\nu_\ell$ and $\bar{t} \rightarrow \bar{b}\ell'^-\bar{\nu}_{\ell'}$, it can be made use of the fact that the width of the top-quark is quite small. In the Narrow-Width-Approximation (NWA) a factorization of the production amplitudes from the decay-amplitudes is achieved in the limit $\frac{\Gamma_t}{m_t} \rightarrow 0$. Indeed, with the measured value of the top-quark mass and the top-quark width the ratio $\frac{\Gamma_t}{m_t}$ is of $\mathcal{O}(1\%)$.

At lowest order in QCD the partonic cross section entering formula (2.8) is given by

$$\hat{\sigma}_{ab}^{(0)}(p_1, p_2) = \frac{1}{2\hat{s}} \frac{1}{\mathcal{N}} \int d\Phi_6(P) \langle \mathcal{M}_{ab \rightarrow 6}^{(0)} | \mathcal{M}_{ab \rightarrow 6}^{(0)} \rangle \quad (2.53)$$

with $P = p_1 + p_2$. When considering the full process, various Feynman diagrams enter the matrix element $\langle \mathcal{M}_{ab \rightarrow 6}^{(0)} | \mathcal{M}_{ab \rightarrow 6}^{(0)} \rangle$. Some generic examples are shown in figure 2.1. They

2. The Top-Quark in Theory

can be classified in double resonant (a), single resonant (b) and continuum diagrams (c), depending on the number of appearing top-quark propagators. Consider the contribution of a double or single resonant diagram type. The top-quark propagator in the amplitude (in the complex mass scheme ¹ [123, 124]) is given by

$$p_t \longrightarrow p_t = \frac{i}{\not{p}_t - \mu_t + i\eta} \quad \text{with} \quad \mu_t^2 = m_t^2 - im_t\Gamma_t. \quad (2.54)$$

Thus, after squaring the amplitude, the denominator is given by

$$D(p_t^2) = \frac{1}{(p_t^2 - m_t^2)^2 + m_t^2\Gamma_t^2}. \quad (2.55)$$

and the corresponding contribution to the matrix element can be written as

$$D(p_t^2) \langle \mathcal{M}_{\text{res.}} | \mathcal{M}_{\text{res.}} \rangle (p_t^2) \in \left\langle \mathcal{M}_{ab \rightarrow 6}^{(0)} \left| \mathcal{M}_{ab \rightarrow 6}^{(0)} \right. \right\rangle \quad (2.56)$$

Additionally, the phase space integral

$$d\Phi_6(P; \{p_i\}_{i=1,6}) = (2\pi)^4 \delta^{(4)}(P - \sum_{i=1}^6 p_i) \prod_{j=1}^n \frac{d^3 \vec{p}_j}{(2\pi)^3 2E_j}. \quad (2.57)$$

can be split into a phase space integral over the production of an intermediate particle with invariant mass p_t^2 and its subsequent decay

$$d\Phi_6(P; \{p_i\}_{i=1,6}) = d\Phi_4(P; \{p_i\}_{i=1,3}, p_t) \frac{dp_t^2}{2\pi} d\Phi_3(p_t; \{p_i\}_{i=4,6}) \equiv \frac{dp_t^2}{2\pi} d\Phi_r(p_t^2). \quad (2.58)$$

With this at hand, the contribution of (2.56) to the cross section (2.53), can be expressed through

$$\hat{\sigma}_B(p_1, p_2) \ni \frac{1}{2\hat{s}} \frac{1}{\mathcal{N}} \int_{q_{\min}}^{q_{\max}} \frac{dp_t^2}{2\pi} D(p_t^2) \int d\Phi_r(p_t^2) \langle \mathcal{M}_{\text{res.}} | \mathcal{M}_{\text{res.}} \rangle (p_t^2). \quad (2.59)$$

In the limit $\frac{\Gamma_t}{m_t} \rightarrow 0$ the denominator asymptotically behaves like a δ function such that

$$\int_{-\infty}^{\infty} \frac{dp_t^2}{2\pi} D(p_t^2) \rightarrow \int_{-\infty}^{\infty} dp_t^2 \frac{\delta(p_t^2 - m_t^2)}{2m_t\Gamma_t}. \quad (2.60)$$

Assuming that the regions $(-\infty, q_{\min})$ and (q_{\max}, ∞) give only a negligible contribution to the integral over dp_t^2 , they can be added to the p_t^2 integral without large change. This leads to the following simplification

$$\begin{aligned} \frac{1}{2\hat{s}} \frac{1}{\mathcal{N}} \int_{q_{\min}}^{q_{\max}} \frac{dp_t^2}{2\pi} D(p_t^2) \int d\Phi_r(p_t^2) \langle \mathcal{M}_{\text{res.}} | \mathcal{M}_{\text{res.}} \rangle (p_t^2) \longrightarrow \\ \frac{1}{2\hat{s}} \frac{1}{\mathcal{N}} \int \frac{d\Phi_r(m_t^2) \langle \mathcal{M}_{\text{res.}} | \mathcal{M}_{\text{res.}} \rangle (m_t^2)}{2m_t\Gamma_t}. \end{aligned} \quad (2.61)$$

¹The complex mass scheme also generates additional terms $\sim \Gamma_t$ in the numerator. In NWA all additionally generated terms are sub-leading.

2.1. Factorization in production and decay

This construction can be applied to both top-quark propagators. Before further discussing the structure of $\mathcal{M}_{\text{res}}^2$, let us turn to other types of diagrams. The decomposition of phase space is valid independent of the matrix element. Therefore, in absence of a top-quark propagator, their contribution is negligible in comparison to the Breit-Wigner resonance. Thus, the contribution of the double resonant diagrams dominates in the cross section and all other contributions are suppressed by Γ_t/m_t [125].

After stripping off the propagator denominator and reverting the polarization sum for on-shell top-quark spinors, the structure of the amplitude $|\mathcal{M}_{\text{res.}}\rangle$ reads

$$|\mathcal{M}_{\text{res.}}\rangle(m_t) = \sum_{h_t} \langle h_t | \Gamma \rangle \langle h_t | \mathcal{M}_{\text{prod}} \rangle \quad (2.62)$$

where $\langle h_t | \Gamma \rangle$ denotes the on-shell decay amplitude with fixed top-quark polarization h_t , and $\langle h_t | \mathcal{M}_{\text{prod.}} \rangle$ the corresponding on-shell top-quark production amplitude.

2.1.5. Spinor-Helicity method

When combining production and decay within the Narrow-Width-Approximation, or in general whenever evaluating matrix elements depending on external polarization, a method to evaluate polarized amplitudes is essential. Spinor-helicity methods are a commonly used approach since they are easy to implement and suitable for automatization ([126, 127] and references therein). Different variants of these methods differ in terms of conventions and notation. In this section some necessary concepts of spinor-helicity formalism presented in [128] are reviewed. They serve as reference the later discussion of polarized $t\bar{t}$ amplitudes.

Basic spinors and 4-vectors

The basic object are two-component spinors

$$\psi_A \text{ and } \psi^{\dot{A}} \quad (2.63)$$

which transform under the irreducible representations $D(\frac{1}{2}, 0)$ and $D(0, \frac{1}{2})$ of the Lorentz-group, respectively. The Lorentz invariant spinor product of two spinors of the same representation is defined by

$$\langle \phi \psi \rangle \equiv \phi_A \epsilon^{AB} \psi_B = \phi_1 \psi_2 - \phi_2 \psi_1. \quad (2.64)$$

The matrix ϵ^{AB} is given in terms of Pauli matrices σ^a .

$$\epsilon^{AB} = \epsilon^{\dot{A}\dot{B}} = \epsilon_{AB} = \epsilon_{\dot{A}\dot{B}} = i\sigma^2. \quad (2.65)$$

The Pauli matrices themselves belong to the $D(\frac{1}{2}, \frac{1}{2})$ representation and the definition

$$\sigma^{\mu, \dot{A}B} = (\sigma^0, \sigma), \sigma^{\mu}_{\dot{A}B} = (\sigma^0, -\sigma) \quad (2.66)$$

allows to represent a Minkowski 4-vector k^μ as

$$K_{\dot{A}B} = k^\mu \sigma_{\mu, \dot{A}B} = \begin{pmatrix} k^0 + k^3 & k^1 + ik^2 \\ k^1 - ik^2 & k^0 - k^3 \end{pmatrix}. \quad (2.67)$$

2. The Top-Quark in Theory

Using properties of the σ^μ one can show that a Minkowski product can be written as:

$$2k \cdot p = K_{\dot{A}B} P^{\dot{A}B} . \quad (2.68)$$

Assuming that k is real, $K_{\dot{A}B}$ is obviously a Hermitian matrix and thus can be written in terms of two eigenvectors $n_{i,A}$ and their eigenvalues λ_i . In case of a time-like vector $k = (k^0, \mathbf{k})$ a particular decomposition is

$$K_{\dot{A}B} = \sum_{i=1,2} \kappa_{i,\dot{A}} \kappa_{i,B} , \quad (2.69)$$

where $\lambda_{1,2} = k^0 \pm |\mathbf{k}|$ and

$$\kappa_{1,A} = \sqrt{\lambda_1} \begin{pmatrix} e^{-i\phi} \cos \frac{\theta}{2} \\ \sin \frac{\theta}{2} \end{pmatrix} \quad \kappa_{2,A} = \sqrt{\lambda_2} \begin{pmatrix} \sin \frac{\theta}{2} \\ -e^{i\phi} \cos \frac{\theta}{2} \end{pmatrix} . \quad (2.70)$$

The angles θ and ϕ are determined through the direction of $\mathbf{k} = |\mathbf{k}| \mathbf{e}$:

$$\mathbf{e} = \begin{pmatrix} \cos \phi \sin \theta \\ \sin \phi \sin \theta \\ \cos \theta \end{pmatrix} . \quad (2.71)$$

In the light-like case ($k^2 = 0$) one of the eigenvalues vanishes and only one spinor remains. Therefore one obtains

$$K_{\dot{A}B} = k_{\dot{A}} k_B \quad (2.72)$$

with the so-called momentum spinor

$$k_A = \sqrt{2k^0} \begin{pmatrix} e^{-i\phi} \cos \frac{\theta}{2} \\ \sin \frac{\theta}{2} \end{pmatrix} . \quad (2.73)$$

Dirac matrices can also be expressed through σ^μ . In the chiral representation the relation reads

$$\gamma^\mu = \begin{pmatrix} 0 & \sigma_{\dot{A}B}^\mu \\ \sigma^{\mu,\dot{A}B} & 0 \end{pmatrix} . \quad (2.74)$$

External wave-functions

Fermions External fermion wave functions are given by Dirac-spinors Ψ ($D(\frac{1}{2}, 0) \oplus D(0, \frac{1}{2})$ representation):

$$\Psi = \begin{pmatrix} \phi_A \\ \psi^{\dot{A}} \end{pmatrix} \quad (2.75)$$

which fulfill the Dirac equation

$$(i\cancel{\partial} - m)\Psi = 0 . \quad (2.76)$$

2.2. Production and Decay

With the plane wave ansatz for fermions ($e^{-ikx}\Phi_k^+$) and anti-fermions ($e^{ikx}\Phi_k^-$) the two solutions

$$\Psi_{k,1}^{(\pm)} = \begin{pmatrix} \kappa_{1,A} \\ \mp \kappa_{2,A}^A \end{pmatrix} \quad \Psi_{k,2}^{(\pm)} = \begin{pmatrix} \pm \kappa_{2,A}^A \\ \kappa_{1,A}^A \end{pmatrix} \quad (2.77)$$

can be constructed. In case of a massless fermion the solutions simplify to

$$\Psi_{k,1}^{(\pm)} = \begin{pmatrix} k_A \\ 0 \end{pmatrix} \quad \Psi_{k,2}^{(\pm)} = \begin{pmatrix} 0 \\ k^A \end{pmatrix}. \quad (2.78)$$

Polarization vectors External vector particles are parametrized by a polarization vector ϵ^μ , a complex/valued four-vector. This leads to the fact that $\epsilon_{\dot{A}B}$ is not necessarily Hermitian and the decomposition in equation (2.69) is not applicable. However, starting with the equation of motion for a free (massive) vector particle (Proca equation)

$$[(\partial^2 + m^2)g^{\mu\nu} - \partial^\mu \partial^\nu] V_\nu = 0 \quad (2.79)$$

and inserting the plane wave ansatz $V^\mu = e^{\mp ikx} \epsilon^\mu(k)$, three solutions in the massive ($m^0 \neq 0$) case

$$\epsilon_{+,\dot{A}B}(k) = \sqrt{2} \kappa_{2,\dot{A}} \kappa_{1,B} / \sqrt{\lambda_1 \lambda_2} \quad (2.80)$$

$$\epsilon_{-,\dot{A}B}(k) = \sqrt{2} \kappa_{1,\dot{A}} \kappa_{2,B} / \sqrt{\lambda_1 \lambda_2} \quad (2.81)$$

$$\epsilon_{0,\dot{A}B}(k) = \frac{1}{m} \left(\kappa_{1,\dot{A}} \kappa_{1,B} - \kappa_{2,\dot{A}} \kappa_{2,B} \right), \quad (2.82)$$

and two solutions in the massless case

$$\epsilon_{+,\dot{A}B}(k) = \sqrt{2} g_{+,\dot{A}} k_B / \langle g_+ k \rangle^*, \quad \epsilon_{-,\dot{A}B}(k) = \sqrt{2} k_{\dot{A}} g_{-,B} / \langle g_- k \rangle \quad (2.83)$$

can be constructed. The vectors g_\pm are arbitrary light-like reference vectors with $g_\pm k \neq 0$.

2.2. Production and Decay

One pillar of the success of top-quark phenomenology is an accurate theoretical description and modelling. The core of any prediction is the fixed order calculation it is based on, and the starting point of any prediction for hadron colliders is the factorization formula 2.3. Considering the production of colored particles, it is evident that the final (and initial) state in fixed order calculations is not very realistic, since this is in contrast to the observation that all 'stable' particles are color neutral due to confinement. Also their multiplicity, which is usually of $\mathcal{O}(1)$ at fixed order, does not match the busy events measured at colliders. However, more realistic final states are not directly accessible through perturbation theory for two reasons: on the one hand, high multiplicity processes are not doable from a practical point of view, and on the other hand, most of the physics beyond the hard scattering is governed by low energy physics where perturbation theory breaks down. Fortunately, many techniques exist that go beyond fixed order and complement fixed order calculations by

2. The Top-Quark in Theory

including leading contributions from this regimes. Resummation² is a wide field of research whose goal is the accumulation of soft or collinear effects of radiation to all orders. There are many different approaches, reaching from specialized procedures for single observables to more general ones like parton-showers. The transformation to measurable final states cannot be achieved by these methods, since confinement in color-neutral particles is a highly non-perturbative feature of QCD. The usual way to obtain detector level final states is the modelling of this transition by parameterized functions that are fitted to measurements. This can happen at different stages, one might be interested in the transition of jet to the energy deposit in the hadronic calorimeter without taking into account the formation of stable hadrons and mesons. Another example are fragmentation functions describing the transition of a quark to a certain meson or hadron, like the transition from b quarks to B -mesons. They are similar to the PDFs which are also determined by fitting to data. By modelling the transition to actual measurable quantities, it is possible to relate observables which are accessible in fixed order calculations to data. This is a non-trivial step in any analysis and requires careful calibration and simulation. In context of top-quark production this point is of particular importance. To relate measurements with observables on top-quark level their decay plays a relevant role in different aspects. One important aspect is that the decays are mediated by the electroweak force and thus exhibit a $V - A$ coupling structure. The approximately massless decay products (light quarks and leptons) therefore induce a dependence on the top-quark polarization. This affects, for example, angular correlations between the final state particles. The experiments at the LHC are not covering the full available phase space but rather only a certain rapidity range. Additionally, further experimental cuts on the phase space may apply, like p_T cuts on jets, leptons and so on. Thus measurements do not yield total cross sections, but rather fiducial cross sections. Also, due to the decay, covering a certain range in rapidity of the measured objects, for instance, does not correspond to covering the same range for the top-quarks. Therefore, an extrapolation is required to extract quantities like the total $t\bar{t}$ cross section. This introduces systematic uncertainties on such quantities. Those uncertainties can be reduced by including the decay in the fixed-order part of the calculation and by directly evaluating quantities on observable particle level in the relevant region of phase space.

2.2.1. Stable top-quark production

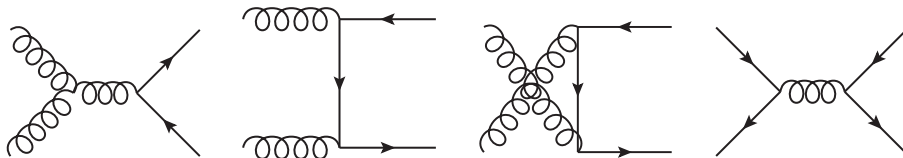


Figure 2.2.: Tree-level diagrams contributing to $t\bar{t}$ production in hadron-hadron collisions.

The partonic cross section entering equation 2.8 is described at lowest order in perturbation theory through the diagrams in figure 2.2. There are two channels at lowest order, the gg - and the $q\bar{q}$ -channel with $q \in \{u, d, c, s, b\}$. Depending on the nature of the incoming hadrons, they contribute with quite different fractions to the cross section. In case

² Resummation is a broad topic and is not discussed in any detail in this work. A review and collection of references can be found for instance in [129]

of proton-proton collisions the gg clearly dominates, making up 80-90% of the total cross section. In proton-antiproton collision, on the other hand, the situation is reversed and the $q\bar{q}$ -channel dominates. Due to their abundance in protons, u and d quarks are the most important quark channels. At higher order more channels are allowed. At next-to-leading order the qg -channel opens up and contributes through real radiation diagrams. The qq' - and $q\bar{q}'$ -channels, with two different quarks in the initial state, arise at NNLO. They both give a relatively small contribution to total cross section. Numbers for the total cross section at the different orders for the Tevatron and LHC @ 7 TeV are collected in table 2.1. The numbers have been obtained for a top mass parameter of $m_t = 173.3$ GeV and the MSTW2008 PDF [104]. The estimation of uncertainties is an intricate procedure since there are different ways in which they enter predictions. The treatment of the partonic cross section in perturbation theory and the finite expansion in couplings is an important origin of the uncertainties. Since higher orders are usually unknown, the uncertainty needs to be estimated. A useful tool is provided by the renormalization and factorization scale. Formally dependence of the (differential) cross section on those scales for each separate order is of higher order in the perturbative expansion. The actual dependence of a prediction on these scales can then be interpreted as the effect of the higher orders that are missing. In practice the error estimation is performed by varying the scale choice around a reasonable central scale by a factor of two or four and taking the envelope. There is no proof that this gives a reliable estimate, but practice and application shows that in many cases the uncertainty estimated in this way is reasonable. Parametric uncertainties enter through uncertainties of the input parameters. Masses, couplings and in some sense the PDFs belong to this type of uncertainties. However, depending on the application of the calculation, the dependence on these inputs might be used for parameter extraction rather than considering them as an origin of uncertainty. Especially the estimation of PDFs uncertainty requires some more details since from the theory point of view they are arbitrary functions of the momentum fraction x (with some constraints like sum rules and normalization). PDF sets are provided with additional PDFs (also denoted as eigenvectors of the Hessian), besides the central PDF. They differ from the central prediction by varying individual fit parameters within their uncertainty band³. Performing the calculation with each of these PDFs again results in an uncertainty band. However, in practice, this requires large computing power, since one is additionally interested in the effect of different PDFs sets (e.g. parameterizations and fitting procedures).

	LO [pb]	NLO [pb]	NNLO [pb]	NNLO+NNLL[pb]
Tevatron	$6.619^{+2.932}_{-1.862}$	$6.682^{+0.356}_{-0.125}$	$7.009^{+0.259}_{-0.374}$	$7.164^{+0.109}_{-0.200}$
LHC 7 TeV	$120.8^{+48.3}_{-31.8}$	$158.1^{+19.5}_{-21.2}$	$167.0^{+6.7}_{-10.7}$	$172.2^{+4.7}_{-5.9}$

Table 2.1.: Total cross section for $t\bar{t}$ production at Tevatron and LHC at LO, NLO, NNLO fixed order as well as for NNLO plus NNLL soft gluon resummation. The MSTW2008 PDF set is used for these predictions, while the error is estimated from scale variations.

The errors quoted in table 2.1 are estimates obtained from scale variations only. As expected, the NLO calculation [38–40] exhibits a reduced scale uncertainty with respect to

³ In case of NNPDF the additional PDFs are given by a sample of replica [130].

2. The Top-Quark in Theory

the LO prediction. That the NLO prediction for the total cross section stays within the error estimate of the LO cross section indicates a well-behaved convergence of perturbation theory. The full NNLO result has been obtained in ref. [51], which constitutes the progress of many years. The double/real contribution to the NNLO cross section was the first application of the novel Sector-improved residue subtraction scheme (or SecToR Improved Phase sPacE for real Radiation (STRIPPER)) [131, 132], which is discussed in chapter 4 in great detail. The double-virtual contribution requires two-loop amplitudes which have been presented in [133]. Details on the used techniques can be found in chapter 3 since the calculation of the polarized two-loop amplitudes presented in this work follows along the same lines as the original calculation. The reduction on the scale dependence results in a theory uncertainty of only 4 – 6%. The result was further improved by performing a NNLL soft-gluon resummation, as discussed in [47]. The resummation lowers the scale uncertainty to 4%.

Also, differential distributions have been investigated and compared to measurements at the Tevatron and the LHC. An example for a Tevatron measurement is given in figure 2.3 [55]. The differential cross sections with respect to the invariant mass of the $t\bar{t}$ system and the top transverse momentum are shown in comparison with D0 data [134]. Even though the experimental errors are quite large, the theory predictions matches the measurements nicely. For the LHC, an example of a comparison between data measured by CMS [135] and a NNLO calculation [54] is given in figure 2.4. Similar to the total cross section, the higher order calculations result in greatly reduced theory uncertainties. In figure 2.4, a further effect of the higher order corrections can be seen. There, higher order correction pull the tails of the differential distributions towards the correct shape. The large corrections in the tail of p_T distributions originate from the real radiation contributions which start at NLO. In these contributions the $t\bar{t}$ system recoils from the additional radiation, an effect not possible at LO. Beyond the bare comparison against data, the differential distribution can be used for parameter extraction. The shape of differential cross sections like $d\sigma/dp_T$ or $d\sigma/dm_{t\bar{t}}$ depends on the top-quark mass. This was used for example in [58] to extract the top-quark mass to be 169.1 ± 2.5 GeV from D0 measurements.

There are further interesting observables which profit from higher order theory predictions that are not discussed here. An important example are asymmetries [53] or the extraction of PDFs using differential $t\bar{t}$ cross sections [136]. Also, observables which are related to associated production, where the top pair is produced accompanied by an additional jet or a vector boson, are omitted here.

2.2.2. Top-quark decay

The top-quark decay is mediated by the weak interaction and the central observable to investigate is the decay width Γ_t . The strong hierarchy in the CKM matrix leaves the decay into bottom quark and a W boson as the dominating contribution to the width. The width is a quantity which can be calculated within perturbation theory and reads up to NNLO in the strong coupling constant

$$\Gamma_t = \Gamma_t^{(0)} + \alpha_s \Gamma_t^{(1)} + (\alpha_s)^2 \Gamma_t^{(2)} + \mathcal{O}(\alpha_s^3). \quad (2.84)$$

At lowest order in perturbation theory this decay process is described by the process $t(p_t) \rightarrow W^+(p_W) + b(p_b)$ with the Feynman diagram in figure 2.5. The leading order width

2.2. Production and Decay

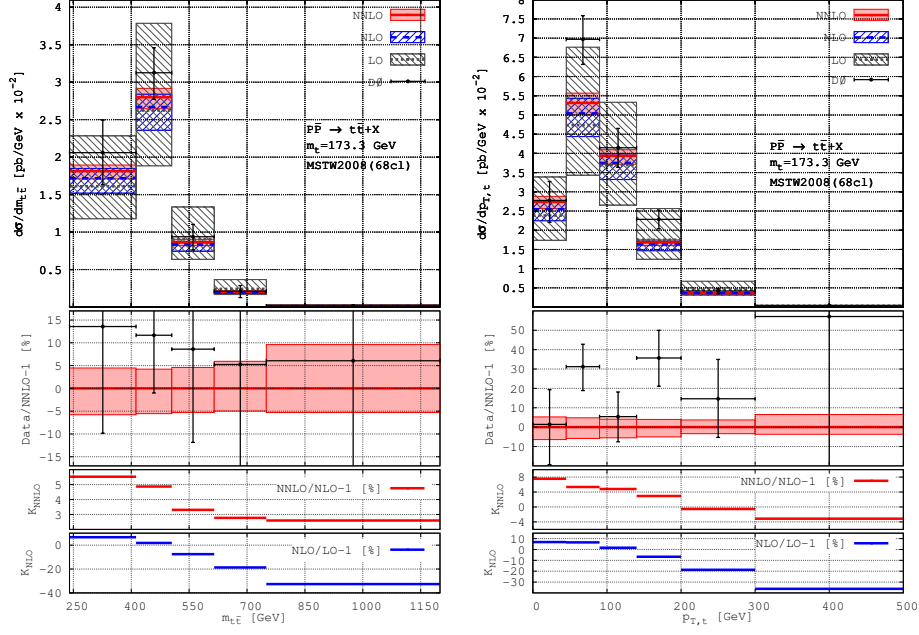


Figure 2.3.: Differential cross sections at Tevatron at different orders in perturbation theory compared to D0 data [55].

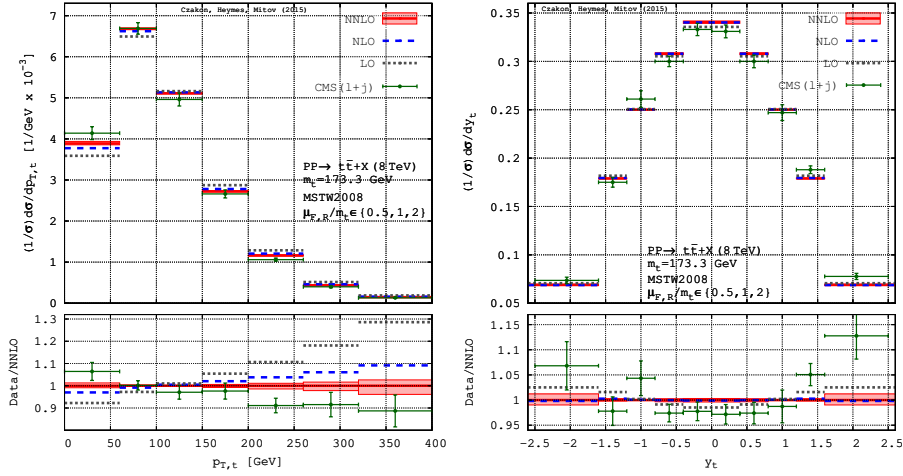


Figure 2.4.: Normalised differential cross sections at LHC @ 8 TeV at different orders in perturbation theory compared to CMS data [54].

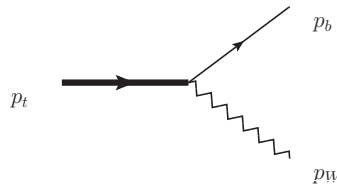


Figure 2.5.: Leading order diagram contributing to the decay width $\Gamma_t(t \rightarrow bW^+)$.

2. The Top-Quark in Theory

evaluates to

$$\Gamma^{(0)} = \frac{G_F m_t^3}{8\pi\sqrt{2}}(1-x)^2(1+2x) \quad \text{with} \quad x = \frac{p_W^2}{m_t^2}, \quad (2.85)$$

where the weak coupling constant was expressed through the Fermi constant $G_F = 1.16379 \cdot 10^{-5} \text{ GeV}^2$. For on-shell W -bosons, $p_W^2 = m_W^2$, the width is a function of the top-quark and W mass as well as coupling constants. Beyond leading order, it is convenient to express the virtual contributions to the width in terms of form factors. The general form of decay amplitudes can be written as a function of the top-quark polarization state h_t

$$\Gamma_t^{h_t} = \langle h_t | \Gamma_t \rangle = \bar{u}(p_b) \Gamma^\mu u_{h_t}(p_t) \epsilon_\mu(p_W), \quad (2.86)$$

with all other polarization indices suppressed. The vertex Γ^μ can be decomposed into three structures

$$\Gamma^\mu = C_1 \gamma^\mu P_L + C_2' \frac{P_R p_W^\mu}{2m_t} + C_3 \frac{P_R \tilde{q}^\mu}{2m_t}, \quad (2.87)$$

with projectors $P_{L/R} = (1 \pm \gamma_5)/2$ and the momentum $\tilde{q} = p_t + p_b$. In case of decay of the W -boson,

$$W^+(p_W) \rightarrow \ell^+(p_{\ell^+}) \nu(p_\nu) \quad \text{or} \quad W^-(p_W) \rightarrow \ell^-(p_{\ell^-}) \nu(p_{\bar{\nu}}) \quad (2.88)$$

is considered as well, the same decomposition holds with the polarization vector replaced by

$$\epsilon_\mu(p_W) \rightarrow \frac{-g_{\mu\nu}}{p_W^2 - m_W^2 + i\Gamma_W m_W} \bar{u}(p_\nu) \gamma^\nu P_L v(p_{\ell^+}) \quad (2.89)$$

and similarly for the anti-top decay. At leading order only C_1 is non-vanishing. For physical amplitudes, the transversality of the W -boson, $\epsilon \cdot p_W = 0$, implies that the second structure does not contribute. The coefficients are known up to NNLO in QCD and NLO in EW. They can be found in the literature [137–139] and are not reproduced here. Also, the full width has been calculated through NLO [140] and NNLO [96, 97, 141] in QCD, fully inclusive as well as differentially. For the total width, results are summarized in table 2.2 which has been taken from [97]. The higher orders in QCD have sizeable impact on the value of Γ_t which shows the necessity to include them in calculations with decaying top-quarks.

The incorporation of the decays within the NWA approach can be achieved by means of spin-correlators as shown in equation 2.62. In that case, the on-shell top-quark propagator is written in terms of the spin sum. However, when the W decays as well, another possibility to incorporate the decay is to keep the spin sum and define “decay-spinors”

$$\bar{U}(p_t) = \tilde{\Gamma}_t(t \rightarrow b\ell^+\nu) \frac{i(\not{p}_t + m_t)}{\sqrt{2m_t\Gamma_t}}, \quad (2.90)$$

$$V(p_t) = \frac{i(-\not{p}_t + m_t)}{\sqrt{2m_t\Gamma_t}} \tilde{\Gamma}(\bar{t} \rightarrow \bar{b}\ell^-\nu). \quad (2.91)$$

which replace the spinors in the production amplitude. This can be done since the external

m_t	Γ_t	δ_{EW}	$\delta_{QCD}^{(1)}$	$\delta_{QCD}^{(2)}$
172.5 GeV	1.4806 GeV	1.68	-8.58	-2.09
173.5 GeV	1.5109 GeV	1.69	-8.58	-2.09
174.5 GeV	1.5415 GeV	1.69	-8.58	-2.09

Table 2.2.: The top-quark width $\Gamma^{(0)}$ and corrections in (%) from higher orders in QCD and EW for different top masses.

particles are massless and thus their polarizations are fixed due to the $V - A$ structure of the coupling. This method was used, for instance, in [59].

2.2.3. Unstable top-quarks

The inclusion of the top-quark decays is an important step towards a realistic modelling of top-quark processes at any collider. There are basically two possible ways to proceed: either one considers a full process like $pp \rightarrow b\bar{b}\ell^+\ell^-\nu\bar{\nu}$ or one uses the Narrow-Width-Approximation. Both approaches have advantages and disadvantages.

NWA. The advantage of the NWA approach is that it is considerably easier to compute. Due to the factorization of the matrix elements and the suppression of off-shell contributions, only low-multiplicity matrix elements are required. The on-shellness of the top-quarks additionally simplifies the phase space integration. Another advantage is that the spin-correlation is fully kept and its effect can be investigated with predictions in NWA. Since the decay kinematics are included, differential distributions of the final state particles can be used with less unfolding for parameter extraction, as to top-quark mass, and thus have a smaller theoretical uncertainty. An example for an observable that encodes spin-correlation effects in the di-lepton channel is the azimuthal distance of two charge leptons (see figure 1.5). The NLO calculation of $t\bar{t}$ within NWA were presented in [59, 60]. An important finding of these calculations was that the NLO corrections of the decay have sizable impact on certain results. An example is the reconstructed W -mass in the lepton plus jet decay channel in figure 2.6. While the leptonic decaying W^+ can be perfectly reconstructed, there is an ambiguity in the reconstruction of the W^- boson from the light jets. Since this decay to light quarks is subject to NLO QCD corrections, the impact is quite strong here. The NNLO corrections to the top-quark pair production and decay are presented in chapter 5.

Off-shell effects. An even more accurate description of top-quark production is given by full off-shell calculations taking into account the finite width of the top. Such a calculation has been performed in [61, 62] at NLO. A nice summary of the results can be found in [142]. The finite top-quark width has only a very small effect on total crosssection of $\mathcal{O}(1\%)$ with respect to the NWA results. This coincides with the naive expectations of the NWA error Γ_t/m_t . However, depending on the observable, the effect on differential distributions can be quite substantial. An example for such an observable is the minimal invariant mass of a charged lepton and a b -jet (figure 2.7). Two conclusions can be drawn from this. On the one hand, the NLO have a large impact on the shape and normalization of the distributions. On the other hand, one can divide the phase space in two regions: One region where the NWA approximation gives reliable results and one where finite width

2. The Top-Quark in Theory

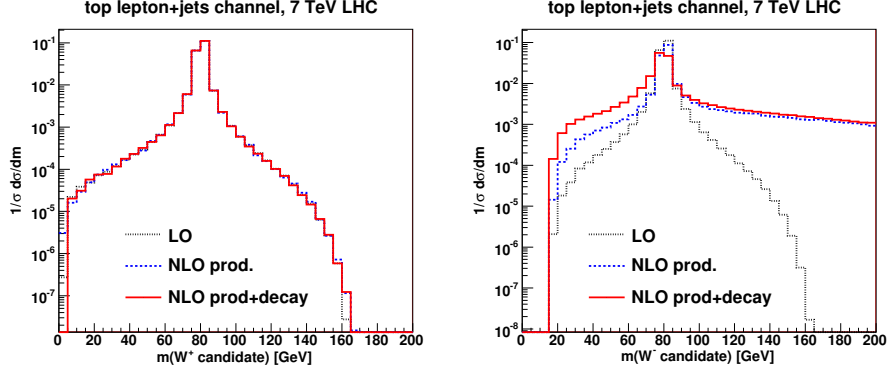


Figure 2.6.: Reconstructed W^\pm mass in the leptons+jets channel, taken from [60].

effects become important. The two regions are separated by the kinematic edge in the distribution. This is caused by the existence of a sharp boundary depending on the t and W masses for on-shell top-quarks (at LO). By including the off-shell contributions, this region can be filled and thus may give a completely different result than in the NWA case. However, the cross section is strongly suppressed in that region.

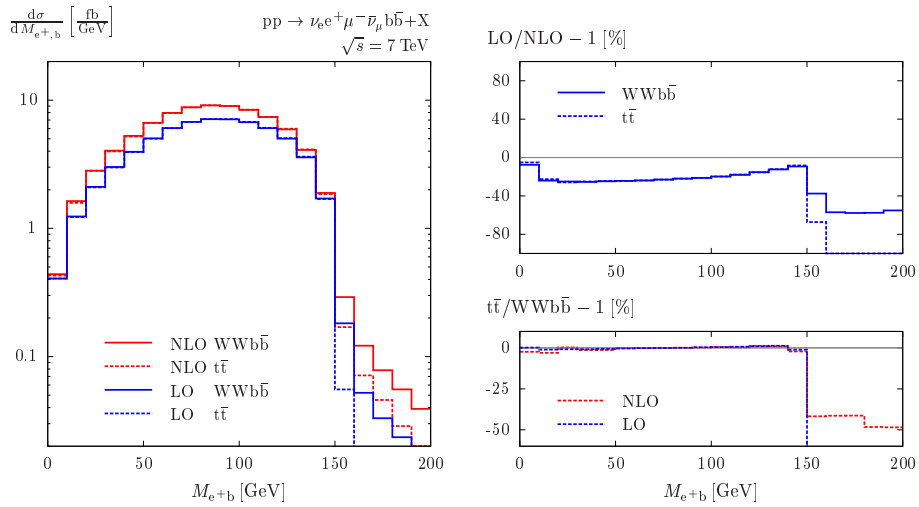


Figure 2.7.: Minimal invariant mass of e^+ and a b -jet compared between a NWA and an off-shell calculation. [142]

3. Polarized Double Virtual Top-Quark Pair Production

This chapter reviews the results for the polarized double virtual matrix elements published in [1]. It gives some further details on methods applied and a more detailed analysis of kinematic limits. Furthermore a representation of the result in form correlation matrices is presented.

3.1. Decomposition of Amplitudes

In order to obtain the matrix elements such that they can be evaluated for arbitrary polarization states of the external particles, a projection method is employed. The problem in the evaluation of polarized matrix-elements originates from the Lorentz structures appearing in the expressions. While at tree-level it is still feasible and quite efficient to evaluate helicity-amplitudes directly, for instance in terms of a spinor-helicity method, at loop-level the reduction of tensor-integrals to scalar ones becomes the bottle neck. However, at one loop there exist automated frameworks that can achieve these reductions [20, 21, 26]. The automated evaluation of two-loop is up to now a unsolved problem. Some progress was made in the past few years, for example with the numerical unitarity framework [143] or the integrand reduction method [144]. However, there is still a long way to go until these and other methods reach the status of practicability. As long as the multiplicity of the process under consideration is not too huge (in practice it is restricted to more or less four external particles) a projection method is a reasonable approach to this problem. It was successfully applied in [145–147]

This method starts from an analysis of the functional dependence of the amplitude on external quantities, to determine linear independent structures from which the amplitude can be build up. These structures can be regarded as a basis, and a projection onto this basis can be performed. The projection itself then leads to traces over γ -matrices and contracted Lorentz indices, which can be evaluated with computer algebra systems like FORM [148]. In this way a reduction to scalar integrals is achieved. The number of structures appearing is process- dependent and grows dramatically with the number of external particles and thus independent quantities.

3.1.1. Spin and Color structures

Onshell top-quark pair production in QCD involves two partonic processes

$$g(p_1)g(p_2) \rightarrow t(p_3)\bar{t}(p_4) \quad \text{and} \quad q(p_1)\bar{q}(p_2) \rightarrow t(p_3)\bar{t}(p_4) . \quad (3.1)$$

with

$$p_1^2 = p_2^2 = 0 , \quad p_3^2 = p_4^2 = m_t^2 , \quad (3.2)$$

3. Polarized Double Virtual Top-Quark Pair Production

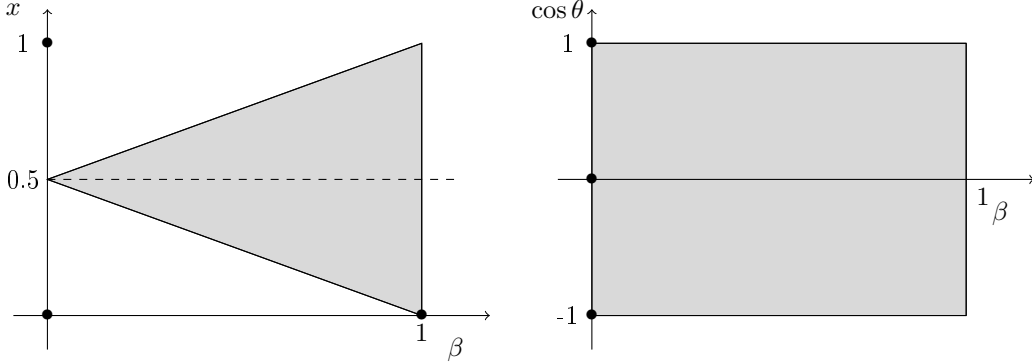


Figure 3.1.: Physically allowed phase space region in two parameterizations.

where m_t is the top-quark mass. With these momenta three Lorentz invariants can be formed

$$s \equiv (p_1 + p_2)^2, \quad t \equiv m_t^2 - (p_1 - p_3)^2, \quad u \equiv m_t^2 - (p_2 - p_3)^2. \quad (3.3)$$

Only two of them are independent due to momentum conservation which implies $s - t - u = 0$. The invariants can be expressed through the scattering angle θ of the top-quark with respect to p_1 and the 'velocity' β of the top-quark

$$t = \frac{s}{2} (1 - \beta \cos \theta), \quad u = \frac{s}{2} (1 + \beta \cos \theta), \quad \text{with } \beta = \sqrt{1 - 4 \frac{m_t^2}{s}}. \quad (3.4)$$

The physical phase space expressed through the different variables is visualised in figure 3.1. The amplitudes for this process are functions of s, t (or $\cos(\theta), \beta$) and m_t . Simple power counting reveals that the amplitudes have no energy dimension and therefore depend only on dimensionless ratios. The amplitude can be expanded in a perturbative series in $\alpha_s = g_s^2/4\pi$. Up to next-to-next-to-leading order the amplitude reads

$$|\mathcal{M}_{g,q}(\alpha_s, m_t, \epsilon)\rangle = 4\pi\alpha_s \left[|\mathcal{M}_{g,q}^{(0)}(m_t, \epsilon)\rangle + \left(\frac{\alpha_s}{2\pi}\right) |\mathcal{M}_{g,q}^{(1)}(m_t, \epsilon)\rangle + \left(\frac{\alpha_s}{2\pi}\right)^2 |\mathcal{M}_{g,q}^{(2)}(m_t, \epsilon)\rangle \right]. \quad (3.5)$$

The amplitudes depend on the color and spin degrees of freedom of the involved particles. It is possible to write the amplitude decomposed in terms of scalar coefficients times structures $|C_i^{g,q}\rangle \otimes |S_j^{g,q}\rangle$ in the color \otimes spin spin space of external particles

$$|\mathcal{M}_{g,q}^{(l)}(m_t, \epsilon)\rangle = \sum_{i,j} c_{ij}^{(l)}(m_t, s, t, \epsilon) |C_i^{g,q}\rangle \otimes |S_j^{g,q}\rangle. \quad (3.6)$$

The color structures $|C_i^{g,q}\rangle$ are vectors in color space such that, if color state of the external particles is denoted by $|a, b, c, d\rangle$, the contraction yields in case of initial state gluons

$$\langle a, b, c, d | C_i^g \rangle = (C_i^g)_{cd}^{ab} \quad (3.7)$$

3.1. Decomposition of Amplitudes

and in case of quarks

$$\langle a, b, c, d | C_i^q \rangle = (C_i^q)_{abcd} . \quad (3.8)$$

Similar for the spin structures $|S_j^{g,q}\rangle$. An external state is represented by $|h_1, h_2, h_3, h_4\rangle$, and the contraction gives

$$\langle h_1, h_2, h_3, h_4 | S_i^g \rangle = \epsilon_1(h_1)_\mu \epsilon_2(h_2)_\nu \bar{u}_3(h_3) (S_i)^{g\mu\nu} v_4(h_4) , \quad (3.9)$$

$$\langle h_1, h_2, h_3, h_4 | S_i^q \rangle = \bar{v}_2(h_2) \Gamma_i u_1(h_1) \bar{u}_3(h_3) \Gamma_i' v_4(h_4) . \quad (3.10)$$

Color structures. To determine which color structures are necessary to decompose the amplitude it is sufficient to examine the external indices of $C_i^{g,q}$.

In case of gluons there are two indices of adjoint representation a, b (gluons) and two of the fundamental representation (top-quarks). One can simply write down all linear independent combinations of generators and color structure constants, with this external index structure. This set is also a natural basis for the color decomposition.

$$C_1^g = (T^a T^b)_{cd}, \quad C_2^g = (T^b T^a)_{cd}, \quad C_3^g = \text{Tr}\{T^a T^b\} \delta_{cd} . \quad (3.11)$$

This particular choice is the one used for the calculation presented in this chapter, but is not unique. A different, but also useful color basis is used in the evaluation of the spin-summed matrix-elements in [51]. This basis can be obtained through linear combinations of the structures in (3.11)

$$C_{\mathbf{8}_S}^g = \sqrt{\frac{2N_C}{(N_C^2 - 1)(N_C^2 - 4)}} \left(C_1^g + C_2^g - \frac{2}{N_C} C_3^g \right) , \quad (3.12)$$

$$C_{\mathbf{8}_A}^g = \sqrt{\frac{2}{N_C(N_C - 1)}} (C_1^g - C_2^g) , \quad (3.13)$$

$$C_{\mathbf{1}}^g = \frac{2}{\sqrt{N_C(N_C - 1)}} C_3^g . \quad (3.14)$$

Here $\mathbf{8}_S$, $\mathbf{8}_A$ denote the symmetric and anti-symmetric octet states respectively, while $\mathbf{1}$ denotes the singlet state. This basis has the neat property that the structures are orthogonal to each other, such that there is no mixing between color coefficients when contracting the amplitudes when, for instance, color-summed quantities need to be evaluated. The same procedure applies to the quark amplitude. Here four fundamental indices have to be represented by a combination of generators and structure constants. It turns out that the basis is particularly simple in this case

$$C_1^q = \delta_{ab} \delta_{cd} , C_2^q = \delta_{ad} \delta_{cb} . \quad (3.15)$$

Spin structures. After color decomposition, each of the coefficients of $C_i^{g,q}$ is further decomposed into a set of spin-structures. Even though the calculation of the amplitudes is performed completely in CDR, let us assume that the external particles are confined to the 4-dimensional space, onshell, and are in a physical polarization state. With other words they obey the four-dimensional equation of motion. Then there are $2^4 = 16$ different

3. Polarized Double Virtual Top-Quark Pair Production

helicity configuration for both partonic processes. This translates to 16 linear independent spin-structures. However, there are further symmetries of the amplitude that reduce this number. Since only QCD interactions are considered, the amplitudes are invariant under parity transformations. The parity transformation does not effect the color-structure, but the helicity of all particles is flipped. This leaves only 8 independent structures. Also, charge conjugation is a valid symmetry of QCD amplitudes. However, C-symmetry interferes with the color-structures and is therefore not used to further constrain the independent structures. In case of gluons, there is even a further symmetry, the Bose-symmetry. The symmetry is not used in the calculation, but rather serves as a check of obtained results.

In the gluon case the 8 structures

$$\begin{aligned}
S_1^{g\mu\nu} &= \frac{1}{s} (\gamma^\mu p_3^\nu + \gamma^\nu p_3^\mu) , & S_2^{g\mu\nu} &= \frac{m_t}{s} g^{\mu\nu} \mathbf{1} , \\
S_3^{g\mu\nu} &= \frac{1}{s m_t} p_3^\mu p_3^\nu \mathbf{1} , & S_4^{g\mu\nu} &= \frac{1}{s m_t^2} \not{p}_1 p_3^\mu p_3^\nu , \\
S_5^{g\mu\nu} &= \frac{1}{s} \not{p}_1 g^{\mu\nu} , & S_6^{g\mu\nu} &= \frac{1}{s m_t} \not{p}_1 (\gamma^\nu p_3^\mu + \gamma^\mu p_3^\nu) , \\
S_7^{g\mu\nu} &= \frac{1}{s} (\gamma^\mu p_3^\nu - \gamma^\nu p_3^\mu) , & S_8^{g\mu\nu} &= \frac{1}{s} (\not{p}_1 g^{\mu\nu} - \not{p}_1 \gamma^\mu \gamma^\nu) .
\end{aligned} \tag{3.16}$$

form a suitable set for decomposition. Here the spinor indices are suppressed. It is also assumed that the gluons are transverse and the polarization vectors fulfill, in addition to the equation of motion,

$$\epsilon_1 \cdot p_2 = \epsilon_2 \cdot p_1 = 0 . \tag{3.17}$$

This can be implemented by using the following polarization sum when the amplitude is contracted

$$\sum_h \epsilon_\mu^*(h) \epsilon_\nu(h) = \left(-g_{\mu\nu} + \frac{p_{1\mu} p_{2\nu} + p_{1\nu} p_{2\mu}}{p_1 \cdot p_2} \right) \equiv d_{\mu\nu} . \tag{3.18}$$

Also, some normalization factors in form of m_t and s are included to make the structures dimensionless. That this set of structures is indeed linear independent can be tested through through the Gram-determinant. The Gram-determinant is defined as

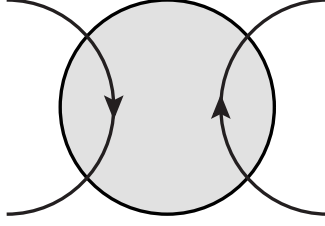
$$\Delta = \det \left((\langle S_i | S_j \rangle)_{ij} \right) \tag{3.19}$$

where the 'scalar-product' $\langle S_i | S_j \rangle$ is defined through

$$\langle S_i | S_j \rangle = \sum_{\text{spin states}} \langle S_i | h_1, h_2, h_3, h_4 \rangle \langle h_1, h_2, h_3, h_4 | S_j \rangle . \tag{3.20}$$

The spin-sum in case of gluons is then given by

$$\begin{aligned}
\left\langle S_i^g \middle| S_j^g \right\rangle &= \sum_{\text{spin}} \epsilon_1^*(h_1)_\alpha \epsilon_2^*(h_2)_\beta \bar{v}_4(h_4) ((S_i)^{\alpha\beta})^\dagger u_3(h_3) \epsilon_1(h_1)_\mu \\
&\quad \epsilon_2(h_2)_\nu \bar{u}_3(h_3) (S_i)^{\mu\nu} v_4(h_4)
\end{aligned}$$


 Figure 3.2.: Generic structure of $q\bar{q} \rightarrow t\bar{t}$ amplitudes.

$$= \text{Tr} \left\{ (\not{p}_4 - m) ((S_i)^{\alpha\beta})^\dagger (\not{p}_3 + m) (S_i)^{\mu\nu} \right\} d_{\mu\alpha} d_{\nu\beta} \quad (3.21)$$

The particular choice of basis was made because of the symmetry property when exchanging $\mu \leftrightarrow \nu$. The structures S_1, \dots, S_6 are symmetric under this symmetry and S_7 and S_8 are anti-symmetric. This property leads to the fact that the "scalar-product" of a symmetric and anti-symmetric structure vanished

$$\langle S_{\text{sym}}^g | S_{\text{asym.}}^g \rangle = 0. \quad (3.22)$$

Now the quark process. Before specifying the basis, a special feature of the quark amplitudes needs to be discussed. Since only QCD couplings are considered the heavy top-quark fermion line and the light fermion line are disconnected, see figure 3.2. In QCD, chirality is conserved and therefore half of the structures can be independent of each other, since only half of the light-quark helicity combinations can contribute. Consequently, the basis only consists of four structures

$$\begin{aligned} S_1^q &= \frac{1}{s m_t} \not{p}_3 \otimes \mathbf{1}, & S_2^q &= \frac{1}{s m_t^2} \not{p}_3 \otimes \not{p}_1, \\ S_3^q &= \frac{1}{s} \gamma^\mu \otimes \gamma_\mu, & S_4^q &= \frac{1}{s m_t} \gamma^\mu \otimes (\not{p}_1 \gamma_\mu), \end{aligned} \quad (3.23)$$

which are of the general form $S = \Gamma \otimes \Gamma'$ (Γ denotes a string of γ -matrices). The "scalar-product" of two quark structures is given by

$$\langle S_i^q | S_j^q \rangle = \text{Tr} \left\{ \not{p}_2 (\Gamma_i)^\dagger \not{p}_1 \Gamma_j \right\} \text{Tr} \left\{ (\not{p}_4 - m) (\Gamma'_i)^\dagger (\not{p}_3 + m) \Gamma'_j \right\} \quad (3.24)$$

Spin structures beyond four dimensions The determined set of spin structure relies on the 4-dimensional polarization states of the external particle. However, the calculation of the loop-amplitudes is done in $d = 4 - 2\epsilon$ dimensions. Since the d dimensional space is infinite dimensional, one can also find an infinite amount of linear independent spin-structures in d dimensions. This however does not cause any problems, due to the following argument. Assume that an infinitely large set of independent spin-structures is added to the already existing "four-dimensional" set. By basis transformation, this set can be made orthogonal to the "four-dimensional" set. In this way, they do not mix and in the limit $\epsilon \rightarrow 0$ they have to vanish after infrared renormalization, since the chosen spin structures form a basis in 4 dimensions.

3. Polarized Double Virtual Top-Quark Pair Production

3.1.2. Projection method

The actual decomposition of the tree-, one- and two-loop amplitudes is done with a projection approach. The basic idea is to construct projectors $\langle P|$ acting on color and/or spin space such that they single out a specific coefficient of the decomposition in (3.6). The color and spin states live in different spaces and thus the projectors can be constructed independently for color and spin structures. Assume an amplitude \mathcal{A} can be written as a decomposition of independent spin structures

$$\mathcal{A} = \sum c_i |S_i\rangle . \quad (3.25)$$

A proper ansatz for a projector for the coefficient c_j is

$$\langle P_j| = \sum_i b_{ji} \langle S_i| \quad (3.26)$$

as long as the S_i 's build up a basis. By demanding that

$$\langle P_j|\mathcal{A}\rangle \stackrel{!}{=} c_j \quad (3.27)$$

a system of algebraic equations of the coefficients b_{ji} is obtained. Inversion yields the projectors $\langle P_j|$. The same concept applies for the color structures. Combining color and spin projectors, the final form of the projector for a coefficient c_{ij} is

$$\langle P_{ij}| = \left(\sum_k b_{ik}^c \langle C_k| \right) \otimes \left(\sum_l b_{jl}^s \langle S_l| \right) . \quad (3.28)$$

The expression for the projector coefficients for the two partonic process are quite lengthy and are given in the appendix D. The coefficients are functions of the variable s, t, m_t , as well as the dimensional regularization parameter ϵ since the calculation is done completely in d dimensions. Also, starting at one-loop, scalar Feynman integrals appear in the coefficients. At one-loop 68 and at two-loop 9350 different scalar integrals appear in the gg -channel.

3.2. Evaluation of Feynman Integrals

A huge amount of scalar integrals appear in the coefficients. It is not feasible to evaluate them one-by-one. One method quite often used in practical calculations is the reduction to a set of master integrals using Integration-by-Parts identities (IBP-identities) [149]. Any scalar N_l -loop integral might be written in the following form

$$I(\{p_k\}, \{m_l\}, \{n_j\}) = \mathcal{N}_l^{N_l 2\epsilon} \int \prod_i^{N_l} \frac{d^d k_i}{(2\pi)^d} \prod_j \frac{1}{(D_j(\{p_k\}, \{m_l\}, \{k_n\}))^{n_j}} , \quad (3.29)$$

with the normalization factor $\mathcal{N}_l = \mu_R^2 e^{\gamma_E} / 4\pi$, where the denominators D_j can depend on the set of external momenta $\{p_k\}$, external and internal masses $\{m_l\}$ and on the loop

momenta $\{k_n\}$. They do not necessary have to be propagators of form

$$D = \left(\sum q_i \right)^2 - m^2 \text{ with } q_i \in \{p_k\} \cup \{k_n\}, \quad (3.30)$$

but also can be scalar products

$$D = k_n \cdot p_k. \quad (3.31)$$

Using translation invariance and integration-by-parts, it is evident that

$$0 = \mathcal{N}_l^{N_l 2\epsilon} \int \prod_i^{N_l} \frac{d^d k_i}{(2\pi)^d} \frac{\partial}{\partial k^\mu} q^\mu \prod_j \frac{1}{(D_j(\{p_k\}, \{m_l\}, \{k_n\}))^{n_j}}, \quad (3.32)$$

where k is any of the loop momenta and q any occurring momentum. The application of the derivative leads to a linear combination of scalar integrals with powers n_j increased or decreased by at most 1, and thus relates different scalar integrals. Generating many different of these relations leads to a system of equations. The reduction of this system down to a small set of linear independent integrals is called the IBP reduction. The Laporta algorithm [150] is a method specially designed for this type of equations. There are many publicly available software packages that implement this algorithm (for example Reduze [151], FIRE [152] or KIRA [153]). An in-house implementation was used to perform the IBP reduction in the $t\bar{t}$ case. The left-over integrals are called the master integrals of the system. The master integrals build up a basis for the functions space spanned by the scalar-integrals. If the master integrals are known, all the scalar integrals are also known. In addition to finding and reducing to a set of master integrals, IBP relations can be used to evaluate them, by generating a system of differential equations. The master integral basis is not unique. This freedom can be used to optimize the set of master integrals such that their evaluation, for example through differential equations, is as simple as possible.

Fortunately, in the case at hand, i.e. the scalar-integrals appearing in the coefficients of the structure decomposition 3.6, the same set of master integrals appear as in the calculation of the spin-summed two-loop matrix-elements. They are not known analytically, even though progress is made in that direction [154–158]. With the use of differential equations they can be evaluated numerically with high precision. In total there are 422 master integrals [133] to be evaluated.

As discussed in [133] there is an enhancement of the amplitudes in the limit of high energy and large/small scattering angles due to diagrams with the topology indicated in Fig. 3.3. This enhancement increases the demand on precision in the numerical evaluation. To improve on the numerical stability, a change of the master integral basis was performed. A basis obeying differential equations which are in the so called ϵ -form seemed to be especially useful.

3.2.1. Canonicalization

It has been shown [159], that under certain circumstances the differential equations of master integrals can be brought into a special form, where the right-hand side is proportional to ϵ and the divergences appearing in the differential equations are single poles in the kinematic variables. The variables in the case at hand would be x and m_s . This form is particularly useful since it allows for straightforward evaluation of the differential equa-

3. Polarized Double Virtual Top-Quark Pair Production

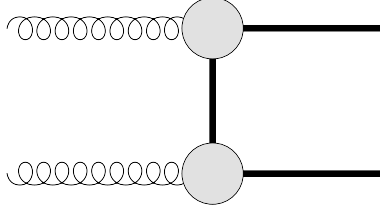


Figure 3.3.: Class of diagrams leading to enhanced matrix elements at high energy and low scattering angle.

tions. The basic idea is to achieve this form by basis transformations. The transformation can be given in terms of a transformation matrix whose coefficients are rational functions of the kinematic variables. It is not always possible to obtain the ϵ -form with these rational transformations and not even with more general transformations like the change of kinematic variables [160–162]. In the work presented in Ref. [162] a criterion in case of one kinematic variable was given that such a ϵ -form exist. There are many examples where it is not possible to reach the canonical form, for instance the differential equations of the master of the two-loop sunset topology with equal masses [163, 164]. The solution involves elliptic integrals, which are a good sign that a ϵ -form is not possible. Unfortunately, the same topology appears in $gg \rightarrow t\bar{t}$ master integral set. Therefore it is not possible to bring all of them into the canonical form. Many of the master integrals can be brought to the ϵ -form only by additional coordinate transformations. The existing setup, however, requires to integrate the hole system at once and thus these kind of transformations can not be applied. This restricts the number of integrals that can be brought into the ϵ -form quite drastically. Basically all master integrals that fulfill one of the following three conditions are not touched

- 1) their expressions involve elliptic integrals;
- 2) coordinate transformations are required in order to reach their ϵ -form;
- 3) their derivatives involve any one of the aforementioned two kinds of master integrals.

This leaves in total 65 out of 422 master integrals that can be brought directly into ϵp -form without any coordinate changes. The package CANONICA [165] was used to perform this task. This 65-by-65 system was moved to the top of the system of the differential system such that all other integrals can profit from the more stable evaluation of those masters.

3.2.2. Evaluation of master integrals

Using the partially canonicalized basis, the differential equations are used extensively to obtain numerical values for the master integrals over the full phase space. The scalar integrals can be written as functions of two dimensionless variables

$$x = \frac{t}{s} \text{ and } m_s = \frac{m_t^2}{s}, \quad (3.33)$$

and potentially an overall trivial factor of s to some power. Differentiating the master integrals with respect to those and performing another IBP reduction, yields a coupled

system of differential equations of the form

$$m_s \frac{\partial}{\partial m_s} \vec{\Gamma}(m_s, x, \epsilon) = \underline{A}^{m_s}(m_s, x, \epsilon) \vec{\Gamma}(m_s, x, \epsilon) \quad (3.34)$$

$$x \frac{\partial}{\partial x} \vec{\Gamma}(m_s, x, \epsilon) = \underline{A}^x(m_s, x, \epsilon) \vec{\Gamma}(m_s, x, \epsilon) \quad (3.35)$$

with $\vec{\Gamma}$ representing the vector of all master integrals. The matrices \underline{A}^{m_s} and \underline{A}^x are rational functions of m_s, x, ϵ . The evaluation is done in three stages:

1. Determination of high precision boundary values
2. The numerical integration to fixed points across the phase space
3. Matching of numerical result to threshold expansion in order to cover singular threshold region

The boundary conditions. For the numerical integration are obtained in the high energy limit $m_s \rightarrow 0$, from the original set of master-integrals, with the help of the rational transformation matrix obtained with CANONICA. In the high-energy limit the masters can be expanded in a power-logarithmic expansion in m_s . A few terms of this expansions can be obtained with Mellin-Barns (MB) techniques. The *MB.m* package [166] was employed for this task. In most case the obtained expansions are exact in x , but in some cases it was necessary to employ the differential equations to extract the exact dependence from the limit $x \rightarrow 0$. This was done as follows. In this double limit $m_s \rightarrow 0$ and $x \rightarrow 0$ it is possible to evaluate the integrals numerically with very high precision. The numerical values then can be resummed, where the PSLQ algorithm [167] and XSummer [168] were used. The idea behind this is simple. Suppose it is known that an integral, or its coefficients of an asymptotic expansion, evaluates to certain set of real numbers such as $\zeta(2)$ with rational coefficients. Then one can make an ansatz in form of a linear combination of all these real numbers and try to match the numerical value. With this method and high enough numerical precision, the analytic form of the integrals can be restored. The high-energy expansions obtained this way are not precise enough in a reasonable distance to the actual boundary. However, the differential equations can be used to improve the series expansion. Inserting an ansatz for the master integrals as a very deep power-logarithmic expansion in differential equation and consistently expanding the equations, yields an algebraic system of equations for the coefficients of the ansatz. Most of the coefficients are constrained through the system and the remaining ones can be matched to expansions obtained before. This allows for a very precise numerical evaluation at some point reasonably close to the boundary. By expanding in m_s , it was implicitly assumed that x is reasonable far away from 0 (or 1). The expansions fail to give reliable approximations of the integrals in these limits. Therefore the starting point for the numerical integration has to be chosen with moderate x . In practice $x = 0.35$, ($x = 0.45$ for cross-checks) was used.

The numerical integration. The solution of the differential equations starts from the boundary and evolves the system of master-integrals along contours in the complex-plane to specified points in the physical phase space. An example for such a contour is given in figure 3.4. To solve the differential equations numerically, software from [169] was incorporated, while the high precision numerics was handle with the QUAD package [170].

3. Polarized Double Virtual Top-Quark Pair Production

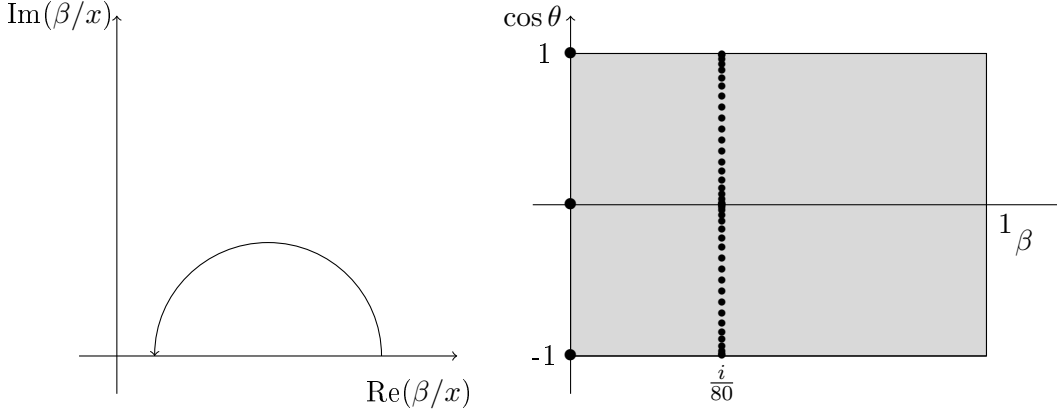


Figure 3.4.: Schematic contour of numeric integration (left). Positions of grid points for representative β value (right). All other points are obtained by shifting to $\beta = i/80$ with $i \in \{1, \dots, 79\}$ and to $\beta = 999/1000$ and $\beta = 9997/10000$.

By performing this numerical integration to a set of points an interpolation grid is created. The position of the points $\{\beta_i, (\cos\theta)_j\}$ in the β and $\cos\theta$ plane is given by the following set:

$$\beta_i = i/80 \text{ with } i \in \{1, \dots, 79\} \quad (3.36)$$

$$(\cos\theta)_j = \pm x_j \text{ with } j \in \{1, \dots, 21\} \quad (3.37)$$

where the x_i are obtained from the Gauss-Kronrod integration rule. They can be obtained for instance with MATHEMATICA [171]. Two points in the high-energy limit $\beta_{80} = 0.999$ and $\beta_{81} = 0.9997$ were added to have better control over the $\cos\theta \rightarrow \pm 1$ limits. The position of the points in physical phase space is visualized in figure 3.4. The results of the numerical integration were checked against the original set on amplitude level.

Threshold expansions. Close to the production threshold, $\beta \rightarrow 0$ some of the integrals show divergent behavior. The numerical integration method does not work well in such cases, due to increasing demand on numerical precision. To obtain reliable results in that limit, a power-logarithmic expansions in β was performed. Using the same technique as in the high-energy case, the differential equations were expanded together with an ansatz for integrals. The unconstrained coefficients are matched to results of the numerical integration at $\beta = 1/10$. With this method a deep expansion up to $\mathcal{O}(\beta^{50})$ and $\mathcal{O}(\ln^{10} \beta)$ is obtained for several fixed values of the angle $\cos\theta$.

3.3. Renormalization

The virtual amplitudes contain infrared and ultraviolet divergences. A finite result is obtained after performing ultraviolet and infrared renormalization. This way, so-called finite-remainder functions are obtained. They are scheme dependent due to freedom in the finite part of the infrared renormalization procedure. First, the UV renormalization is

performed. The amplitude reads

$$\left| \mathcal{M}_{g,q}(\alpha_s^{(n_f)}, m, \mu, \epsilon) \right\rangle = \left(\frac{\mu^2 e^{\gamma_E}}{4\pi} \right)^{-2\epsilon} Z_{g,q} Z_Q \left| \mathcal{M}_{g,q}^0(\alpha_s^0, m^0, \epsilon) \right\rangle. \quad (3.38)$$

For wave functions on-shell renormalization is employed with the renormalization constants Z_g , Z_q and Z_Q , see Appendix B. The coupling constant is renormalized in the $\overline{\text{MS}}$ scheme with $n_f = n_l + n_h$ active flavors (equation 2.12)

$$\alpha_s^0 = \left(\frac{e^{\gamma_E}}{4\pi} \right)^\epsilon \mu^{2\epsilon} Z_{\alpha_s}^{(n_f)} \alpha_s^{(n_f)}(\mu). \quad (3.39)$$

As argued in section 2.1.2, the top-quark mass is decoupled from the running of α_s . The decoupling can be achieved by the replacement

$$\alpha_s^{(n_f)} = \zeta_{\alpha_s} \alpha_s^{(n_l)}, \quad (3.40)$$

where ζ_{α_s} is the decoupling constant. Both renormalizations act multiplicatively on the amplitude and therefore on the coefficients of the color- and spin-decomposed amplitude. The mass renormalization enters with additional insertions of top-quark propagators. Thus they are not purely multiplicative and term arising from the expansion 2.19 have to be projected on the structures. In terms of the coefficients the UV renormalized coefficients $c_{ij}^{(l)}$ is given by

$$c_{ij}^{(l)} = c_{ij}^{0(l)} + c_{ij}^{UV(l)} \quad (3.41)$$

where $c_{ij}^{0(l)}$ is the bare coefficient and $c_{ij}^{UV(l)}$ the collection of UV counter terms.

Finite remainder After UV renormalization, the amplitude still contains infrared singularities. As discussed in more detail in section 2.1.2, the structure of these divergences is completely known [172]. They can be extracted from the UV renormalized amplitude

$$\left| \mathcal{M}_{g,q}^{(0)} \right\rangle = \left| \mathcal{F}_{g,q}^{(0)} \right\rangle, \quad (3.42)$$

$$\left| \mathcal{M}_{g,q}^{(1)} \right\rangle = \mathbf{Z}_{g,q}^{(1)} \left| \mathcal{M}_{g,q}^{(0)} \right\rangle + \left| \mathcal{F}_{g,q}^{(1)} \right\rangle, \quad (3.43)$$

$$\left| \mathcal{M}_{g,q}^{(2)} \right\rangle = \mathbf{Z}_{g,q}^{(2)} \left| \mathcal{M}_{g,q}^{(0)} \right\rangle + \mathbf{Z}_{g,q}^{(1)} \left| \mathcal{F}_{g,q}^{(1)} \right\rangle + \left| \mathcal{F}_{g,q}^{(2)} \right\rangle \quad (3.44)$$

$$= \left(\mathbf{Z}_{g,q}^{(2)} - \mathbf{Z}_{g,q}^{(1)} \mathbf{Z}_{g,q}^{(1)} \right) \left| \mathcal{M}_{g,q}^{(0)} \right\rangle + \mathbf{Z}_{g,q}^{(1)} \left| \mathcal{M}_{g,q}^{(1)} \right\rangle + \left| \mathcal{F}_{g,q}^{(2)} \right\rangle, \quad (3.45)$$

using the infrared renormalization constant $\mathbf{Z} = \mathbf{1} + \mathbf{Z}^{(1)} + \mathbf{Z}^{(2)} + \mathcal{O}(\alpha_s^3)$. $\mathbf{Z}_{g,q}^{(l)}$ can be obtained from the anomalous dimension $\mathbf{\Gamma}_{g,q}$ which read for $q\bar{q}/gg \rightarrow t\bar{t}$:

$$\begin{aligned} \mathbf{\Gamma}_{g,q} = & \mathbf{T}_1 \cdot \mathbf{T}_2 \gamma_{\text{cusp}} \ln \frac{\mu^2}{-s} + 2\gamma^{g,q} - \mathbf{T}_3 \cdot \mathbf{T}_4 \gamma_{\text{cusp}}(\beta) + 2\gamma^Q \\ & + (\mathbf{T}_3 \cdot \mathbf{T}_1 + \mathbf{T}_4 \cdot \mathbf{T}_2) \gamma_{\text{cusp}} \ln \frac{2m_t \mu}{t} + (\mathbf{T}_3 \cdot \mathbf{T}_2 + \mathbf{T}_4 \cdot \mathbf{T}_1) \gamma_{\text{cusp}} \ln \frac{2m_t \mu}{u} \\ & + i2f^{abc} T_3^a T_4^b T_1^c f_2 \left(b, \ln \frac{u}{t} \right) + i2f^{abc} T_3^a T_4^b T_2^c f_2 \left(b, \ln \frac{t}{u} \right) \end{aligned} \quad (3.46)$$

3. Polarized Double Virtual Top-Quark Pair Production

Of special interest are the terms with triple-correlators. In spin and color summed QCD matrix elements this term does not contribute [173]. The reason is that up to two-loops the triple-correlator is only contracted with tree-level matrix elements, which are real as long as no complex-coupling occur. At three loops however they would be contracted with one loop matrix elements and their imaginary part would give rise to contributing terms. Since spin and color information is kept here, they do contribute in this calculation. Due to the absence of a third massive quark, only the triple-correlator term (the last line in 3.46

$$\sum_{(I,J)} \sum_k i f^{abc} \mathbf{T}_I^a \mathbf{T}_J^b \mathbf{T}_k^c f_2 \left(\beta_{IJ}, \ln \frac{-\sigma_{Jk} v_J \cdot p_k}{-\sigma_{Ik} v_I \cdot p_k} \right),$$

contributes. This is the first calculation in which this contribution is needed to obtain all poles correctly, and therefore the first non-trivial cross-check of the corresponding part in the anomalous dimension matrix, which were calculated in [118].

Since \mathbf{Z} acts on color space, the $\mathbf{z}_{g,q}^{(k)} \left| \mathcal{M}_{g,q}^{(l)} \right\rangle$ terms need to be projected to the color and spin structures again. Thus the l -loop IR counter term $c_{ij}^{IR,(l)}$ for the coefficient $c_{ij}^{(l)}$ is given by

$$c_{ij}^{IR,(1)} = \langle P_{ij} | \mathbf{z}_{g,q}^{(1)} \left| \mathcal{M}_{g,q}^{(0)} \right\rangle \quad (3.47)$$

$$c_{ij}^{IR,(2)} = \langle P_{ij} | \left(\mathbf{z}_{g,q}^{(2)} - \mathbf{z}_{g,q}^{(1)} \mathbf{z}_{g,q}^{(1)} \right) \left| \mathcal{M}_{g,q}^{(0)} \right\rangle + \langle P_{ij} | \mathbf{z}_{g,q}^{(1)} \left| \mathcal{M}_{g,q}^{(1)} \right\rangle \quad (3.48)$$

The finite remainder coefficient $c_{ij}^{F,(l)}$ is then given by

$$c_{ij}^{F,(l)} = c_{ij}^{(l)} + c_{ij}^{IR,(l)} \quad (3.49)$$

3.4. Finite-remainder functions

Application of the described projection and renormalization procedure yields finite remainder for all the coefficients at tree, one-loop and two-loop level. There are in total $3 \times 8 = 24$ gluon and $2 \times 4 = 8$ quark coefficients. Starting at one-loop the coefficients obtain a imaginary part and are polynomials in n_l (the number of light quarks). At one loop a n_l^1 term appears where at two-loops potentially n_l^2 terms contribute. Thus at two-loops there would be $32 \times 2 \times 3 = 224$ different real contributions. From these quantities various representations of the spin-information can be obtained. A representation within the spin-density approach is given in section 3.5. For the application to top-quark decays, which is the final goal of this work, the representation in form of correlators of the top- and anti-top-quark helicity is used to cross check implementation of the polarized amplitudes, see section 3.6.2. As 224 different plots are far to much to visualise, the other representations are condensed since color and spin sums over the initial state are performed. However, some general properties of the coefficients $c_{ij}^{F,(l)}$ can be discussed.

At tree-level the following coefficients are found in case of $gg \rightarrow t\bar{t}$

$$c_{11}^{(0)} = \frac{-1}{x}, \quad c_{21}^{(0)} = \frac{-1}{1-x}, \quad (3.50)$$

3.4. Finite-remainder functions

$$c_{15}^{(0)} = \frac{2x-1}{x}, \quad c_{25}^{(0)} = \frac{2x-1}{1-x}, \quad (3.51)$$

$$c_{17}^{(0)} = c_{18}^{(0)} = -c_{11}^{(0)}, \quad c_{27}^{(0)} = c_{28}^{(0)} = -c_{21}^{(0)}. \quad (3.52)$$

where all other coefficients vanish. As expected, these coefficients are symmetric under the replacement $\cos \theta \rightarrow -\cos \theta$ or $x \rightarrow 1-x$. For the $q\bar{q} \rightarrow t\bar{t}$ process only the two coefficients

$$c_{13}^{(0)} = \frac{1}{2}, \quad c_{23}^{(0)} = \frac{-1}{6}. \quad (3.53)$$

contribute at tree-level. Beyond tree-level all coefficients are non-vanishing except the coefficients c_{i6} in case of gluons and c_{i4} in case of quarks. A further pattern emerging here, is that only the S_5^g and S_3^g obtain contributions from the highest available power of n_l . This means that all diagrams with one at 1-loop and all diagrams with two separated closed light fermion loops are projected to the same spin structure.

At two-loop the master integrals are available in different forms for different phase space regions.

High-energy region A high energy expansion of the finite remainder coefficients is obtained after inserting the corresponding expansion of the master integrals and renormalization. The expansion was performed up to $\mathcal{O}(m_s^4)$ for each coefficient. The quality of the expansions can be investigated by comparing the results with those obtained from the numerical integration. In figure 3.5 the relative differences of the real part

$$c_{ij}^{\text{diff}} = \left| \frac{c_{ij}^{\text{HE}}}{c_{ij}^{\text{num}}} - 1 \right| \quad (3.54)$$

between both results for fixed, quite central value of $\cos \theta$ are shown. The coefficients are evaluated for $n_l = 5$. A reasonable description of the amplitude by the expansion is only obtained in the central region. The same quantity is shown in figure 3.5 for fixed $\beta = 9997/10000$. The difference grows in the limit $\cos \theta \rightarrow \pm 1$. In the forward/backward scattering region the applied expansion in m_s is not valid anymore, as expected. A necessary simultaneous expansion in m_s and x (or $1-x$, respectively), is left for future investigation.

Bulk region. In the region where the numerical integration is feasible, the finite remainder coefficients are obtained at the same points as the master integrals in form of an interpolation grid. A visualisation of the large set of coefficients is omitted here. In the form of the spin density matrix in the next section this region is visualised in form of 3D plots.

The Threshold region Similar to the high-energy expansion of the coefficient, an expansion in β was performed using the threshold expression for the master integrals. The master integral expansions were done for fixed angles $\cos \theta_n$, thus an expansion

$$c_{ij}(\beta, \cos \theta_n) = \sum_{k=-2}^2 \sum_{l=0}^2 \tilde{c}_{ij,kl,n} \beta^k \ln^l \beta$$

3. Polarized Double Virtual Top-Quark Pair Production

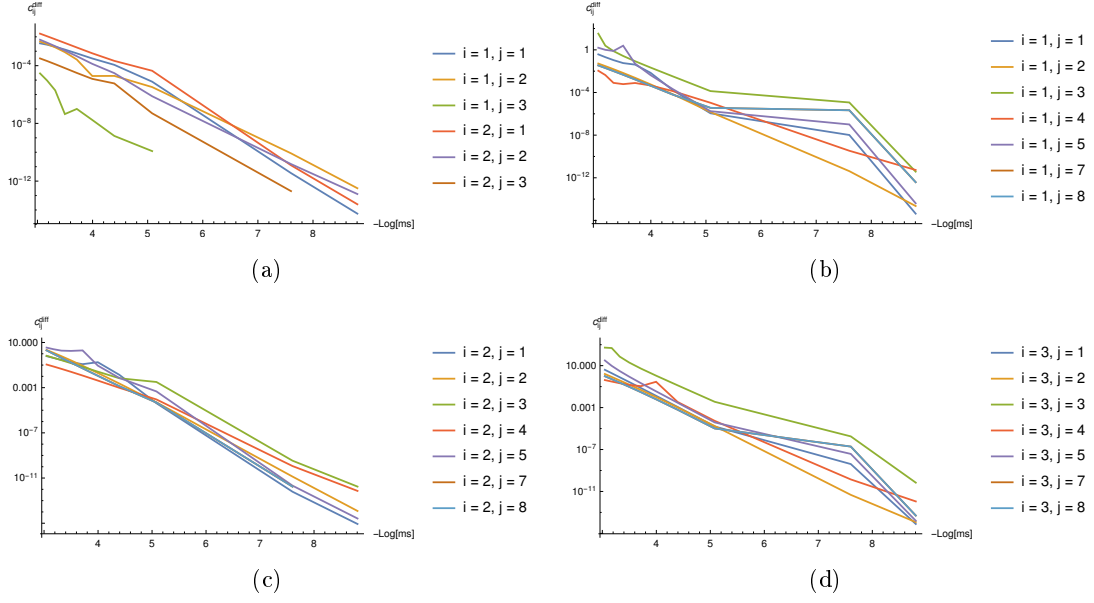


Figure 3.5.: Difference between the high energy expansion and the results of the numerical integration of the finite remainder coefficients for $-(\cos\theta)_{14} \approx -0.7166976$. (a) qq (b) gg color structure C_1 (c) gg color structure C_2 (d) gg color structure C_3 . Stopping lines indicate that all digits of c_{ij}^{num} match the result from the expansion.

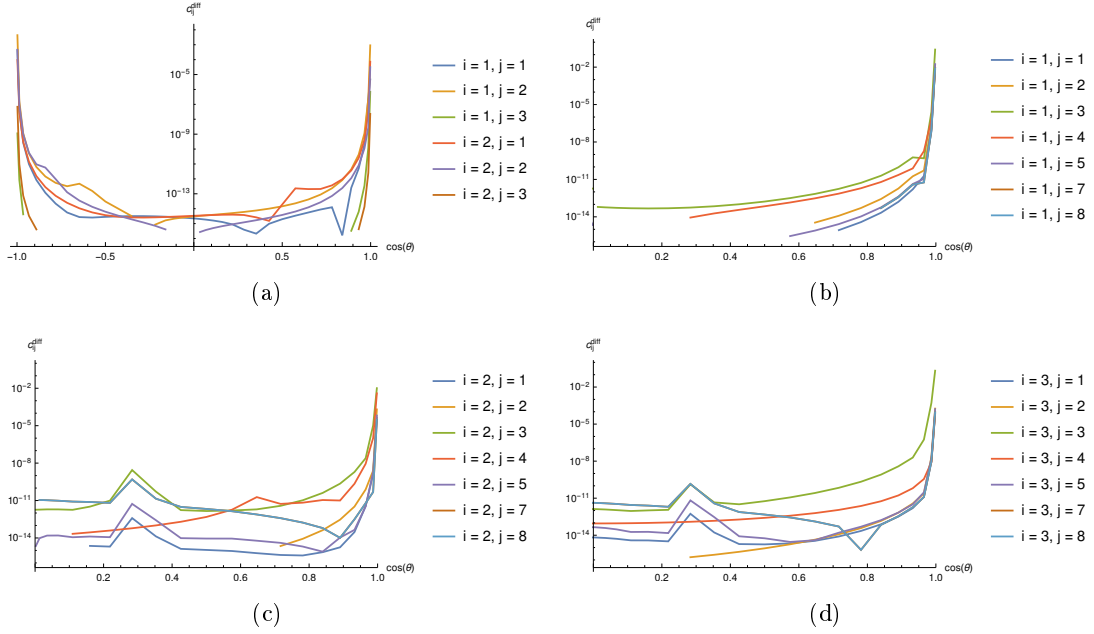


Figure 3.6.: Difference between the high energy expansion and the results of the numerical integration of the finite remainder coefficients for $\beta = 9997/10000$. (a) qq (b) gg color structure C_1 (c) gg color structure C_2 (d) gg color structure C_3 . Stopping lines indicate that all digits of c_{ij}^{num} match the result from the expansion.

of the coefficients, was obtained. To restore the dependence on $\cos\theta$ a fit to a polynomial

$$\tilde{c}_{ij,kl} = \sum_{n=0}^{2+k} a_n \cos^n \theta \quad (3.55)$$

was performed for the imaginary and real part and each n_l coefficient separately.

3.5. Spin-Density Matrix

A different way to represent spin dependent matrix elements is given by the spin density matrix. In the rest frames of the top-quarks the spin can be described by two 3-vectors

$$\hat{\mathbf{s}}_t \quad \text{and} \quad \hat{\mathbf{s}}_{\bar{t}} \quad (3.56)$$

which are normalized to 1. The corresponding four-vectors are

$$s_t^r = \begin{pmatrix} 0 \\ \hat{\mathbf{s}}_t \end{pmatrix} \quad \text{and} \quad s_{\bar{t}}^r = \begin{pmatrix} 0 \\ \hat{\mathbf{s}}_{\bar{t}} \end{pmatrix} \quad (3.57)$$

In the center of mass system of a top-quark pair these correspond to two four-vectors s_t and $s_{\bar{t}}$, with

$$s_t^2 = s_{\bar{t}}^2 = -1 \quad \text{and} \quad p_3 \cdot s_t = p_4 \cdot s_{\bar{t}} = 0. \quad (3.58)$$

A corresponding projector can be applied on the top-quark spinors to obtain the amplitude for a top-quark with spin in s_t direction. When calculating matrix elements, this results in the insertion of the following projector in the spin sum

$$u(p_3, s_t) \bar{u}(p_3, s_t) = (\not{p}_3 + m) \frac{1}{2} (1 + \gamma_5 \not{s}_t), \quad (3.59)$$

$$v(p_4, s_{\bar{t}}) \bar{v}(p_4, s_{\bar{t}}) = (\not{p}_4 - m) \frac{1}{2} (1 + \gamma_5 \not{s}_{\bar{t}}). \quad (3.60)$$

A matrix element with this projector insertion is denoted by

$$\langle \mathcal{M} | \mathcal{M} \rangle (s_t, s_{\bar{t}}) \quad (3.61)$$

and is related to the spin density matrix as defined in [174]

$$\langle \mathcal{M} | \mathcal{M} \rangle (s_t, s_{\bar{t}}) = \frac{1}{4} \text{Tr} [R^{q,g} (\mathbf{1} + \hat{\mathbf{s}}_t \sigma) \otimes (\mathbf{1} + \hat{\mathbf{s}}_{\bar{t}} \sigma)] \Big|_{2\text{-loop}}. \quad (3.62)$$

The two-loop finite remainder contribution to this matrix element can be decomposed in the following way

$$\begin{aligned} \mathcal{R}_{q,g}^F(s_t, s_{\bar{t}}) &= 2 \text{Re} \langle \mathcal{M}_{q,g}^0 | \mathcal{F}_{q,g}^2 \rangle (s_t, s_{\bar{t}}) \\ &= A_{q,g} + (C)_{q,g} \left((s_t \cdot s_{\bar{t}}) \right) + \\ &\quad (B_t)_{q,g} \left(\epsilon^{\mu\nu\alpha\beta} p_{1\mu} p_{2\nu} p_{3\alpha} s_{t\beta} \right) + (B_{\bar{t}})_{q,g} \left(\epsilon^{\mu\nu\alpha\beta} p_{1\mu} p_{2\nu} p_{3\alpha} s_{\bar{t}\beta} \right) + \end{aligned} \quad (3.63)$$

3. Polarized Double Virtual Top-Quark Pair Production

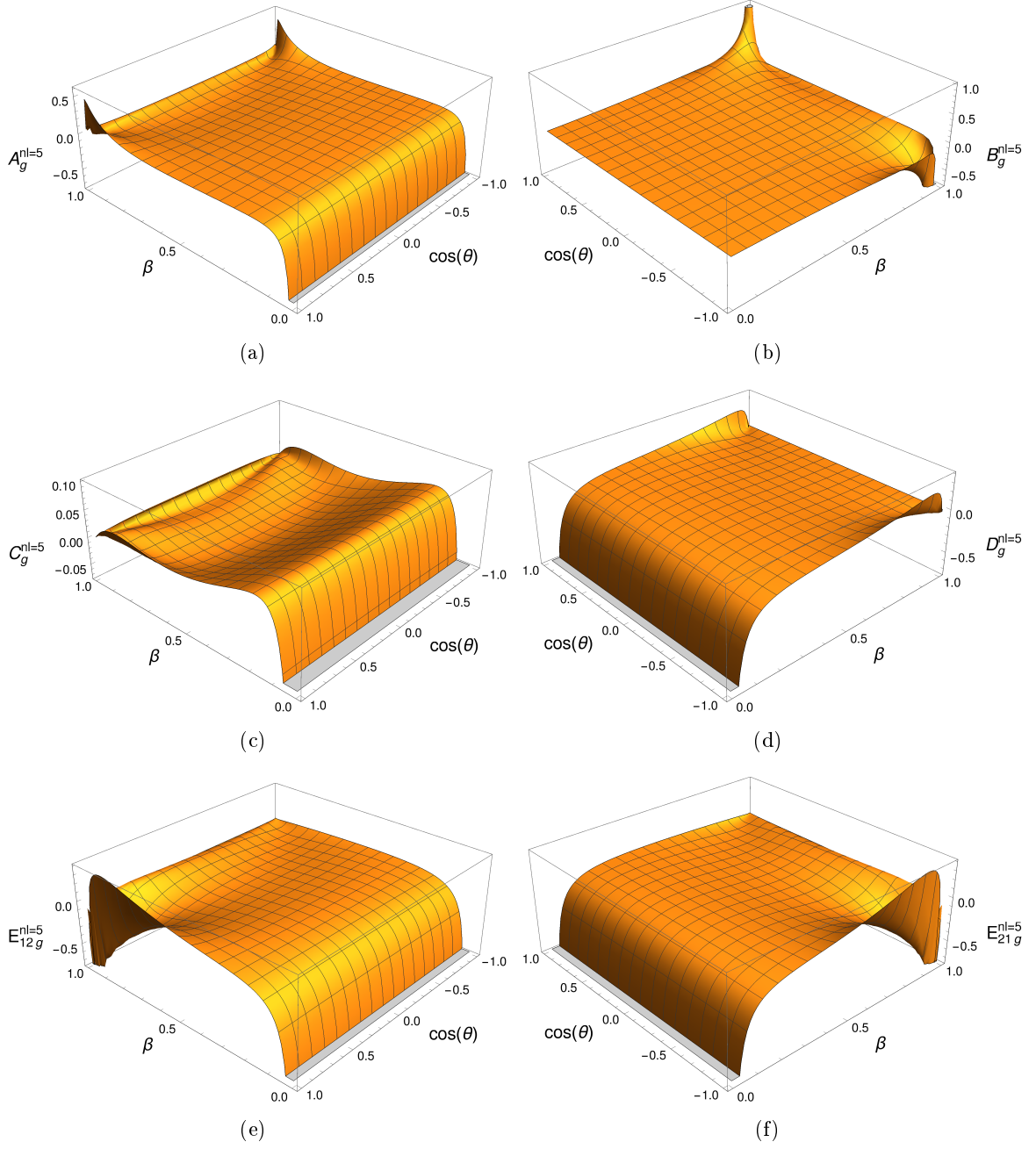


Figure 3.7.: Finite remainder coefficient functions of the spin-density matrix in case of initial state gluons for $n_l = 5$.

$$\begin{aligned}
 & (D_1)_{q,g} \left((p_1 \cdot s_t)(p_1 \cdot s_{\bar{t}}) \right) + (D_2)_{q,g} \left((p_2 \cdot s_t)(p_2 \cdot s_{\bar{t}}) \right) + \\
 & (E_{12})_{q,g} \left((p_1 \cdot s_t)(p_2 \cdot s_{\bar{t}}) \right) + (E_{21})_{q,g} \left((p_2 \cdot s_t)(p_1 \cdot s_{\bar{t}}) \right). \quad (3.64)
 \end{aligned}$$

3.5. Spin-Density Matrix

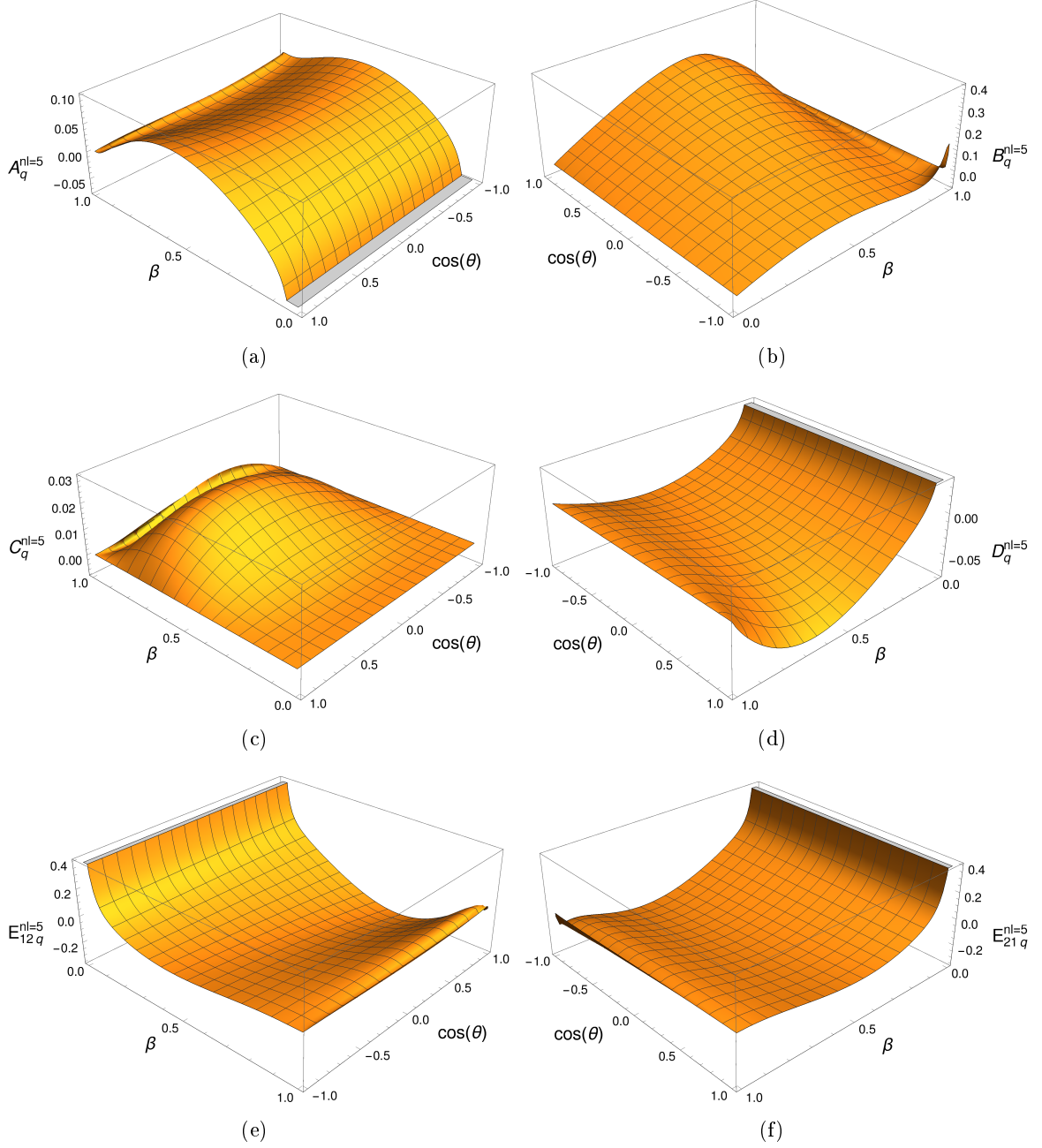


Figure 3.8.: Finite remainder coefficient functions of the spin-density matrix in case of initial state quarks for $n_l = 5$.

Since the finite remainder coefficients are completely free of poles in ϵ , the treatment of γ_5 does not cause any problems, and everything can be treated in 4 dimensions.

Since in QCD parity (P), charge conjugation (C) and the combination (CP) are good symmetries, the transformation properties of the structures imply constraints on the coefficients[174]:

$$B_t = B_{\bar{t}} = B \quad \text{and} \quad D_1 = D_2 = D . \quad (3.65)$$

3. Polarized Double Virtual Top-Quark Pair Production

Thus, the decomposition can be simplified to

$$\begin{aligned}
\mathcal{R}_{q,g}^F &= A_{q,g} + (B)_{q,g} \left(\epsilon^{\mu\nu\alpha\beta} p_{1\mu} p_{2\nu} p_{3\alpha} s_{t\beta} + \epsilon^{\mu\nu\alpha\beta} p_{1\mu} p_{2\nu} p_{3\alpha} s_{\bar{t}\beta} \right) \\
&+ (C)_{q,g} \left((s_t \cdot s_{\bar{t}}) \right) + (D)_{q,g} \left((p_1 \cdot s_t)(p_1 \cdot s_{\bar{t}}) + (p_2 \cdot s_t)(p_2 \cdot s_{\bar{t}}) \right) \\
&+ (E_{12})_{q,g} \left((p_1 \cdot s_t)(p_2 \cdot s_{\bar{t}}) \right) + (E_{21})_{q,g} \left((p_2 \cdot s_t)(p_1 \cdot s_{\bar{t}}) \right). \quad (3.66)
\end{aligned}$$

The additional Bose-symmetry in case of gluon initiated top-pair production induces another symmetry in the coefficient. The Bose-symmetry amounts to interchanging the two gluons and replacing $\cos\theta \rightarrow -\cos\theta$ in the coefficients. This implies that the functions A_g, C_g, D_g are symmetric in $\cos\theta$ and that B_g has to be an antisymmetric function in $\cos\theta$. Additionally this implies the relation $E_{12g}(\cos\theta) = E_{21g}(-\cos\theta)$. The coefficient $A_{q,g}$ is the spin summed matrix-element and thus can be obtained from the original calculation. However, this coefficient was re-calculated using the decomposed amplitude. The original calculation then constituted as a check for the new result. The coefficients $B_{q,g}$ describe the transverse polarization with respect to the scattering plane spanned by p_1, p_2, p_3, p_4 . Only absorptive parts of the amplitudes can contribute this coefficient. Thus, at tree-level this coefficient vanishes. All others describe spin-correlation between the top- and anti-top-quark.

To present the results the two normalization factors

$$N_g = \frac{\beta(1-\beta^2)}{4096\pi} \quad \text{and} \quad N_q = \frac{\beta(1-\beta^2)}{576\pi}, \quad (3.67)$$

are introduced to damp the singular behaviour close to threshold and in the high energy limit. The normalized coefficient functions of \mathcal{R}_g^F and \mathcal{R}_q^F are visualised in Figs. 3.7 and 3.8 for $n_l = 5$.

3.5.1. Threshold expansions

From the threshold expansion of the structure coefficients, a threshold expansion of the spin-density matrix can be derived. Due to the smaller number of different coefficients, the spin-density matrix is a good quantity to study the threshold expansion. To do so, threshold expansions of the coefficients up to $\mathcal{O}(\beta^6)$ are derived for a fixed point for $\cos\theta$. The point was arbitrarily chosen to be $\cos\theta = x_9$. In the region where the numerical integration of the master integrals was successful, e.g. $\beta > 0.1$, a comparison with the threshold expansion can be made. The difference¹ between the expansion and the integration result is given by

$$\left(X_{\text{diff}}^{n_l=5} \right) (\beta, x_9) = \left(X_{\text{thres}}^{n_l=5} \right) (\beta, x_9) - \left(X_{\text{grid}}^{n_l=5} \right) (\beta, x_9), \quad (3.68)$$

with $X \in \{A_g, B_g, C_g, D_g, E_{12g}\}$ for different expansion depths of $\left(X_{\text{thres}}^{n_l=5} \right) (\beta, x_9)$. This comparison is shown in figure 3.9 and 3.10. The series converges quite nicely and a decent prescription of the coefficients with expansion is possible up to $\beta \sim 0.3$, when expanding

¹The relative difference is not used, because the coefficient functions have a zero in the plotted region.

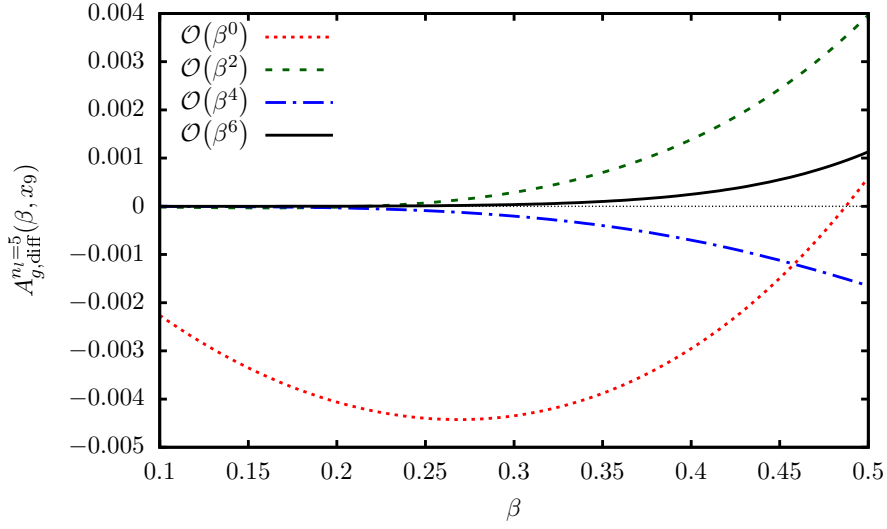


Figure 3.9.: The difference between the threshold expansion for coefficient A_g up to β^n with $n = 0, 2, 4, 6$ and results from numerical integration for a fixed angle θ .

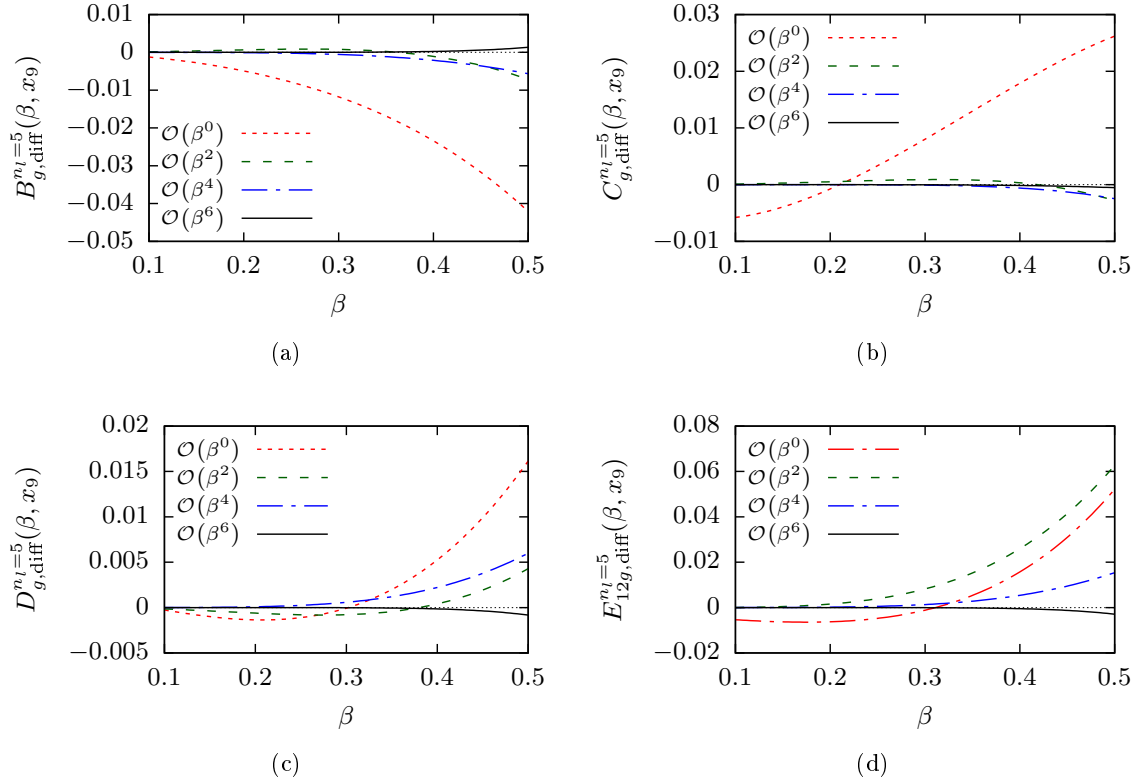


Figure 3.10.: The difference between the threshold expansion for coefficient B_g, C_g, D_g, E_{12g} up to β^n with $n = 0, 2, 4, 6$ and results from numerical integration for a fixed angle θ .

3. Polarized Double Virtual Top-Quark Pair Production

up to $\mathcal{O}(\beta^6)$. In practice however, the threshold expansion of the coefficients is used only for $\beta < 1/80$.

3.6. Spin structures and correlation matrices

In order to use the results generated above for the actual calculation of top-quark production and decays (see chapter 5) it is necessary to be able to evaluate the finite remainder $|\mathcal{F}_{q,g}^l\rangle$ explicitly, for a specified spin state. On the one hand, the coefficients are trivial in this context since they are just functions of kinematic invariants. On the other hand, the spin-structures can be evaluated using spin-helicity methods. Since finally only color-summed quantities are of interest in this calculation, the color sum can be done analytically. The derivation of the amplitude decomposition was wholly general in the sense that any spin-helicity method with any convention can be used to evaluate the spin structures. In order to obtain correlation matrices that can easily be combined with decay amplitude, the WvdW formalism discussed in section 2.1.5 was used. The reason for this choice is that massive external spinors are helicity eigenstates. The advantage arises from simple properties of appearing objects when investigating symmetries like parity.

3.6.1. Spin-structures

The wave-functions for the top-quarks can be directly read off equation 2.77. For the two helicity states of the top-quark there are

$$\bar{u}_3(+)=\left(-\kappa_2^A(p_3)\ \kappa_{1,\dot{A}}(p_3)\right),\quad \bar{u}_3(-)=\left(\kappa_1^A(p_3)\ \kappa_{2,\dot{A}}(p_3)\right). \quad (3.69)$$

And similar for the anti-top the states read

$$v_4(-)=\left(\begin{array}{c} \kappa_{1,A}(p_4) \\ \kappa_2^{\dot{A}} \end{array}\right),\quad v_4(+)=\left(\begin{array}{c} -\kappa_{2,A}(p_4) \\ \kappa_1^{\dot{A}} \end{array}\right). \quad (3.70)$$

For the gluon amplitude the two polarization vectors $\epsilon_{\pm}^{\mu}(p_1)$ and $\epsilon_{\pm}^{\mu}(p_2)$ can be expressed through WvdW spinors in the following way

$$\epsilon_{+,\dot{A}B}(p_1)=\frac{\sqrt{2}p_{2\dot{A}}p_{1B}}{\langle p_2p_1\rangle^*},\quad \epsilon_{-,\dot{A}B}(p_1)=\frac{\sqrt{2}p_{1\dot{A}}p_{2B}}{\langle p_2p_1\rangle}, \quad (3.71)$$

$$\epsilon_{+,\dot{A}B}(p_2)=\frac{\sqrt{2}p_{1\dot{A}}p_{2B}}{\langle p_1p_2\rangle^*},\quad \epsilon_{-,\dot{A}B}(p_2)=\frac{\sqrt{2}p_{2\dot{A}}p_{1B}}{\langle p_1p_2\rangle}. \quad (3.72)$$

In case of the quark amplitude the spinors of the massless quarks are given by

$$u_1(+)=\left(\begin{array}{c} \kappa_A(p_1) \\ 0 \end{array}\right),\quad u_1(-)=\left(\begin{array}{c} 0 \\ \kappa^{\dot{A}}(p_1) \end{array}\right) \quad (3.73)$$

$$\bar{v}_2(-)=\left(0\ \kappa_{\dot{A}}(p_2)\right),\quad \bar{v}_2(+)=\left(\kappa^A(p_2)\ 0\right) \quad (3.74)$$

To write the spin structures in terms of spinor products the following identity needs to

be employed

$$\not{p} = \begin{pmatrix} 0 & p_{A\dot{B}} \\ p^{\dot{A}B} & 0 \end{pmatrix}. \quad (3.75)$$

In case of the quark structures, the contraction between the light and heavy quark line needs to be performed. This is also straight forward, due to the following relation

$$\gamma_{(D\dot{C})}^\mu \bar{v}_2(+)\gamma_\mu u_1(-) = \gamma^\mu \kappa^A(p_2)\sigma_{A\dot{B},\mu}\kappa^{\dot{B}}(p_1) = \begin{pmatrix} 0 & 2\kappa_D(p_2)\kappa_{\dot{C}}(p_1) \\ 2\kappa^{\dot{D}}(p_1)\kappa^C(p_2) & 0 \end{pmatrix} \quad (3.76)$$

and a similar one for flipped helicities. Straightforward application of these rules provides a set of expressions for all helicity combinations. A final remark on complex phases. Due to the definition of the of the spinor $\kappa(p)$, the angle ϕ describing the rotation around the z -axis enters the amplitude. However, the dependence is only through a phase factor $e^{i\phi}$ which cancels when calculating quantities like

$$\langle \mathcal{M}|h_1, h_2, h_3, h_4\rangle \langle h_1, h_2, h_3, h_4|\mathcal{M}\rangle, \quad (3.77)$$

but when calculating the off-diagonal contributions for a correlation matrix such like

$$\langle \mathcal{M}|h_1, h_2, h_3, -h_4\rangle \langle h_1, h_2, h_3, h_4|\mathcal{M}\rangle \quad (3.78)$$

this phase stays and has to be taken into account. Conversely, when contracting the correlator with decay-correlators, i.e. when the off-diagonal parts matter, this phase factor cancels against a similar phase factor in the decay correlator. Since the whole system is invariant under rotation of the z -axis, this is of course expected.

3.6.2. Helicity correlation matrices

When calculating matrix elements in NWA naturally correlation matrices are encountered, see section 2.1.4. For the top-quark pair the following matrix is of interest

$$\mathcal{M}^{\text{cor.}}(h_3, h_4, h'_3, h'_4) = \sum_{h_1, h_2} \langle \mathcal{M}|h_1, h_2, h_3, h_4\rangle \langle h_1, h_2, h'_3, h'_4|\mathcal{M}\rangle \quad (3.79)$$

with $h_i \in \{+1, -1\}$. Due to symmetry under the parity transformation this matrix has the property

$$\mathcal{M}^{\text{cor.}}(h_3, h_4, h'_3, h'_4) = h_3 h_4 h'_3 h'_4 \mathcal{M}^{\text{cor.}}(-h_3, -h_4, -h'_3, -h'_4) \quad (3.80)$$

Thus only half of the signatures are independent. For both channels eight coefficients are independent. As an example the coefficients for the gg -channel are visualized with $n_l = 5$ in figure 3.11. For the plots a normalization of $\beta(1 - \beta^2)/(576\pi)$ has been applied. This method of including the decays was used to cross check the implementation of the polarized amplitudes. In practice the method of decay spinors (see section 2.2.2) is used since it is more flexible and allows also for polarized gluons needed for collinear subtraction in case of one-loop matrix element appearing in NNLO calculations.

3. Polarized Double Virtual Top-Quark Pair Production

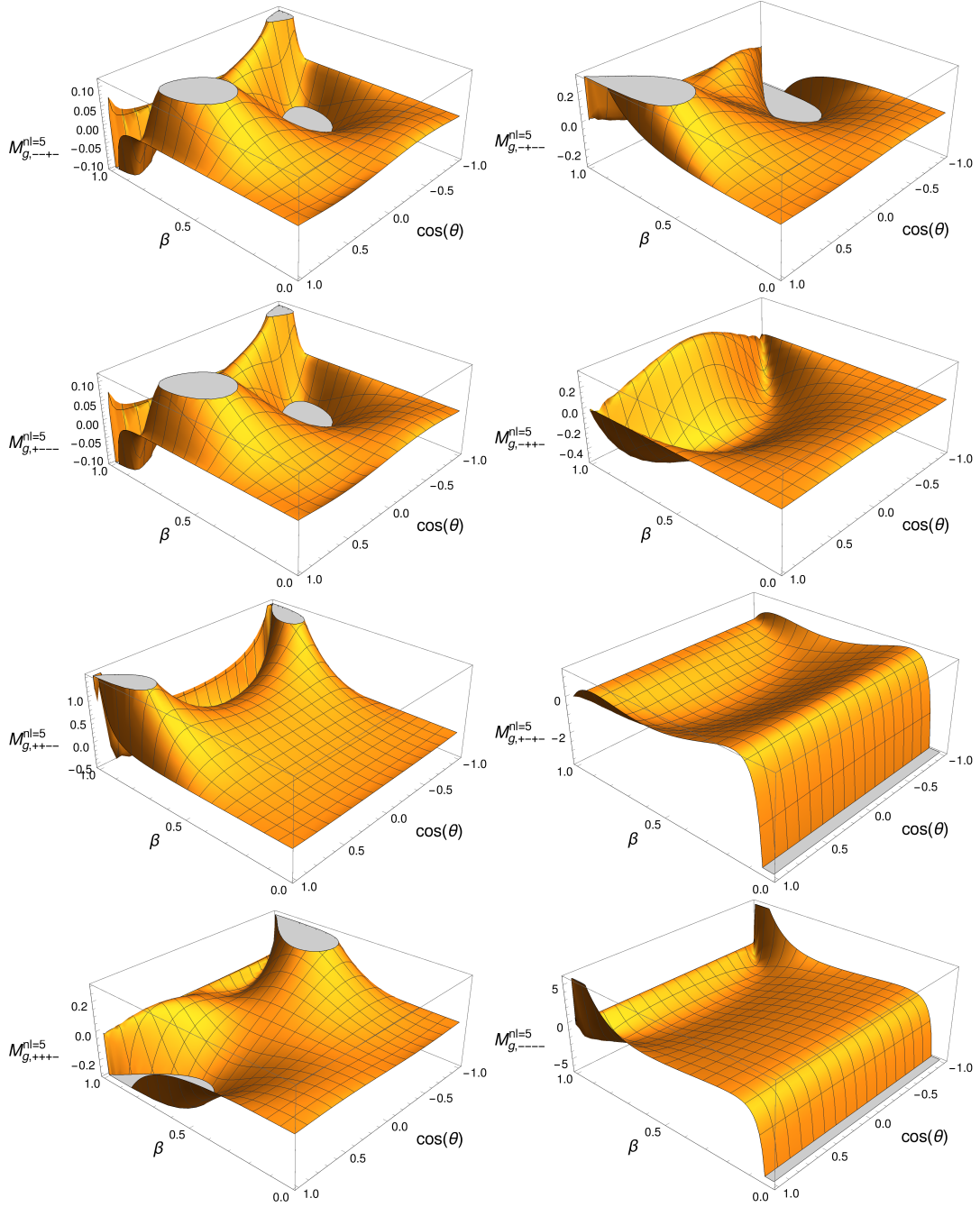


Figure 3.11.: Real part of the coefficients of the correlation matrix $\mathcal{M}^{\text{cor.}}$ in the gg -channel for $n_l = 5$.

4. Real radiation contribution

Calculations beyond the lowest order in perturbation theory consist, for a given process, of many contributions which only together provide a finite and meaningful calculation. The task of a subtraction scheme is to facilitate this combination. The difficulty arises through the divergences present in the various contributions. Considering higher order calculations in QCD, two types of contributions for the case of one additional power in α_s can be identified, on one hand the (un-)resolved emission of one additional parton and on the other hand corrections from one additional quantum-loop. Also, as discussed in section 2.1.1 there are potential contributions from collinear factorization if there are composite objects in the initial state. Each contribution is divergent on their own in four space-time dimensions and by working with convention dimensional regularization, thus in $d = 4 - 2\epsilon$ dimensions, the divergences manifest as poles of a Laurent-series in ϵ for different contributions separately. Due to the KLN theorem these divergences cancel for all infrared safe observables if one combines all necessary parts. The difficult part here is the extraction of the Laurent-series for each contribution. In case of the virtual contribution, many different methods directly yield a Laurent-series expansion. Conceptually, in case of the real radiation, it would necessary to evaluate the d dimensional phase space integral over additional emissions in an analytic form within all kinematic constraints to obtain a similar series. This is sometimes possible for inclusive enough quantities like total cross-sections, but becomes increasingly more challenging for differential observables. The feasibility of such a calculation depends strongly on the process and/or observable under consideration. A further issue here is that it is not directly possible to switch to a numerical evaluation approach due to the divergent nature of these integrals. However, in the past two decades methods were developed to handle the problem of numerical evaluation of real-radiation contribution. There are two main classes of approaches: slicing and subtraction. Both approaches use factorization of QCD amplitudes in infrared limits (see section 2.1.3) to regularize the divergences in the real radiation contribution and evaluate the divergent part separately in a less complicated kinematic configuration either numerically or analytically.

In case of slicing methods, a cutoff in the real radiation phase space is introduced, which cuts out the divergent region. Close to the divergent region the integrand, phase-space weight, and matrix element can be simplified by applying factorization formulae for the corresponding kinematic limit. These resulting expressions are then simple enough to evaluate them analytically or numerically. This of course introduces logarithms of the cutoff parameter in the real as well as in the integrated part, which have to cancel between both objects.

Subtraction methods take a different path. In these methods, one adds and subtracts approximations of the matrix elements in divergent infra-red regions, using again some form of matrix-element factorization. These approximations are done in such a way, that an integrand, consisting of the matrix-element and the approximation, is finite in the complete phase space, while the subtraction term should be simple enough that the term which is added back can be evaluated either analytically or numerically in the form of a Laurent expansion in ϵ .

4. Real radiation contribution

The automation of these procedures was a crucial building block of the broad success of next-to-leading order calculations. Together with automated one-loop amplitudes the paved the way for the "NLO-revolution". Automated frameworks allow for convenient and flexible NLO QCD calculations. Also combinations with NLO EW corrections are accessible. Looking at the NNLO QCD, the situation is different. On the real radiation side a vast landscape of techniques are in development and step to full automatization and generality is some cases already possible as discussed in the next section. But the practical applicability of a certain method for a given problem is still not guaranteed. On the loop side there are two important aspects. The main issue towards automated NNLO QCD calculations are the two-loop amplitudes. Even though progress is made with different techniques, the automation seems not reachable in the near future. Another issue is given by the requirement of numerically stable one-loop amplitudes which allow for phase space integration close to infrared regions.

4.1. Subtraction Schemes at NNLO

In this section an overview over the different ideas and methods that are used for the task of handling real-radiation contributions is given. The sector-improved residue subtraction scheme is discussed in great detail afterwards.

4.1.1. Slicing methods

The q_T subtraction/slicing method The idea of the q_T subtraction was originally formulated for a specific class of processes at hadron colliders [175]. The processes that are considered are productions of colorless final states F at lowest order in perturbation theory with an invariant mass Q

$$h_1 h_2 \rightarrow F(Q) + X \quad (4.1)$$

where $Q^2 = (\sum q_i)^2$. The q_i are the momenta of the particles in F . The scheme is completely general for final states that meet this requirement. If there is no further radiation the total transverse momentum

$$q_T = \sum q_{T,i} \quad (4.2)$$

has to vanish due to momentum conservation. To the NNLO cross section $d\sigma_{(N)NLO}^F$ double real, real virtual and double virtual corrections contribute. If $q_T \neq 0$ is required the double virtual vanishes due to its born kinematics, F_n parts from real radiation contributions vanish too. Indeed, as long $q_T \neq 0$ the NLO cross-section to a F +jet final state is obtained

$$d\sigma_{(N)NLO}^F \Big|_{q_T \neq 0} = d\sigma_{(N)LO}^{F+jet} \quad (4.3)$$

The NNLO contributions and their divergences are obtained in the limit $q_T \rightarrow 0$. The idea is now to perform a subtraction of these divergences in the limit $q_T \rightarrow 0$ with the help of factorization formula obtained from resummation techniques. The subtraction term may

be written as

$$d\sigma^{CT} = d\sigma_{LO}^F \otimes \Sigma^F(q_T/Q) d^2q_T. \quad (4.4)$$

thus in terms of the LO cross section combined with an approximation of the higher multiplicity matrix elements in $q_T \rightarrow 0$ limit. With this the full NNLO cross section can be written as

$$d\sigma_{(N)\text{NLO}}^F = \mathcal{H}_{(N)\text{NLO}}^F \otimes d\sigma_{LO}^F + \left[d\sigma_{(N)\text{NLO}}^{F+\text{jet}} - d\sigma_{(N)\text{NLO}}^{CT} \right] \quad (4.5)$$

where the *hard* function \mathcal{H}^F represents the contribution that needed to be added back at $q_T = 0$ to obtain the full NNLO cross-section. It contains the information of the one and two-loop matrix-elements with tree-level kinematics. The exact form is fixed through the specific form of the counter term. The first application of this scheme was Higgs-boson production at LHC [175] but meanwhile it was applied to various processes with colorless final-states at the LHC. In a series of calculations the production of vector bosons (WH [176], V [177], W^+W^- [178], ZZ [179], $Z\gamma$ [180]) was extensively studied. The results were combined in the program MATRIX [181] which allows for NNLO calculations for all $2 \rightarrow 1, 2$ vector and vector-pair production processes. Also an extension for massive colored states was investigated in [182]. The implementation of this scheme is done in practice as a slicing method, where the real-radiation part is evaluated for a finite but small cut-off q_T^{cut} and the phase space region below approximated by the resummation formula.

N -jettiness subtraction/slicing. A quite similar method is the N -jettiness subtraction first presented in [183]. The crucial idea of the q_T subtraction was the separation of NNLO contributions from the NLO contribution using the transverse momentum observable. The idea works also for other observables that can accomplish this job, as long as corresponding resummation and factorization formula are known. The N -jettiness observable is such a candidate, for Born configuration with N jets it is defined as

$$\mathcal{T}_N = \sum_k \min_i \left\{ \frac{2p_i \cdot q_k}{Q_i} \right\} \quad (4.6)$$

where the sum is over all final state parton. The momenta p_i on the other hand are the N -jettiness axes and are obtained from a projection of the full phase space point to a Born phase space point. A suitable projection would be a cluster algorithm which terminates when all partons are clustered in N jets, combined with a projection of the massive jet momenta to massless ones. The initial state momenta are included as beam jets in the evaluation of the minimum, while the normalization factors Q_i can be fixed to the corresponding jet energy such that p_i/Q_i gives the direction of the i -th jet. For the Born kinematics the variable vanishes always since each parton momentum is associated with one jet. If there is additional resolved radiation the N -jettiness variable becomes larger than zero since at least of the minima is unequal to zero. The total cross-section might be written as

$$\sigma = \int d\mathcal{T}_N \frac{d\sigma}{d\mathcal{T}_N} = \int_0^{\mathcal{T}_N^{\text{cut}}} d\mathcal{T}_N \frac{d\sigma}{d\mathcal{T}_N} + \int_{\mathcal{T}_N^{\text{cut}}} d\mathcal{T}_N \frac{d\sigma}{d\mathcal{T}_N}. \quad (4.7)$$

4. Real radiation contribution

For $\mathcal{T}_N \geq \mathcal{T}_N^{\text{cut}} > 0$ at least one additionally emitted parton forms a resolved jet and therefore the integral over this region may be evaluated with standard NLO techniques, similar to the q_T case. For a small enough cut $\mathcal{T}_N^{\text{cut}}$ the other integrals might be expanded as

$$\int_0^{\mathcal{T}_N^{\text{cut}}} d\mathcal{T}_N \frac{d\sigma}{d\mathcal{T}_N} = \sigma^{\text{sing}}(\mathcal{T}_N^{\text{cut}}) + \mathcal{O}(\mathcal{T}_N^{\text{cut}}) \quad (4.8)$$

where the singular cross section σ^{sing} can be obtained from soft-collinear effective field theory (SCET) [184]. It contains double virtual contributions as well as contributions from the unresolved double real and real-virtual radiation. From the infrared divergences large logarithm of the cutoff variable arise in both integrals which need to be cancel against each other. Therefore, in practice it is necessary to introduce a further subtraction on integrand level. A suitable subtraction term is given by the singular cross section itself close to the cutoff. With the introduction of another cutoff $\mathcal{T}_N^{\text{off}}$

$$\sigma = \sigma^{\text{sing}}(\mathcal{T}_N^{\text{off}}) + \int_{\mathcal{T}_N^{\text{cut}}} d\mathcal{T}_N \left[\frac{d\sigma}{d\mathcal{T}_N} - \frac{d\sigma^{\text{sing}}}{d\mathcal{T}_N} \Theta(\mathcal{T}_N < \mathcal{T}_N^{\text{off}}) \right] + \mathcal{O}(\mathcal{T}_N^{\text{cut}}) \quad (4.9)$$

In contrast to the q_T subtraction this method can be applied directly to colored final states, as long as the singular part is known. It was successfully applied to processes like Higgs or vector boson plus jet production [185–188].

4.1.2. Subtraction methods

CoLoRFuINNLO. The "Completely Local subRaction for Fully differential Predictions at NNLO" method is a subtraction method in the more traditional sense. Formulated for colorless initial states, local subtraction terms matching the infrared limits of the double real radiation contribution as well as real-virtual contributions are obtained from factorization formulae. The overlap between different singularities is taken into account such that the method provides completely integrable contributions to the cross section. Moreover, the subtraction terms are designed in such a way that the analytical integration is conceptually possible. In a series of publications [189–196] all necessary integrated subtraction terms were derived. Due to the absence of colored initial states, the NNLO contribution to the cross section is divided in three contributions

$$\sigma^{\text{NNLO}} = \sigma_{n+2}^{\text{NNLO}} + \sigma_{n+1}^{\text{NNLO}} + \sigma_n^{\text{NNLO}} \quad (4.10)$$

which contain the double real, real virtual and double virtual contribution, respectively. Local subtraction terms are introduced such that they can be organised like

$$\sigma_{n+2}^{\text{NNLO}} = \int \left[d\hat{\sigma}_{n+2}^{RR} F_{n+2} - d\hat{\sigma}_{n+2}^{RR,S_2} F_n - \left(d\hat{\sigma}_{n+1}^{RR,S_1} F_{n+1} - d\hat{\sigma}_{n+2}^{RR,S_{12}} F_n \right) \right]_{\epsilon=0} \quad (4.11)$$

$$\sigma_{n+1}^{\text{NNLO}} = \int \left[\left(d\hat{\sigma}_{n+1}^{RV} + \int_1 d\hat{\sigma}_{n+2}^{RR,S_1} \right) F_{n+1} + \left(d\hat{\sigma}_{n+1}^{RV} + \left(\int_1 d\hat{\sigma}_{n+2}^{RR,S_1} \right)^{S_1} \right) F_n \right]_{\epsilon=0} \quad (4.12)$$

$$\sigma_n^{\text{NNLO}} = \int \left[d\hat{\sigma}_n^{VV} + \int_2 \left(d\hat{\sigma}_{n+1}^{RR,S_2} - d\hat{\sigma}_{n+2}^{RR,S_{12}} \right) \right]$$

$$+ \int_1 \left(d\hat{\sigma}_{n+1}^{RV,S_1} + \left(\int_1 d\hat{\sigma}_{n+2}^{RR,S_1} \right)^{S_1} \right) \Big]_{\epsilon=0} F_n \quad (4.13)$$

The symbols S_1, S_2, S_{12} denote single, double and iterated double unresolved limits. The subscript of the measurement function F_m denotes the number of resolved momenta entering the hard matrix-element in the various contributions. The appearing integrals \int_1, \int_2 represent the analytic integrations over the unresolved particles. The CoLoRFulNNLO method was applied to Higgs decays into $b\bar{b}$ pairs [197, 198] as well as electron-positron annihilation to jets [199]. The extension to colored initial states is in progress [200].

Antenna Subtraction at NNLO. The Antenna Subtraction method was introduced for NLO calculations [201, 202] and later generalized to NNLO [203]. The subtraction here is based on the usage of color-ordered amplitudes $|\mathcal{M}_k\rangle$ which are defined such that

$$|\mathcal{M}_n\rangle = \sum_k C_{n,k}(N_C) |\mathcal{M}_k\rangle. \quad (4.14)$$

The sum is performed over all non-cyclic permutations of the external partons. The color-ordered amplitudes have simpler factorization formulae which allow for a simplified analytical integration. The subtraction term are written in terms of so-called antenna functions X_{ijk}^0 for single and X_{ijkl}^0 for double unresolved limits of the parton flavors $i, j, k, l \in \{g, q, \bar{q}\}$. They can be calculated from ratios of color-ordered matrix elements

$$X_{ijk}^0(p_i, p_j, p_k) \sim \frac{|M_{ijk}^{(0)}|^2}{|M_{IK}^{(0)}|^2}, \quad X_{ijkl}^0(p_i, p_j, p_k, p_l) \sim \frac{|M_{ijkl}^{(0)}|^2}{|M_{IL}^{(0)}|^2}. \quad (4.15)$$

The color-ordered matrix elements entering these expressions are chosen in such a way that they allow for an easy evaluation and analytical integration over the unresolved phase space

$$\mathcal{X}_{ijk}^{(0)} = \int_1 X_{ijk}^0, \quad \mathcal{X}_{ijkl}^{(0)} = \int_2 X_{ijkl}^0. \quad (4.16)$$

Similar expression are obtained for the real virtual contribution. The integrated contributions are then combined in a similar way as in the CoLoRFulNNLO scheme. The prescription to obtain the subtraction terms does not allow for spin correlation, which are however needed to have a fully local subtraction. To obtain nevertheless stable results, such cases need to be treated in a special way. A possibility is to average out the correlation by combining suitable phase space points. Up to now only the leading color parts of this subtraction scheme are known. But nevertheless the scheme was applied to various processes. The first application was in $e^+e^- \rightarrow$ jets [204, 205]. After the extension of the scheme to heavy final state particles also the production of top-quark pairs in e^+e^- collision was considered [206, 207]. The production of the top-quark pairs at hadron colliders however, was performed only in $q\bar{q}$ channel so far [208–210]. More recently the scheme was used to evaluate the NNLO corrections to Higgs production [211]. Another important application was calculation of the NNLO corrections to the dijet [212] and single inclusive jet [213] observables.

4.2. Sector-improved Residue Subtraction Scheme

The sector-improved residue subtraction scheme (STRIPPER) has been proposed a few years ago as general method of handling real-radiation contributions up to next-to-next-to-leading order [131, 132]. It combines ideas from the FKS-approach [23] with the sector-decomposition method [214–216] to a general scheme which provides a set of subtraction and integrated subtraction terms for arbitrary processes. Originally formulated completely in CDR [131], the scheme was reformulated in four dimensions [217] a few years later. The scheme was applied successfully in calculations of differential distributions at next-to-next-to-leading order for various processes [31, 51, 136, 218–220], most prominently to the production of top-quark pairs at hadron colliders. The STRIPPER scheme is used as well to perform the calculation of top-quark production including their decays in this work. A conceptual new phase space parameterization is introduced to overcome inefficiencies in convergence of differential distributions. The four dimensional formulation presented in [217] depends on the specific parameterization used in the construction, and is therefore not compatible with the new phase space approach. In this chapter, the new phase space parameterization is presented and combined with some of the original concepts that remain unchanged. For completeness these concepts are reviewed in necessary detail, closely following the original construction.

4.2.1. General setup

The STRIPPER scheme is general in the sense that it can be used for next-to-next-to-leading calculations in QCD for arbitrary processes, in hadron-hadron, hadron-lepton or lepton-lepton collisions or heavy-particle decays. The most complicated type, and most complete in terms on necessary considerations, are the hadron-hadron collisions. Considering the (differential) production cross section of some final state Y consisting of n particles, the process in mind is $h_1(P_1)h_2(P_2) \rightarrow Y$, where h_1, h_2 denote the incoming hadrons with momentum P_1, P_2 . The construction starts with the well-known factorization of a hadronic process

$$\sigma_{h_1 h_2}(P_1, P_2) = \sum_{ab} \int \int_0^1 dx_1 dx_2 \phi_a^1(x_1, \mu_F^2) \phi_b^2(x_2, \mu_F^2) \hat{\sigma}_{ab}(x_1 P_1, x_2 P_2, \alpha_s(\mu_R^2), \mu_R^2, \mu_F^2) \quad (4.17)$$

into partonic cross sections $\hat{\sigma}_{ab}$ convoluted with PDFs ϕ^i of the incoming hadrons. The PDFs are evaluated at the factorization scale μ_F . The renormalization scale μ_R enters through the running of α_s and higher order contributions. The partonic cross-section is a quantity which can be calculated in perturbative QFT (at least conceptually) to the desired order. At next-to-next-to-leading order $\hat{\sigma}_{ab}$ has to be expanded up to two additional orders in $\alpha_s(\mu_R^2)$,

$$\hat{\sigma}_{ab} = \hat{\sigma}_{ab}^{(0)} + \hat{\sigma}_{ab}^{(1)} + \hat{\sigma}_{ab}^{(2)}. \quad (4.18)$$

The lowest order consist of the Born process only:

$$\hat{\sigma}_{ab}^{(0)} = \hat{\sigma}_{ab}^B. \quad (4.19)$$

4.2. Sector-improved Residue Subtraction Scheme

The expression of $\hat{\sigma}_{ab}^B$ is given in the Appendix A.3, together with all contributions appearing at higher order. At next-to-leading order three contributions arise:

$$\hat{\sigma}_{ab}^{(1)} = \hat{\sigma}_{ab}^R + \hat{\sigma}_{ab}^V + \hat{\sigma}_{ab}^C. \quad (4.20)$$

In the real contribution $\hat{\sigma}_{ab}^R$ the contribution from one additional parton emission is included, while in $\hat{\sigma}_{ab}^V$ the contribution from one quantum-loop appears. The $\hat{\sigma}_{ab}^C$ contains all terms originating from collinear renormalization of initial state singularities. Finally at next-to-next-to-leading order there is

$$\hat{\sigma}_{ab}^{(2)} = \hat{\sigma}_{ab}^{RR} + \hat{\sigma}_{ab}^{RV} + \hat{\sigma}_{ab}^{VV} + \hat{\sigma}_{ab}^{C1} + \hat{\sigma}_{ab}^{C2}. \quad (4.21)$$

The emission of two additional partons ($\hat{\sigma}_{ab}^{RR}$), the emission of one additional parton combined with one quantum loop ($\hat{\sigma}_{ab}^{RV}$) and two quantum loops ($\hat{\sigma}_{ab}^{VV}$) contribute. The factorization contributions $\hat{\sigma}_{ab}^{C1}$ and $\hat{\sigma}_{ab}^{C2}$ contain various convolutions, needed for the collinear renormalization.

The measurement function All previously mentioned contributions are defined together with a *measurement function* F_m where $m = n, n + 1, n + 2$, compare Appendix A.3. The function F defines an infrared safe observable, such as total cross sections or differential distributions. The measurement function F_n depends on the momenta of a n -particle configuration and ensures that these are well out-side any infrared singular limit, otherwise the tree-level cross section would not be defined. The F_{n+1} function on the other hand allows for one unresolved momentum, e.g. one momentum that approaches a singular limit, either soft or collinear. Such a configuration cannot be distinguished from an n -particle configuration such that $F_{n+1} \rightarrow F_n$ in any infrared limit. The same is true for F_{n+2} but with up to two unresolved momenta allowed. If one momentum becomes unresolved, $F_{n+2} \rightarrow F_{n+1}$ holds and obvious extension in case of two unresolved momenta.

Selector function Since single/double unresolved limits are allowed in contributions with F_{n+1}/F_{n+2} measurement functions, these contributions are not finite. These allowed divergences are need to be canceled against divergences of other contributions. In CDR, these divergences manifest in terms of poles when expanding the contribution in a Laurent-series in ϵ . Since an analytical extraction is not always feasible, numerical methods are required. However, these cannot deal with the divergent behaviour of the integrals. In order to extract the Laurent expansion the phase space is decomposed with the help of a selector function. The selector function selects specific partons (two in case of a contribution coming with F_{n+1} and three or two pairs of two partons in case of F_{n+2}) and allows only the infrared limit of one(two) of them. Either of the chosen unresolved parton(s) can become soft or collinear to the other parton(s). All other collinear and soft limits of partons are suppressed such that the corresponding divergence is regulated. The selector function is not unique, but does also not effect the further construction of the scheme. There are two properties of this selector functions that are important. The selector function has to be a partition of unity

$$\sum_{ik} \mathcal{S}_{i,k} = 1 \quad \text{and} \quad \sum_{ij} \left(\sum_k \mathcal{S}_{ij,k} + \sum_{kl} \mathcal{S}_{i,k;j,l} \right) = 1. \quad (4.22)$$

4. Real radiation contribution

The single-collinear selector function $\mathcal{S}_{i,k}$ allows only for the soft limit of parton i and the collinear limit of i and k . Whereas the triple-collinear selector function $\mathcal{S}_{ij,k}$ allows only for the soft limit of parton i and j as well as all possible collinear limits between i,j and k . The double collinear selector function $\mathcal{S}_{i,k;j,l}$ similarly allows for the soft limits of i and j but only for the collinear limits of the pairs i,k and j,l . One implementation of such a function, which is also used in the calculations presented in section 5, can be found in [217].

4.3. Phase Space Parameterization

So far, all contributions containing additional radiation are decomposed into sectors, while in each sector two, three or four particles are singled out. In case of a single-collinear decomposition in each sector $\mathcal{S}_{i,k}$ the momentum of parton i is named u and that of parton k , r . In case of triple-collinear sector $\mathcal{S}_{ij,k}$ the momenta of i,j and k are labeled as u_1, u_2 and r . Finally, in a double-collinear sector $\mathcal{S}_{i,k;j,l}$ the momenta u_1 and r_1 are assigned to parton i and k while u_2 and r_2 are assigned to j and l . In each sector, a parameterization of the phase space needs to be specified such that an easy extraction of the ϵ in each sector is possible. Since the divergences are related to the soft and collinear limits, a direct parameterization of the energy and the angular distance to the reference is desirable.

Note on notation The momenta u, u_i are frequently called unresolved momenta in the following, even when they are well separated. Accordingly, the corresponding phase space is called unresolved phase. If a momentum actually is unresolved in some discussion, this should be clear from the context.

4.3.1. Original phase space parameterization

In the original formulation of the STRIPPER scheme the phase space of the unresolved partons can be found in [217]. Schematically, the parameterization start from fixed incoming momenta, determined by the initial state. After fixing the direction of the reference momenta, the unresolved phase space is parameterized with respect to the reference momentum (momenta), potentially using the complete available energy. This restricts the energy available for the reference momentum as well as the rest of the phase space. When generating the subtraction terms needed to make the integrals integrable, this procedure lead to the phenomenon that many different kinematics configurations are obtained. This is not a conceptual issue but might have practical consequences in terms of *miss-binning*. In table 4.5 the numbers of different kinematic configurations in each sector are given. A more detailed discussion follows together with the subtraction kinematics of the alternative phase space parameterization.

Miss-binning

The term *miss-binning* refers to a practical problem apparent in all subtraction schemes when calculating binned differential distributions. Suppose, for a real-radiation contribution, one generates a well-separated full configuration, which enters some bin with its weight. The weight contains besides the phase space, initial and/or integration weights the matrix element. The important feature of this weight is that if the full configuration approaches a singular limit this weight will become large. The subtraction then regulates

this divergent behaviour in the infrared limit. In the well-separated case, the weight is not especially large, however subtraction terms are still present. They also come with a small weight but might enter completely different bins. Only in the infrared limit the subtraction terms are bound to end up in the same bin as the full configuration. Suppose now, that the full configuration is indeed quite close to a singular configuration that lies quite near the boundary of a bin. Then it can happen that the weight becomes already sizeable but nevertheless the subtraction term can enter a neighbouring bin, also with a sizeable weight with opposite sign. In each bin this will be observed as a fluctuation in the accumulated weights and thus will increase the estimated error and will shift the estimated value of the binned quantity. This does not spoil the integrability but may spoil the convergence. It is intuitive that frequency of this *miss-binning* may depend on the number of different kinematic configurations present in the subtraction. There is no apparent way of proving this statement; rather it is a matter of experimentation. This is the reason for the new attempt to formulate a parameterization which minimizes this problem within the STRIPPER scheme.

4.3.2. New phase space parameterization

The phase space parameterization presented here is a conceptually new idea, worked out by Michal Czakon. Some concepts already appear in phase space parameterizations and mappings for the POWHEG box in the context of parton shower matching [221, 222]. The guiding idea is to find a parameterization which is defined in such a way that the subtraction term terms generated within the STRIPPER scheme automatically come with a minimal number of different kinematics. That there is only a small number of necessary configurations to regulate all infrared limits in one sector follows from the simple observation that the physical limits are described by one or two partons become unresolved. Thus, naively for the double real contribution there one might expect that one $n + 1$ and one n configuration should be enough.

General considerations

Consider the n -particle phase space where certain momenta are labeled according to their role within an sector. In this sector n_r reference partons are identified, of which n_{f_r} are in the final state. Furthermore n_u unresolved partons and $n_q = n - n_{f_r} - n_u$ Born partons are specified with the help of the selector function. The type of the decomposition (single-, double-, or triple-collinear) fixes n_r , n_{f_r} and n_u . The full phase space might be written in the following form:

$$d\Phi_n = \prod_{i=1}^{n_q} d\mu_{m_i}(q_i) \prod_{j=1}^{n_{f_r}} d\mu_0(r_j) \prod_{k=1}^{n_u} d\mu_0(u_k) (2\pi)^d \delta^{(d)} \left(\sum_{i=1}^{n_q} q_i + \sum_{j=1}^{n_{f_r}} r_j + \sum_{k=1}^{n_u} u_k - P \right) \quad (4.23)$$

where P is the total initial state momentum and the single particle measures are defined as

$$d\mu_m(k) \equiv \frac{d^d k}{(2\pi)^d} 2\pi \delta(k^2 - m^2) \theta(k^0) \equiv \frac{d^d k}{(2\pi)^d} 2\pi \delta_+(k^2 - m^2), \quad (4.24)$$

4. Real radiation contribution

where the δ_+ function was introduced as a short hand for the on-shell and positive energy condition. The phase space for the reference and unresolved momenta can be decoupled from the remaining momenta by introducing an integration over a auxiliary momentum q with invariant mass $Q \geq \sum_{i=1}^{n_q} m_i$.

$$\begin{aligned} d\Phi_n = & \frac{dQ^2}{2\pi} d\mu_Q(q) \prod_{j=1}^{n_{fr}} d\mu_0(r_j) \prod_{k=1}^{n_u} d\mu_0(u_k) (2\pi)^d \delta^{(d)}\left(q + \sum_{j=1}^{n_{fr}} r_j + \sum_{k=1}^{n_u} u_k - P\right) \\ & \cdot \prod_{i=1}^{n_q} d\mu_{m_i}(q_i) (2\pi)^d \delta^{(d)}\left(\sum_{i=1}^{n_q} q_i - q\right) \end{aligned} \quad (4.25)$$

The integration over q can be used to eliminate the delta function containing the reference and unresolved momenta to achieve the following form

$$\begin{aligned} d\Phi_n = & dQ^2 \left[\prod_{j=1}^{n_{fr}} d\mu_0(r_j) \prod_{k=1}^{n_u} d\mu_0(u_k) \delta_+\left(\left(P - \sum_{j=1}^{n_{fr}} r_j - \sum_{k=1}^{n_u} u_k\right)^2 - Q^2\right) \right] \\ & \cdot \prod_{i=1}^{n_q} d\mu_{m_i}(q_i) (2\pi)^d \delta^{(d)}\left(\sum_{i=1}^{n_q} q_i - q\right). \end{aligned} \quad (4.26)$$

The full phase space can be mapped to the Born phase space with $n - n_u$ particles,

$$\{P, r_j, u_k\} \rightarrow \{\tilde{P}, \tilde{r}_j\}. \quad (4.27)$$

This mapping is by no means unique and there are possibly many ways to do this. By imposing additional constraints on the mapping, it can be uniquely defined. In this case the following three constraints are imposed:

- The mapping is invertible for fixed unresolved momenta,

$$\{\tilde{P}, \tilde{r}_j, u_k\} \rightarrow \{P, r_j, u_k\}. \quad (4.28)$$

- The invariant mass of the auxiliary momentum is preserved

$$\tilde{q}^2 = q^2, \quad \text{where} \quad \tilde{q} = \tilde{P} - \sum_{j=1}^{n_{fr}} \tilde{r}_j. \quad (4.29)$$

- The reference momenta are transformed only by rescaling.

The last condition is the key idea of the parameterization which will lead to a reduced set of subtraction kinematics. This condition reads a little bit different depending on the position of the reference parton. If it is in the final state it can be written as

$$r = x\tilde{r}, \quad (4.30)$$

where x is determined by the full kinematics. Denoting by $f_x(r)$ the function that determines the value of x , the phase space measure can be written in the following form

$$d\mu_0(r) = d\mu_0(r) dx \delta(x - f_x(r)) d^d \tilde{r} \delta^{(d)}(\tilde{r} - r/x) \quad (4.31)$$

4.3. Phase Space Parameterization

$$= d\mu_0(\tilde{r}) dx \theta(x) x^{d-2} \delta(x - f_x(x \tilde{r})) \quad (4.32)$$

$$= d\mu_0(\tilde{r}) \theta(x) x^{d-3} \left[-\frac{\partial}{\partial x} \frac{f_x(x \tilde{r})}{x} \right]^{-1} \Big|_{x=f_x(x \tilde{r})}. \quad (4.33)$$

And similar, in case of initial state references, the rescaling is defined as

$$r = \tilde{r}/z. \quad (4.34)$$

In this case the integration over the parton distribution functions needs to be taken into account. The incoming momentum is parameterized by the momentum fraction x of the momentum of the hadrons. Similar to the final state case, the rescaling factor z depends on the full kinematics described through the function $f_z(x p_h)$, which depends on the original momentum fraction x ,

$$dx \phi(x) = dx \phi(x) d\tilde{x} \delta(\tilde{x} - f_z(x p_h) x) \quad (4.35)$$

$$= d\tilde{x} \phi(\tilde{x}/z) \theta(z - \tilde{x}) \left[-z^2 \frac{\partial}{\partial z} \frac{f(\tilde{r}/z)}{z} \right]^{-1} \Big|_{z=f(\tilde{r}/z)}. \quad (4.36)$$

Using this specific transformation, the full phase space can be written as

$$\begin{aligned} d\Phi_n = & dQ^2 \left[\prod_{j=1}^{n_{fr}} d\mu_0(\tilde{r}_j) \delta_+ \left(\left(\tilde{P} - \sum_{j=1}^{n_{fr}} \tilde{r}_j \right)^2 - Q^2 \right) \prod_{k=1}^{n_u} d\mu_0(u_k) \theta(\{u_l\} \in \mathcal{U}) \mathcal{J} \right] \\ & \cdot \prod_{i=1}^{n_q} d\mu_{m_i}(\tilde{q}_i) (2\pi)^d \delta^{(d)} \left(\sum_{i=1}^{n_q} \tilde{q}_i - \tilde{q} \right), \end{aligned} \quad (4.37)$$

where \mathcal{J} represents the necessary Jacobians for the transformation. For a specific Born configuration $\{\tilde{P}, \tilde{r}\}$ the integration volume over the unresolved momenta is constrained by $\theta(\{u_l\})$. The set \mathcal{U} is the collection of unresolved momenta. The relation $q^2 = \tilde{q}^2$ implies that there is a Lorentz transformation which transforms \tilde{q} into q . Since the one particle measures $d\mu_{m_i}(q_i)$ are Lorentz invariant the phase space measure can be written as

$$\begin{aligned} d\Phi_n = & dQ^2 \left[\prod_{j=1}^{n_{fr}} d\mu_0(\tilde{r}_j) \delta_+ \left(\left(\tilde{P} - \sum_{j=1}^{n_{fr}} \tilde{r}_j \right)^2 - Q^2 \right) \prod_{k=1}^{n_u} d\mu_0(u_k) \theta(\{u_l\} \in \mathcal{U}) \mathcal{J} \right] \\ & \prod_{i=1}^{n_q} d\mu_{m_i}(q_i) (2\pi)^d \delta^{(d)} \left(\sum_{i=1}^{n_q} q_i - \tilde{q} \right). \end{aligned} \quad (4.38)$$

The Jacobian depends clearly on the sector under consideration and can be constructed from the general derivations. The constraints for the unresolved phase space can be derived from equation (4.29) and the requirement that the Born configuration remains physical. The details of this constraints can be found in the following discussion, where the different placements of the references are separately investigated.

At this point it is instructive to change the point view. In formula (4.38) the integration over the full Born phase space is factorized from the integration over the unresolved phase space. This, together with the inverse of the transformation, suggests that the phase space

4. Real radiation contribution

construction can be viewed in the following way: Instead of generating a full configuration and derive some Born configuration from there, create first a Born configuration and derive the full configuration from that. To be able to do this, the unresolved momenta need to be generated in a way that the constraints are fulfilled.

The full configuration is then determined by rescaling parameters x and/or z which are again fixed by the condition 4.29. The important feature here is that the conditions only involve the sum, in case of final state references, or the difference, in case of initial state references, of the reference and the unresolved momenta, $r \pm u$. In the infrared limits, where u becomes soft $u \rightarrow 0$ or collinear $u \rightarrow \alpha r$, the conditions become independent of u . In other words, it does not matter if u is soft, collinear or soft-collinear with respect to r , the full configuration obtained from \tilde{r}, \tilde{P} and $\{q\}$ are always the same. As shown in the next section, this leads to the minimal number of subtraction configuration in each sector, except in case of a single unresolved configuration in two triple collinear sectors. The details about the obtained configurations are discussed after defining further details of the phase space parameterization.

Parameterization in single-collinear sectors

In case of a $n + 1$ particle phase spaces a single-collinear sector decomposition is used. If the reference parton is an initial state parton, the integration over the momentum fraction x is incorporated in the phase space integral over some function $f(r, u)$ (dependence on the other Born momenta is suppressed)

$$\int dx d\Phi_{n+1} \phi_k(x) f(r, u) = \int d\tilde{x} d\mu_0(u) \theta(u) \phi(\tilde{x}/z) \theta(z - \tilde{x}) \mathcal{J} d\Phi_n(\tilde{q}) f(\tilde{r}/z, u) \quad (4.39)$$

where $\tilde{q}^2 = (\tilde{r} + p)^2$ where p is the other initial state momentum and $\tilde{r} = \tilde{x} p_h$. The function $\theta(u)$ encodes the constraints on the unresolved phase space originating from Born mapping. Equation (4.29) implies the relation which yields the constraints on the unresolved momentum:

$$(r + p - u)^2 = (\tilde{r} + p)^2, \quad (4.40)$$

replacing either r by \tilde{r}/z or vice versa, yields the following expressions for the rescaling parameter z

$$z = \frac{(r + p) \cdot (r - u)}{p \cdot r}, \quad z = \frac{(p - u) \cdot \tilde{r}}{p \cdot (\tilde{r} + u)}. \quad (4.41)$$

Differentiating the first equation with respect to z after replacing $r \rightarrow \tilde{r}/z$ yields, combined with equation (4.36), the Jacobian

$$\mathcal{J} = \frac{p \cdot \tilde{r}}{(p - u) \cdot \tilde{r}}. \quad (4.42)$$

Writing $u = u^0 \hat{u}$ and noting that $r + p$ is a time-like four-vector it is evident that z is a monotonically decreasing function of u^0 . Together with the fact that it is defined for any full configuration, this ensures that the transformation can be inverted and that any full configuration has a well defined Born configuration. Using the fact that z has to be larger than \tilde{x} , the maximum energy $(u^0)_{\max}$ is given for specified \tilde{r}, p and \hat{u} through equation

4.3. Phase Space Parameterization

(4.41)

$$(u^0)_{\max} = (1 - \tilde{x}) \frac{p \cdot \tilde{r} / \tilde{x}}{(\tilde{r} / \tilde{x} + p) \cdot \hat{u}}. \quad (4.43)$$

Thus the phase space integral reads

$$\int dx d\Phi_{n+1} \phi_k(x) f(r, u) = \int d\tilde{x} d\mu_0(u) \phi(\tilde{x}/z) \frac{p \cdot \tilde{r}}{(p - u) \cdot \tilde{r}} d\Phi_n(\tilde{q}) f(\tilde{r}/z, u), \quad (4.44)$$

where the constraints on the unresolved phase space are hidden in the unresolved phase space measure

$$d\mu_0(u) = \mathcal{N}^\epsilon \mu_R^{2\epsilon} \int d^{2-2\epsilon} \Omega \int_0^1 d\eta \int_0^{(u^0)_{\max}(\eta)} du^0 \frac{(u^0)^{1-2\epsilon}}{2(2\pi)^{(3-2\epsilon)}}. \quad (4.45)$$

The normalization factor \mathcal{N} is defined as $(\frac{e^{\gamma_E}}{4\pi})$.

In case of a final state reference the relation

$$(P - r - u)^2 = (P - \tilde{r})^2 \quad (4.46)$$

fixes x and the maximum of unresolved parton energy (obtained at $x = 0$) in a similar way to be

$$x = \frac{P \cdot r}{(P - r) \cdot (r + u)}, \quad x = \frac{P \cdot (\tilde{r} - u)}{(P - u) \cdot \tilde{r}}, \quad (u^0)_{\max} = \frac{P \cdot \tilde{r}}{P \cdot \hat{u}} \quad (4.47)$$

where the Jacobian evaluates to

$$\mathcal{J} = \frac{x^{d-3} P \cdot \tilde{r}}{(P - u) \cdot \tilde{r}}. \quad (4.48)$$

Also, x is a monotonically decreasing function of u^0 since $(P - r)^2 > 0$ and it is defined for any full configuration.

In both cases the direction of the unresolved momentum is parameterized with respect to the reference parton. Writing

$$r = r^0 \hat{r} = r^0 \begin{pmatrix} 1 \\ \hat{\mathbf{r}} \end{pmatrix} \quad \text{with} \quad \hat{\mathbf{r}} = \hat{\mathbf{n}}^{(3-2\epsilon)}(\alpha_1, \alpha_2, \dots), \quad (4.49)$$

\hat{u} is given by

$$\hat{u} = \begin{pmatrix} 1 \\ \hat{\mathbf{u}} \end{pmatrix} \quad \text{with} \quad \hat{\mathbf{u}} = \mathbf{R}_1^{(3-2\epsilon)}(\alpha_1, \alpha_2, \dots) \hat{\mathbf{n}}^{(3-2\epsilon)}(\theta, \phi, \rho_1). \quad (4.50)$$

Details on the definition of the versors $\hat{\mathbf{n}}$ and matrices \mathbf{R} can be found in appendix A.2. After introducing the variables η and ξ

$$\eta = \frac{1}{2}(1 - \cos \theta), \quad u^0 = \xi (u^0)_{\max}, \quad (4.51)$$

4. Real radiation contribution

the unresolved phase space integral can then be written as

$$d\mu_0(u) = \mathcal{N}^\epsilon \int \frac{d^{1-2\epsilon}\Omega(\phi, \rho_1, \dots)}{(2\pi)^{1-2\epsilon}} \int_0^1 d\eta \int_0^1 d\xi \frac{(u^0)_{\max}^2}{(2\pi)^2} \left(\frac{(u^0)_{\max}}{\mu_R} \right)^{2\epsilon} (1-\eta)^\epsilon \eta^{-\epsilon} \xi^{1-2\epsilon} \quad (4.52)$$

$$\equiv \int d\tilde{\mu}(u) \eta \xi^2 \quad (4.53)$$

where $d\tilde{\mu}(u)$ is defined for convenience in later expressions. It can be divided into a regular and a singular part (in the limits $\eta/\xi \rightarrow 0$)

$$d\tilde{\mu}(u) = \frac{d\eta}{\eta^{1+\epsilon}} \frac{d\xi}{\xi^{1+2\epsilon}} d\tilde{\mu}_{\text{reg}}(\eta, \xi). \quad (4.54)$$

Triple-collinear sector parameterization

The phase space parameterization in triple-collinear sectors follows, at first, the same lines as the single-collinear parameterization. The triple-collinear selector function $\mathcal{S}_{ij,k}$ allows to identify three partons, the reference momentum r of parton k and the two unresolved momenta u_1 ("i") and u_2 ("j"). Following the general construction in section 4.38 a phase space integral over some function $f(r, u_1, u_2)$ can be written as

$$\int dx d\Phi_{n+2} \phi_k(x) f(r, u_1, u_2) = \int d\tilde{x} d\mu_0(u_1) d\mu_0(u_2) \theta(u_1, u_2) \quad (4.55)$$

$$\phi(\tilde{x}/z) \theta(z - \tilde{x}) \mathcal{J} d\Phi_n(\tilde{q}) f(\tilde{r}/z, u_1, u_2) \quad (4.56)$$

in case of a initial state reference, and as

$$\int d\Phi_{n+2} f(r, u_1, u_2) = \int d\mu_0(u_1) d\mu_0(u_2) d\mu_0(\tilde{r}) \theta(u_1, u_2) \mathcal{J} d\Phi_{n-1}(\tilde{q}) f(x\tilde{r}, u_1, u_2) \quad (4.57)$$

in case of a final state reference. Again equation (4.29) provides the constraints that fix x or z .

$$\text{final:} \quad (P - r - u_1 - u_2)^2 = (P - \tilde{r})^2 \Rightarrow x = \frac{P \cdot r}{(P - r) \cdot (r + u_1 + u_2) - u_1 \cdot u_2} \quad (4.58)$$

$$x = \frac{P \cdot (\tilde{r} - u_1 - u_2) + u_1 \cdot u_2}{(P - u_1 - u_2) \cdot \tilde{r}} \quad (4.59)$$

$$\text{initial:} \quad (r + p - u_1 - u_2)^2 = (\tilde{r} + p)^2 \Rightarrow z = \frac{(r + p) \cdot (r - u_1 - u_2) + u_1 \cdot u_2}{p \cdot r} \quad (4.60)$$

$$z = \frac{(p - u_1 - u_2) \cdot \tilde{r}}{p \cdot (\tilde{r} + u_1 + u_2) - u_1 \cdot u_2} \quad (4.61)$$

Expressing the unresolved momentum as $u_1 = u_1^0 \hat{u}_1$ and $u_2 = u_2^0 \hat{u}_2$, the first thing to note is that x and z are monotonically decreasing functions of u_i^0 if u_j^0 with $i \neq j$ is fixed, which follows again from the fact that $r + p$ or $P - r$ are time-like vectors. The transformation is defined for any full configuration which reflects in the fact that $x, z, \tilde{q}^0 \geq 0$ and $x, z \leq 1$. The monotonic dependence of x and z allows to parameterize energies of u_1 and u_2 in an iterative way to cover full phase space volume. This iterative parameterization leads to

4.3. Phase Space Parameterization

the following energy bounds for u_1 and u_2

$$\begin{aligned} \text{final: } (u_1^0)_{\max} &= \frac{P \cdot \tilde{r}}{P \cdot \hat{u}_1}, & (u_2^0)_{\max} &= \frac{P \cdot (\tilde{r} - u_1)}{(P - u_1) \cdot \hat{u}_2}, \\ \text{initial: } (u_1^0)_{\max} &= (1 - \tilde{x}) \frac{p \cdot \tilde{r}/\tilde{x}}{(\tilde{r}/\tilde{x} + p) \cdot \hat{u}_1}, & (u_2^0)_{\max} &= \frac{(\tilde{r}/\tilde{x} + p) \cdot ((1 - \tilde{x}) \tilde{r}/\tilde{x} - u_1)}{(\tilde{r}/\tilde{x} + p - u_1) \cdot \hat{u}_2}. \end{aligned} \quad (4.62)$$

$$(4.63)$$

From equation (4.33) and (4.36) the Jacobians

$$\text{final: } \mathcal{J} = \frac{x^{d-3} P \cdot \tilde{r}}{(P - u_1 - u_2) \cdot \tilde{r}} \quad (4.64)$$

$$\text{initial: } \mathcal{J} = \frac{p \cdot \tilde{r}}{(p - u_1 - u_2) \cdot \tilde{r}} \quad (4.65)$$

can be derived. The directions of u_1 and u_2 are parameterized in with respect to the reference momentum r

$$\hat{u}_1 = \begin{pmatrix} 1 \\ \hat{\mathbf{u}}_1 \end{pmatrix} \text{ with } \hat{\mathbf{u}}_1 = \mathbf{R}_1^{(3-2\epsilon)}(\alpha_1, \alpha_2, \dots) \hat{\mathbf{n}}^{(3-2\epsilon)}(\theta_1, \phi_1, \rho_1, \rho_2, \dots) \quad (4.66)$$

$$\hat{u}_2 = \begin{pmatrix} 1 \\ \hat{\mathbf{u}}_2 \end{pmatrix} \text{ with } \hat{\mathbf{u}}_2 = \mathbf{R}_1^{(3-2\epsilon)}(\alpha_1, \alpha_2, \dots) \mathbf{R}_2^{(3-2\epsilon)}(\phi_1, \rho_1, \rho_2, \dots) \hat{\mathbf{n}}^{(3-2\epsilon)}(\theta_2, \phi_2, \sigma_1, \sigma_2) \quad (4.67)$$

Furthermore, as discussed in section 2.1.3, the double soft limits require a hierarchy in the unresolved partons energy $u_1^0 \geq u_2^0$ and therefore the phase space is split up by introducing the partition of unity

$$1 = \theta(u_1^0 - u_2^0) + \theta(u_2^0 - u_1^0). \quad (4.68)$$

Together with the constraints on the maximum energies from equation (4.63), the following parameterization for the energies can be employed

$$u_1^0 = (u_1^0)_{\max} \xi_1, \quad u_2^0 = \xi_1 \xi_2 \underbrace{(u_1^0)_{\max}}_{\equiv (u_2^0)_{\max}(u_1, \hat{u}_2)} \min \left[1, \frac{1}{\xi_1} \frac{(u_2^0)_{\max}}{(u_1^0)_{\max}} \right], \quad \xi_{1,2} \in [0, 1], \quad (4.69)$$

which covers the part of the phase space where $u_1^0 > u_2^0$. Instead of introducing a similar parameterization to cover the $u_2^0 > u_1^0$ case, the same contribution can be obtained from the sector where u_1 and u_2 are swapped, thus only the $u_1^0 > u_2^0$ case needs to be considered. In addition, parameterizations of the angular variables $\theta_{1,2}$ and ϕ_2 by $\hat{\eta}_{1,2}$ and ζ

$$\cos \theta_1 = 1 - 2\hat{\eta}_1, \quad \cos \theta_2 = 1 - 2\hat{\eta}_2, \quad \cos \phi_2 = \frac{1 - 2\hat{\eta}_3 - (1 - 2\hat{\eta}_1)(1 - 2\hat{\eta}_2)}{4\sqrt{(1 - \hat{\eta}_1)\hat{\eta}_1(1 - \hat{\eta}_2)\hat{\eta}_2}}, \quad (4.70)$$

$$\eta_3 = \frac{\hat{u}_1 \cdot \hat{u}_2}{2} = \frac{1 - \cos \theta_{12}}{2} = \frac{(\hat{\eta}_1 - \hat{\eta}_2)^2}{\hat{\eta}_1 + \hat{\eta}_2 - 2\hat{\eta}_1\hat{\eta}_2 - 2(1 - 2\zeta)\sqrt{\hat{\eta}_1(1 - \hat{\eta}_1)\hat{\eta}_2(1 - \hat{\eta}_2)}}, \quad (4.71)$$

4. Real radiation contribution

sector	$\hat{\eta}_1$	$\hat{\eta}_2$	$(r + u_1 + u_2)^2$
\mathcal{S}_1	η_1	$\eta_1\eta_2/2$	$\xi_1\eta_1 \times \text{regular}$
\mathcal{S}_{23}	$\eta_1\eta_2/2$	η_2	$\xi_1\eta_2 \times \text{regular}$
\mathcal{S}_4	η_1	$\eta_1(1 - \eta_2/2)$	$\xi_1\eta_1 \times \text{regular}$
\mathcal{S}_5	$\eta_1(1 - \eta_2/2)$	η_2	$\xi_1\eta_2 \times \text{regular}$

Table 4.1.: Sector parameterization and factorization of the three particle invariant s_{123}

are introduced. It is convenient to write ζ in terms of an angle ϕ_ζ such that

$$\zeta = \frac{1}{2} (1 + \cos(\pi\phi_\zeta)) \quad \text{and} \quad (4.72)$$

$$d\phi_2 \sin^{-2\epsilon} \phi_2 = d\phi_\zeta d(\phi)^{1-2\epsilon} \quad (4.73)$$

where the function $d(\phi)$ contains the Jacobian which depends on ϕ_ζ , $\hat{\eta}_1$ and $\hat{\eta}_2$. The phase space needs to be further decomposed to factorize all triple collinear limits. There are four invariants that appear in the amplitudes as propagators or equivalently in the corresponding triple-collinear splitting functions which give rise to the divergent behaviour in these limits

$$(r + u_1)^2 = 4r^0(u_1^0)_{\max} \xi_1 \hat{\eta}_1 \quad (4.74)$$

$$(r + u_2)^2 = 4r^0(u_2^0)_{\max} (u_1, \hat{u}_2) \xi_1 \xi_2 \hat{\eta}_2 \quad (4.75)$$

$$(u_1 + u_2)^2 = 4(u_1^0)_{\max} (u_2^0)_{\max} (u_1, \hat{u}_2) \xi_1^2 \xi_2 \eta_3 \quad (4.76)$$

$$(r + u_1 + u_2)^2 = 4\xi_1 (r^0(u_1^0)_{\max} \hat{\eta}_1 + r^0(u_2^0)_{\max} (u_1, \hat{u}_2) \xi_2 \hat{\eta}_2 + (u_1^0)_{\max} (u_2^0)_{\max} (u_1, \hat{u}_2) \xi_1 \xi_2 \eta_3) \quad (4.77)$$

The soft and collinear limit of the first and second invariant is directly factorized. Due to the introduction of ζ the third invariant vanishes if $\hat{\eta}_1 = \hat{\eta}_2$, while the last one vanishes in various ways, depending how the two angles $\hat{\eta}_1$ and $\hat{\eta}_2$ are related to each other. The phase space can be decomposed into four regions (sub-sectors) $\theta(0 < \hat{\eta}_2 < \hat{\eta}_1/2)$ (\mathcal{S}_1), $\theta(0 < \hat{\eta}_1 < \hat{\eta}_2/2)$ (\mathcal{S}_{23} , the origin of this numbering has historical reasons), $\theta(\hat{\eta}_1/2 < \hat{\eta}_2 < \hat{\eta}_1)$ (\mathcal{S}_4) and $\theta(\hat{\eta}_2/2 < \hat{\eta}_1 < \hat{\eta}_2)$ (\mathcal{S}_5), which translates to the prescription in figure 4.1. In each sub-sector the invariants fully factorize (see table 4.1).

In the original formulation the sector \mathcal{S}_{23} was further decomposed into two sectors \mathcal{S}_2 and \mathcal{S}_3 (which is the origin of the strange naming). In [219] it was pointed out that this decomposition is not necessary to factorize all singular limits. The reason is commutativity of the soft and collinear limits, also called color-coherence. Originally the collinear limit of u_1 was assumed to be correlated with the soft limit of u_2 , such so that in \mathcal{S}_2 a single limit of collinear u_1 implied a soft (and not collinear) limit of u_2 and vice versa in \mathcal{S}_3 . This makes the factorization of $(r + u_1 + u_2)^2$ explicit in this soft-collinear limit. However, the factorization also occurs in \mathcal{S}_{23} .

With parameterizations (4.71) the unresolved phase space integrals can be expressed in each sector as

$$d\mu_0(u_1)d\mu_0(u_2) = \int d\tilde{\mu}_i(u_1)d\tilde{\mu}_i(u_2)\eta_1^{a_1}\xi_1^{a_2}\eta_2^{a_3}\xi_2^{a_4} \quad (4.78)$$

4.3. Phase Space Parameterization

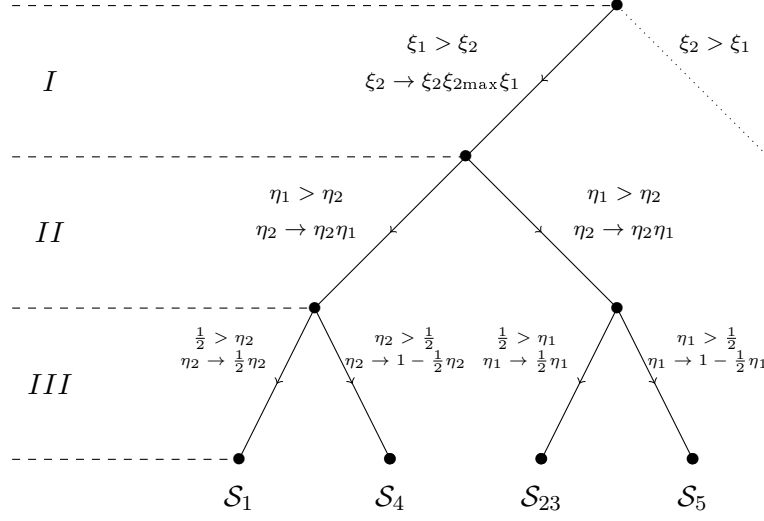


Figure 4.1.: Sector decomposition in triple-collinear sectors

with

$$d\tilde{\mu}_i(u_1)d\tilde{\mu}_i(u_2) = \frac{d\eta_1}{\eta_1^{1+b_1\epsilon}} \frac{d\xi_1}{\xi_1^{1+b_2\epsilon}} \frac{d\eta_2}{\eta_2^{1+b_3\epsilon}} \frac{d\xi_2}{\xi_2^{1+b_4\epsilon}} d\tilde{\mu}_{\text{reg}}^1(\{x\})d\tilde{\mu}_{\text{reg}}^2(\{x\}) \quad (4.79)$$

with sector dependent values for a_i and b_i (see table 4.2). The set of all four variables $\{\eta_1, \xi_1, \eta_2, \xi_2\}$ is denoted by $\{x\}$. The explicit forms of $d\tilde{\mu}_{\text{reg}}^i(\{x\})$ also depends on the sector, but are, as indicated, functions of the sector variables and further angular parameterizations. As in the single collinear case, these measures are completely regular in all limits $\eta_i, \xi_i \rightarrow 0$ and contain integrals over the $1 - 2\epsilon$ dimensional unit sphere. Using the ϕ_ζ replacement the general structure is

$$d\tilde{\mu}_{\text{reg}}^1(\{x\}) = \mathcal{N}^\epsilon \int \frac{d^{1-2\epsilon}\Omega(\phi_1, \rho_1, \dots)}{(2\pi)^{1-2\epsilon}} \frac{(u_1^0)_{\text{max}}^2}{(2\pi)^2} \left(\frac{(u_1^0)_{\text{max}}}{\mu_R} \right)^{2\epsilon} (1 - \hat{\eta}_1)^\epsilon \hat{\eta}_{1,reg}^{-\epsilon} \quad (4.80)$$

$$d\tilde{\mu}_{\text{reg}}^2(\{x\}) = \mathcal{N}^\epsilon \int d\phi_\zeta \frac{d^{-2\epsilon}\Omega(\sigma_1, \dots)}{(2\pi)^{-2\epsilon}} \frac{d(\phi)_{\text{reg}}^{1-2\epsilon}}{2} \frac{(u_2^0)_{\text{max}}^2}{(2\pi)^2} \left(\frac{(u_2^0)_{\text{max}}}{\mu_R} \right)^{2\epsilon} (1 - \hat{\eta}_2)^\epsilon \hat{\eta}_{2,reg}^{-\epsilon}. \quad (4.81)$$

The variables $\eta_{i,reg}$ are obtained after factoring out all vanishing parts from $\hat{\eta}_i$ in the $\eta_i \rightarrow 0$ limit, e.g

sector	$\eta_{1,reg}$	$\eta_{2,reg}$
\mathcal{S}_1	1	$\frac{1}{2}$
\mathcal{S}_{23}	$\frac{1}{2}$	1
\mathcal{S}_4	1	$\frac{1}{2}(2 - \eta_2)$
\mathcal{S}_5	$\frac{1}{2}(2 - \eta_1)$	1

and the $\hat{\eta}$ variables are replaced by the corresponding parameterization from table 4.1.

Special energy parameterization of sector \mathcal{S}_4 and \mathcal{S}_5 The sectors \mathcal{S}_4 and \mathcal{S}_5 parameterize the limits where the two unresolved partons can become collinear to each other. The

4. Real radiation contribution

sector	a_i	b_i
\mathcal{S}_1	$\{2, 4, 1, 2\}$	$\{2, 4, 1, 2\}$
\mathcal{S}_{23}	$\{1, 4, 2, 2\}$	$\{1, 4, 2, 2\}$
\mathcal{S}_4	$\{2, 4, 2, 2\}$	$\{2, 4, 2, 2\}$
\mathcal{S}_5	$\{2, 4, 2, 2\}$	$\{2, 4, 2, 2\}$

Table 4.2.: Sector parameterization and factorization of the three particle invariant s_{123}

iterative energy parameterization discussed before would result in non unique configurations. In these limits the resolved parton is described by the sum and ratio of the energies and the sum of the energies depend on the u_2 . Thus the single collinear and single soft-collinear limit would result in different $u_1 + u_2$. This can be circumvented by discarding the iterative approach and directly parameterize the sum and the energy ratio

$$u_{12}^0 \equiv u_1^0 + u_2^0, \quad \xi_2 = \frac{2u_2^0}{u_1^0 + u_2^0}. \quad (4.82)$$

The requirement that $u_1^0 > u_2^0$ can be build in by restricting $\xi_2 \in [0, 1]$. Inserting this parameterization in the equations for x and z (4.61), both quantities are found to be decreasing functions of u_{12}^0 for fixed ξ_2 . The maximum value of u_{12}^0 can then be achieved in the same manner as in iterated parameterization by inverting the equations for $x = 0$ (or $z = \tilde{x}$). There is

$$\text{final: } (u_{12}^0)_{\max} = \frac{2P \cdot \tilde{r}}{P \cdot \bar{u}_{12} + \sqrt{(P \cdot \bar{u}_{12})^2 - 2\bar{u}_{12}^2 P \cdot \tilde{r}}}, \quad (4.83)$$

$$\text{initial: } (u_{12}^0)_{\max} = \frac{2p \cdot \tilde{r}/\tilde{x}}{(\tilde{r}/\tilde{x} + p) \cdot \bar{u}_{12} + \sqrt{((\tilde{r}/\tilde{x} + p) \cdot \bar{u}_{12})^2 - 2\bar{u}_{12}^2 p \cdot (1 - \tilde{x})\tilde{r}/\tilde{x}}} \quad (4.84)$$

with the definition

$$\bar{u}_{12} = (1 - \xi_2/2)\hat{u}_1 + \xi_2/2\hat{u}_2. \quad (4.85)$$

The energies of u_1 and u_2 are then parameterized as

$$u_1^0 = (u_{12}^0)_{\max} \xi_1 (1 - \xi_2/2) \quad u_2^0 = (u_{12}^0)_{\max} \xi_2/2 \quad (4.86)$$

$$\text{with } du_1^0 du_2^0 = \frac{1}{2} (u_{12}^0)_{\max}^2 \xi_1 d\xi_1 d\xi_2. \quad (4.87)$$

Double-collinear sector parameterization

In the following, it is assumed that $n > n_{fr} + n_u$ and the special case $n = n_{fr} + n_u$ is discussed at the end of the section. Since there are two reference momenta in double-collinear sectors, four different possibilities of their placement arise: initial-initial, final-initial, initial-final, final-final. In all cases two scaling parameters have to be fixed, but there is only one condition (equation (4.29)). Thus, a second condition has to be imposed to specify the mapping to the Born configuration uniquely. Since the double-collinear is similar to the combination of two single-collinear cases, a natural choice for the second condition would be that single-collinear condition for u_1 and r_1 has to hold, too. The

4.3. Phase Space Parameterization

final-final:

$$\begin{aligned}
(P - r_1 - u_1 - r_2 - u_2)^2 &= (P - \tilde{r}_1 - \tilde{r}_2)^2, & (P - r_1 - u_1)^2 &= (P - \tilde{r}_1)^2, \\
x_1 &= \frac{P \cdot r_1}{(P - u_1) \cdot (r_1 + u_1)}, & x_2 &= \frac{(P - r_1/x_1) \cdot r_2}{(P - r_1 - u_1 - u_2) \cdot (r_2 + u_2)}, \\
x_1 &= \frac{P \cdot (\tilde{r}_1 - u_1)}{(P - u_1) \cdot \tilde{r}_1}, & x_2 &= \frac{(P - \tilde{r}_1) \cdot \tilde{r}_2 - (P - x_1 \tilde{r}_1 - u_1) \cdot u_2}{(P - x_1 \tilde{r}_1 - u_1 - u_2) \cdot \tilde{r}_2}, \\
(u_1^0)_{\max} &= \frac{P \cdot \tilde{r}_1}{P \cdot \hat{u}_1}, & (u_2^0)_{\max} &= \frac{(P - \tilde{r}_1) \cdot \tilde{r}_2}{(P - x_1 \tilde{r}_1 - u_1) \cdot \hat{u}_2}, \\
\mathcal{J} &= \frac{x_1^{d-3} P \cdot \tilde{r}_1}{(P - u_1) \cdot \tilde{r}_1} \frac{x_2^{d-3} (P - \tilde{r}_1) \cdot \tilde{r}_2}{(P - x_1 \tilde{r}_1 - u_1 - u_2) \cdot \tilde{r}_2},
\end{aligned}$$

final-initial:

$$\begin{aligned}
(p + r_2 - r_1 - u_1 - u_2)^2 &= (p + \tilde{r}_2 - \tilde{r}_1)^2, & (p + \tilde{r}_2 - r_1 - u_1)^2 &= (p + \tilde{r}_2 - \tilde{r}_1)^2, \\
z_2 &= \frac{(p - r_1 - u_1 - u_2) \cdot (r_2 - u_2)}{(p - r_1 - u_1) \cdot r_2}, & x_1 &= \frac{(p + z_2 r_2) \cdot r_1}{(p + z_2 r_2 - u_1) \cdot (r_1 + u_1)}, \\
x_1 &= \frac{(p + \tilde{r}_2) \cdot (\tilde{r}_1 - u_1)}{(p + \tilde{r}_2 - u_1) \cdot \tilde{r}_1}, & z_2 &= \frac{(p - x_1 \tilde{r}_1 - u_1 - u_2) \cdot \tilde{r}_2}{(p - x_1 \tilde{r}_1 - u_1) \cdot (\tilde{r}_2 + u_2)}, \\
(u_1^0)_{\max} &= \frac{(p + \tilde{r}_2) \cdot \tilde{r}_1}{(p + \tilde{r}_2) \cdot \hat{u}_1}, & (u_2^0)_{\max} &= (1 - \tilde{x}_2) \frac{(p - x_1 \tilde{r}_1 - u_1) \cdot \tilde{r}_2 / \tilde{x}_2}{(p + \tilde{r}_2 / \tilde{x}_2 - x_1 \tilde{r}_1 - u_1) \cdot \hat{u}_2}, \\
\mathcal{J} &= \frac{x_1^{d-3} (p + \tilde{r}_2) \cdot \tilde{r}_1}{(p + \tilde{r}_2 - u_1) \cdot \tilde{r}_1} \frac{(p - x_1 \tilde{r}_1 - u_1) \cdot \tilde{r}_2}{(p - x_1 \tilde{r}_1 - u_1 - u_2) \cdot \tilde{r}_2}.
\end{aligned}$$

Table 4.3.: Rescaling parameters, Jacobians and mapping condition for the double collinear phase space parameterization for final-final and final-initial reference momentum configurations.

actual conditions for the various cases are collected in table 4.3 and 4.4, together with the results for the rescaling parameter, the Jacobian, and the boundaries for the unresolved partons energies. Here, the energy parameterization can also be done in an iterative way. The scaling parameters x_1, z_1 are monotonically decreasing functions of u_1^0 , completely independent of u_2 as a consequence of the additional condition. The rescaling parameter x_2, z_2 in their turn are also monotonically decreasing functions of u_2^0 as soon as u_1 is fixed. As in the triple-collinear case a hierarchy in the unresolved parton energies needs to be imposed. Only the $u_1^0 > u_2^0$ case needs to be considered when adding the contribution with swapped references instead of introducing a parameterization with $u_1^0 < u_2^0$. Evidently this swapping leads to different Born frames if at least one of the references is in the initial state. Since the problem does not arise when the parameterization is done directly in the laboratory frame, this is the reason for the choice of the laboratory frame as starting point.

4. Real radiation contribution

initial-final:

$$\begin{aligned}
(r_1 + p - u_1 - r_2 - u_2)^2 &= (\tilde{r}_1 + p - \tilde{r}_2)^2, & (r_1 + p - u_1)^2 &= (\tilde{r}_1 + p)^2, \\
z_1 &= \frac{(r_1 + p) \cdot (r_1 - u_1)}{p \cdot r_1}, & x_2 &= \frac{(z_1 r_1 + p) \cdot r_2}{(r_1 + p - u_1 - u_2) \cdot (r_2 + u_2)}, \\
z_1 &= \frac{(p - u_1) \cdot \tilde{r}_1}{p \cdot (\tilde{r}_1 + u_1)}, & x_2 &= \frac{(\tilde{r}_1 + p) \cdot \tilde{r}_2 - (\tilde{r}_1/z_1 + p - u_1) \cdot u_2}{(\tilde{r}_1/z_1 + p - u_1 - u_2) \cdot \tilde{r}_2}, \\
(u_1^0)_{\max} &= (1 - \tilde{x}_1) \frac{p \cdot \tilde{r}_1/\tilde{x}_1}{(\tilde{r}_1/\tilde{x}_1 + p) \cdot \hat{u}_1}, & (u_2^0)_{\max} &= \frac{(\tilde{r}_1 + p) \cdot \tilde{r}_2}{(\tilde{r}_1/z_1 + p - u_1) \cdot \hat{u}_2}, \\
\mathcal{J} &= \frac{p \cdot \tilde{r}_1}{(p - u_1) \cdot \tilde{r}_1} \frac{x_2^{d-3} (\tilde{r}_1 + p) \cdot \tilde{r}_2}{(\tilde{r}_1/z_1 + p - u_1 - u_2) \cdot \tilde{r}_2},
\end{aligned}$$

initial-initial:

$$\begin{aligned}
(r_1 + r_2 - u_1 - u_2)^2 &= (\tilde{r}_1 + \tilde{r}_2)^2, & (r_1 + \tilde{r}_2 - u_1)^2 &= (\tilde{r}_1 + \tilde{r}_2)^2, \\
z_2 &= \frac{(r_1 - u_1 - u_2) \cdot (r_2 - u_2)}{(r_1 - u_1) \cdot r_2}, & z_1 &= \frac{(z_2 r_2 - u_1) \cdot (r_1 - u_1)}{z_2 r_2 \cdot r_1}, \\
z_1 &= \frac{(\tilde{r}_2 - u_1) \cdot \tilde{r}_1}{\tilde{r}_2 \cdot (\tilde{r}_1 + u_1)}, & z_2 &= \frac{(\tilde{r}_1/z_1 - u_1 - u_2) \cdot \tilde{r}_2}{(\tilde{r}_1/z_1 - u_1) \cdot (\tilde{r}_2 + u_2)}, \\
(u_1^0)_{\max} &= (1 - \tilde{x}_1) \frac{\tilde{r}_2 \cdot \tilde{r}_1/\tilde{x}_1}{(\tilde{r}_1/\tilde{x}_1 + \tilde{r}_2) \cdot \hat{u}_1}, & (u_2^0)_{\max} &= (1 - \tilde{x}_2) \frac{(\tilde{r}_1/z_1 - u_1) \cdot \tilde{r}_2/\tilde{x}_2}{(\tilde{r}_1/z_1 + \tilde{r}_2/\tilde{x}_2 - u_1) \cdot \hat{u}_2}, \\
\mathcal{J} &= \frac{\tilde{r}_2 \cdot \tilde{r}_1}{(\tilde{r}_2 - u_1) \cdot \tilde{r}_1} \frac{(\tilde{r}_1/z_1 - u_1) \cdot \tilde{r}_2}{(\tilde{r}_1/z_1 - u_1 - u_2) \cdot \tilde{r}_2}.
\end{aligned}$$

Table 4.4.: Rescaling parameters, Jacobians and mapping condition for the double collinear phase space parameterization for initial-final and initial-initial reference momentum configurations.

With this in mind, the energies of the unresolved partons can be parameterized as

$$u_1^0 = (u_1^0)_{\max} \xi_1, \quad u_2^0 = \underbrace{\xi_1 \xi_2 (u_1^0)_{\max}}_{\equiv (u_2^0)_{\max}(u_1, \hat{u}_2)} \min \left[1, \frac{1}{\xi_1} \frac{(u_2^0)_{\max}}{(u_1^0)_{\max}} \right], \quad \xi_{1,2} \in [0, 1]. \quad (4.88)$$

The angular parameterization of u_1 is identical to the single-collinear case, while u_2 is parameterized with respect r_2 , for the first five dimensions and with respect u_1 in all $(-1 - 2\epsilon)$ -dimensional angles.

$$r_1 = r_1^0 \hat{r}_1 = r_1^0 \begin{pmatrix} 1 \\ \hat{\mathbf{r}}_1 \end{pmatrix} \quad \text{with } \hat{\mathbf{r}}_1 = \hat{\mathbf{n}}^{(3-2\epsilon)}(\alpha_1, \alpha_2, \dots), \quad (4.89)$$

$$r_2 = r_2^0 \hat{r}_2 = r_2^0 \begin{pmatrix} 1 \\ \hat{\mathbf{r}}_2 \end{pmatrix} \quad \text{with } \hat{\mathbf{r}}_2 = \hat{\mathbf{n}}^{(3-2\epsilon)}(\beta_1, \beta_2, \dots), \quad (4.90)$$

4.3. Phase Space Parameterization

$$u_1 = u_1^0 \hat{u}_1 = u_1^0 \begin{pmatrix} 1 \\ \hat{\mathbf{u}}_1 \end{pmatrix}$$

with $\hat{\mathbf{u}}_1 = \mathbf{R}_1^{(3-2\epsilon)}(\alpha_1, \alpha_2, \dots) \hat{\mathbf{n}}^{(3-2\epsilon)}(\theta_1, \phi_1, \rho_1, \rho_2, \dots)$,

(4.91)

$$u_2 = u_2^0 \hat{u}_2 = u_2^0 \begin{pmatrix} 1 \\ \hat{\mathbf{u}}_2 \end{pmatrix}$$

with $\hat{\mathbf{u}}_2 = \mathbf{R}_1^{(3-2\epsilon)}(\beta_1, \beta_2, \dots) \mathbf{R}_4^{(3-2\epsilon)}(\rho_2, \rho_3, \dots) \hat{\mathbf{n}}^{(3-2\epsilon)}(\theta_2, \phi_2, \sigma_1, \sigma_2, \dots)$.

(4.92)

For two initial state references the phase space integral over some function $f(r_1, u_1, r_2, u_2)$ reads

$$\begin{aligned} \int dx_1 dx_2 d\Phi_{n+2} \phi_k(x_1) \phi_l(x_2) f(r_1, u_1, r_2, u_2) = \\ \int d\tilde{x} d\mu_0(u_1) d\mu_0(u_2) \theta(u_1, u_2) \phi(\tilde{x}_1/z_1) \theta(z_1 - \tilde{x}_1) \phi(\tilde{x}_2/z_2) \theta(z_2 - \tilde{x}_2) \\ \cdot \mathcal{J} d\Phi_n(\tilde{q}) f(\tilde{r}_1/z_1, u_1, \tilde{r}_2/z_2, u_2) \end{aligned}$$
(4.93)

while for the initial-final configuration it is

$$\begin{aligned} \int dx_1 d\Phi_{n+2} \phi_k(x_1) f(r_1, u_1, r_2, u_2) = \\ \int d\tilde{x}_1 d\mu_0(r_2) d\mu_0(u_1) d\mu_0(u_2) \theta(u_1, u_2) \phi(\tilde{x}_1/z_1) \theta(z_1 - \tilde{x}_1) \mathcal{J} \\ \cdot d\Phi_{n-1}(\tilde{q}) f(\tilde{r}_1/z_1, u_1, x_2 \tilde{r}_2, u_2) \end{aligned}$$
(4.94)

and a corresponding expression of the final-initial case. Finally, the final-final case is given by

$$\begin{aligned} \int d\Phi_{n+2} f(r_1, u_1, r_2, u_2) = \\ \int d\mu_0(r_1) d\mu_0(r_2) d\mu_0(u_1) d\mu_0(u_2) \theta(u_1, u_2) \mathcal{J} d\Phi_{n-1}(\tilde{q}) f(x_1 \tilde{r}_1, u_1, x_2 \tilde{r}_2, u_2) \end{aligned}$$
(4.95)

The function $\theta(u_1, u_2)$ denotes the phase space constraints from the mapping on the unresolved phase space. With the replacement for the angles $\eta_{1,2} = \frac{1}{2}(1 - \cos \theta_{1,2})$ the unresolved phase space can be written as

$$d\mu_0(u_1) d\mu_0(u_2) = \int d\tilde{\mu}_i(u_1) d\tilde{\mu}_i(u_2) \eta_1 \xi_1^4 \eta_2 \xi_2^2$$
(4.96)

with

$$d\tilde{\mu}_i(u_1) d\tilde{\mu}_i(u_2) = \frac{d\eta_1}{\eta_1^{1+\epsilon}} \frac{d\xi_1}{\xi_1^{1+4\epsilon}} \frac{d\eta_2}{\eta_2^{1+2\epsilon}} \frac{d\xi_2}{\xi_2^{1+2\epsilon}} d\tilde{\mu}_{\text{reg}}^1(\{x\}) d\tilde{\mu}_{\text{reg}}^2(\{x\}).$$
(4.97)

The regular parts of the phase space measures read

$$d\tilde{\mu}_{\text{reg}}^1(\{x\}) = \mathcal{N}^\epsilon \int \frac{d^{1-2\epsilon} \Omega(\phi_1, \rho_1, \dots)}{(2\pi)^{1-2\epsilon}} \frac{(u_1^0)_{\text{max}}^2}{(2\pi)^2} \left(\frac{(u_1^0)_{\text{max}}}{\mu_R} \right)^{2\epsilon} (1 - \eta_1)^\epsilon$$
(4.98)

4. Real radiation contribution

$$d\tilde{\mu}_{\text{reg}}^2(\{x\}) = \mathcal{N}^\epsilon \int \frac{d^{1-2\epsilon}\Omega(\phi_2, \sigma_1, \dots)}{(2\pi)^{-2\epsilon}} \frac{(u_2^0)^2}{(2\pi)^2} \left(\frac{(u_2^0)_{\text{max}}}{\mu_R} \right)^{2\epsilon} (1 - \eta_2)^\epsilon. \quad (4.99)$$

Special case with $n = n_{fr} + n_u$ A special situation arises in a double collinear sector when all final state momenta are picked to be reference or unresolved. This system is more constrained than the other cases and it is not possible to apply the new phase space construction in this case, since it is assumed that a boost can be performed to recoil against the reference and unresolved momenta. Therefore, the original parameterization in [217] of this sector is used without any changes and a derivation is omitted here.

Transverse momenta

Splitting functions that occur in subtraction terms depend on the transverse components of the collinear momenta. For the single collinear parameterization the transverse momentum

$$u_\perp^\mu = \begin{pmatrix} 0 \\ \hat{\mathbf{u}}_\perp \end{pmatrix}, \quad \hat{\mathbf{u}}_\perp = \lim_{\theta \rightarrow 0} \frac{\hat{\mathbf{u}} - \hat{\mathbf{r}}}{\|\hat{\mathbf{u}} - \hat{\mathbf{r}}\|} = \left. \frac{\partial \hat{\mathbf{u}}}{\partial \theta} \right|_{\theta=0} \quad (4.100)$$

is constructed. For the double and triple collinear case similarly $u_{i\perp}$ ($i = 1, 2$) are defined

$$u_{i\perp}^\mu = \begin{pmatrix} 0 \\ \hat{\mathbf{u}}_{i\perp} \end{pmatrix}, \quad \hat{\mathbf{u}}_{i\perp} = \lim_{\theta_i \rightarrow 0} \frac{\hat{\mathbf{u}}_i - \hat{\mathbf{r}}_i}{\|\hat{\mathbf{u}}_i - \hat{\mathbf{r}}_i\|} = \left. \frac{\partial \hat{\mathbf{u}}_i}{\partial \theta_i} \right|_{\theta_i=0} \quad (4.101)$$

Additionally, for collinear limits of the two unresolved partons in the triple-collinear sector parameterization a third transverse momentum is necessary. $u_{3\perp}$ is determined through the limit

$$\hat{\mathbf{u}}_{3\perp}^\pm = \lim_{\theta_2 \rightarrow \theta_1^\pm} \frac{\hat{\mathbf{u}}_2 - \hat{\mathbf{u}}_1}{\|\hat{\mathbf{u}}_2 - \hat{\mathbf{u}}_1\|} \quad (4.102)$$

4.4. Subtraction terms

4.4.1. Generation of subtraction terms

All contributions incorporating emissions of one or two particles needs subtraction terms to be numerically accessible. After introducing the partition of unity with the selector function like

$$\int d\Phi_{n+1} = \sum_{ik} \int d\Phi_{n+1} \mathcal{S}_{i,k} \quad \text{or} \quad (4.103)$$

$$\int d\Phi_{n+2} = \sum_{ij} \sum_k \int d\Phi_{n+2} \mathcal{S}_{ij,k} + \sum_{ij} \sum_{kl} \int d\Phi_{n+2} \mathcal{S}_{i,k;j,l} \quad (4.104)$$

and the phase space parameterizations discussed in the previous section, the integrals over the unresolved phase spaces within each sector look like

$$\hat{\sigma}^{R,RV,C1} = \int_0^1 \int_0^1 \frac{d\eta}{\eta^{1+\epsilon}} \frac{d\xi}{\xi^{1+2\epsilon}} d\tilde{\mu} \eta \xi^2 \mathcal{M} F_{n+1} \quad (4.105)$$

in case of the single sector parameterization and

$$\hat{\sigma}^{RR} = \int_0^1 \int_0^1 \int_0^1 \int_0^1 \frac{d\eta_1}{\eta_1^{1+b_1\epsilon}} \frac{d\xi_1}{\xi_1^{1+b_2\epsilon}} \frac{d\eta_2}{\eta_2^{1+b_3\epsilon}} \frac{d\xi_2}{\xi_2^{1+b_4\epsilon}} d\tilde{\mu}_{\text{reg}}^1 d\tilde{\mu}_{\text{reg}}^2 \eta_1^{a_1} \xi_1^{a_2} \eta_2^{a_3} \xi_2^{a_4} \mathcal{M} F_{n+2} \quad (4.106)$$

in case of double- and triple collinear parameterizations. The symbol \mathcal{M} stands for the matrix elements in the different contributions including the selector function, further phase space measures and integrations, convolutions, Jacobians and normalization factors. They contain no divergences not related to the η_i, ξ_i . The measurement function F depends on the full kinematics. In each case the infrared structure of QCD ensures that the combination

$$\mathcal{M}_{\text{reg}} = \prod_i x_i^{a_i} \mathcal{M} \quad (4.107)$$

is a finite quantity in all limits $x_i \rightarrow 0$ where $x_i \in \{\eta_1, \xi_1, \eta_2, \xi_2\}$ or $x_i \in \{\eta, \xi\}$.

The subtraction terms are generated by applying the relation

$$\frac{1}{x^{1+a\epsilon}} = -\frac{1}{a\epsilon} \delta(x) + \left[\frac{1}{x^{1+a\epsilon}} \right]_+ \quad (4.108)$$

where the "+"-prescription is defined by

$$\int_0^1 dx \left[\frac{1}{x^{1+a\epsilon}} \right]_+ f(x) = \int_0^1 dx \frac{f(x) - f(0)}{x^{1+a\epsilon}}. \quad (4.109)$$

In the further discussion the end-point term of the "+"-distribution is called the subtraction term while the δ function part is called the integrated subtraction term or pole term. Applying this formula recursively to the integrals above generates subtraction terms for all divergent limits and a bunch of integrated subtraction terms which themselves need subtraction terms obtained in the same manner. Once there are no singular limits left, this recursion terminates and left are integrals of regularized integrands as well as explicit poles in ϵ times integrals with less integration variables. The procedure is slightly more complicated in case of the real-virtual contribution. The virtual loop integration creates terms whose scaling in the limit $x_i \rightarrow 0$ differ from the naive expectations. Schematically this look as follows

$$\lim_{x \rightarrow 0} f(x) \rightarrow f_0 + x^{-b\epsilon} f_\epsilon \quad (4.110)$$

The prescription for generating subtraction terms needs to be modified to

$$\int_0^1 \frac{dx}{x^{1+a\epsilon}} f(x) = -\frac{1}{a\epsilon} f_0 - \frac{1}{(a+b)\epsilon} f_\epsilon + \int_0^1 \frac{dx}{x^{1+a\epsilon}} \left(f(x) - f_0 - x^{-b\epsilon} f_\epsilon \right). \quad (4.111)$$

Again recursive application of the formula lead to set of integrable expressions.

4.4.2. Subtraction kinematics

In the end-point and pole terms (the subtraction and integrated subtraction terms) one or more variables x_i are set to zero. Besides setting the corresponding variable in the regular

4. Real radiation contribution

Original parameterization			New parameterization		
\mathcal{S}	unresolved config.	number	\mathcal{S}	unresolved config.	number
single	$\{r\}, \{r + u\}$	2	single	$\{r + u\}$	1
triple	double unres. $\{r\}, \{r + u_1\}, \{r + u_1 + u_2\}$ single unres.	3	triple	double unres. $\{r + u_1 + u_2\}$ single unres.	1
\mathcal{S}_1	$\{u_1, r\}, \{u_1, r + u_2\}$	2	\mathcal{S}_1	$\{u_1, r + u_2\}$	1
\mathcal{S}_2	$\{u_1, r\}$	1	$\mathcal{S}_{2,3}$	$\{u_1, r\}/\{u_2, r + u_1\}$	2
\mathcal{S}_3	$\{u_2, r + u_1\}$	1	\mathcal{S}_4	$\{u_1 + u_2, r\}$	1
\mathcal{S}_4	$\{u_1, r\}, \{u_1 + u_2, r\}$	2	\mathcal{S}_5	$\{u_1, r\}, \{u_1 + u_2, r\}$	2
\mathcal{S}_5	$\{u_1, r\}, \{u_1 + u_2, r\},$ $\{u_1 + \text{soft}u_2, r\}$	3	double	double unres. $\{r_1 + u_1, r_2 + u_2\}$ single unres. $\{u_1, r_1, r_2 + u_2\},$ $\{u_2, r_1 + u_1, r_2\},$	1
double	double unres. $\{r_1, r_2\}, \{r_1 + u_1, r_2\},$ $\{r_1 + u_1, r_2 + u_2\}$ single unres. $\{u_1, r_1, r_2\}, \{u_1, r_1, r_2 + u_2\},$ $\{r_1 + u_1, r_2, u_2\}$	3			2

Table 4.5.: Listing of the subtraction kinematics for the original and new phase space parameterization. The notation is discussed in the text.

phase space weights to zero, this changes the kinematic configuration entering the matrix element as well as the measurement function F . Each vanishing of a variable corresponds to a physical limit, which depends on the sector parameterization.

Single-collinear The following limits are obtained, following straightforwardly from the parameterization:

$$\xi \rightarrow 0 \quad \Rightarrow \quad u \rightarrow 0 \quad \{r\} \quad (4.112)$$

$$\eta \rightarrow 0 \quad \Rightarrow \quad u||r \quad \{r + u\} \quad (4.113)$$

the expression in the curly brackets indicates the resolved momenta, omitting the momenta $\{q_i\}$. The special feature of the new parameterization is that the two different looking kinematic configurations are actually the same. Indeed, inspecting the equation in the soft and collinear limit yields (for the final state reference case, initial state analogous)

$$x_{\text{soft}} = \frac{P \cdot (\tilde{r} - 0)}{(P - 0) \cdot \tilde{r}} = 1 \quad \Rightarrow \quad r = \tilde{r} \quad (4.114)$$

$$x_{\text{col.}} = \frac{P \cdot \tilde{r}(1 - \xi)}{P \cdot \tilde{r}} = 1 - \xi \quad \Rightarrow \quad r + u = x_{\text{col.}}\tilde{r} + u = (1 - \xi)\tilde{r} + \xi\tilde{r} = \tilde{r} \quad (4.115)$$

Furthermore, the obtained configuration corresponds to the original Born configuration from which the phase space construction started.

Double- and triple-collinear In the triple- and double-collinear case much more limits are possible, and due to the sector decomposition, different limits arise in different sub-sectors.

There are single and double unresolved subtraction kinematics, with one or two partons become unresolved. Considering the double unresolved kinematics, there are naively three "different" resolved configurations possible

$$\{r + u_1 + u_2\}, \{r + u_1\}, \{r\} \quad (4.116)$$

in triple collinear sectors and also three

$$\{r_1 + u_1, r_2 + u_2\}, \{r_1 + u_1, r_2\}, \{r_1, r_2\} \quad (4.117)$$

in double-collinear sectors. Since soft particles do not influence the kinematics, other configurations are not possible, due to the iterative energy parameterization. It can be shown analogous to the single-collinear case that all these double unresolved limits are the same configuration, which is again the Born configuration from which the construction started. In figure 4.2 the evolution of the momenta when approaching the triple-collinear ($\eta_1 \rightarrow 0$) and the double-soft ($\xi_1 \rightarrow 0$) limit is demonstrated for sector \mathcal{S}_1 .

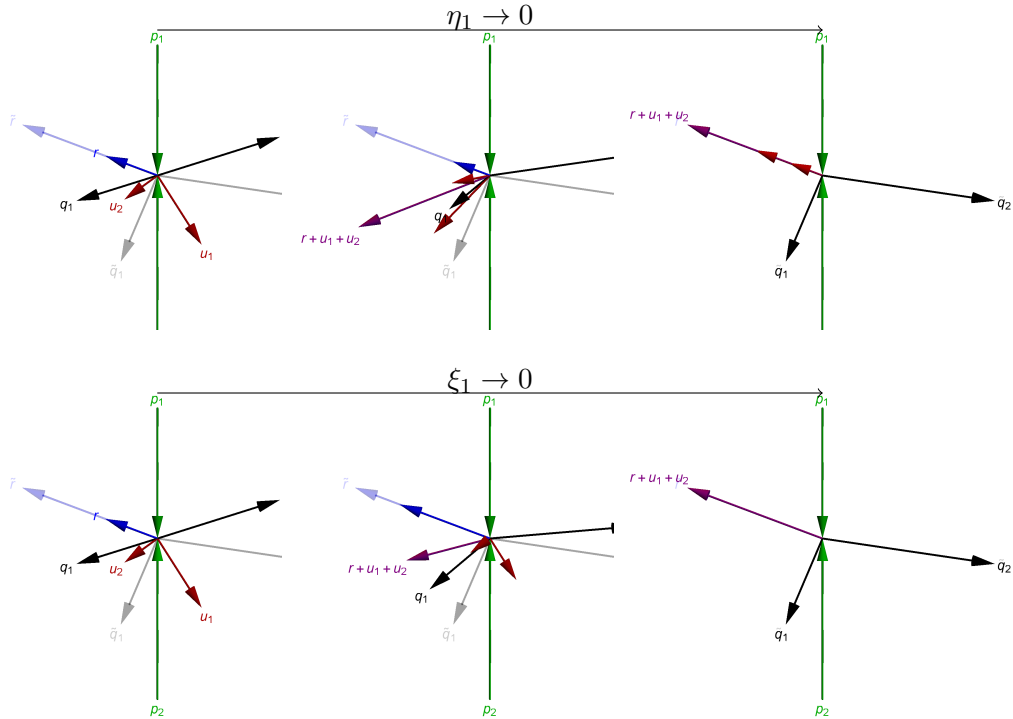


Figure 4.2.: Triple-collinear and double soft limit in sector \mathcal{S}_1 from the same full configuration (left figure). The limit configuration (right figure) is the same and coincides with the underlying Born configuration (grey shaded).

The discussion of the single-unresolved limits depends on the sector. In table 4.5 the list of all single-unresolved configurations is given. The table can be summarized as follows:

- There is only 1 single-unresolved configuration in sectors 1 and 4

4. Real radiation contribution

- There are 2 single-unresolved configurations in sector 2,3 and 5, as well as in the double-collinear sector

That there are two single-unresolved contributions arising in \mathcal{S}_5 originates from the soft u_2 limit. In this case, the angular parameterization of u_2 determines the direction of u_1 . When comparing this with the original parameterization, the number of subtraction kinematics is significantly reduced. Another advantageous feature follows from the fact that there is only one double unresolved configuration across all sectors which coincides with the Born configuration. In the four-dimensional formulation presented below, all contributions containing poles in the regularization parameter ϵ are shifted to contributions which contain doubly unresolved kinematics only. Since there is only one configuration it is possible to fix the Born configuration and check the pole cancellation numerically. While the pole cancellation in the original formulation was also checked numerically, the advantage is that here the integration over Born phase space is not necessary. This results in a strong test of the implementation of the subtraction scheme.

4.4.3. Azimuthal averaging

In collinear limits the generated subtraction terms possibly contain spin-correlations. They are necessary for point-wise convergence of the integrands. However, in the corresponding pole terms the spin correlation is not needed (since the term is not needed as a subtraction) and can be averaged out as demonstrated in [217]. Since the angular parameterization is not changed, the original description how to deal with those splitting functions also applies for the construction presented here. The integral over the correlator can be performed explicitly by

$$\left[\int d^{1-2\epsilon}\Omega \right]^{-1} \int d^{1-2\epsilon}\Omega(\phi, \rho_1, \rho_2, \dots) \frac{u_{\perp}^{\mu} u_{\perp}^{\nu}}{u_{\perp}^2} = \frac{1}{2(1-\epsilon)} \left(g^{\mu\nu} - \frac{r^{\mu} \bar{r}^{\nu} + r^{\nu} \bar{r}^{\mu}}{r \cdot \bar{r}} \right), \quad (4.118)$$

in case of the single collinear parameterization. In case of two unresolved momenta the higher dimensional angles depend on each other, compare definitions (4.67) and (4.92). In the triple collinear limit ($u_1||u_2||r$) or double-collinear limit ($u_1||r_1$ and $u_2||r_2$), the directions can be decoupled using rotational invariance of the measure. Then the same formula for the averaging applies for each parton. In the single collinear limits one can proceed similarly, except in sector \mathcal{S}_4 and \mathcal{S}_5 . There the special treatment of the case $u_1||u_2 \not\parallel r$ presented in [217], has to be performed.

4.5. Four-Dimensional Formulation

Up to here everything was defined and constructed in CDR, by numerical evaluation of the various integrals all contributions are obtained in from of Laurent-series expansions in ϵ . The divergences present cancel among all contributions, which is a consequence of the finiteness of the next-to-next-to-leading order cross-section. However, the situation is not optimal in terms of computational efficiency. With increasing multiplicity the d -dimensional phase space parameterization becomes more and more complicated and number of effective dimensions grows. With the aim of developing a general framework the invocation of a automated generator for tree-level and maybe one-loop matrix-elements is necessary. But the CDR formulation requires the ϵ expansions of matrix elements beyond

ϵ^0 , which are usually not provided in such programs. This motivates a four-dimensional formulation of the scheme, which allows to circumvent the aforementioned bottlenecks.

4.5.1. Separately finite contributions

A crucial step towards a four-dimensional formulation is the identification of combinations of contributions that are finite by themselves. The application of master formula (4.108) to the various contributions yields a vast landscape of different integrals containing suitable subtractions. Everything is defined in d dimensions. Therefore each integral corresponds to Laurent series in ϵ , with poles up to ϵ^{-4} . The sum over all integrals and contributions then yields a finite result in the limit $\epsilon \rightarrow 0$ for any infrared safe observable defined through the measurement function. However, it is possible to organize the integrals in such a way that different subsets are separately finite in d dimensions, in other words, all poles in ϵ cancel among these smaller set of integrals.

At leading order, this statement is trivial since no poles are present at all and $\hat{\sigma}^B$ is finite on its own. At next-to-leading order, the whole construction is formed by three contributions $\hat{\sigma}^R$, $\hat{\sigma}^V$ and $\hat{\sigma}^C$. Only $\hat{\sigma}^R$ needs subtraction, and after application of the master formula, the integrals are organised in two contributions

$$\hat{\sigma}^R = \hat{\sigma}_F^R + \hat{\sigma}_U^R \quad \text{where} \quad (4.119)$$

$$\hat{\sigma}_F^R = \frac{1}{2\hat{s}} \frac{1}{N} \int \left[d\Phi_{n+1} \left\langle M_{n+1}^{(0)} \left| M_{n+1}^{(0)} \right\rangle F_{n+1} + \text{subt. terms with } F_n \right]. \quad (4.120)$$

The integrated subtraction terms are collected in $\hat{\sigma}_U^R$. They are all proportional to the n -particle measurement F_n and due to the specific parameterization one might write them in following form

$$\hat{\sigma}_U^R = \frac{1}{2\hat{s}} \frac{1}{N} \int d\Phi_n \sum_{\text{pole terms}} d\tilde{\mu} [\text{pole terms with } F_n + \text{subt. to pole terms with } F_n] \quad (4.121)$$

The measure $d\tilde{\mu}$ denotes integrations over remaining parameters of the unresolved parton, which depends on the specific sector and pole term. The virtual contribution can also be split up into the finite remainder part and the \mathbf{Z} operator as defined in section 2.1.2. Thus two contributions are obtained:

$$\hat{\sigma}_F^V = \frac{1}{2\hat{s}} \frac{1}{N} \int d\Phi_n 2 \text{Re} \left\langle \mathcal{M}_n^{(0)} \left| \mathcal{F}_n^{(1)} \right\rangle F_n \quad (4.122)$$

$$\hat{\sigma}_U^V = \frac{1}{2\hat{s}} \frac{1}{N} \int d\Phi_n 2 \text{Re} \left\langle \mathcal{M}_n^{(0)} \left| \mathbf{Z}^{(1)} \left| \mathcal{M}_n^{(0)} \right\rangle F_n \right. \right. \quad (4.123)$$

Since $\hat{\sigma}_F^V$ and $\hat{\sigma}_F^R$ are finite by construction and $\hat{\sigma}^C$ is not decomposed further, three separately finite contributions can be identified

$$\hat{\sigma}_F^R, \quad \hat{\sigma}_F^V, \quad \hat{\sigma}_U = \hat{\sigma}_U^R + \hat{\sigma}_U^V + \hat{\sigma}^C. \quad (4.124)$$

One detail to emphasize here is the fact that all contribution with poles in ϵ , e.g. within $\hat{\sigma}_U$, have a n -particle measurement function and n -particle phase space integral, plus possibly further integration over unresolved momenta.

4. Real radiation contribution

The formulation at next-to-next-to-leading order starts with five contributions. The double-real radiation can be organized in three parts, determined by the multiplicity of the resolved particle phase space

$$\hat{\sigma}^{RR} = \hat{\sigma}_F^{RR} + \hat{\sigma}_{SU}^{RR} + \hat{\sigma}_{DU}^{RR}. \quad (4.125)$$

The full $n + 2$ particle phase space integral, together with the corresponding subtraction terms, is contained in the real-radiation finite part $\hat{\sigma}_F^{RR}$

$$\hat{\sigma}_F^{RR} = \frac{1}{2\hat{s}} \frac{1}{N} \int d\Phi_{n+2} \left[\langle \mathcal{M}_{n+2}^{(0)} | \mathcal{M}_{n+2}^{(0)} \rangle F_{n+2} + \text{subt. terms with } F_{n+1} \text{ and } F_n \right] \quad (4.126)$$

which is, as the name suggests, by construction finite and does not contain any poles in ϵ . The other two parts containing poles in ϵ and by adapting the notation from the $\hat{\sigma}_U^R$ case, the single (SU) and double (DU) unresolved double-real-radiation contribution $\hat{\sigma}_{SU}^{RR}$ and $\hat{\sigma}_{DU}^{RR}$ might be written as

$$\hat{\sigma}_{SU}^{RR} = \frac{1}{2\hat{s}} \frac{1}{N} \int d\Phi_{n+1} \sum_{\text{pole terms}} d\tilde{\mu} [\text{pole terms} \times F_{n+1} + \text{subt. with } F_{n+1} \text{ and } F_n], \quad (4.127)$$

$$\hat{\sigma}_{DU}^{RR} = \frac{1}{2\hat{s}} \frac{1}{N} \int d\Phi_n \sum_{\text{pole terms}} d\tilde{\mu} [\text{pole terms} \times F_n + \text{subt. with } F_n]. \quad (4.128)$$

The real-virtual contribution can be split up in a similar manner. It contains the one-loop matrix element which can be decomposed into a finite remainder function and the corresponding divergent part given by the \mathbf{Z} operator

$$2 \text{Re} \langle \mathcal{M}_{n+1}^{(0)} | \mathcal{M}_{n+1}^{(1)} \rangle = 2 \text{Re} \langle \mathcal{M}_{n+1}^{(0)} | \mathcal{F}_{n+1}^{(1)} \rangle + 2 \text{Re} \langle \mathcal{M}_{n+1}^{(0)} | \mathbf{Z}^{(1)} | \mathcal{M}_{n+1}^{(0)} \rangle. \quad (4.129)$$

Generating corresponding subtraction terms yields the following decomposition

$$\hat{\sigma}^{RV} = \hat{\sigma}_F^{RV} + \hat{\sigma}_{SU}^{RV} + \hat{\sigma}_{FR}^{RV} + \hat{\sigma}_{DU}^{RV} \quad (4.130)$$

with

$$\hat{\sigma}_F^{RV} = \frac{1}{2\hat{s}} \frac{1}{N} \int d\Phi_{n+1} \left[2 \text{Re} \langle \mathcal{M}_{n+1}^{(0)} | \mathcal{F}_{n+1}^{(1)} \rangle F_{n+1} + \text{subt. with } F_n \right] \quad (4.131)$$

$$\hat{\sigma}_{SU}^{RV} = \frac{1}{2\hat{s}} \frac{1}{N} \int d\Phi_{n+1} \left[2 \text{Re} \langle \mathcal{M}_{n+1}^{(0)} | \mathbf{Z}^{(1)} | \mathcal{M}_{n+1}^{(0)} \rangle F_{n+1} + \text{subt. with } F_n \right] \quad (4.132)$$

$$\hat{\sigma}_{FR}^{RV} = \frac{1}{2\hat{s}} \frac{1}{N} \int d\Phi_n \sum_{\text{pole terms with } |\mathcal{F}_n^{(1)}\rangle} d\tilde{\mu} [\text{pole terms} \times F_n + \text{subt. with } F_n] \quad (4.133)$$

$$\hat{\sigma}_{DU}^{RV} = \frac{1}{2\hat{s}} \frac{1}{N} \int d\Phi_n \sum_{\text{pole terms with } |\mathcal{M}_n^{(0)}\rangle} d\tilde{\mu} [\text{pole terms} \times F_n + \text{subt. with } F_n] \quad (4.134)$$

The reason for distinguishing $\hat{\sigma}_{DU}^{RV}$ and $\hat{\sigma}_{FR}^{RV}$ becomes evident in the discussion of separately finite contributions. Here all contributions except $\hat{\sigma}_F^{RV}$ contain poles in ϵ .

The double virtual contribution is treated similarly to the virtual contribution. In this

case one finite ($\hat{\sigma}_F^{VV}$) and two ϵ pole containing contributions are formed

$$\hat{\sigma}_F^{VV} = \frac{1}{2\hat{s}} \frac{1}{N} \int d\Phi_n \left[2 \operatorname{Re} \langle \mathcal{M}_n^{(0)} | \mathcal{F}_n^{(2)} \rangle + \langle \mathcal{F}_n^{(1)} | \mathcal{F}_n^{(1)} \rangle \right] F_n , \quad (4.135)$$

$$\hat{\sigma}_{FR}^{VV} = \frac{1}{2\hat{s}} \frac{1}{N} \int d\Phi_n \left[2 \operatorname{Re} \langle \mathcal{M}_n^{(0)} | (\mathbf{Z}^{(1)\dagger} + \mathbf{Z}^{(1)}) | \mathcal{M}_n^{(0)} \rangle \right] F_n , \quad (4.136)$$

$$\hat{\sigma}_{DU}^{VV} = \frac{1}{2\hat{s}} \frac{1}{N} \int d\Phi_n \left[2 \operatorname{Re} \langle \mathcal{M}_n^{(0)} | \mathbf{Z}^{(2)} | \mathcal{M}_n^{(0)} \rangle + \langle \mathcal{M}_n^{(0)} | \mathbf{Z}^{(1)\dagger} \mathbf{Z}^{(1)} | \mathcal{M}_n^{(0)} \rangle \right] F_n . \quad (4.137)$$

The single convolution contribution $\hat{\sigma}^{C1}$ splits into two part after applying the decomposition for $\hat{\sigma}^R$

$$\hat{\sigma}^{C1} = \hat{\sigma}_{SU}^{C1} + \hat{\sigma}_{DU}^{C1} \quad (4.138)$$

where $\hat{\sigma}_{SU}^{C1}$ contains $\hat{\sigma}_F^R$ while $\hat{\sigma}_{DU}^{C1}$ keeps $\hat{\sigma}_U^R$. However, both contributions contain however divergences in ϵ . The double convolution contribution contains double convolutions over tree-level matrix-elements as well as single convolutions over one-loop virtual contributions. The decomposition of $\hat{\sigma}^V$ is applied and all terms containing the finite remainder function $|\mathcal{F}^{(1)}\rangle$ are put into $\hat{\sigma}_{FR}^{C2}$, and all those without it into $\hat{\sigma}_{DU}^{C2}$. Both parts have explicit poles ϵ and are proportional to the n -particle measurement function.

By construction three contributions can be easily identified to be separately finite:

$$\hat{\sigma}_F^{RR} , \quad \hat{\sigma}_F^{RV} , \quad \hat{\sigma}_F^{VV} . \quad (4.139)$$

As the next-to-next-to-leading order cross-section is also finite, it can be concluded that all remaining parts together have to be finite in d dimensions

$$\hat{\sigma}_{DU} + \hat{\sigma}_{SU} + \hat{\sigma}_{FR} = \text{finite} \quad (4.140)$$

with the definitions

$$\hat{\sigma}_{FR} = \hat{\sigma}_{FR}^{RV} + \hat{\sigma}_{FR}^{VV} + \hat{\sigma}_{FR}^{C2} , \quad (4.141)$$

$$\hat{\sigma}_{SU} = \hat{\sigma}_{SU}^{RR} + \hat{\sigma}_{SU}^{RV} + \hat{\sigma}_{SU}^{C1} , \quad (4.142)$$

$$\hat{\sigma}_{DU} = \hat{\sigma}_{DU}^{RR} + \hat{\sigma}_{DU}^{RV} + \hat{\sigma}_{DU}^{C1} + \hat{\sigma}_{DU}^{VV} + \hat{\sigma}_{DU}^{C2} . \quad (4.143)$$

Further, it can be argued that σ_{FR} has to be finite separately. As discussed above in the σ_{FR}^c (with $c \in \{RV, VV, C2\}$) contributions appear only term with one-loop finite-remainder matrix-elements. One can easily convince one-self that the only way they arise they give the same terms as the next-to-leading order contribution $\hat{\sigma}_U$ with the replacement

$$\langle \mathcal{M}_n^{(0)} | \mathcal{M}_n^{(0)} \rangle \rightarrow 2 \operatorname{Re} \langle \mathcal{M}_n^{(0)} | \mathcal{F}_n^{(1)} \rangle . \quad (4.144)$$

In this sense $\hat{\sigma}_{FR}^{RV}$ corresponds to $\hat{\sigma}_U^R$, $\hat{\sigma}_{FR}^{VV}$ to $\hat{\sigma}_U^V$ and $\hat{\sigma}_{FR}^{C2}$ to $\hat{\sigma}^C$. The functional dependence of the n -particle matrix-elements (at least after azimuthal averaging) does not influence the finiteness of the next-to-leading order cross-section. This only depends on the unresolved integrals over the soft and splitting functions, as well explicit poles from the virtual contribution. Therefore the finiteness of the next-to-leading order cross-section implies the finiteness of σ_{FR} . The mechanism behind this argument can be made more ob-

4. Real radiation contribution

vious with the new phase space parameterization. Since there is only one fully unresolved configuration the cancellation in $\hat{\sigma}_U$ happens for a fixed Born configuration. For fixed Born momenta all the matrix elements across all contributions are just the same number (or to be more precise, an expansion in ϵ with constant coefficients) which could be taken out of the contributions, without spoiling the pole cancellation. The same holds for the n -particle finite remainder functions appearing in $\hat{\sigma}_{FR}$. A detailed discussion can be found in [217].

This leaves $\hat{\sigma}_{DU} + \hat{\sigma}_{SU}$ as a finite quantity in d dimensions. As discussed at the end of this section, a four-dimensional formulation would yield four-dimensional resolved momenta and polarizations. Its not possible to go to four-dimensions directly, since $\hat{\sigma}_{SU}$ contains inclusive d -dimensional phase space integrals over the resolved additional radiation. The terms of order up to $\mathcal{O}(\epsilon^2)$ of this integral contribute to the finite part of the cross section as long as the poles in $\hat{\sigma}_{SU}$ do not cancel separately. Consequently, a direct four dimensional limit would yield wrong and not even finite quantities. However, as demonstrated in [217], it is possible to construct special counter terms that allow to render $\hat{\sigma}_{SU}$ and $\hat{\sigma}_{DU}$ separately finite. The construction of the counter terms depends on the specific choice of the phase space parameterization. Since a different phase space parameterization is employed, new counter terms need to be calculated (see section 4.6).

Assuming for now that a set of terms exists, such that

$$\hat{\sigma}_{\tilde{S}U} = \hat{\sigma}_{SU} - \hat{\sigma}_{HV} \quad \text{and} \quad (4.145)$$

$$\hat{\sigma}_{\tilde{D}U} = \hat{\sigma}_{DU} + \hat{\sigma}_{HV} \quad (4.146)$$

are separately finite and the HV regularization can be finally constructed.

In the HV regularization scheme all resolved momenta and polarizations are taken to be four dimensional, in contrast to d dimensions in CDR. This has a number of non-trivial consequences. It has to be ensured that the finite result, hence the ϵ^0 coefficient of the sum over all contributions is correct. The HV scheme will introduce errors at $\mathcal{O}(\epsilon)$ in the final result, which are, however, not of interest for physical predictions. The first thing to note is, that for four-dimensional polarizations all tree-level matrix elements have no expansions in ϵ , since the dependence can only enter through spin sums of external particles. In case of finite remainder functions this is not so easy anymore since virtual integrations also introduce an ϵ dependence. That terms of the finite remainder functions of order ϵ or higher are not necessary to correctly calculate the ϵ^0 is discussed below. The second thing is a modification of the phase space due to the four-dimensional resolved momenta, which schematically will lead to a partially four dimensional resolved phase space and a partially d -dimensional phase space wherever unresolved momenta appear.

All contributions which do not contain poles in ϵ , namely

$$\hat{\sigma}^B, \hat{\sigma}_F^R, \hat{\sigma}_F^V, \hat{\sigma}_F^{RR}, \hat{\sigma}_F^{RV}, \hat{\sigma}_F^{VV}, \quad (4.147)$$

can simply be evaluated for $\epsilon = 0$ and immediately yield the correct ϵ^0 results. All contributions that contain only F_n measurement functions as well as poles in ϵ are

$$\hat{\sigma}_U, \hat{\sigma}_{FR}, \hat{\sigma}_{DU}. \quad (4.148)$$

The ϵ expansion of the matrix elements can be dropped, since the cancellation of the ϵ -poles in each contribution does not depend on the functional dependence on the kinematics of the amplitudes, but rather on the unresolved phase space integrals over factorization formulae

4.5. Four-Dimensional Formulation

and the form of $\mathbf{Z}^{(1,2)}$, similar to the discussion of finiteness of $\hat{\sigma}_{FR}$. Another way to see this is that phase space parameterization results in a unique Born configuration, independent of unresolved phase space integrals and across all sectors. Since the F_n measurement function could be used to single out a specific Born configuration, the finiteness of the cross-section implies that for each Born configuration the poles have to cancel (after integration over unresolved degrees of freedom) within each separately finite contribution. But for a specific Born configuration the n -particle matrix-elements are fixed numbers (or expansions in ϵ with constant coefficients), which cannot influence the pole cancellation. Indeed the dropped terms would add up to zero at ϵ^0 as long as the poles cancel. Removing the ϵ terms of the matrix elements corresponds to four dimensional polarizations. The four-dimensional momenta are obtained using a modified measurement function

$$F_n \rightarrow F_n \mathcal{N}^{-(n-1)\epsilon} \left[\prod_{i=1}^{n-1} (2\pi)^{-2\epsilon} \delta^{(-2\epsilon)}(q_i) \right] \quad (4.149)$$

which sets all resolved momenta to four dimensions after performing the integrals over the δ functions. In case of no or only initial state references this idea directly applies. In case of final state references, it is not the reference alone which appears in the δ function but rather the resolved momentum combination which amounts to

$$\text{single-collinear sectors: } \delta^{(-2\epsilon)}(r+u) = (r^0+u^0)^{2\epsilon} \delta^{(-2\epsilon)}(\hat{r}), \quad (4.150)$$

$$\text{triple-collinear sectors: } \delta^{(-2\epsilon)}(r+u_1+u_2) = (r^0+u_1^0+u_2^0)^{2\epsilon} \delta^{(-2\epsilon)}(\hat{r}), \quad (4.151)$$

$$\text{double-collinear sectors: } \prod_{i=1,2} \delta^{(-2\epsilon)}(r_i+u_i) = \prod_{i=1,2} (r_i^0+u_i^0)^{2\epsilon} \delta^{(-2\epsilon)}(\hat{r}_i). \quad (4.152)$$

While the direction of the reference are restricted to four dimensions, the energy factor together with the factor $(r^0)^{(-2\epsilon)}$ from the phase space measure of the reference parton give rise to a non-trivial ϵ depending factor which needs to be included. Since the form of the measurement function does not affect the pole cancellation, the replacement in equation (4.149) does not change the finite result at ϵ^0 since removed integrals are at least of order ϵ and thus vanish in the limit $\epsilon \rightarrow 0$.

The contribution $\hat{\sigma}_{SU}$ is slightly more involved since here two different types of matrix elements appear: n and $n+1$ particle ones. The complication arise due to the subtraction terms which consist of factorization formula for d dimensional matrix-elements. If the resolved parton, whose soft and collinear limits are regularized by these factorization formula, is set to four dimensions using the replacement (4.149) the factorization formula do not match anymore. This can be circumvented by evaluating the factorization formula at $\epsilon = 0$. This is straight-forward in case of $\hat{\sigma}_{SU}^{RV}$ and $\hat{\sigma}_{SU}^{C1}$. Both contributions are simply evaluated with a four-dimensional phase space and four-dimensional matrix-elements (and four-dimensional factorization formula). In case of $\hat{\sigma}_{SU}^{RR}$ it is important to note that the splitting function arising from taking a pole has still to be treated in d dimensions since it belongs to the limit of the still unresolved momentum which is not affected by the replacement (4.149). The subtraction terms to these terms on the other hand need to be evaluated at $\epsilon = 0$ since those belong to limit of the four dimensional momentum. This triple-collinear limit is an iterated one and thus the triple-collinear splitting function factorizes into the product of two splitting functions. Similar to the previous case, the δ functions appearing in replacement might contain combinations of reference and unre-

4. Real radiation contribution

Sector(pole)	δ -function	energy factor
triple collinear:		
$\mathcal{S}_1(\eta_1)$	$\delta^{(-2\epsilon)}(r + u_2)\delta^{(-2\epsilon)}(u_1)$	$(r^0 + u_2^0)^{2\epsilon}(u_1^0)^{2\epsilon}$
$\mathcal{S}_{23}(\eta_2)$	$\delta^{(-2\epsilon)}(r + u_1)\delta^{(-2\epsilon)}(u_2)$	$(r^0 + u_1^0)^{2\epsilon}(u_2^0)^{2\epsilon}$
$\mathcal{S}_4(\eta_1)$	$\delta^{(-2\epsilon)}(r)\delta^{(-2\epsilon)}(u_1 + u_2)$	$(r^0)^{2\epsilon}(u_1^0 + u_2^0)^{2\epsilon}$
$\mathcal{S}_5(\eta_2)$	$\delta^{(-2\epsilon)}(r)\delta^{(-2\epsilon)}(u_1 + u_2)$	$(r^0)^{2\epsilon}(u_1^0 + u_2^0)^{2\epsilon}$
$\mathcal{S}_i(\xi_2) i \in \{1, 23, 4, 5\}$	$\delta^{(-2\epsilon)}(r)\delta^{(-2\epsilon)}(u_1)$	$(r^0)^{2\epsilon}(u_1^0)^{2\epsilon}$
double collinear		
(η_1)	$\delta^{(-2\epsilon)}(r_1 + u_1)\delta^{(-2\epsilon)}(r_2)\delta^{(-2\epsilon)}(u_2)$	$(r_1^0 + u_1^0)^{2\epsilon}(r_2^0)^{2\epsilon}(u_2^0)^{2\epsilon}$
(η_2)	$\delta^{(-2\epsilon)}(r_1)\delta^{(-2\epsilon)}(r_2)\delta^{(-2\epsilon)}(u_1)$	$(r_1^0)^{2\epsilon}(r_2^0 + u_2^0)^{2\epsilon}(u_1^0)^{2\epsilon}$
(ξ_2)	$\delta^{(-2\epsilon)}(r_1)\delta^{(-2\epsilon)}(r_2 + u_2)\delta^{(-2\epsilon)}(u_1)$	$(r_1^0)^{2\epsilon}(r_2^0)^{2\epsilon}(u_1^0)^{2\epsilon}$

Table 4.6.: Energy factors arising from -2ϵ -dimensional delta function in $\hat{\sigma}_{SU}^{RR}$.

solved momenta if the reference is in the final state. Which combination arises depends on the sector and the pole taken to end up in $\hat{\sigma}_{SU}^{RR}$, but they lead to similar expressions as in (4.152). They are listed in table 4.6

A last remark on the number of dimensions for the unresolved phase spaces should be made. In collinear poles the integration over the angles of the collinear parton can be performed analytically since nothing depends on them. One has to be careful in some cases arising in the σ^{RR} , since the angular parameterization of u_1 and u_2 is not fully independent. In these cases one has to decouple them. In case of soft limits this situation is different since scalar products between the resolved and the unresolved partons depend on their angles beyond four dimensions. If there is only one soft non-collinear parton, there is an additional fifth dimension to be integrated over. In case of double-soft, non-collinear limits, a sixth dimension needs to be taken into account.

4.6. 't Hooft-Veltman Corrections

The discussion of the 't Hooft-Veltman regularization relied on the assumption that it is possible to identify or construct a set of corrections $\hat{\sigma}_{HV}$ such that

$$\hat{\sigma}_{SU,HV} = \hat{\sigma}_{SU} - \hat{\sigma}_{HV} = \text{finite} , \quad (4.153)$$

$$\hat{\sigma}_{DU,HV} = \hat{\sigma}_{DU} + \hat{\sigma}_{HV} = \text{finite} . \quad (4.154)$$

Indeed it is possible to formulate an algorithmic approach which generates such a set of corrections. This set, or distinct terms inside the set, will be called 't Hooft-Veltman corrections. The algorithm presented below is in a certain sense independent of the exact details of phase space parameterization as long as some general assumptions about the parameterization hold. The details of this assumptions become clear during the derivation. The way separately finite SU and DU contributions are obtained is completely different and independent from that presented in [217]. After outlining the general idea the 't Hooft-Veltman corrections for the parameterization, presented in section 4.3, are derived.

4.6.1. Measurement function based approach

The approach of generating the correction terms will make extensive use of the measurement function F_m . Assume that the next-to-next-to-leading order measurement function F appearing in all the contributions is replaced by a next-to-leading order measurement function which would have the property $F_{n+1} \neq 0$ and $F_n = 0$. Obviously, this would render $\hat{\sigma}_{DU}$ and $\hat{\sigma}_{FR}$ to zero since they are proportional to F_n . This also implies, through the finiteness of the next-to-leading order cross section that $\hat{\sigma}_{SU}$ has to be finite. Indeed $\hat{\sigma}_{SU}$ then corresponds to contributions of a next-to-leading order calculation with a $n + 1$ particle Born process:

$$\hat{\sigma}_{SU}^{RU} \rightarrow \hat{\sigma}_U^R, \quad \hat{\sigma}_{SU}^{RV} \rightarrow \hat{\sigma}_U^V, \quad \hat{\sigma}_{SU}^{C1} \rightarrow \hat{\sigma}^C. \quad (4.155)$$

The contributions $\hat{\sigma}_U^R, \hat{\sigma}_U^V$ and $\hat{\sigma}^C$ may be written in the following form

$$\hat{\sigma}_U^V = \int d^d \Phi_{n+1} \mathcal{I}_{n+1}^V F_{n+1} \quad (4.156)$$

$$\hat{\sigma}^C = \int d^d \Phi_{n+1} \mathcal{I}_{n+1}^C F_{n+1} \quad (4.157)$$

$$\hat{\sigma}_U^R = \sum_{\text{pole terms}} \int d^d \Phi_{n+1} \mathcal{I}_{n+1}^R F_{n+1}. \quad (4.158)$$

The sum in the $\hat{\sigma}_U^R$ case is performed over all sectors and all pole terms therein. That the phase space integral Φ_{n+1} can factorized out in real emission case, is a non trivial statement and one requirement on the phase space parameterization. In case of the proposed parameterization this feature can easily achieved, details follow in the next section. The integrands \mathcal{I}_{n+1}^c are quite different. In case of \mathcal{I}_{n+1}^V the expression can be obtained from the $\mathbf{Z}^{(1)}$ operator. The essential point here is that \mathcal{I}_{n+1}^V are only the explicit poles given in expression (2.29) together with d dimensional (color-correlated) matrix-elements. If one would expand \mathcal{I}_{n+1}^V in ϵ while keeping the matrix-elements unexpanded, the series would terminate at $\mathcal{O}(\epsilon^{-1})$:

$$\mathcal{I}_{n+1}^V = \frac{\mathcal{I}_{n+1}^{V(-2)}}{\epsilon^2} + \frac{\mathcal{I}_{n+1}^{V(-1)}}{\epsilon}. \quad (4.159)$$

The convolution integrand \mathcal{I}_{n+1}^C contains an explicit pole in ϵ while the only other ϵ dependent term is the scale ratio $(\mu_R^2/\mu_F)^{\epsilon}$. An expansion in ϵ could be written as

$$\mathcal{I}_{n+1}^C = \frac{\mathcal{I}_{n+1}^{C(-1)}}{\epsilon} + \mathcal{I}_{n+1}^{C(0)} + \mathcal{O}(\epsilon) \quad (4.160)$$

the coefficients $\mathcal{I}_{n+1}^{C(i)}$ still contain the convolution integrals over z and unexpanded d -dimensional matrix-elements. Note that the coefficient $\mathcal{I}_{n+1}^{C(0)}$ is proportional to $\ln(\mu_R^2/\mu_F^2)$ and vanishes if both scales are chosen to be the same.

The integrand \mathcal{I}_{n+1}^R is slightly more complicated. Due to sector decomposition, this term is build up from pole terms from possibly many different sectors indicated by the unspecified sum in front. It includes the selector functions, factorization formulae and (color-correlated) $n + 1$ particle matrix elements. In addition, there might be further phase

4. Real radiation contribution

space integrations over the unresolved momentum. The pole terms come with explicit poles in ϵ , which might reach ϵ^{-2} . In each sector the integrand \mathcal{I}_{n+1}^R could be written as

$$\mathcal{I}_{n+1}^R = \frac{\mathcal{I}_{n+1}^{R(-2)}}{\epsilon^2} + \frac{\mathcal{I}_{n+1}^{R(-1)}}{\epsilon} + \mathcal{I}_{n+1}^{R(0)} + \mathcal{O}(\epsilon). \quad (4.161)$$

Here again the d dimensional matrix elements are not expanded. However, the factorization formula generated by writing these terms down are expanded in ϵ , as well as the unresolved phase space integral $d\tilde{\mu}$.

The matrix-elements are kept d -dimensional because in case of the next-to-next-to-leading order calculation a further parton can be unresolved and the full d -dimensional factorization formula are needed in order to not modify the finite part with the 't Hooft-Veltman corrections. As argued before, the finiteness of the next-to-leading order cross-section implies that the pole cancellation does not depend on some special dependence on the kinematics of the matrix elements, and therefore pole cancellation, also hold without taking their expansion in ϵ into account. The statement of finiteness of the next-to-leading order cross-section can now be phrased in the following way

$$\sum_c \int d\Phi_{n+1} \left[\frac{\mathcal{I}_{n+1}^{c(-2)}}{\epsilon^2} + \frac{\mathcal{I}_{n+1}^{c(-1)}}{\epsilon} \right] F_{n+1} \equiv \sum_c \mathcal{I}^c = 0 \quad (4.162)$$

where $c \in \{R, V, C\}$. The sum over different sectors in the R case is implicit. The NNLO case with a next-to-leading order measurement function can be recovered by replacing $R \rightarrow RR$, $V \rightarrow RV$ and $C \rightarrow C1$. There is no difference in the structure, nor changes in the argumentation in that case.

Parameterized measurement function Before returning to the next-to-next-to-leading order case, a tool in form of a parameterized measurement needs to be introduced. Let F_{n+1}^α be a family of measurement functions with the following properties:

- Like all measurement functions it has to be infrared safe.
- If $\alpha \neq 0$ then $F_n^\alpha \equiv 0$, while for $\alpha = 0$, F_n^0 can be any measurement function. In other words, $\alpha \neq 0$ corresponds to a next-to-leading order calculation within a next-to-next-to-leading order calculation, a general next-to-next-to-leading order calculation otherwise.

There are various ways to define an explicit measurement functions which fulfills these properties. However, the following form allows for a simple construction of the 't Hooft-Veltman corrections. The explicit form is motivated by phase space slicing methods. In order to distinguish a $n+1$ and n particle configurations, a set of global infrared sensitive observables is introduced. Here the variables used are the minimum angle between any partons and the minimal energy-fraction of any parton with respect to some arbitrary energy-scale E_{norm}

$$\alpha_\eta = \min_{i,j} \eta_{ij}, \quad \text{with} \quad \eta_{ij} = \frac{1}{2} (1 - \cos \theta_{ij}), \quad (4.163)$$

$$\alpha_\xi = \min_i \xi_i, \quad \text{with} \quad \xi_i = \frac{p_i^0}{E_{\text{norm}}}, \quad (4.164)$$

are used, i, j run over all resolved momenta entering the measurement function. The parameterized measurement function can then be implemented as

$$F_{n+1}^\alpha = F_{n+1} \theta(\alpha_\eta - \alpha) \theta(\alpha_\xi - \alpha) \equiv F_{n+1} \theta_\eta \theta_\xi \quad (4.165)$$

with the usual Heaviside function θ and a usual measurement function F_{n+1} . For $\alpha \neq 0$ this is a well-defined next-to-leading order measurement function and a proper next-to-next-to-leading order measurement function for $\alpha = 0$ which is inherited from F_{n+1} .

Identification of 't Hooft-Veltman corrections Using the parameterized measurement function the finiteness of the next-to-leading order statement becomes

$$\sum_c \int d\Phi_{n+1} \left[\frac{\mathcal{I}_{n+1}^{c(-2)}}{\epsilon^2} + \frac{\mathcal{I}_{n+1}^{c(-1)}}{\epsilon} \right] F_{n+1} \theta(\alpha_\eta - \alpha) \theta(\alpha_\xi - \alpha) \equiv \sum_c \mathcal{I}^c = 0. \quad (4.166)$$

Returning to the full next-to-next-to-leading order case the structure of the contributions $\hat{\sigma}_{SU}^c$ becomes slightly more complicated. Mainly, due to the presence of further subtraction terms needed for the additional infrared limits which are now allowed again. The subtraction terms are valid for each term in the ϵ expansion such that the contribution can be written as

$$\begin{aligned} \hat{\sigma}_{SU}^c &= \int d^d\Phi_{n+1} [\mathcal{I}_{n+1}^c F_{n+1} + \mathcal{I}_n^c F_n] \quad (4.167) \\ &= \int d^d\Phi_{n+1} \left\{ \left[\frac{\mathcal{I}_{n+1}^{c(-2)}}{\epsilon^2} + \frac{\mathcal{I}_{n+1}^{c(-1)}}{\epsilon} + \mathcal{I}_{n+1}^{c(0)} \right] F_{n+1} + \left[\frac{\mathcal{I}_n^{c(-2)}}{\epsilon^2} + \frac{\mathcal{I}_n^{c(-1)}}{\epsilon} + \mathcal{I}_n^{c(0)} \right] F_n \right\}. \quad (4.168) \end{aligned}$$

The factorization formulae arising from the limits of the d -dimensional $n+1$ matrix elements in $\mathcal{I}_{n+1}^{c(i)}$ coefficients are also kept unexpanded in the corresponding $\mathcal{I}_n^{c(i)}$ terms. Lets investigate the difference $\hat{\sigma}_{SU}^c - \mathcal{I}^c$. Reshuffling the different terms one finds

$$\hat{\sigma}_{SU}^c - \mathcal{I}^c = \int d^d\Phi_{n+1} \left[\frac{\mathcal{I}_{n+1}^{c(-2)} F_{n+1} + \mathcal{I}_n^{c(-2)} F_n}{\epsilon^2} + \frac{\mathcal{I}_{n+1}^{c(-1)} F_{n+1} + \mathcal{I}_n^{c(-1)} F_n}{\epsilon} \right] (1 - \theta_\eta \theta_\xi) \quad (4.169)$$

$$+ \int d^d\Phi_{n+1} [\mathcal{I}_{n+1}^{c(0)} F_{n+1} + \mathcal{I}_n^{c(0)} F_n] + \int d^d\Phi_{n+1} \left[\frac{\mathcal{I}_n^{c(-2)}}{\epsilon^2} + \frac{\mathcal{I}_n^{c(-1)}}{\epsilon} \right] F_n \theta_\eta \theta_\xi \quad (4.170)$$

$$\equiv Z^c(\alpha) + C^c + N^c(\alpha). \quad (4.171)$$

Nothing happened except reordering different terms. However, the functions $Z^c(\alpha)$, C^c and $N^c(\alpha)$ have some remarkable properties. Firstly, C^c does not depend on the parameter α at all and it does not contain any poles in ϵ . Secondly, $Z^c(\alpha)$ consist of a phase space integral over an integrable function times the factor $(1 - \theta_\eta \theta_\xi)$ which restricts the phase space domain. If α now would tend to zero, the integration volume and therefore $Z^c(\alpha)$ vanish, i.e. $\lim_{\alpha \rightarrow 0} Z^c(\alpha) = 0$. All contributions to poles in ϵ that do not vanish in the

4. Real radiation contribution

limit $\alpha \rightarrow 0$ are located in the function

$$N^c(\alpha) = \int d^d\Phi_{n+1} \left[\frac{\mathcal{I}_n^{c(-2)}}{\epsilon^2} + \frac{\mathcal{I}_n^{c(-1)}}{\epsilon} \right] F_n \theta_\eta \theta_\xi \quad (4.172)$$

The phase space integral over $d\Phi_{n+1}$ contains the integration over the angle and energy variables η and ξ of an unresolved momentum which give rise to divergences, which are regulated by α . The integrals are all of the form

$$\int_0^1 \frac{dx}{x^{1+a\epsilon}} \theta(x - f\alpha). \quad (4.173)$$

Thus the integration gives rise to logarithms of the parameter α , similar to those in slicing methods, and N^c can be expressed as a power log series

$$N^c(\alpha) = \sum_{k=0}^{l_{\max}} \ln^k(\alpha) N_k^c(\alpha). \quad (4.174)$$

where the coefficients $N_k^c(\alpha)$ are regular functions in α . In particular, the limit $\lim_{\alpha \rightarrow 0} N_k^c(\alpha)$ must exist.

For the complete single unresolved contribution $\hat{\sigma}_{SU}$ the following rearrangement can be made:

$$\hat{\sigma}_{SU} = \hat{\sigma}_{SU} - \underbrace{\sum_c \mathcal{I}^c}_{=0} = \sum_c (\hat{\sigma}_{SU}^c - \mathcal{I}^c) = \sum_c (Z^c(\alpha) + C^c + N^c(\alpha)) \quad (4.175)$$

Since the left-hand side of this equation does not depend on α , also the right-hand side has to be independent of α . The $Z^c(\alpha)$ are regular functions of α ; in particular they vanish in the limit $\alpha \rightarrow 0$. This leads to the conclusion that the logarithms appearing in expression 4.174 have to cancel across the different contributions c . Therefore all terms proportional to a logarithm can be safely removed and an expression arises where the limit $\alpha \rightarrow 0$ can be performed safely. In this limit only

$$\sum_c N_0^c(0) \equiv \hat{\sigma}_{HV} \quad (4.176)$$

remains. After subtracting $\hat{\sigma}_{HV}$ from $\hat{\sigma}_{SU}$, all poles are removed and finite quantity is obtained. Adding them back to $\hat{\sigma}_{DU}$, which is possible since $\hat{\sigma}_{HV}$ is also proportional to F_n , yields the two separately finite contributions

$$\hat{\sigma}_{SU,HV} = \hat{\sigma}_{SU} - \hat{\sigma}_{HV} \text{ and } \hat{\sigma}_{DU,HV} = \hat{\sigma}_{DU} + \hat{\sigma}_{HV}. \quad (4.177)$$

This evaluation has to be done completely in d dimensions. However after this procedure the 't Hooft-Veltman regularization discussed in the previous section can be applied. The last missing pieces are the functions $N_0^c(0)$. Their form depends on the parameterization and the explicit form of the θ function used. For the specific choice for θ in equation (4.165) and the phase space parameterization their derivation can be found in the next section.

4.6.2. Calculation of 't Hooft-Veltman corrections

In order to obtain $N_0^c(0)$, the integrals in $N^c(\alpha)$ over the angle and energy of the unresolved parton have to be evaluated, whose limits are regulated by the θ step functions. Fortunately, the integrands are end-point subtraction terms generated through the master formula. Therefore the subtraction term $f(0)$ for variable x depends only trivially on x through the denominator. The minimum condition in the definition (4.164) needs some additional discussion, since the step functions are not affected by the plus description. It is essential that only the relevant angle and energy fraction in each sector give rise to a non vanishing contribution in the limit $\alpha \rightarrow 0$. This is true since all other singular limits, i.e. $\eta_{ij} \rightarrow 0$ and/or $\xi_i \rightarrow 0$ with $i \neq u$ and $j \neq r$, are regulated by the selector function. Thus they give a contribution $\sim \alpha$ after integration which can therefore be neglected and the α_η and α_ξ variables adapt to the relevant expression in each sector. A toy-model for such a situation would be a function $f(x)$ that depends only on one variable x and after the procedure described above the following integral needs to be evaluated

$$N(\alpha) = \int_0^1 \frac{dx f(0)}{x^{1+a\epsilon}} \theta(x - \alpha). \quad (4.178)$$

The integral can be simply performed and yields

$$N(\alpha) = -\frac{1 - \alpha^{-a\epsilon}}{a\epsilon}. \quad (4.179)$$

Thus the calculation of the 't Hooft-Veltman corrections boils down to integrals over step functions. There are two important aspects that have to be taken into account, especially in the double real contribution. As one can see in the toy-model, the simple form of the step function there generates only logarithms α . If such an integral is encountered in the evaluation of the corrections, this term can immediately be dropped, since the logarithms have to cancel in the final result. This is certainly not the case if, for instance, the step function would look like $\theta(x - c\alpha)$ where c is some constant or even a function of x . If it is a constant in x , logarithms of c are generated in addition to those of α . It is slightly more complicated if the function depends on x . The first thing to note is, that this function has to have a non-vanishing limit for $x \rightarrow 0$, e.g. $c(0) = c_0 \neq 0$. If this would not be the case the θ function would not regulate the infrared limits, and the construction would not make any sense, therefore it is assumed by construction. This then leads to the following way to handle such situations

$$N(\alpha) = f(0) \int_0^1 \frac{dx}{x^{1+a\epsilon}} \theta(x - c(x)\alpha) \quad (4.180)$$

$$= f(0) \int_0^1 \frac{dx}{x^{1+a\epsilon}} \theta(x - c(0)\alpha) + f(0) \int_0^1 \frac{dx}{x^{1+a\epsilon}} (\theta(x - c(x)\alpha) - \theta(x - c(0)\alpha)) . \quad (4.181)$$

The first term can be evaluated easily while the second vanishes in the limit $\alpha \rightarrow 0$. With this general considerations the evaluation of corrections can be performed.

Notation Some notation needs to be introduced to organize the calculation. The relevant variables are $x = \{\eta_1, \xi_1, \eta_2, \xi_2\}$ in the double real contribution and $x = \{\eta, \xi\}$ in real-

4. Real radiation contribution

virtual and single-convolution contributions. The object x is used to identify the various terms. Whenever there is a pole term the corresponding variable is replaced by "Pole", if it is an endpoint-subtraction the variable is replaced by "Subt". The explicit integrations are always over "Subt"-terms and performed integrations will be denoted by "Int" for the corresponding variable. If the variable is not treated in any way the label is "Reg". For example denotes

$$\{\text{Reg, Int, Pole, Subt}\} \quad (4.182)$$

a term which is obtained from taking the subtraction term in ξ_2 and ξ_1 for pole term generated by the "+"-prescription in the variable η_2 and integrate explicitly over ξ_1 .

Double-real contributions

The contribution from single-unresolved double-real radiation to $\hat{\sigma}_{HV}$ is split up across different sectors. Fortunately, the correction terms can be written in a form such that they can be applied for any process under consideration. Process and sector specific information like the flavor structure and position of the reference momentum do not influence the derivation and can be restored afterwards. The structure of double pole terms ($x_i = x_j =$ "pole") with no further subtraction appearing in $\hat{\sigma}_{SU}^{RR}$ is the following

$$\dots \int_0^1 \int_0^1 dx_i dx_j \prod_{k \neq i, j} \int_0^1 \frac{dx_k}{x_k^{1-b_k \epsilon}} d\tilde{\mu}_{\text{reg}}^1(x) d\tilde{\mu}_{\text{reg}}^2(x) \mathcal{M}_{\text{reg}} F_{n+2} \left(\frac{-\delta(x_i)}{b_i \epsilon} \right) \left(\frac{-\delta(x_j)}{b_j \epsilon} \right). \quad (4.183)$$

The integration over the δ functions results in one of the momenta entering the matrix element become soft-collinear to the reference. Let us assume that u_2 is the unresolved momentum. The matrix element then factorizes

$$\mathcal{M}_{\text{reg}} = f_{\text{reg}}(x) \mathcal{M}'_{\text{reg}} \quad (4.184)$$

where the function $f_{\text{reg}}(x)$ denotes the factorization formula describing limit of $|\mathcal{M}_{n+2}^0|^2$ regularized by suitable powers of the x_i . Expanding f_{reg} and $d\tilde{\mu}_{\text{reg}}^2$ together with the ϵ^{-2} pole in ϵ up to ϵ^{-1} yields the expression for $\mathcal{I}_{n+1}^{RR,(-1,-2)}$. Since this is a soft limit $f_{\text{reg}} = f_{\text{reg}}^0$ does not depend on ϵ ,

$$\dots \prod_{k \neq i, j} \int_0^1 \frac{dx_k}{x_k^{1+b_k \epsilon}} d\tilde{\mu}_{\text{reg}}^1(x) \left(\underbrace{\frac{d\tilde{\mu}_{\text{reg}}^{2,(0)}(x) f_{\text{reg}}^0(x) \mathcal{M}'_{\text{reg}}}{\epsilon^2}}_{\mathcal{I}_{n+1}^{RR,(-2)}(x)} + \underbrace{\frac{d\tilde{\mu}_{\text{reg}}^{2,(1)}(x) f_{\text{reg}}^0(x) \mathcal{M}'_{\text{reg}}}{\epsilon^1}}_{\mathcal{I}_{n+1}^{RR,(-1)}(x)} \right) F_{n+1} \quad (4.185)$$

Using the master-formula on the remaining x_i 's generates then the corresponding $\mathcal{I}_n^{RR,(-1,-2)}$ terms. Renaming the remaining two variables y and z , one finds

$$\mathcal{I}_n^{RR,(i)} = -\mathcal{I}_{n+1}^{RR,(i)}(y, 0) - \mathcal{I}_{n+1}^{RR,(i)}(0, z) + \mathcal{I}_{n+1}^{RR,(i)}(0, 0). \quad (4.186)$$

4.6. 't Hooft-Veltman Corrections

Due to the additional limit (y and/or $z \rightarrow 0$) the coefficients $\mathcal{I}_{n+1}^{RR,(i)}$ take the form

$$d\tilde{\mu}_{\text{reg}}^{2,(0)} f_{\text{reg}}^0 f'_{\text{reg}} \mathcal{M}'' \quad (4.187)$$

with a tree-level matrix-element \mathcal{M}'' . Putting this formula into (4.172) the contribution to $N^{RR}(\alpha)$ is

$$N^{RR}(\alpha) \ni \int_0^1 \frac{dy}{y^{1+b_y\epsilon}} \frac{dz}{z^{1+b_z\epsilon}} \left(-f^{(i)}(y, 0) - f^{(i)}(0, z) + f^{(i)}(0, 0) \right) \theta_\alpha \quad (4.188)$$

the function $f^{(i)}$ abbreviates the unresolved phase space weight $d\tilde{\mu}_{\text{reg}}^1(x), \mathcal{I}_{n+1}^{RR,(i)}$, the measurement function F_n and the tree-level phase space integration, while θ_α are the regularizing step functions. This integral can now be evaluated by simple reshuffling of terms of three integrals.

$$- \int_0^1 \frac{dy}{y^{1+b_y\epsilon}} \frac{dz}{z^{1+b_z\epsilon}} \left(f^{(i)}(y, 0) - f^{(i)}(0, 0) \right) \theta_\alpha \quad (4.189)$$

$$- \int_0^1 \frac{dy}{y^{1+b_y\epsilon}} \frac{dz}{z^{1+b_z\epsilon}} \left(f^{(i)}(0, z) - f^{(i)}(0, 0) \right) \theta_\alpha \quad (4.190)$$

$$+ \int_0^1 \frac{dy}{y^{1+b_y\epsilon}} \frac{dz}{z^{1+b_z\epsilon}} f^{(i)}(0, 0) \theta_\alpha \quad (4.191)$$

In the last integral nothing depends on the integration variables, except the step-function. Therefore the integration can be performed directly. In the other cases, one integration variable is regulated by a subtraction term. The corresponding integration can not be performed in general since the dependence might be complicated, but the step-function does not have to regularize the corresponding limit anymore. This means that there are no logarithm connected to this variable after integration. The other integration can however be performed and give rise to corresponding logarithms and other terms.

After discussing this at length all other cases are following along the same lines. Single-pole contributions are simpler in respect of the expansion in ϵ since only the lowest order contributes there. But they become more complicated due to an additional integrations over the angle or energy of the unresolved momentum. However, the same procedure works for all contributions. Only in the special case, further discussion is necessary due to the different way of constructing the phase space.

Since the integrals over the step-functions are trivial, only the pole and subtraction combinations that will contribute to the corrections which do not cancel are stated in table 4.7. Some of the details for each sector are discussed below.

Sector \mathcal{S}_1 In sector \mathcal{S}_1 u_1 is the resolved momentum in the single-unresolved configurations and therefore the step-functions in all pole-terms are

$$\theta(\eta_1 - \alpha) \theta(\xi_1(u_1^0)_{\max}(\eta_1) / E_{\text{norm}} - \alpha). \quad (4.192)$$

Thus, whenever an integration over η_1 can be performed, the result will always be proportional to logarithms of α , and therefore it cancels.

4. Real radiation contribution

Sector	SU pole	contributing terms $\{\eta_1, \xi_1, \eta_2, \xi_2\}$
\mathcal{S}_1	$\{\eta_2, \xi_2\}$	{Reg, Int, Pole, Pole}
	$\{\eta_2\}$	{Reg, Int, Pole, Reg}
	$\{\xi_2\}$	{Reg, Int, Reg, Pole}
\mathcal{S}_{23}	$\{\eta_1\}$	{Pole, Int, Reg, Int}, {Pole, Int, Reg, Reg}, {Pole, Reg, Reg, Int}
	$\{\xi_2\}$	{Int, Int, Int, Pole}, {Reg, Int, Int, Pole}, {Int, Reg, Int, Pole}
		{Int, Int, Reg, Pole}, {Reg, Reg, Int, Pole}, {Reg, Int, Reg, Pole}
		{Int, Reg, Reg, Pole}
\mathcal{S}_4	$\{\eta_2, \xi_2\}$	{Reg, Int, Pole, Pole}
	$\{\eta_2\}$	{Reg, Int, Pole, Reg}
	$\{\xi_2\}$	{Reg, Int, Reg, Pole}
\mathcal{S}_5	$\{\eta_1, \xi_2\}$	{Pole, Int, Reg, Pole}
	$\{\eta_1\}$	{Pole, Int, Reg, Reg}
	$\{\xi_2\}$	{Reg*, Int, Int, Pole}, {Reg, Int, Reg, Pole}
\mathcal{S}_6	$\{\eta_2, \xi_2\}$	{Reg, Int, Pole, Pole}
	$\{\eta_2\}$	{Reg, Int, Pole, Reg}
	$\{\xi_2\}$	{Reg, Int, Reg, Pole}
	$\{\eta_1\}$	{Pole, Int, Reg, Int}, {Pole, Int, Reg, Reg}, {Pole, Reg, Reg, Int}
special case :		all terms contribute

Table 4.7.: Contributing terms from triple-collinear sectors. All Reg's can also be Subt, except for Reg* which is only Reg.

Sector \mathcal{S}_{23} In sector \mathcal{S}_{23} two different situations arise depending one the pole that has to be taken. In case of the ξ_2 pole, u_1 is resolved in SU and the step-function reads

$$\theta(\eta_1 \eta_2 / 2 - \alpha) \theta(\xi_1 (u_1^0)_{\max}(\eta_1 \eta_2 / 2) / E_{\text{norm}} - \alpha). \quad (4.193)$$

Both step functions contain non trivial functions and therefore all possible integrations contribute. In case of a η_1 pole, u_2 is the resolved momentum and the step function is

$$\theta(\eta_2 - \alpha) \theta(\xi_2 \xi_1 (u_2^0)_{\max}(0, \eta_2, \xi_1) / E_{\text{norm}} - \alpha). \quad (4.194)$$

Therefore all integrations over η_2 generate only logarithms. The other integrations, however, give non-trivial terms.

Sector \mathcal{S}_4 The situation in sector \mathcal{S}_4 is identical to \mathcal{S}_1 , since the resolved parton is either u_1 (soft pole in ξ_2) or $u_1 + u_2$ (collinear pole in η_2) which behaves in both cases like u_1 in sector \mathcal{S}_1 due to the special energy parameterization.

Sector \mathcal{S}_5 Here the resolved parton, similar to \mathcal{S}_4 is either u_1 or $u_1 + u_2$. As discussed in section 4.4.2, in the soft case the directions of the unresolved parton determines the direction of the resolved parton which leads to a special pattern in the θ functions. They are in case of a collinear or soft-collinear pole

$$\theta(\eta_2 - \alpha) \theta(\xi_1 (u_{12}^0) / E_{\text{norm}} - \alpha) \quad (4.195)$$

similar to sector \mathcal{S}_4 . But in the soft case they read

$$\theta(\eta_2(1 - \eta_1/2) - \alpha)\theta(\xi_1(u_{12}^0)/E_{\text{norm}} - \alpha). \quad (4.196)$$

the dependence in the first θ -function is such that in case of a subtraction term in η_1 only logarithms arise from the η_2 integration. Therefore, only for regular η_1 there is a non trivial contribution to the correction terms.

Sector \mathcal{S}_6 Here two case have to distinguished. If the SU pole is not η_1 , u_1 is the resolved momentum and the same θ -functions as in sector \mathcal{S}_1 are found, with the same corrections. Otherwise the case of the η_1 pole in sector \mathcal{S}_{23} is recovered with the same conclusions.

Sector \mathcal{S}_6 - special case In all other cases the parameterization of the unresolved and reference momenta is done directly in the laboratory frame. Therefore the angular and energy variables correspond directly to the variables entering the step function. In the special case, where $n = 2$ and both references are located in the final state, this is different as discussed in section 4.3. The angles and energies are parameterized in the center-of-mass frame of the references. The momenta are boosted afterwards to the lab-frame. The boosted angles and energies then enter the θ -functions. This affects the corrections obtained. The laboratory and center-of-mass system are connected by a boost in z direction with a rapidity y , where

$$\exp(y) = \frac{|\vec{q}| + q^0}{q^2} \text{ with } q = r_1 + r_2 \quad (4.197)$$

The effect of this boost on the unresolved momenta can be written as

$$u_{\text{lab}}^0 = u_{\text{cms}}^0 \left(\cosh(y) + \hat{u}\hat{z} \sinh(y) \right) \quad (4.198)$$

$$\vec{u}_{\text{lab}} = \vec{u}_{\text{cms}} + u_{\text{cms}}^0 \hat{z} \left(\sinh(y) + \hat{u}\hat{z}(\cosh(y) - 1) \right) \quad (4.199)$$

and thus the θ -function can be written as

$$\theta(\eta_{\text{lab}} - \alpha)\theta(\xi_{\text{lab}} - \alpha) = \theta \left(\eta \left[\frac{r_{\text{lab}}^0}{r_{\text{cms}}^0} \frac{u_{\text{lab}}^0}{u_{\text{cms}}^0} \right]^{-1} - \alpha \right) \theta(\xi u_{\text{lab}}^0/E_{\text{norm}} - \alpha) \quad (4.200)$$

The additional factor in front of η will result in more terms contributing across all pole cases, since this integral does not create only pure logarithms of α anymore.

Real-virtual contribution

The real-virtual contribution is given by

$$\hat{\sigma}^{RV} = \frac{1}{2s} \frac{1}{N} \int d\Phi_{n+1} \left[2 \text{Re} \left\langle \mathcal{M}_{n+1}^{(0)} \left| \mathcal{M}_{n+1}^{(1)} \right. \right\rangle F_{n+1} + (\text{subt. terms} \sim F_n) \right] \quad (4.201)$$

In each sector the phase space is parameterized with the single-collinear parameterization and the one-loop matrix element can be viewed as a function $f(\xi, \eta)$. The dependence on the other angular variables as well as the Born kinematic is suppressed here. Due to the virtual integrations the scaling behaviour of this function is not trivial in the infrared

4. Real radiation contribution

limits $\eta, \xi \rightarrow 0$. Relevant for the discussion of the 't Hooft-Veltman corrections are only the parts proportional to tree-level matrix elements, since only those contribute to $\hat{\sigma}_{SU}^{RV}$. In the collinear limit, the one-loop matrix element factorizes as in formula (2.49). The terms

$$(s_{12})^{-\epsilon} \quad \text{and} \quad \left(\frac{z}{1-z} \right)^\epsilon \quad (4.202)$$

give rise to altered scaling, schematically

$$\lim_{\eta \rightarrow 0} f(\eta, \xi) = f^{(\eta,0)}(\xi) + \eta^{-\epsilon} \xi^{-\epsilon} f^{(\eta,1)}(\xi) + \eta^{-\epsilon} \xi^{-2\epsilon} f^{(\eta,2)}(\xi) . \quad (4.203)$$

In the soft limit $\xi \rightarrow 0$ the formula (2.47) applies and a term with

$$(S_{ij})^\epsilon \quad (4.204)$$

arises and introduces the following limit behaviour

$$\lim_{\xi \rightarrow 0} f(\eta, \xi) = f^{(\xi,0)}(\eta) + \xi^{-2\epsilon} f^{(\xi,1)}(\eta) . \quad (4.205)$$

By investigating, for instance, the soft limit of the collinear limit the scaling of the soft-collinear limit can be determined to be

$$\lim_{\eta \rightarrow 0, \xi \rightarrow 0} f(\eta, \xi) = f^{(\eta\xi,0)} + \eta^{-\epsilon} \xi^{-2\epsilon} f^{(\eta\xi,1)} \quad (4.206)$$

with $f^{(\eta\xi,0)} \equiv f^{(\eta,0)}(0)$ and $f^{(\eta\xi,1)} \equiv f^{(\eta,2)}(0)$. Furthermore, one can show that $f^{(\eta,1)}(0) = 0$. The soft and the collinear commute and therefore the following relation holds for the soft subtraction terms

$$\lim_{\eta \rightarrow 0} f^{(\xi,1)}(\eta) = \eta^{-\epsilon} f^{(\eta\xi,1)} \quad (4.207)$$

or, equivalently, a function $f^{(\xi,\text{reg})} = f^{(\xi,1)}(\eta) - \eta^{-\epsilon} f^{(\eta\xi,1)}$ can be defined which vanishes in the $\eta \rightarrow 0$ limit. Using the above limit expression as subtraction terms, expanding everything in ϵ up to ϵ^{-1} and keeping the part contributing to $N^{RV}(\alpha)$, results in

$$N^{RV}(\alpha)|_{\epsilon^{-2}} = \int_{\xi\eta} \frac{1}{\epsilon^2} \left[-f^{\eta,0(-2)} - f^{\eta,1(-2)} - f^{\eta,2(-2)} - f^{\xi,0(-2)} - f^{\xi,\text{reg}(-2)} + f^{\eta\xi,0(-2)} \right] \quad (4.208)$$

$$\begin{aligned} N^{RV}(\alpha)|_{\epsilon^{-1}} = \int_{\xi\eta} \frac{1}{\epsilon^1} & \left[-f^{\eta,0(-1)} - f^{\eta,1(-1)} - f^{\eta,2(-1)} - f^{\xi,0(-1)} - f^{\xi,\text{reg}(-1)} + f^{\eta\xi,0(-1)} \right. \\ & + \ln(\eta) \left(f^{\eta,1(-2)} + f^{\eta,2(-2)} \right) \\ & - \ln(\mu) \left(f^{\eta,1(-2)} + f^{\eta,2(-2)} + f^{(\xi,\text{reg})(-2)} \right) \\ & \left. + \ln(\xi) \left(f^{\eta,1(-2)} + 2f^{\eta,2(-2)} + 2f^{\xi,\text{reg}(-2)} \right) \right] \quad (4.209) \end{aligned}$$

where the ϵ expansions

$$f^a = \sum_{i=-2} f^{a(i)} \epsilon^i \quad (4.210)$$

are used. Additionally, the dependence on the renormalization scale through the one-loop splitting and soft function is made explicit. Similar to the double-pole case in the double-real contribution the different terms can be rearranged such that the either integrals over η and/or ξ can be performed or are regulated by subtraction terms. Whenever an integral over η can be performed the result is proportional to $\ln \alpha$. For functions not related to altered scaling, the $f^{c,0(i)}$ functions, one finds

$$\begin{aligned} N_0^{RV}(0) \ni & \frac{-1}{2\epsilon} \left(\frac{f^{\xi,0(-2)}(\eta)}{\epsilon^2} + \frac{f^{\xi,0(-1)}(\eta)}{\epsilon} \right) \cdot \left[\left(\frac{E_{\text{norm}}}{u_{\text{max}}^0(\eta)} \right)^{-2\epsilon} - 1 \right] \\ & - \frac{-1}{2\epsilon} \left(\frac{f^{\eta\xi,0(-2)}}{\epsilon^2} + \frac{f^{\eta\xi,0(-1)}}{\epsilon} \right) \cdot \left[\left(\frac{E_{\text{norm}}}{u_{\text{max}}^0(0)} \right)^{-2\epsilon} - 1 \right]. \end{aligned} \quad (4.211)$$

The functions $f^{\xi,1}$ and $f^{\eta\xi,1}$ also contribute to the 't Hooft-Veltman corrections:

$$\begin{aligned} N_0^{RV}(0) \ni & \frac{-1}{2\epsilon} \left(\frac{f^{\xi,0(-2)}(\eta)}{\epsilon^2} \right) \cdot \left[2\epsilon \left(\frac{E_{\text{norm}}}{u_{\text{max}}^0(\eta)} \right)^{-2\epsilon} \ln \left(\frac{E_{\text{norm}}}{u_{\text{max}}^0(\eta)} \right) \right] \\ & + \left(\frac{f^{\xi,0(-1)}(\eta)}{\epsilon} \right) \cdot \left[\left(\frac{E_{\text{norm}}}{u_{\text{max}}^0(\eta)} \right)^{-2\epsilon} - 1 \right] \end{aligned} \quad (4.212)$$

and

$$\begin{aligned} N_0^{RV}(0) \ni & -\frac{-1}{2\epsilon} \left(\frac{f^{\eta\xi,0(-2)}(0)}{\epsilon^2} \right) \cdot \left[2\epsilon \left(\frac{E_{\text{norm}}}{u_{\text{max}}^0(0)} \right)^{-2\epsilon} \ln \left(\frac{E_{\text{norm}}}{u_{\text{max}}^0(\eta)} \right) \right] \\ & + \left(\left(\frac{E_{\text{norm}}}{u_{\text{max}}^0(\eta)} \right)^{-2\epsilon} - 1 \right) \ln \eta \right] + \left(\frac{f^{\eta\xi,0(-1)}(0)}{\epsilon} \right) \cdot \left[\left(\frac{E_{\text{norm}}}{u_{\text{max}}^0(0)} \right)^{-2\epsilon} - 1 \right]. \end{aligned} \quad (4.213)$$

Finally, the following set of terms involving the renormalization scale concludes the real-virtual corrections

$$\begin{aligned} N_0^{RV}(0) \ni & \frac{-1}{2\epsilon} \left(\frac{f^{\xi,1(-2)}(\eta)}{\epsilon} \ln \mu^2 \right) \cdot \left[\left(\frac{E_{\text{norm}}}{u_{\text{max}}^0(\eta)} \right)^{-2\epsilon} - 1 \right] \\ & - \frac{-1}{2\epsilon} \left(\frac{f^{\eta\xi,1(-2)}}{\epsilon} \ln \mu^2 \right) \cdot \left[\left(\frac{E_{\text{norm}}}{u_{\text{max}}^0(0)} \right)^{-2\epsilon} - 1 \right]. \end{aligned} \quad (4.214)$$

4. Real radiation contribution

Collinear factorization contribution

Finally, there is the collinear factorization contribution. The contribution $\hat{\sigma}_{SU}^{C1}$ starts at ϵ^{-1} and since the matrix elements are not expanded, only

$$\hat{\sigma}_{SU}^{C1} \sim \frac{1}{\epsilon} \left(\frac{\mu_F}{\mu_R} \right)^\epsilon = \frac{1}{\epsilon} + \mathcal{O}(\epsilon^0) \quad (4.215)$$

has to be considered. Since the convolution does not interfere with the integration over η or ξ , the contribution, similar to the real-virtual case, can be considered as

$$\hat{\sigma}_{SU}^{C1} \sim \int d\xi d\eta (f(\eta, \xi) - f(\eta, 0) - f(0, \xi) + f(0, 0)) \quad (4.216)$$

One immediately finds by applying the same techniques as discussed above

$$N_0^{C1}(0) = \frac{-1}{2\epsilon} \frac{f(\eta, 0)}{\epsilon} \left[\left(\frac{E_{\text{norm}}}{u_{\text{max}}^0(\eta)} \right)^{-2\epsilon} - 1 \right] - \frac{-1}{2\epsilon} \frac{f(0, 0)}{\epsilon} \left[\left(\frac{E_{\text{norm}}}{u_{\text{max}}^0(0)} \right)^{-2\epsilon} - 1 \right] \quad (4.217)$$

Final remarks

The derived corrections need to be subtracted from $\hat{\sigma}_{SU}$ and added back $\hat{\sigma}_{DU}$. However, the corrections are similar to terms already contained in $\hat{\sigma}_{DU}^{RR}, \hat{\sigma}_{DU}^{RV}$ and $\hat{\sigma}_{DU}^{C1}$. They can be matched by identifying integrated variables with pole terms. Then the corrections amount to multiplications of the derived factors without the function placeholder f .

The finite results of a next-to-next-to-leading order calculation does not depend on the introduced energy scale E_{norm} . Thus it can be set to an arbitrary value. This on the one hand can be used to check the implementation by varying the value and on the other hand to steer a little bit the cancellation of the corresponding logarithms.

5. Top-pair production and decay at NNLO in QCD

In the previous three chapters, all necessary components for top-quark pair production and decay in NWA were presented. Consider the following processes

$$pp \rightarrow t\bar{t} \rightarrow b\bar{b}W^+W^- \rightarrow b\bar{\ell}^+\ell'^-\nu_\ell\bar{\nu}_{\ell'} \quad (5.1)$$

with $\ell = \{e, \mu\}$. The top-quarks, as well as the W -bosons, are treated within the Narrow-Width-Approximation. In this chapter the calculation of this process through NNLO in QCD is presented. The implementation of the four-dimensional STRIPPER scheme was modified in such a way that it can handle decaying massive particles and spin-correlations.

5.1. Treatment of top-quark width in perturbation theory

The width of the top-quark Γ_t entering the calculation needs an additional discussion. As discussed, the width can be evaluated in perturbation theory and enters within the Narrow-Width-Approximation through the on-shell top quark propagators. Schematically the (differential) cross section might be written as follows

$$d\sigma = d\sigma_{t\bar{t}} \times \frac{d\Gamma_t}{\Gamma_t} \times \frac{d\Gamma_{\bar{t}}}{\Gamma_t} \quad (5.2)$$

with the total top-decay width Γ_t , the on-shell top-quark production $\sigma_{t\bar{t}}$ and the differential decay rate $d\Gamma_{t,l}$ to leptons. The \times symbol represents the treatment of the spin-correlation which is taken into account here. Since also the W -bosons are also treated within the NWA the total decay rate can be further factorized to

$$\Gamma_t = \Gamma(t \rightarrow bW^+) \sum_{ff'} \frac{\Gamma(W^+ \rightarrow ff')}{\Gamma_W}, \quad (5.3)$$

assuming a diagonal CKM matrix. When interested in leptonic final states, the differential decay rate is given by

$$d\Gamma_t = d\Gamma(t \rightarrow bW^+) \sum_{f \in \{e, \mu\}} \frac{d\Gamma(W^+ \rightarrow f\nu_f)}{\Gamma_W}; \quad (5.4)$$

and similar for the anti-top-quark. Assuming that there are no phase space cuts involved, the integration over the phase space would yield

$$\sigma = \sigma_{t\bar{t}} \left(\sum_{f, f' \in \{e, \mu\}} \text{BR}(W^+ \rightarrow f^+\nu_f) \text{BR}(W^- \rightarrow f'^-\bar{\nu}_{f'}) \right) \quad (5.5)$$

5. Top-pair production and decay at NNLO in QCD

Thus just the production cross section times the branching fractions of the channel are under consideration. This property should hold in perturbation theory to all orders. This can be achieved by consistently expanding expression 5.2 in α_s [60]. Each component can be written as an expansion in α_s

$$d\sigma_{t\bar{t}} = d\sigma_{t\bar{t}}^{(0)} + \alpha_s d\sigma_{t\bar{t}}^{(1)} + \alpha_s^2 d\sigma_{t\bar{t}}^{(2)} \quad (5.6)$$

$$d\Gamma_{t(\bar{t})} = d\Gamma_{t(\bar{t})}^{(0)} + \alpha_s d\Gamma_{t(\bar{t})}^{(1)} + \alpha_s^2 d\Gamma_{t(\bar{t})}^{(2)} \quad (5.7)$$

$$\Gamma_t = \Gamma_t^{(0)} + \alpha_s \Gamma_t^{(1)} + \alpha_s^2 \Gamma_t^{(2)}. \quad (5.8)$$

Up to NNLO the expansion to the full expression reads

$$d\sigma = d\sigma^{\text{LO}} + \alpha_s d\sigma^{\text{NLO}} + \alpha_s^2 d\sigma^{\text{NNLO}} \quad (5.9)$$

with

$$d\sigma^{\text{LO}} \equiv \sigma^{\text{LOxLO}} \quad (5.10)$$

$$d\sigma^{\text{NLO}} = d\sigma^{\text{NLOxLO}} + d\sigma^{\text{LOxNLO}} - \frac{2\Gamma_t^{(1)}}{\Gamma_t^{(0)}} d\sigma^{\text{LO}} \quad (5.11)$$

$$d\sigma^{\text{NNLO}} = d\sigma^{\text{NNLOxLO}} + d\sigma^{\text{NLOxNLO}} + d\sigma^{\text{LOxNNLO}} - \frac{2\Gamma_t^{(1)}}{\Gamma_t^{(0)}} d\sigma^{\text{NLO}} + \left(\frac{3\Gamma_t^{(1)2}}{\Gamma_t^{(0)2}} - \frac{2\Gamma_t^{(0)}\Gamma_t^{(2)}}{\Gamma_t^{(0)2}} \right) d\sigma^{\text{LO}} \quad (5.12)$$

where contributions are combined according to whether the corrections are located in the production and/or decays, which gives

$$d\sigma^{\text{LOxLO}} = d\sigma_{t\bar{t}}^{(0)} \times \frac{d\Gamma_t^{(0)}}{\Gamma_t^{(0)}} \times \frac{d\Gamma_{\bar{t}}^{(0)}}{\Gamma_{\bar{t}}^{(0)}} \quad (5.13)$$

$$d\sigma^{\text{NLOxLO}} = d\sigma_{t\bar{t}}^{(1)} \times \frac{d\Gamma_t^{(0)}}{\Gamma_t^{(0)}} \times \frac{d\Gamma_{\bar{t}}^{(0)}}{\Gamma_{\bar{t}}^{(0)}} \quad (5.14)$$

$$d\sigma^{\text{NNLOxLO}} = d\sigma_{t\bar{t}}^{(2)} \times \frac{d\Gamma_t^{(0)}}{\Gamma_t^{(0)}} \times \frac{d\Gamma_{\bar{t}}^{(0)}}{\Gamma_{\bar{t}}^{(0)}} \quad (5.15)$$

$$d\sigma^{\text{LOxNLO}} = d\sigma_{t\bar{t}}^{(0)} \times \left(\frac{d\Gamma_t^{(1)}}{\Gamma_t^{(0)}} \times \frac{d\Gamma_{\bar{t}}^{(0)}}{\Gamma_{\bar{t}}^{(0)}} + \frac{d\Gamma_t^{(0)}}{\Gamma_t^{(0)}} \times \frac{d\Gamma_{\bar{t}}^{(1)}}{\Gamma_{\bar{t}}^{(0)}} \right) \quad (5.16)$$

$$d\sigma^{\text{LOxNNLO}} = d\sigma_{t\bar{t}}^{(0)} \times \left(\frac{d\Gamma_t^{(2)}}{\Gamma_t^{(0)}} \times \frac{d\Gamma_{\bar{t}}^{(0)}}{\Gamma_{\bar{t}}^{(0)}} + \frac{d\Gamma_t^{(0)}}{\Gamma_t^{(0)}} \times \frac{d\Gamma_{\bar{t}}^{(2)}}{\Gamma_{\bar{t}}^{(0)}} + \frac{d\Gamma_t^{(1)}}{\Gamma_t^{(0)}} \times \frac{d\Gamma_{\bar{t}}^{(1)}}{\Gamma_{\bar{t}}^{(0)}} \right) \quad (5.17)$$

$$d\sigma^{\text{NLOxNLO}} = d\sigma_{t\bar{t}}^{(1)} \times \left(\frac{d\Gamma_t^{(1)}}{\Gamma_t^{(0)}} \times \frac{d\Gamma_{\bar{t}}^{(0)}}{\Gamma_{\bar{t}}^{(0)}} + \frac{d\Gamma_t^{(0)}}{\Gamma_t^{(0)}} \times \frac{d\Gamma_{\bar{t}}^{(1)}}{\Gamma_{\bar{t}}^{(0)}} \right). \quad (5.18)$$

It can be checked explicitly that this treatment preserves the property 5.5. A further advantage of this approach is that all calculations can be performed with the leading order width, and the additional terms can be obtained by simple rescaling. The dependence of the width on the renormalization scale is kept and the complete expression 5.12 is evaluated

5.2. Dipole subtraction for decay corrections

consistently at the same scale μ .

The total top decay width with $\mu = m_t = 173.3$ GeV, is up to $\mathcal{O}(\alpha_s^2)$, given by

$$\Gamma(t \rightarrow bW^+) = \Gamma^{(0)} (1 - 1.20\alpha_s(\mu) - \alpha_s^2(\mu)2.67). \quad (5.19)$$

For an on-shell renormalized top-quark mass, only α_s depends on μ and the RGE equation

$$\frac{d\Gamma}{d \ln \mu^2} = 0 \quad (5.20)$$

holds. From this the scale dependence can easily be restored.

5.2. Dipole subtraction for decay corrections

The next-to-leading order corrections to the decay is done in a special way. The reason is their appearance in the contribution

$$d\sigma^{\text{NLO}\times\text{NLO}} = d\sigma_{t\bar{t}}^{(1)} \times \left(\frac{d\Gamma_t^{(1)}}{\Gamma_t^{(0)}} \times \frac{d\Gamma_{\bar{t}}^{(0)}}{\Gamma_{\bar{t}}^{(0)}} + \frac{d\Gamma_t^{(0)}}{\Gamma_t^{(0)}} \times \frac{d\Gamma_{\bar{t}}^{(1)}}{\Gamma_{\bar{t}}^{(0)}} \right). \quad (5.21)$$

Here, next-to-leading order contributions from the production and the decay have to be handled at the same time. There is no conceptual problem in performing this calculation with the STRIPPER scheme, but it became evident that it is not very convenient to build this in the existing code. Therefore the NLO corrections to the decay are treated outside the STRIPPER scheme. Writing the NLO contribution of the decay width as

$$\Gamma_t^{(1)} = \Gamma_t^R + \Gamma_t^V \quad (5.22)$$

$$= \int d^d\Phi_3 \langle \mathcal{M}_3^{(0)} | \mathcal{M}_3^{(0)} \rangle + \int d^d\Phi_2 2 \text{Re} \langle \mathcal{M}_2^{(0)} | \mathcal{M}_2^{(1)} \rangle \quad (5.23)$$

the infrared divergencies are handled with the methods presented in [223], i.e. with a dipole subtraction scheme.

To the real radiation contribution Γ^R only the process

$$t \rightarrow bW^+g \quad (5.24)$$

contributes. The matrix element can be written in a factorized form

$$\begin{aligned} \langle \Gamma_{+1} | \Gamma_{+1} \rangle = g^2 C_F \left\{ \left[\frac{1}{p_b \cdot p_g} \left(\frac{2}{1-z} - 1 - z \right) - \frac{m_t^2}{(p_t \cdot p_g)^2} \right] \langle \Gamma | \Gamma \rangle \right. \\ \left. + 8m_t^2 \frac{G_F}{\sqrt{2}} \left[\frac{y}{1-z} \left(\frac{3}{(1+r)} - r^2 + 2r - \frac{5}{2} \right) + \frac{(1+2r^2)}{(1-z)} - 1 \right] \right\}. \end{aligned} \quad (5.25)$$

Two singular limits need to be regulated. The soft limit of the gluon, where $p_t \cdot p_g$ and $p_b \cdot p_g$ vanish, as well as the collinear limit of the gluon and the b -quark, where only $p_b \cdot p_g$ generates a divergence. Following the form of the matrix element, the subtraction term is

5. Top-pair production and decay at NNLO in QCD

chosen to be

$$D((p_t + p_g)^2, (p_b + p_g)^2, m_t^2, m_W^2) = 4\pi C_F \left[\frac{1}{p_b \cdot p_g} \left(\frac{2}{1-z} - 1 - z - \epsilon(1-z) \right) - \frac{m_t^2}{(p_t \cdot p_g)^2} \right] \quad (5.26)$$

such that

$$\int d^d\Phi_3 \left(\langle \mathcal{M}_3^{(0)} | \mathcal{M}_3^{(0)} \rangle - D \cdot \langle \mathcal{M}_2^{(0)} | \mathcal{M}_2^{(0)} \rangle \right) \quad (5.27)$$

is integrable. The momenta \tilde{p}_b and \tilde{p}_W entering the matrix-element $\langle \mathcal{M}_2^{(0)} | \mathcal{M}_2^{(0)} \rangle$ are obtained by a mapping from the full kinematics. One can achieve this by a Lorentz-transformation such that

$$\tilde{p}_W = \alpha \left(p_W - \frac{p_t \cdot p_W}{p_t^2} p_t \right) + \beta p_t \quad \text{with} \quad \alpha = \frac{p_t^2 - p_W^2}{2\sqrt{(p_t \cdot p_W)^2 - p_W^2 p_t^2}} \quad \beta = \frac{p_t^2 + p_W^2}{2p_t^2} \quad (5.28)$$

and \tilde{p}_b is fixed through $\tilde{p}_b = p_t - \tilde{p}_W$. The integrated dipole can then be obtained from the integration over the gluon phase space. Due to the Lorentz invariance of the phase space measure the integrated dipole can be written as

$$d\Gamma^I = d\Phi_3 D \cdot \langle \mathcal{M}_2 | \mathcal{M}_2 \rangle = d\Phi_2(\tilde{p}_w, \tilde{p}_b) \langle \mathcal{M}_2 | \mathcal{M}_2 \rangle \int d\mu_0(p_g) D \quad (5.29)$$

where the integral evaluates to

$$\begin{aligned} \int d\mu_0(p_g) D &= \frac{\alpha_s C_F}{2\pi} \frac{(4\pi)^\epsilon}{\Gamma(1-\epsilon)} \left(\frac{\mu^2}{m_t^2} \right)^\epsilon \left[\frac{1}{\epsilon^2} + \frac{1}{\epsilon} \left(\frac{5}{2} - 2\ln(1-x) \right) \right. \\ &\quad + \frac{25}{4} + \frac{1}{2} \left(\frac{1}{(1-x)^2} - \frac{8}{1-x} + 7 \right) \ln x + \frac{1}{2(1-x)} + 2\text{Li}_2(1-x) \\ &\quad \left. - \frac{5\pi^2}{6} - 5\ln(1-x) + 2\ln^2(1-x) + \frac{1}{2} \right]. \end{aligned} \quad (5.30)$$

The virtual corrections at one-loop are given in terms of a form-factor, see equation 2.87 in section 2,

$$\langle h_t, h_b, h_W | \Gamma_2 \rangle = \bar{u}(h_b, p_b) F^\mu u(h_t, p_t) \epsilon_\mu(h_W, p_W) \quad (5.31)$$

$$\text{with } F^\mu = \gamma^\mu P_L \left[1 + \frac{\alpha_s}{4\pi} C_0 \right] + P_R p_b^\mu \left[\frac{\alpha_s}{4\pi} C_1 \right] \quad (5.32)$$

The virtual contribution needs to be combined with the integrated dipole in equation 5.30 and the cancellation of poles can be performed on form factor level, since one might write the integrated dipole as

$$d\Gamma^I = d\Phi_2 2 \text{Re} \left\langle \Gamma^{(0)} | \mathcal{I} \right\rangle \quad (5.33)$$

due to the absence of an imaginary part in 5.30. The next-to-leading order decay rate can

then be phrased as

$$\Gamma_t^{(1)} = \Gamma^{RS} + \Gamma^{VI} \quad (5.34)$$

$$= \int d^d\Phi_3 \left(\langle \Gamma_3^{(0)} | \Gamma_3^{(0)} \rangle - D \langle \Gamma_0^{(2)} | \Gamma_0^{(2)} \rangle \right) + \int d^d\Phi_2 2 \operatorname{Re} \langle \Gamma^{(0)} | \Gamma^{(1)} + \mathcal{I} \rangle. \quad (5.35)$$

The construction holds in a similar manner in case of polarized top-quarks and can therefore be incorporated in a straight forward manner in the Narrow-Width-Approximation.

5.3. Results for LHC

Equipped with the methods discussed so far, many different particle phenomena can be investigated and the phenomenology discussed here is only the starting point for various investigations. In this section, a first application of the developed framework to LHC phenomenology is presented. All results are preliminary in the sense that they are checked for consistency and also a set of cross-checks of different parts against existing calculations were performed, but they are not published yet. This is the first calculation of this process (within NWA) through NNLO in QCD, even though the production and the decay at NNLO are known already for quite some time. The double polarized matrix-element, were the missing piece to perform the combination of the known results. The setup presented below is chosen such that a comparison with CMS [135] data and the approximate calculation presented in [224] can be performed.

m_t	173.3 GeV
m_W	80.385 GeV
m_Z	91.1876 GeV
Γ_W	2.0928 GeV
G_F	$1.16379 \cdot 10^{-5} \text{ GeV}^2$

Table 5.1.: Input parameters for calculation

For all calculations presented in the following, the input parameters listed in table 5.1 were used. The G_F -scheme for the electro-weak sector is employed. Then the electro-weak coupling and mixing-angle are defined by m_Z , m_W and G_F

$$\sin \theta_W = \frac{m_W}{m_Z} \quad (5.36)$$

$$g_w = \sqrt{\frac{G_F 8 m_W^2}{\sqrt{2}}}. \quad (5.37)$$

The leading order decay width of the top-quark evaluated with this input amounts to

$$\Gamma^{(0)} = 1.5048 \text{ GeV} \quad (5.38)$$

while equation 5.19 can be used to obtain higher order coefficients appearing in 5.12 and their scale dependence. The width is evaluated at the same scale as all other contributions and is subject to the scale variations for the uncertainty estimation. The *MMHT2014* LO, NLO, NNLO PDF sets together with their values for $\alpha_s(m_Z)$ were used for the corresponding predictions.

5. Top-pair production and decay at NNLO in QCD

Setup	LO [pb]	NLO [pb]	NNLO [pb]	NNLO [pb]	CMS [pb]
CMS @ 8TeV	$3.780^{+37\%}_{-25\%}$	$4.48^{+9\%}_{-11\%}$	$4.61^{+1\%}_{-4\%}$	$4.87^{+2.5\%}_{-6.8\%}$	$4.73^{+4.7\%}_{-4.7\%}$

Table 5.2.: Fiducial cross section predictions for the CMS setup at LO, NLO, NNLO in QCD as well as NNLO predictions from [224]. The theory is compared to measurements of CMS [135].

The estimation of the theoretical uncertainty is made with the help of scale variations. Formally, the dependence of a theory prediction from perturbation theory up to given order on the renormalization and factorization scale is of one order higher in the coupling. Consequently, the dependence of the results are expected to become smaller when moving to higher orders in perturbation theory. The residual scale dependence might be used to estimate the effect of higher orders. Heuristically this method provides reasonable error estimates and in many cases the next order lies within the uncertainty bands of the previous order. In the case at hand, the uncertainty bands are estimated by varying the renormalization and factorization scale simultaneously with $\mu = \mu_R = \mu_F \in [m_t/2, 2m_t]$. A more rigorous estimation of the error, including off-diagonal variations and PDF uncertainties, is left for further investigations.

5.3.1. Fiducial cross sections

The most inclusive observable is the total cross-section. From a theory point of view, no phase space cuts are necessary to define the final state. However, at CMS and ATLAS only fiducial cross-sections are measured, since the detectors do not cover the full phase space. In table 5.2 fiducial cross-section predictions for various fiducial volumes are presented. They are compared to measurements from CMS [135]. Predictions for CMS are presented in the full dilepton channel at 8 TeV. The fiducial volumes are defined through cuts on the final state lepton and reconstructed b -jets. For the leptons a p_T of 20 GeV and $|\eta(\ell)| < 2.4$ is required. Additionally, two b -jets (anti- k_t , $R = 0.5$) with $p_T(J_b) > 30$ GeV and $|\eta(J_b)| < 2.4$ have to be present.

The transverse momentum p_T of a particle (or jet) with momentum p is defined as

$$p_T = \sqrt{p_x^2 + p_y^2}. \quad (5.39)$$

The rapidity is defined for massless particles as

$$y = \frac{1}{2} \ln \left(\frac{p_0 + p_z}{p_0 - p_z} \right) \quad (5.40)$$

and corresponds to the boost that has to be applied in z direction to bring the particle in the transverse plane with respect to the beam. It can be generalized to massive particles, by defining

$$\eta = \frac{1}{2} \ln \left(\frac{|\vec{p}| + p_z}{\vec{p} - p_z} \right), \quad (5.41)$$

which coincides with the rapidity definition for massless particles.

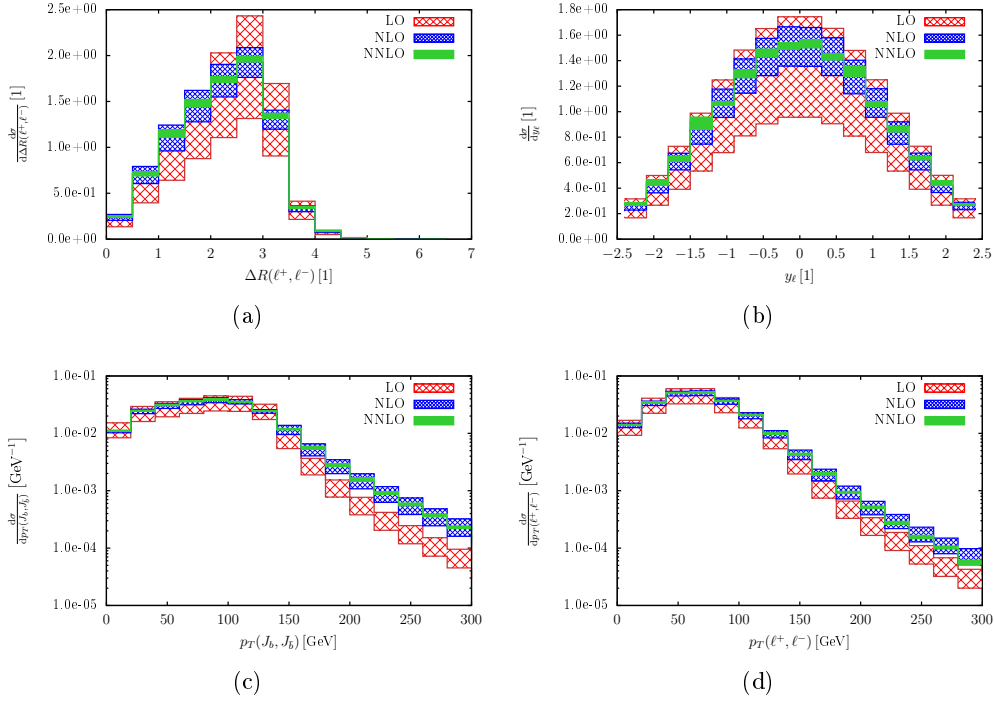


Figure 5.1.: Predictions for differential distributions inside the fiducial volume of the CMS setup in table for LO, NLO and NNLO in QCD. The uncertainty bands are obtained from scale variations $\mu = \mu_R = \mu_F \in [m_t/2, 2m_t]$.

The dependence on the scale μ nicely reduces with increasing perturbative order down to $\mathcal{O}(5\%)$ and an improving description of the measured cross-section.

5.3.2. Differential distributions

Besides cross sections for fiducial volumes, differential cross sections are of particular interest in general. The dependence of the cross section on various kinematic observables encodes fundamental properties of the particles involved in the process under consideration. In the case of top-quark pair production they are extremely important for many measurements, ranging from determination of the top quark mass, through template fits, to the investigation of spin properties [225]. As mentioned in previous discussions about the motivation of this project, due to its short lifetime, the top-quark is not observed directly but rather reconstructed from the decay products. Properties of the top-quark are inferred through the modelling of production and decay. The more accurate the modelling the more accurate are the measurements. The most precise prediction for differential properties of top-quarks are performed at NNLO QCD plus NLO EW corrections[31], for stable top-quarks. One crucial problem in comparing these predictions to measurements is the reconstruction of the top-quarks and their four-momenta. Including the decays in the calculation allows to directly model the decay products and their kinematic distribution and so improves the measurements. Most importantly, keeping the spin-correlation between production and decay in this calculation may provide a direct handle on the spin-properties of the top-quarks.

5. Top-pair production and decay at NNLO in QCD

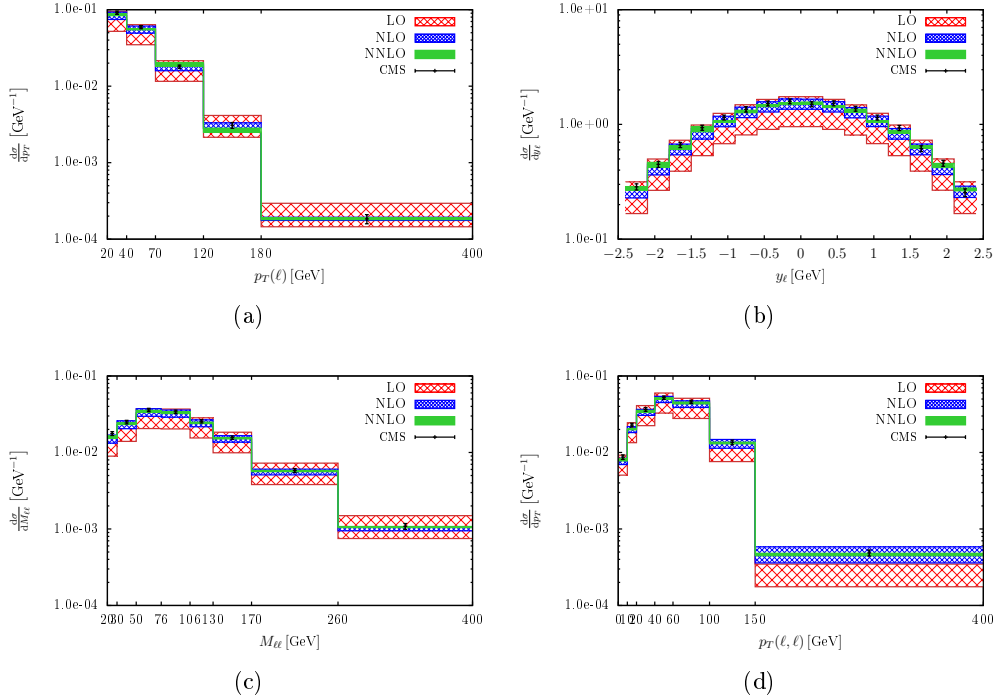


Figure 5.2.: Comparison of LO, NLO and NNLO predictions for lepton observables to CMS measurements. The theory uncertainty bands are obtained from scale variations $\mu = \mu_R = \mu_F \in [m_t/2, 2m_t]$, while the data presented here are taken from [135].

For the CMS setups differential distributions were calculated. The focus is here on the momenta of the leptons and b -jets. Since the neutrinos are unobserved, only imbalances in the measured momentum configuration of the leptons and b -jets can be related to them, as for instance the missing transverse energy E_T . However, neutrino related observables are not discussed here in further detail. In figure 5.1 the dependencies of the cross section on the pseudo-rapidity of the lepton averaged over all considered lepton species, the $\Delta R(\ell^+, \ell^-)$ distance between the oppositely charged leptons, as well as the transverse momentum of the lepton pair $p_T(\ell^+, \ell^-)$ and the two reconstructed b -jets are demonstrated at LO, NLO and NNLO in perturbation theory. The uncertainty bands are obtained with the same scale variation as is used for the total cross section. One observes a reducing scale dependence with increasing order in perturbation theory, which indicates that the perturbative expansion converges well. In the p_T distribution, the NNLO prediction stabilises the tail while a significant change in shape happened between LO and NLO. At leading order, there is no real radiation and only the distribution of the balanced transverse momentum between the decay products is observed, while starting at NLO, additional radiation recoils from the top-quark pair system.

Additionally, a comparison to CMS measurements of differential level is performed. In [135], measurements of normalized differential cross-sections for the di-lepton channel are presented for observables related to the b -jets and leptons. For the comparisons the data were normalized again to the measured fiducial cross-section in table 5.2. The error on the fiducial cross-section is propagated with quadrature. The reason for this is that the way

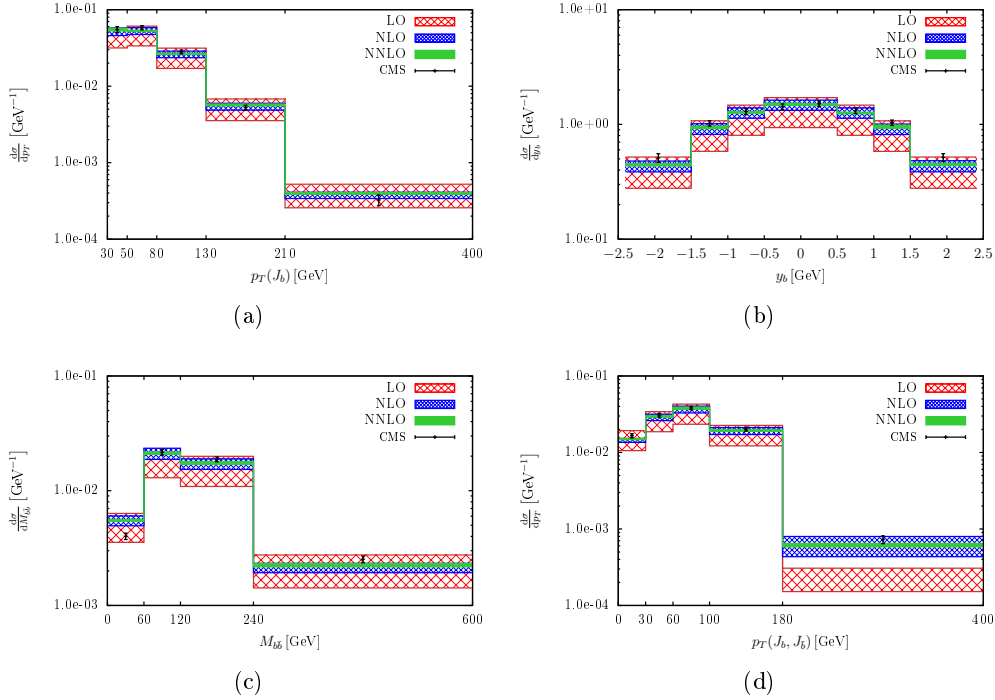


Figure 5.3.: Comparison of LO, NLO and NNLO predictions for b -jet observables to CMS measurements. The theory uncertainty bands are obtained from scale variations $\mu = \mu_R = \mu_F \in [m_t/2, 2m_t]$, while the data presented here are taken from [135].

the theory uncertainty is estimated in this calculation is not feasible for normalized distributions. For instance, at leading order only the value of α_s and the evolution of the PDFs depend on the scale. Due to the fixed scale choice, the effect on α_s is just a normalization and in normalized distribution only the difference between the PDF evaluated at different scales is visible. Since the variation of the PDF evaluated at scales in $[m_t/2, 2m_t]$ is not very strong the error estimate would basically amount to zero. Also for NLO and NNLO the cancellation in normalization reduces the error to a small unreliable value. Dynamical scales and more rigorous study of the scale dependence as well as the PDF uncertainties needs to be discussed in the future.

A comparison of lepton-related observables can be found in figure 5.2. Shown are the transverse momentum $p_T(\ell)$, the rapidity y_ℓ averaged over both charged leptons, as well as their invariant mass $M_{\ell\ell}$ and combined transverse momentum $p_T(\ell, \ell)$. In all cases striking agreement between the NNLO calculation and the CMS measurement can be found. In combination with the fact that the theory uncertainties become visibly smaller, one can conclude that a significantly better description of the data is found.

In figure 5.3 a similar comparison is made for b -jet observables. Here also, the NNLO prediction provides a very competitive description of the measurements with small uncertainties in comparison with NLO. Both cases show that the higher order calculations are needed to obtain a reasonable description of the data. Especially in the tails of transverse momentum distributions the improvements are quite impressive.

6. Summary and Conclusions

The motivation of the work presented in this thesis originated from the observation that higher order perturbative calculations are the backbone of theoretical descriptions at hadron colliders, in particular the LHC. The production of top-quark pairs, the heaviest known particle, was identified as a window to precision physics in the Standard Model and searches beyond it. The accurate modelling of top-quarks is essential to gain the maximum use out of the large amount of data available. The calculation of the production and the decay into the di-leptonic final state of a top-quark pair within the Narrow-Width-Approximation was presented through NNLO in QCD. All necessary components were discussed in detail. The starting point were the foundations of top-quark physics at hadron colliders and the separation of partonic physics, accessible through perturbation theory, from hadronic physics was presented by facilitating a factorization theorem. The perturbative treatment of the partonic cross section in terms of higher order QCD corrections was investigated.

The polarised two-loop amplitude of the $t\bar{t}$ -pair production is a necessary building block of $t\bar{t}$ production with decays. Its calculation was a substantial part of this work and was discussed in detail. A broad band of computational techniques for multi-loop amplitudes were employed. The reduction of tensor to scalar integrals was performed by a projection approach which kept the spin and color information. Integration-by-parts identities were used for the reduction of the occurring scalar integrals to master integrals. The master integrals were evaluated by numerical integration of the system of differential equations obeyed by the master integrals. The preparation of the amplitude for implementation was also discussed.

The handling of real-radiation contributions in NNLO calculations is a dynamically developing field of research. In this work the STRIPPER scheme was presented in a modified version. A new phase space parameterization was introduced with the intention to optimize the convergence in differential distributions. The change of parameterization needed a reevaluation of the four dimensional formulation of this scheme. The introduction of "t Hooft-Veltman"-corrections is necessary to correctly evaluate the occurring integrals. A method to identify the necessary modifications was developed and its application discussed. The C++ implementation of the original scheme was modified to the new parameterization and the determined corrections were implemented. The STRIPPER implementation thus now represents a fully general NNLO QCD subtraction framework.

The first application of this framework is the calculation of $t\bar{t}$ production with leptonic decays. The framework was enhanced by the possibility to treat decays of on-shell top-quarks and W bosons within the NWA. First phenomenological results in terms of fiducial and differential cross sections were presented and compared to CMS data. Improving theoretical error estimates from scale variations and astonishing agreement with CMS data have been found.

This work marks the starting point for a broad band of phenomenological studies for top-quark physics and application of the obtained STRIPPER framework. The presented top-quark pair calculation can be used for a variety of measurements, and due to the high

6. Summary and Conclusions

order in perturbation theory combined with the included modelling of the decay a reduction of the theory error in many measurements is to be expected. Many of the applications of NNLO top-quark phenomenology can now be repeated based on the new predictions. For example, the top-quark mass extraction based on differential distribution or the extraction of PDFs are going to profit from this new result. The inclusion of the decay allows to reduce systematic uncertainties in the fits and comparisons. The results can be used to investigate spin-correlation observables like the angular separation between the two charged leptons at a new level of precision. In this work the leptonic decays were presented, but the extension to also include the hadronic decay channels of the W -boson (as long as likewise treated in NWA) is straightforward.

The automatised STRIPPER framework is the ideal basis for phenomenological applications at NNLO for a variety of processes. The development of the framework has two main perspectives. An important goal is going to be the inclusion of further available two-loop matrix elements. An example could be the amplitudes needed for vector pair production which are publicly available. Moreover, matrix elements for di-jet, vector-boson plus jet, Higgs-boson with or without jet, or lepton pair production are known and available. The framework would directly allow for the inclusion of heavy particle decays, like W , Z and H decays. This would provide the most comprehensive collection of available processes at NNLO. In the same context, one might think about the inclusion of automatised one-loop matrix elements provided by libraries like OPENLOOPS or RECOLA. As soon as they are stable and flexible enough to provide matrix elements in the infrared limits and spin correlated matrix elements for subtraction terms, this will be a sensible item to incorporate in the STRIPPER framework. Since the subtraction is completely automatised, the framework is conceptually ready for higher multiplicity processes. The bottle-neck is the availability of two-loop matrix-elements. The only candidate process exhibiting $2 \rightarrow 3$ kinematics whose two-loop matrix elements are known is the three-jet production. At some point these matrix elements will be fast enough for phenomenological applications. However, practice must show if the subtraction scheme can handle this complicated process with reasonable efficiency and/or convergence. This leads to the next, even more important prospect: efficiency. Even though the set of subtraction terms provided in the software is general and can be used for any process, this does not necessarily mean that the subtraction scheme results in *good* performance. The newly implemented phase space parameterization needs to be investigated in terms of its impact on the convergence. This is a critical point for future investigations, since the demand on computing power increases dramatically for progressively complex processes and thus an efficient way to perform the calculations is essential. A starting point for improving on this, is not only the phase space parameterization, but also other ideas like event smearing, a method where several events close in the phase space are averaged over to improve convergence, are waiting for implementation and testing.

As shown above, the number of prospective processes to be integrated, and the possibilities of further improvement are vast. All this summarizes the prospects for the near future: There are interesting times ahead!

A. General Notation and conventions

A.1. Notation

Conventions, notations and definitions that appear in various places are collected in this section. The notation is as far as possible oriented on the notation in [217] and many formula and conventions are directly from that work.

Spacetime dimension

$$d = 4 - 2\epsilon . \quad (\text{A.1})$$

Bare strong coupling

$$\alpha_s^0 = \left(\frac{\mu_R^2 e^{\gamma_E}}{4\pi} \right)^\epsilon Z_{\alpha_s} \zeta_{\alpha_s} \alpha_s , \quad (\text{A.2})$$

- μ_R – renormalization scale ,
- Z_{α_s} – $\overline{\text{MS}}$ renormalization constant ,
- ζ_{α_s} – heavy-quark decoupling constant [226] .

Matrix elements

$$\mathcal{M}_{a_1, \dots, a_n}^{c_1, \dots, c_n; s_1, \dots, s_n}(p_1, \dots, p_n) = \left(\langle c_1, \dots, c_n | \otimes \langle s_1, \dots, s_n | \right) |\mathcal{M}_{a_1, \dots, a_n}(p_1, \dots, p_n)\rangle , \quad (\text{A.3})$$

$$|\mathcal{M}_n\rangle = |\mathcal{M}_{a_1, \dots, a_n}(p_1, \dots, p_n)\rangle , \quad \sum_{\substack{\text{color} \\ \text{spin}}} |\mathcal{M}_n|^2 = \langle \mathcal{M}_n | \mathcal{M}_n \rangle , \quad (\text{A.4})$$

$$|\mathcal{M}_n\rangle = \left(\frac{\mu_R^2 e^{\gamma_E}}{4\pi} \right)^{-l\epsilon} \left(|\mathcal{M}_n^{(0)}\rangle + |\mathcal{M}_n^{(1)}\rangle + |\mathcal{M}_n^{(2)}\rangle + \dots \right) . \quad (\text{A.5})$$

- c_i – color of parton i ,
- s_i – spin of parton i ,
- $\langle c_1, \dots, c_n \rangle$ – color basis vectors,
- l – α_s power of Born approximation.
- a_i – flavor of parton i ,
- p_i – momentum of parton i ,
- $\langle s_1, \dots, s_n \rangle$ – spin basis vectors,

Phase spaces

$$\int d\Phi_n(p_1 + p_2 \rightarrow \sum_{i=1}^n q_i) = \left(\frac{\mu_R^2 e^{\gamma_E}}{4\pi} \right)^{(n-1)\epsilon} \int \prod_{i=1}^n \frac{d^{d-1} q_i}{(2\pi)^{d-1} 2q_i^0} (2\pi)^d \delta^{(d)} \left(\sum_{i=1}^n q_i - p_1 - p_2 \right) . \quad (\text{A.6})$$

A. General Notation and conventions

Sums over partons

$$\sum_{i,j,\dots} \text{ -- sum over all indices } i, j, \dots, \quad \sum_{(i,j,\dots)} \text{ -- sum over distinct indices } i, j, \dots.$$

- i, j, k, \dots -- indices for arbitrary partons, both massless and massive,
- i_0, j_0, k_0, \dots -- indices for massless partons,
- I, J, K, \dots -- indices for massive partons.

Kinematic invariants

$$p_I^2 = m_I^2, \quad v_I = p_I/m_I, \quad v_{IJ} = \sqrt{1 - \frac{m_I^2 m_J^2}{(p_I p_J)^2}}, \quad (\text{A.7})$$

$$s_{ij} = 2\sigma_{ij} p_i \cdot p_j + i0^+. \quad (\text{A.8})$$

$\sigma_{ij} = +1$ -- if the momenta p_i and p_j are both incoming or outgoing, $\sigma_{ij} = -1$ -- otherwise.

Color charge operators [22]

$$\begin{aligned} \langle c_1, \dots, c_i, \dots, c_n, c | \mathbf{T}_i | b_1, \dots, b_i, \dots, b_n \rangle &= \langle c_1, \dots, c_i, \dots, c_n | T_i^c | b_1, \dots, b_i, \dots, b_n \rangle \\ &= \delta_{c_1 b_1} \dots T_{c_i b_i}^c \dots \delta_{c_n b_n}. \end{aligned} \quad (\text{A.9})$$

$$\sum_i \mathbf{T}_i | \mathcal{M}_n \rangle = 0, \quad T_i^c T_j^c = \mathbf{T}_i \cdot \mathbf{T}_j = \mathbf{T}_j \cdot \mathbf{T}_i, \quad \mathbf{T}_i \cdot \mathbf{T}_i = \mathbf{T}_i^2 = C_i = C_{a_i}, \quad (\text{A.10})$$

$$C_g = C_A, \quad C_q = C_{\bar{q}} = C_F. \quad (\text{A.11})$$

$$\begin{aligned} T_{c_1 c_2}^c &= i f^{c_1 c_2 c} \text{ -- emitter is a gluon,} \\ T_{c_1 c_2}^c &= t_{c_1 c_2}^c (= -t_{c_2 c_1}^c) \text{ -- emitter is an outgoing quark (anti-quark),} \\ T_{c_1 c_2}^c &= -t_{c_2 c_1}^c (= t_{c_1 c_2}^c) \text{ -- emitter is an ingoing quark (anti-quark).} \end{aligned}$$

$$\text{Tr} [t^a t^b] = T_F \delta^{ab} = \frac{1}{2} \delta^{ab}. \quad (\text{A.12})$$

A.2. Spherical coordinates in d dimensions

Let $d^d \mathbf{r}$ be the Euclidean integration measure in \mathbb{R}^d . It can be decomposed into a radial and an angular part with the help of a δ -function insertion, if the \mathbf{r} vector is rescaled as $\mathbf{r} = r \hat{\mathbf{n}}$

$$\int_{\mathbb{R}^d} d^d \mathbf{r} = \int_0^\infty dr r^{d-1} \int_{\mathbb{R}^d} d^d \hat{\mathbf{n}} \delta(1 - \|\hat{\mathbf{n}}\|) = \int_0^\infty dr r^{d-1} \int_{\mathcal{S}_1^{d-1}} d\Omega. \quad (\text{A.13})$$

In this way a rotationally invariant measure, $d\Omega$, on the unit $(d-1)$ -sphere, \mathcal{S}_1^{d-1} is defined. From now on the dimensionality is included in the notation of the versors $\hat{\mathbf{n}}$. Let

A.2. Spherical coordinates in d dimensions

us introduce a recursive parameterization in terms of angles

$$\hat{\mathbf{n}}^{(d)}(\theta_1, \theta_2, \dots, \theta_{d-1}) = \begin{pmatrix} \cos \theta_1 \\ \sin \theta_1 \hat{\mathbf{n}}^{(d-1)}(\theta_2, \dots, \theta_{d-1}) \end{pmatrix}, \quad \hat{\mathbf{n}}^{(1)} = 1, \quad (\text{A.14})$$

where

$$\theta_1, \dots, \theta_{d-2} \in [0, \pi], \quad \theta_{d-1} \in [0, 2\pi]. \quad (\text{A.15})$$

An important property of this parameterization is

$$\begin{aligned} \hat{\mathbf{n}}^{(d)}(\theta_1, \dots, \theta_{n-1}, 0, \theta_{n+1}, \dots, \theta_{d-1}) &= \hat{\mathbf{n}}^{(d)}(\theta_1, \dots, \theta_{n-1}, 0, 0, \dots), \\ \hat{\mathbf{n}}^{(d)}(\theta_1, \dots, \theta_{n-1}, \pi, \theta_{n+1}, \dots, \theta_{d-1}) &= \hat{\mathbf{n}}^{(d)}(\theta_1, \dots, \theta_{n-1}, \pi, 0, 0, \dots). \end{aligned} \quad (\text{A.16})$$

The recursive definition of the versor can be implemented in the integration measure

$$\int_{\mathcal{S}_1^{d-1}} d\Omega(\theta_1, \theta_2, \dots, \theta_{d-1}) = \int_0^\pi d\theta_1 \sin^{d-2} \theta_1 \int_{\mathcal{S}_1^{d-2}} d\Omega(\theta_2, \dots, \theta_{d-1}). \quad (\text{A.17})$$

The volume of the unit $(d-1)$ -sphere is

$$\int_{\mathcal{S}_1^{d-1}} d\Omega 1 = \frac{2\pi^{\frac{d}{2}}}{\Gamma(\frac{d}{2})}. \quad (\text{A.18})$$

The following result

$$\int_{\mathcal{S}_1^{d-1}} d\Omega \delta^{(d)}(\alpha \hat{\mathbf{n}}^{(d)}) = \alpha^{1-d} \int_{\mathbb{R}^d} d^d(\alpha \hat{\mathbf{n}}^{(d)}) \delta(\alpha - \|\alpha \hat{\mathbf{n}}^{(d)}\|) \delta^{(d)}(\alpha \hat{\mathbf{n}}^{(d)}) = \frac{1}{\alpha^{d-1}} \delta(\alpha), \quad (\text{A.19})$$

implies the correct reduction of the dimensionality of space

$$\int_{\mathcal{S}_1^{d-1}} d\Omega \delta^{(d-n)}(\hat{\mathbf{n}}^{(d)}) = \int_{\mathcal{S}_1^{n-1}} d\Omega, \quad (\text{A.20})$$

Furthermore a representation of the angular versor parameterization through rotations of a basis vector is introduced. A basis versor is defined

$$\hat{\mathbf{n}}_{\mathbf{0}}^{(d)} = \begin{pmatrix} 1 \\ 0 \\ 0 \\ \vdots \end{pmatrix}, \quad (\text{A.21})$$

$$\hat{\sigma}_{ab}^{\text{C}}(p_1, p_2) = \frac{\alpha_s}{2\pi} \frac{1}{\epsilon} \left(\frac{\mu_R^2}{\mu_F^2} \right)^\epsilon \sum_c \int_0^1 dz \left[P_{ca}^{(0)}(z) \hat{\sigma}_{cb}^{\text{B}}(zp_1, p_2) + P_{cb}^{(0)}(z) \hat{\sigma}_{ac}^{\text{B}}(p_1, zp_2) \right], \quad (\text{A.30})$$

and finally the contributions arising at NNLO:

$$\hat{\sigma}_{ab}^{\text{RR}} = \frac{1}{2\hat{s}} \frac{1}{N_{ab}} \int d\Phi_{n+2} \langle \mathcal{M}_{n+2}^{(0)} | \mathcal{M}_{n+2}^{(0)} \rangle F_{n+2}, \quad (\text{A.31})$$

$$\hat{\sigma}_{ab}^{\text{RV}} = \frac{1}{2\hat{s}} \frac{1}{N_{ab}} \int d\Phi_{n+1} 2\text{Re} \langle \mathcal{M}_{n+1}^{(0)} | \mathcal{M}_{n+1}^{(1)} \rangle F_{n+1}, \quad (\text{A.32})$$

$$\hat{\sigma}_{ab}^{\text{VV}} = \frac{1}{2\hat{s}} \frac{1}{N_{ab}} \int d\Phi_n \left(2\text{Re} \langle \mathcal{M}_n^{(0)} | \mathcal{M}_n^{(2)} \rangle + \langle \mathcal{M}_n^{(1)} | \mathcal{M}_n^{(1)} \rangle \right) F_n, \quad (\text{A.33})$$

with the collinear factorization contributions:

$$\begin{aligned} \hat{\sigma}_{ab}^{\text{C1}}(p_1, p_2) &= \frac{\alpha_s}{2\pi} \frac{1}{\epsilon} \left(\frac{\mu_R^2}{\mu_F^2} \right)^\epsilon \sum_c \int_0^1 dz \left[P_{ca}^{(0)}(z) \hat{\sigma}_{cb}^{\text{R}}(zp_1, p_2) + P_{cb}^{(0)}(z) \hat{\sigma}_{ac}^{\text{R}}(p_1, zp_2) \right], \\ \hat{\sigma}_{ab}^{\text{C2}}(p_1, p_2) &= \frac{\alpha_s}{2\pi} \frac{1}{\epsilon} \left(\frac{\mu_R^2}{\mu_F^2} \right)^\epsilon \sum_c \int_0^1 dz \left[P_{ca}^{(0)}(z) \hat{\sigma}_{cb}^{\text{V}}(zp_1, p_2) + P_{cb}^{(0)}(z) \hat{\sigma}_{ac}^{\text{V}}(p_1, zp_2) \right] \\ &+ \left(\frac{\alpha_s}{2\pi} \right)^2 \frac{1}{2\epsilon} \left(\frac{\mu_R^2}{\mu_F^2} \right)^{2\epsilon} \sum_c \int_0^1 dz \left[P_{ca}^{(1)}(z) \hat{\sigma}_{cb}^{\text{B}}(zp_1, p_2) + P_{cb}^{(1)}(z) \hat{\sigma}_{ac}^{\text{B}}(p_1, zp_2) \right] \\ &+ \left(\frac{\alpha_s}{2\pi} \right)^2 \frac{\beta_0}{4\epsilon^2} \left[\left(\frac{\mu_R^2}{\mu_F^2} \right)^{2\epsilon} - 2 \left(\frac{\mu_R^2}{\mu_F^2} \right)^\epsilon \right] \\ &\cdot \sum_c \int_0^1 dz \left[P_{ca}^{(0)}(z) \hat{\sigma}_{cb}^{\text{B}}(zp_1, p_2) + P_{cb}^{(0)}(z) \hat{\sigma}_{ac}^{\text{B}}(p_1, zp_2) \right] \\ &+ \left(\frac{\alpha_s}{2\pi} \right)^2 \frac{1}{2\epsilon^2} \left(\frac{\mu_R^2}{\mu_F^2} \right)^{2\epsilon} \\ &\cdot \sum_{cd} \int_0^1 dz \left[\left(P_{cd}^{(0)} \otimes P_{da}^{(0)} \right)(z) \hat{\sigma}_{cb}^{\text{B}}(zp_1, p_2) + \left(P_{cd}^{(0)} \otimes P_{db}^{(0)} \right)(z) \hat{\sigma}_{ac}^{\text{B}}(p_1, zp_2) \right] \\ &+ \left(\frac{\alpha_s}{2\pi} \right)^2 \frac{1}{\epsilon^2} \left(\frac{\mu_R^2}{\mu_F^2} \right)^{2\epsilon} \sum_{cd} \iint_0^1 dz d\bar{z} \left[P_{ca}^{(0)}(z) P_{db}^{(0)}(\bar{z}) \hat{\sigma}_{cd}^{\text{B}}(zp_1, \bar{z}p_2) \right], \end{aligned} \quad (\text{A.34})$$

where

$$(f \otimes g)(x) = \iint_0^1 dy dz f(y)g(z) \delta(x - yz). \quad (\text{A.35})$$

B. Renormalization Constants

B.1. UV renormalization constants

The necessary renormalization constants for UV renormalization of the polarized double virtual $t\bar{t}$ amplitude are collected here. The on-shell renormalization constants are

$$\begin{aligned}
Z_g &= 1 + \left(\frac{\alpha_s^{(n_f)}}{2\pi} \right) T_F n_h \left\{ -\frac{2}{3\epsilon} - \frac{2}{3} l_\mu - \frac{1}{3} \epsilon l_\mu^2 - \frac{\pi^2}{18} \epsilon - \frac{1}{9} \epsilon^2 l_\mu^3 - \frac{\pi^2}{18} \epsilon^2 l_\mu + \frac{2}{9} \epsilon^2 \zeta_3 \right\} \\
&+ \left(\frac{\alpha_s^{(n_f)}}{2\pi} \right)^2 T_F n_h \left\{ T_F n_h \left[\frac{4}{9\epsilon} l_\mu + \frac{2}{3} l_\mu^2 + \frac{\pi^2}{27} \right] + T_F n_l \left[-\frac{4}{9\epsilon^2} - \frac{4}{9\epsilon} l_\mu - \frac{2}{9} l_\mu^2 - \frac{\pi^2}{27} \right] \right. \\
&+ \mathcal{F} \left[-\frac{1}{2\epsilon} - l_\mu - \frac{15}{4} \right] + C_A \left[\frac{35}{36\epsilon^2} + \frac{13}{18\epsilon} l_\mu - \frac{5}{8\epsilon} - \frac{5}{4} l_\mu + \frac{1}{9} l_\mu^2 + \frac{13}{48} + \frac{13\pi^2}{216} \right] \left. \right\}, \\
Z_q &= 1 + \left(\frac{\alpha_s^{(n_f)}}{2\pi} \right)^2 \mathcal{F} T_F n_h \left[\frac{1}{4\epsilon} + \frac{1}{2} l_\mu - \frac{5}{24} \right], \\
Z_Q &= 1 + \left(\frac{\alpha_s^{(n_f)}}{2\pi} \right) \mathcal{F} \left\{ -\frac{3}{2\epsilon} - 2 - \frac{3}{2} l_\mu - 4\epsilon - 2\epsilon l_\mu - \frac{3}{4} \epsilon l_\mu^2 - \frac{\pi^2}{8} \epsilon - 8\epsilon^2 - 4\epsilon^2 l_\mu - \epsilon^2 l_\mu^2 \right. \\
&- \left. \frac{1}{4} \epsilon^2 l_\mu^3 - \frac{\pi^2}{6} \epsilon^2 - \frac{\pi^2}{8} \epsilon^2 l_\mu + \frac{1}{2} \epsilon^2 \zeta_3 \right\} + \left(\frac{\alpha_s^{(n_f)}}{2\pi} \right)^2 \mathcal{F} \left\{ T_F n_h \left[\frac{1}{4\epsilon} + \frac{1}{\epsilon} l_\mu + \frac{947}{72} + \frac{11}{6} l_\mu \right. \right. \\
&+ \left. \left. \frac{3}{2} l_\mu^2 - \frac{5\pi^2}{4} \right] + T_F n_l \left[-\frac{1}{2\epsilon^2} + \frac{11}{12\epsilon} + \frac{113}{24} + \frac{19}{6} l_\mu + \frac{1}{2} l_\mu^2 + \frac{\pi^2}{3} \right] + \mathcal{F} \left[\frac{9}{8\epsilon^2} + \frac{51}{16\epsilon} \right. \right. \\
&+ \left. \left. \frac{9}{4\epsilon} l_\mu + \frac{433}{32} + \frac{51}{8} l_\mu + \frac{9}{4} l_\mu^2 - \frac{49\pi^2}{16} + 4 \ln 2\pi^2 - 6\zeta_3 \right] + C_A \left[\frac{11}{8\epsilon^2} - \frac{127}{48\epsilon} - \frac{1705}{96} \right. \right. \\
&- \left. \left. \frac{215}{24} l_\mu - \frac{11}{8} l_\mu^2 + \frac{5\pi^2}{4} - 2 \ln 2\pi^2 + 3\zeta_3 \right] \right\}, \\
Z_m &= 1 + \left(\frac{\alpha_s^{(n_f)}}{2\pi} \right) \mathcal{F} \left\{ -\frac{3}{2\epsilon} - 2 - \frac{3}{2} l_\mu - 4\epsilon - 2\epsilon l_\mu - \frac{3}{4} \epsilon l_\mu^2 - \frac{\pi^2}{8} \epsilon - 8\epsilon^2 - 4\epsilon^2 l_\mu - \epsilon^2 l_\mu^2 \right. \\
&- \left. \frac{1}{4} \epsilon^2 l_\mu^3 - \frac{\pi^2}{6} \epsilon^2 - \frac{\pi^2}{8} \epsilon^2 l_\mu + \frac{1}{2} \epsilon^2 \zeta_3 \right\} + \left(\frac{\alpha_s^{(n_f)}}{2\pi} \right)^2 \mathcal{F} \left\{ T_F n_h \left[-\frac{1}{2\epsilon^2} + \frac{5}{12\epsilon} + \frac{143}{24} \right. \right. \\
&+ \left. \left. \frac{13}{6} l_\mu + \frac{1}{2} l_\mu^2 - \frac{2\pi^2}{3} \right] + T_F n_l \left[-\frac{1}{2\epsilon^2} + \frac{5}{12\epsilon} + \frac{71}{24} + \frac{13}{6} l_\mu + \frac{1}{2} l_\mu^2 + \frac{\pi^2}{3} \right] \right\}
\end{aligned}$$

B. Renormalization Constants

$$\begin{aligned}
& +\mathcal{F}\left[\frac{9}{8\epsilon^2} + \frac{45}{16\epsilon} + \frac{9}{4\epsilon}l_\mu + \frac{199}{32} + \frac{45}{8}l_\mu + \frac{9}{4}l_\mu^2 - \frac{17\pi^2}{16} + 2\ln 2\pi^2 - 3\zeta_3\right] \\
& +C_A\left[\frac{11}{8\epsilon^2} - \frac{97}{48\epsilon} - \frac{1111}{96} - \frac{185}{24}l_\mu - \frac{11}{8}l_\mu^2 + \frac{\pi^2}{3} - \ln 2\pi^2 + \frac{3}{2}\zeta_3\right]\}, \tag{B.1}
\end{aligned}$$

where $l_\mu = \ln \mu^2/m^2$. The on-shell wave-function renormalization constants for the gluon and light quark fields have been taken from [227, 228].

For the heavy-quark wave-function and mass renormalization constants we used expressions from [229]. The $\overline{\text{MS}}$ renormalization constant for the strong coupling up to $\mathcal{O}\left(\alpha_s^{(n_f)^2}\right)$ is given in terms of beta-function coefficients

$$Z_{\alpha_s} = 1 - \left(\frac{\alpha_s^{(n_f)}}{2\pi}\right) \frac{b_0}{2\epsilon} + \left(\frac{\alpha_s^{(n_f)}}{2\pi}\right)^2 \left(\frac{b_0^2}{4\epsilon^2} - \frac{b_1}{8\epsilon}\right), \tag{B.2}$$

where

$$b_0 = \frac{11}{3}C_A - \frac{4}{3}T_F n_f, \quad b_1 = \frac{34}{3}C_A^2 - \frac{20}{3}C_A T_F n_f - 4\mathcal{F}T_F n_f. \tag{B.3}$$

The two-loop decoupling constant for the strong coupling is given by [230]

$$\begin{aligned}
\zeta_{\alpha_s} &= 1 + \left(\frac{\alpha_s^{(n_l)}}{2\pi}\right) T_F n_h \left\{ \frac{2}{3}l_\mu + \frac{1}{3}\epsilon l_\mu^2 + \frac{\pi^2}{18}\epsilon + \frac{1}{9}\epsilon^2 l_\mu^3 + \frac{\pi^2}{18}\epsilon^2 l_\mu - \frac{2}{9}\epsilon^2 \zeta_3 \right\} \\
&+ \left(\frac{\alpha_s^{(n_l)}}{2\pi}\right)^2 T_F n_h \left\{ \frac{4}{9}T_F n_h l_\mu^2 + \mathcal{F}\left[\frac{15}{4} + l_\mu\right] + C_A\left[-\frac{8}{9} + \frac{5}{3}l_\mu\right] \right\}. \tag{B.4}
\end{aligned}$$

B.2. Supplements for IR renormalization

A list of all the anomalous dimensions occurring in Eq. (2.25) necessary to obtain the finite remainders of the two-loop amplitudes are listed here. The anomalous dimensions related to a single parton (collinear in origin for massless partons and soft in origin for massive partons) are [116, 117]

$$\begin{aligned}
\gamma^g\left(\alpha_s^{(n_l)}\right) &= \left(\frac{\alpha_s^{(n_l)}}{2\pi}\right) \left\{ -\frac{11}{6}C_A + \frac{2}{3}T_F n_l \right\} + \left(\frac{\alpha_s^{(n_l)}}{2\pi}\right)^2 \left\{ C_A^2 \left[-\frac{173}{27} + \frac{11\pi^2}{72} + \frac{1}{2}\zeta_3 \right] \right. \\
&\left. + C_A T_F n_l \left[\frac{64}{27} - \frac{\pi^2}{18} \right] + \mathcal{F}T_F n_l \right\}, \tag{B.5}
\end{aligned}$$

$$\begin{aligned}
\gamma^q\left(\alpha_s^{(n_l)}\right) &= -\left(\frac{\alpha_s^{(n_l)}}{2\pi}\right) \frac{3}{2}\mathcal{F} + \left(\frac{\alpha_s^{(n_l)}}{2\pi}\right)^2 \mathcal{F} \left\{ C_A \left[-\frac{961}{216} - \frac{11\pi^2}{24} + \frac{13}{2}\zeta_3 \right] \right. \\
&\left. + \mathcal{F}\left[-\frac{3}{8} + \frac{\pi^2}{2} - 6\zeta_3\right] + T_F n_l \left[\frac{65}{54} + \frac{\pi^2}{6} \right] \right\}, \tag{B.6}
\end{aligned}$$

B.2. Supplements for IR renormalization

$$\gamma^Q(\alpha_s^{(n_l)}) = -\left(\frac{\alpha_s^{(n_l)}}{2\pi}\right)\mathcal{F} + \left(\frac{\alpha_s^{(n_l)}}{2\pi}\right)^2 \mathcal{F} \left\{ C_A \left[-\frac{49}{18} + \frac{\pi^2}{6} - \zeta_3 \right] + \frac{10}{9} T_F n_l \right\}. \quad (\text{B.7})$$

The cusp anomalous dimensions are given by [231, 232]

$$\gamma_{\text{cusp}}(\alpha_s^{(n_l)}) = \frac{\alpha_s^{(n_l)}}{\pi} + \left(\frac{\alpha_s^{(n_l)}}{2\pi}\right)^2 \left\{ C_A \left[\frac{67}{9} - \frac{\pi^2}{3} \right] - \frac{20}{9} T_F n_l \right\}, \quad (\text{B.8})$$

$$\begin{aligned} \gamma_{\text{cusp}}(\beta, \alpha_s^{(n_l)}) &= \gamma_{\text{cusp}}(\alpha_s^{(n_l)}) \beta \coth \beta \\ &+ \left(\frac{\alpha_s^{(n_l)}}{2\pi}\right)^2 2C_A \left\{ \coth^2 \beta \left[\text{Li}_3(e^{-2\beta}) + \beta \text{Li}_2(e^{-2\beta}) - \zeta_3 + \frac{\pi^2}{6} \beta + \frac{1}{3} \beta^3 \right] \right. \\ &+ \coth \beta \left[\text{Li}_2(e^{-2\beta}) - 2\beta \ln(1 - e^{-2\beta}) - \frac{\pi^2}{6}(1 + \beta) - \beta^2 - \frac{1}{3} \beta^3 \right] \\ &\left. + \frac{\pi^2}{6} + \zeta_3 + \beta^2 \right\}. \end{aligned} \quad (\text{B.9})$$

The two functions F_1 and f_2 are given by

$$F_1(\beta_{12}, \beta_{23}, \beta_{31}) = \frac{1}{3} \sum_{I,J,K} \epsilon_{I,J,K} \frac{\alpha_s}{4\pi} g(\beta_{IJ} \gamma_{\text{cusp}}(\beta_{KI}, \alpha_s)) \quad (\text{B.10})$$

$$f_2\left(\beta_{12}, \ln \frac{-\sigma_{23} v_2 p_3}{-\sigma_{13} v_1 p_3}\right) = -\frac{\alpha_s}{3\pi} g(\beta_{12}) \gamma_{\text{cusp}}(\alpha_s) \ln \left(\frac{-\sigma_{23} v_2 p_3}{-\sigma_{13} v_1 p_3} \right) \quad (\text{B.11})$$

with the function

$$g(\beta) = \coth \beta \left[\beta^2 + 2\beta \ln(1 - e^{-2\beta}) - \text{Li}_2(e^{-2\beta}) + \frac{\pi^2}{6} \right] - \beta^2 - \frac{\pi^2}{6} \quad (\text{B.12})$$

C. Factorization Formula

The factorization formula collected here are the same as in [217]. They are reproduced here for completeness and for reference of some discussions.

C.1. Infrared limits of tree-level amplitudes

C.1.1. Collinear limits

The explicit formulae of the splitting functions discussed in section 2.1.3

$$\hat{P}_{gg}^{(0),\mu\nu}(z, k_\perp; \epsilon) = 2C_A \left[-g^{\mu\nu} \left(\frac{z}{1-z} + \frac{1-z}{z} \right) - 2(1-\epsilon)z(1-z) \frac{k_\perp^\mu k_\perp^\nu}{k_\perp^2} \right], \quad (\text{C.1})$$

$$\hat{P}_{q\bar{q}}^{(0),\mu\nu}(z, k_\perp; \epsilon) = \hat{P}_{\bar{q}q}^{(0),\mu\nu}(z, k_\perp; \epsilon) = T_F \left[-g^{\mu\nu} + 4z(1-z) \frac{k_\perp^\mu k_\perp^\nu}{k_\perp^2} \right], \quad (\text{C.2})$$

$$\hat{P}_{qg}^{(0),ss'}(z, k_\perp; \epsilon) = \hat{P}_{\bar{q}g}^{(0),ss'}(z, k_\perp; \epsilon) = \delta^{ss'} C_F \left[\frac{1+z^2}{1-z} - \epsilon(1-z) \right], \quad (\text{C.3})$$

$$\hat{P}_{gq}^{(0),ss'}(z, k_\perp; \epsilon) = \hat{P}_{g\bar{q}}^{(0),ss'}(z, k_\perp; \epsilon) = \hat{P}_{qg}^{(0),ss'}(1-z, k_\perp; \epsilon). \quad (\text{C.4})$$

Additionally to the averaged version of the collinear factorization formula is need and given by

$$\overline{|\mathcal{M}_{a_1, a_2, \dots}^{(0)}(p_1, p_2, \dots)|^2} \simeq 4\pi\alpha_s \frac{2}{s_{12}} \langle \hat{\mathbf{P}}_{a_1 a_2}^{(0)}(z; \epsilon) \rangle |\mathcal{M}_{a, \dots}^{(0)}(p, \dots)|^2, \quad (\text{C.5})$$

with the averaged splitting functions

$$\langle \hat{\mathbf{P}}_{gg}^{(0)}(z; \epsilon) \rangle = 2C_A \left[\frac{z}{1-z} + \frac{1-z}{z} + z(1-z) \right], \quad (\text{C.6})$$

$$\langle \hat{\mathbf{P}}_{q\bar{q}}^{(0)}(z; \epsilon) \rangle = \langle \hat{\mathbf{P}}_{\bar{q}q}^{(0)}(z; \epsilon) \rangle = T_F \left[1 - \frac{2z(1-z)}{1-\epsilon} \right], \quad (\text{C.7})$$

$$\langle \hat{\mathbf{P}}_{qg}^{(0)}(z; \epsilon) \rangle = \langle \hat{\mathbf{P}}_{\bar{q}g}^{(0)}(z; \epsilon) \rangle = C_F \left[\frac{1+z^2}{1-z} - \epsilon(1-z) \right], \quad (\text{C.8})$$

$$\langle \hat{\mathbf{P}}_{gq}^{(0)}(z; \epsilon) \rangle = \langle \hat{\mathbf{P}}_{g\bar{q}}^{(0)}(z; \epsilon) \rangle = \langle \hat{\mathbf{P}}_{qg}^{(0)}(1-z; \epsilon) \rangle. \quad (\text{C.9})$$

Also polarized splitting functions are required for polarized final state gluons with momentum p_1 and polarization vector ε_1^μ , which can be chosen to be real,

$$\hat{P}_{Pgg}^{(0),\mu\nu}(z, k_\perp, \varepsilon_1^\mu) = 2C_A \left[g^{\mu\nu} \frac{(\varepsilon_1 \cdot k_\perp)^2}{k_\perp^2} \left(\frac{1-z}{z} \right) + \left(\frac{z}{1-z} \right) \varepsilon_1^\mu \varepsilon_1^\nu \right]$$

C. Factorization Formula

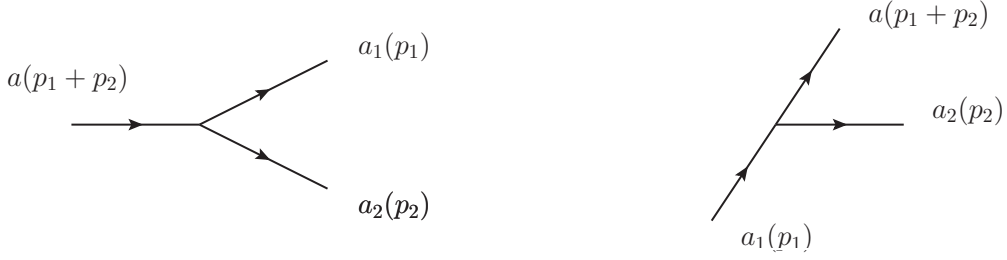


Figure C.1.: Final state collinear splitting configuration (left) vs. initial state collinear splitting configuration (right).

$$-z(1-z) \frac{k_{\perp}^{\mu} k_{\perp}^{\nu}}{k_{\perp}^2} \Big], \quad (\text{C.10})$$

$$\hat{P}_{Pgq}^{(0), ss'}(z, k_{\perp}, \varepsilon_1^{\mu}) = \delta^{ss'} C_F \left[-2 \frac{(\varepsilon_1 \cdot k_{\perp})^2}{k_{\perp}^2} \left(\frac{1-z}{z} \right) + \frac{1}{2} z \right]. \quad (\text{C.11})$$

The crossings needed to obtain the splitting functions can read of the figure C.1. Essentially it amounts to a sign in front of the splitting function:

$$\hat{\mathbf{P}}_{a_1 a_2} \longrightarrow (-)^{2s_a + 2s_{a_1}} \hat{\mathbf{P}}_{a_1 a_2}, \quad (\text{C.12})$$

where s_a and s_{a_1} are the spins of partons a and a_1 respectively, and a replacement of the energy fractions z :

$$z = \frac{p_1^0}{p_1^0 + p_2^0} \in [0, 1] \longrightarrow z = \frac{p_1^0}{p_1^0 - p_2^0} \in [1, +\infty[. \quad (\text{C.13})$$

In the triple collinear limit the splitting functions are parameterized through invariants and the following set of variables

$$z_i = \frac{x_i}{\sum_{j=1}^3 x_j}, \quad \tilde{k}_i^{\mu} = k_{\perp i}^{\mu} - \frac{x_i}{\sum_{k=1}^3 x_k} \sum_{j=1}^3 k_{\perp j}^{\mu}, \quad t_{ij,k} = 2 \frac{z_i s_{jk} - z_j s_{ik}}{z_i + z_j} + \frac{z_i - z_j}{z_i + z_j} s_{ij}. \quad (\text{C.14})$$

The complete set of splitting functions is taken from Ref. [122] (see also [233, 234]). If spin conservation holds for certain flavor combination, only the averaged splitting function $\langle \hat{\mathbf{P}}_{a_1 a_2 a_3} \rangle$ is given, where

$$\hat{P}_{a_1 a_2 a_3}^{ss'} = \delta^{ss'} \langle \hat{\mathbf{P}}_{a_1 a_2 a_3} \rangle. \quad (\text{C.15})$$

First splittings involving only quarks:

$$\langle \hat{\mathbf{P}}_{\bar{q}_1' q_2' q_3} \rangle = \frac{1}{2} C_F T_F \frac{s_{123}}{s_{12}} \left[-\frac{t_{12,3}^2}{s_{12} s_{123}} + \frac{4z_3 + (z_1 - z_2)^2}{z_1 + z_2} + (1 - 2\epsilon) \left(z_1 + z_2 - \frac{s_{12}}{s_{123}} \right) \right]. \quad (\text{C.16})$$

For identical quark flavors symmetrization has to be taken into account

$$\langle \hat{\mathbf{P}}_{\bar{q}_1 q_2 q_3} \rangle = \left[\langle \hat{\mathbf{P}}_{\bar{q}_1' q_2' q_3} \rangle + (2 \leftrightarrow 3) \right] + \langle \hat{\mathbf{P}}_{\bar{q}_1 q_2 q_3}^{(\text{id})} \rangle, \quad (\text{C.17})$$

where

$$\begin{aligned}
 \langle \hat{\mathbf{P}}_{\bar{q}_1 q_2 q_3}^{(\text{id})} \rangle &= C_F \left(C_F - \frac{1}{2} C_A \right) \left\{ (1 - \epsilon) \left(\frac{2s_{23}}{s_{12}} - \epsilon \right) \right. \\
 &+ \frac{s_{123}}{s_{12}} \left[\frac{1 + z_1^2}{1 - z_2} - \frac{2z_2}{1 - z_3} - \epsilon \left(\frac{(1 - z_3)^2}{1 - z_2} + 1 + z_1 - \frac{2z_2}{1 - z_3} \right) - \epsilon^2 (1 - z_3) \right] \\
 &\left. - \frac{s_{123}^2}{s_{12}s_{13}} \frac{z_1}{2} \left[\frac{1 + z_1^2}{(1 - z_2)(1 - z_3)} - \epsilon \left(1 + 2 \frac{1 - z_2}{1 - z_3} \right) - \epsilon^2 \right] \right\} + (2 \leftrightarrow 3). \quad (\text{C.18})
 \end{aligned}$$

The remaining functions are

$$\langle \hat{\mathbf{P}}_{g_1 g_2 q_3} \rangle = C_F^2 \langle \hat{\mathbf{P}}_{g_1 g_2 q_3}^{(\text{ab})} \rangle + C_F C_A \langle \hat{\mathbf{P}}_{g_1 g_2 q_3}^{(\text{nab})} \rangle, \quad (\text{C.19})$$

with

$$\begin{aligned}
 \langle \hat{\mathbf{P}}_{g_1 g_2 q_3}^{(\text{ab})} \rangle &= \left\{ \frac{s_{123}^2}{2s_{13}s_{23}} z_3 \left[\frac{1 + z_3^2}{z_1 z_2} - \epsilon \frac{z_1^2 + z_2^2}{z_1 z_2} - \epsilon(1 + \epsilon) \right] \right. \\
 &+ \frac{s_{123}}{s_{13}} \left[\frac{z_3(1 - z_1) + (1 - z_2)^3}{z_1 z_2} + \epsilon^2(1 + z_3) - \epsilon(z_1^2 + z_1 z_2 + z_2^2) \frac{1 - z_2}{z_1 z_2} \right] \\
 &\left. + (1 - \epsilon) \left[\epsilon - (1 - \epsilon) \frac{s_{23}}{s_{13}} \right] \right\} + (1 \leftrightarrow 2), \quad (\text{C.20})
 \end{aligned}$$

$$\begin{aligned}
 \langle \hat{\mathbf{P}}_{g_1 g_2 q_3}^{(\text{nab})} \rangle &= \left\{ (1 - \epsilon) \left(\frac{t_{12,3}^2}{4s_{12}^2} + \frac{1}{4} - \frac{\epsilon}{2} \right) + \frac{s_{123}^2}{2s_{12}s_{13}} \left[\frac{(1 - z_3)^2(1 - \epsilon) + 2z_3}{z_2} \right. \right. \\
 &+ \left. \frac{z_2^2(1 - \epsilon) + 2(1 - z_2)}{1 - z_3} \right] - \frac{s_{123}^2}{4s_{13}s_{23}} z_3 \left[\frac{(1 - z_3)^2(1 - \epsilon) + 2z_3}{z_1 z_2} + \epsilon(1 - \epsilon) \right] \\
 &+ \frac{s_{123}}{2s_{12}} \left[(1 - \epsilon) \frac{z_1(2 - 2z_1 + z_1^2) - z_2(6 - 6z_2 + z_2^2)}{z_2(1 - z_3)} + 2\epsilon \frac{z_3(z_1 - 2z_2) - z_2}{z_2(1 - z_3)} \right] \\
 &+ \frac{s_{123}}{2s_{13}} \left[(1 - \epsilon) \frac{(1 - z_2)^3 + z_3^2 - z_2}{z_2(1 - z_3)} - \epsilon \left(\frac{2(1 - z_2)(z_2 - z_3)}{z_2(1 - z_3)} - z_1 + z_2 \right) \right. \\
 &\left. \left. - \frac{z_3(1 - z_1) + (1 - z_2)^3}{z_1 z_2} + \epsilon(1 - z_2) \left(\frac{z_1^2 + z_2^2}{z_1 z_2} - \epsilon \right) \right] \right\} + (1 \leftrightarrow 2). \quad (\text{C.21})
 \end{aligned}$$

Similarly

$$\hat{P}_{g_1 q_2 \bar{q}_3}^{\mu\nu} = C_F T_F \hat{P}_{g_1 q_2 \bar{q}_3}^{\mu\nu(\text{ab})} + C_A T_F \hat{P}_{g_1 q_2 \bar{q}_3}^{\mu\nu(\text{nab})}, \quad (\text{C.22})$$

with

$$\begin{aligned}
 \hat{P}_{g_1 q_2 \bar{q}_3}^{\mu\nu(\text{ab})} &= -g^{\mu\nu} \left[-2 + \frac{2s_{123}s_{23} + (1 - \epsilon)(s_{123} - s_{23})^2}{s_{12}s_{13}} \right] \\
 &+ \frac{4s_{123}}{s_{12}s_{13}} \left(\tilde{k}_3^\mu \tilde{k}_2^\nu + \tilde{k}_2^\mu \tilde{k}_3^\nu - (1 - \epsilon) \tilde{k}_1^\mu \tilde{k}_1^\nu \right), \quad (\text{C.23})
 \end{aligned}$$

C. Factorization Formula

$$\begin{aligned}
\hat{P}_{g_1 q_2 \bar{q}_3}^{\mu\nu(\text{nab})} &= \frac{1}{4} \left\{ \frac{s_{123}}{s_{23}^2} \left[g^{\mu\nu} \frac{t_{23,1}^2}{s_{123}} - 16 \frac{z_2^2 z_3^2}{z_1(1-z_1)} \left(\frac{\tilde{k}_2}{z_2} - \frac{\tilde{k}_3}{z_3} \right)^\mu \left(\frac{\tilde{k}_2}{z_2} - \frac{\tilde{k}_3}{z_3} \right)^\nu \right] \right. \\
&\quad + \frac{s_{123}}{s_{12}s_{13}} \left[2s_{123}g^{\mu\nu} - 4(\tilde{k}_2^\mu \tilde{k}_3^\nu + \tilde{k}_3^\mu \tilde{k}_2^\nu - (1-\epsilon)\tilde{k}_1^\mu \tilde{k}_1^\nu) \right] \\
&\quad - g^{\mu\nu} \left[-(1-2\epsilon) + 2\frac{s_{123}}{s_{12}} \frac{1-z_3}{z_1(1-z_1)} + 2\frac{s_{123}}{s_{23}} \frac{1-z_1+2z_1^2}{z_1(1-z_1)} \right] \\
&\quad + \frac{s_{123}}{s_{12}s_{23}} \left[-2s_{123}g^{\mu\nu} \frac{z_2(1-2z_1)}{z_1(1-z_1)} - 16\tilde{k}_3^\mu \tilde{k}_3^\nu \frac{z_2^2}{z_1(1-z_1)} + 8(1-\epsilon)\tilde{k}_2^\mu \tilde{k}_2^\nu \right. \\
&\quad \left. \left. + 4(\tilde{k}_2^\mu \tilde{k}_3^\nu + \tilde{k}_3^\mu \tilde{k}_2^\nu) \left(\frac{2z_2(z_3-z_1)}{z_1(1-z_1)} + (1-\epsilon) \right) \right] \right\} + (2 \leftrightarrow 3). \quad (\text{C.24})
\end{aligned}$$

Finally

$$\begin{aligned}
\hat{P}_{g_1 g_2 g_3}^{\mu\nu} &= C_A^2 \left\{ \frac{(1-\epsilon)}{4s_{12}^2} \left[-g^{\mu\nu} t_{12,3}^2 + 16s_{123} \frac{z_1^2 z_2^2}{z_3(1-z_3)} \left(\frac{\tilde{k}_2}{z_2} - \frac{\tilde{k}_1}{z_1} \right)^\mu \left(\frac{\tilde{k}_2}{z_2} - \frac{\tilde{k}_1}{z_1} \right)^\nu \right] \right. \\
&\quad - \frac{3}{4}(1-\epsilon)g^{\mu\nu} + \frac{s_{123}}{s_{12}} g^{\mu\nu} \frac{1}{z_3} \left[\frac{2(1-z_3) + 4z_3^2}{1-z_3} - \frac{1-2z_3(1-z_3)}{z_1(1-z_1)} \right] \\
&\quad + \frac{s_{123}(1-\epsilon)}{s_{12}s_{13}} \left[2z_1 \left(\frac{\tilde{k}_2^\mu \tilde{k}_2^\nu}{z_3(1-z_3)} \frac{1-2z_3}{z_3} + \frac{\tilde{k}_3^\mu \tilde{k}_3^\nu}{z_2(1-z_2)} \frac{1-2z_2}{z_2} \right) \right. \\
&\quad + \frac{s_{123}}{2(1-\epsilon)} g^{\mu\nu} \left(\frac{4z_2 z_3 + 2z_1(1-z_1) - 1}{(1-z_2)(1-z_3)} - \frac{1-2z_1(1-z_1)}{z_2 z_3} \right) \\
&\quad \left. \left. + \left(\frac{\tilde{k}_2^\mu \tilde{k}_3^\nu}{z_3(1-z_3)} + \frac{\tilde{k}_3^\mu \tilde{k}_2^\nu}{z_3(1-z_3)} \right) \left(\frac{2z_2(1-z_2)}{z_3(1-z_3)} - 3 \right) \right] \right\} + (5 \text{ permutations}). \quad (\text{C.25})
\end{aligned}$$

The averaged splitting functions are

$$\begin{aligned}
\langle \hat{\mathbf{P}}_{g_1 q_2 \bar{q}_3}^{(\text{ab})} \rangle &= -2 - (1-\epsilon)s_{23} \left(\frac{1}{s_{12}} + \frac{1}{s_{13}} \right) + 2\frac{s_{123}^2}{s_{12}s_{13}} \left(1 + z_1^2 - \frac{z_1 + 2z_2 z_3}{1-\epsilon} \right) \\
&\quad - \frac{s_{123}}{s_{12}} \left(1 + 2z_1 + \epsilon - 2\frac{z_1 + z_2}{1-\epsilon} \right) - \frac{s_{123}}{s_{13}} \left(1 + 2z_1 + \epsilon - 2\frac{z_1 + z_3}{1-\epsilon} \right), \quad (\text{C.26})
\end{aligned}$$

$$\begin{aligned}
\langle \hat{\mathbf{P}}_{g_1 q_2 \bar{q}_3}^{(\text{nab})} \rangle &= \left\{ -\frac{t_{23,1}^2}{4s_{23}^2} + \frac{s_{123}^2}{2s_{13}s_{23}} z_3 \left[\frac{(1-z_1)^3 - z_1^3}{z_1(1-z_1)} - \frac{2z_3(1-z_3-2z_1 z_2)}{(1-\epsilon)z_1(1-z_1)} \right] \right. \\
&\quad + \frac{s_{123}}{2s_{13}} (1-z_2) \left[1 + \frac{1}{z_1(1-z_1)} - \frac{2z_2(1-z_2)}{(1-\epsilon)z_1(1-z_1)} \right] \\
&\quad + \frac{s_{123}}{2s_{23}} \left[\frac{1+z_1^3}{z_1(1-z_1)} + \frac{z_1(z_3-z_2)^2 - 2z_2 z_3(1+z_1)}{(1-\epsilon)z_1(1-z_1)} \right] \\
&\quad \left. - \frac{1}{4} + \frac{\epsilon}{2} - \frac{s_{123}^2}{2s_{12}s_{13}} \left(1 + z_1^2 - \frac{z_1 + 2z_2 z_3}{1-\epsilon} \right) \right\} + (2 \leftrightarrow 3), \quad (\text{C.27})
\end{aligned}$$

C.1. Infrared limits of tree-level amplitudes

$$\begin{aligned}
\langle \hat{\mathbf{P}}_{g_1 g_2 g_3} \rangle &= C_A^2 \left\{ \frac{(1-\epsilon)}{4s_{12}^2} t_{12,3}^2 + \frac{3}{4}(1-\epsilon) + \frac{s_{123}}{s_{12}} \left[4 \frac{z_1 z_2 - 1}{1-z_3} + \frac{z_1 z_2 - 2}{z_3} + \frac{3}{2} + \frac{5}{2} z_3 \right. \right. \\
&\quad \left. \left. + \frac{(1-z_3(1-z_3))^2}{z_3 z_1 (1-z_1)} \right] + \frac{s_{123}^2}{s_{12} s_{13}} \left[\frac{z_1 z_2 (1-z_2)(1-2z_3)}{z_3(1-z_3)} + z_2 z_3 - 2 + \frac{z_1(1+2z_1)}{2} \right. \right. \\
&\quad \left. \left. + \frac{1+2z_1(1+z_1)}{2(1-z_2)(1-z_3)} + \frac{1-2z_1(1-z_1)}{2z_2 z_3} \right] \right\} + (5 \text{ permutations}) . \quad (\text{C.28})
\end{aligned}$$

Initial state collinear limits are recovered by crossing (C.12).

C.1.2. Soft limits

The function $\mathcal{I}_{ij}(q_1, q_2)$ needed for the double soft-function in case of a final state $q\bar{q}$ -pair, is given by

$$\mathcal{I}_{ij}(q_1, q_2) = \frac{(p_i \cdot q_1)(p_j \cdot q_2) + (p_j \cdot q_1)(p_i \cdot q_2) - (p_i \cdot p_j)(q_1 \cdot q_2)}{(q_1 \cdot q_2)^2 [p_i \cdot (q_1 + q_2)] [p_j \cdot (q_1 + q_2)]} . \quad (\text{C.29})$$

And the soft function $\mathcal{S}_{ij}(q_1, q_2)$ can be written in terms of massive and a massless contribution

$$\mathcal{S}_{ij}(q_1, q_2) = \mathcal{S}_{ij}^{m=0}(q_1, q_2) + \left(m_i^2 \mathcal{S}_{ij}^{m \neq 0}(q_1, q_2) + m_j^2 \mathcal{S}_{ji}^{m \neq 0}(q_1, q_2) \right) , \quad (\text{C.30})$$

where the first term has been given in [122] and reads

$$\begin{aligned}
\mathcal{S}_{ij}^{m=0}(q_1, q_2) &= \frac{(1-\epsilon)}{(q_1 \cdot q_2)^2} \frac{p_i \cdot q_1 p_j \cdot q_2 + p_i \cdot q_2 p_j \cdot q_1}{p_i \cdot (q_1 + q_2) p_j \cdot (q_1 + q_2)} \\
&\quad - \frac{(p_i \cdot p_j)^2}{2 p_i \cdot q_1 p_j \cdot q_2 p_i \cdot q_2 p_j \cdot q_1} \left[2 - \frac{p_i \cdot q_1 p_j \cdot q_2 + p_i \cdot q_2 p_j \cdot q_1}{p_i \cdot (q_1 + q_2) p_j \cdot (q_1 + q_2)} \right] \\
&\quad + \frac{p_i \cdot p_j}{2 q_1 \cdot q_2} \left[\frac{2}{p_i \cdot q_1 p_j \cdot q_2} + \frac{2}{p_j \cdot q_1 p_i \cdot q_2} - \frac{1}{p_i \cdot (q_1 + q_2) p_j \cdot (q_1 + q_2)} \right] \\
&\quad \times \left(4 + \frac{(p_i \cdot q_1 p_j \cdot q_2 + p_i \cdot q_2 p_j \cdot q_1)^2}{p_i \cdot q_1 p_j \cdot q_2 p_i \cdot q_2 p_j \cdot q_1} \right) . \quad (\text{C.31})
\end{aligned}$$

The massive contribution in Eq. (C.30) was derived in Ref. [132] and reads

$$\begin{aligned}
\mathcal{S}_{ij}^{m \neq 0}(q_1, q_2) &= -\frac{1}{4 q_1 \cdot q_2 p_i \cdot q_1 p_i \cdot q_2} + \frac{p_i \cdot p_j p_j \cdot (q_1 + q_2)}{2 p_i \cdot q_1 p_j \cdot q_2 p_i \cdot q_2 p_j \cdot q_1 p_i \cdot (q_1 + q_2)} \\
&\quad - \frac{1}{2 q_1 \cdot q_2 p_i \cdot (q_1 + q_2) p_j \cdot (q_1 + q_2)} \left(\frac{(p_j \cdot q_1)^2}{p_i \cdot q_1 p_j \cdot q_2} + \frac{(p_j \cdot q_2)^2}{p_i \cdot q_2 p_j \cdot q_1} \right) . \quad (\text{C.32})
\end{aligned}$$

C. Factorization Formula

C.2. Infrared limits of one-loop matrix elements

A one-loop matrix element can be decomposed 2.1.2 into divergent part and the finite remainder function

$$2\text{Re} \langle \mathcal{M}_{n+1}^{(0)} | \mathcal{M}_{n+1}^{(1)} \rangle = 2\text{Re} \langle \mathcal{M}_{n+1}^{(0)} | \mathbf{Z}^{(1)} | \mathcal{M}_{n+1}^{(0)} \rangle + 2\text{Re} \langle \mathcal{M}_{n+1}^{(0)} | \mathcal{F}_{n+1}^{(1)} \rangle . \quad (\text{C.33})$$

The different parts have different factorization formula which are collected in the following. Note that the splitting and soft function for the finite remainder hold only at $\epsilon = 0$.

C.2.1. Collinear limit

The factorization of the one-loop matrix element was derived in [190, 235–239]

$$\begin{aligned} 2\text{Re} \langle \mathcal{M}_{a_1, a_2, \dots}^{(0)}(p_1, p_2, \dots) | \mathcal{M}_{a_1, a_2, \dots}^{(1)}(p_1, p_2, \dots) \rangle \simeq \\ 4\pi\alpha_s \frac{2}{s_{12}} \left[2\text{Re} \langle \mathcal{M}_{a, \dots}^{(0)}(p, \dots) | \hat{\mathbf{P}}_{a_1 a_2}^{(0)}(z, k_\perp; \epsilon) | \mathcal{M}_{a, \dots}^{(1)}(p, \dots) \rangle \right. \\ \left. + \frac{\alpha_s}{4\pi} \langle \mathcal{M}_{a, \dots}^{(0)}(p, \dots) | \hat{\mathbf{P}}_{a_1 a_2}^{(1)}(z, k_\perp; \epsilon) | \mathcal{M}_{a, \dots}^{(0)}(p, \dots) \rangle \right] . \end{aligned} \quad (\text{C.34})$$

The tree-level splitting function occur as well as the one-loop splitting functions $\hat{\mathbf{P}}_{a_1 a_2}^{(1)}(z, k_\perp; \epsilon)$,

$$\langle s | \hat{\mathbf{P}}_{a_1 a_2}^{(1)}(z, k_\perp; \epsilon) | s' \rangle = \hat{P}_{a_1 a_2}^{(1), ss'}(z, k_\perp; \epsilon) , \quad (\text{C.35})$$

with

$$\begin{aligned} \hat{P}_{q\bar{q}}^{(1), \mu\nu}(z, k_\perp; \epsilon) &= \hat{P}_{q\bar{q}}^{(1), \mu\nu}(z, k_\perp; \epsilon) = r_{SR}^{\bar{q}q}(z) \hat{P}_{q\bar{q}}^{(0), \mu\nu}(z, k_\perp; \epsilon) , \\ \hat{P}_{qg}^{(1), ss'}(z, k_\perp; \epsilon) &= \hat{P}_{qg}^{(1), ss'}(z, k_\perp; \epsilon) = r_{SR}^{gg}(z) \hat{P}_{qg}^{(0), ss'}(z, k_\perp; \epsilon) + C_F r_{NS}^{qg} [1 - \epsilon(1 - z)] \delta^{ss'} , \\ \hat{P}_{gq}^{(1), ss'}(z, k_\perp; \epsilon) &= \hat{P}_{gq}^{(1), ss'}(z, k_\perp; \epsilon) = \hat{P}_{qg}^{(1), ss'}(1 - z, k_\perp; \epsilon) . \end{aligned} \quad (\text{C.36})$$

In the expression appears the renormalized singular coefficients $r_{SR}^{a_1 a_2}$. The are obtained from the unrenormalized singular coefficients $r_S^{a_1 a_2}$ by

$$r_{SR}^{a_1 a_2}(z) = 2\text{Re} \left(-\frac{\mu_R^2}{s_{12}} \right)^\epsilon c_\Gamma r_S^{a_1 a_2}(z) - \frac{\beta_0}{\epsilon} , \quad (\text{C.37})$$

where

$$\text{Re} \left(-\frac{\mu_R^2}{s_{12}} \right)^\epsilon = \left(\frac{\mu_R^2}{s_{12}} \right)^\epsilon \cos(\pi\epsilon) , \quad c_\Gamma = e^{\epsilon\gamma_E} \frac{\Gamma^2(1 - \epsilon)\Gamma(1 + \epsilon)}{\Gamma(1 - 2\epsilon)} , \quad (\text{C.38})$$

and

$$r_S^{gg}(z) = -\frac{C_A}{\epsilon^2} \left[\left(\frac{z}{1 - z} \right)^\epsilon \frac{\pi\epsilon}{\sin(\pi\epsilon)} - \sum_{m=1}^{\infty} 2\epsilon^{2m-1} \text{Li}_{2m-1} \left(-\frac{1 - z}{z} \right) \right] , \quad (\text{C.39})$$

C.2. Infrared limits of one-loop matrix elements

$$r_S^{\bar{q}q}(z) = \frac{1}{\epsilon^2} (C_A - 2C_F) + \frac{C_A}{\epsilon^2} \sum_{m=1}^{\infty} \epsilon^m \left[\text{Li}_m \left(-\frac{z}{1-z} \right) + \text{Li}_m \left(-\frac{1-z}{z} \right) \right] \quad (\text{C.40})$$

$$+ \frac{1}{1-2\epsilon} \left[\frac{1}{\epsilon} (\gamma_0^q - \gamma_0^g) + C_A - 2C_F + \frac{C_A + 4T_F n_l}{3(3-2\epsilon)} \right], \quad (\text{C.41})$$

$$r_S^{gg}(z) = -\frac{1}{\epsilon^2} \left[C_A \left(\frac{z}{1-z} \right)^\epsilon \frac{\pi\epsilon}{\sin(\pi\epsilon)} + \sum_{m=1}^{\infty} \epsilon^m [(1 + (-1)^m) C_A - 2C_F] \text{Li}_m \left(-\frac{1-z}{z} \right) \right]. \quad (\text{C.42})$$

The non-singular coefficients read

$$r_{NS}^{gg} = 2\text{Re} \left(-\frac{\mu_R^2}{s_{12}} \right)^\epsilon \text{c}_\Gamma \frac{C_A(1-\epsilon) - 2T_F n_l}{(1-2\epsilon)(2-2\epsilon)(3-2\epsilon)}, \quad r_{NS}^{qg} = 2\text{Re} \left(-\frac{\mu_R^2}{s_{12}} \right)^\epsilon \text{c}_\Gamma \frac{C_A - C_F}{1-2\epsilon}. \quad (\text{C.43})$$

The initial state crossing is a little bit more evolved and besides the crossing (C.12) the following analytical continuation need to be considered

$$\text{Re} \left(-\frac{\mu_R^2}{s_{12}} \right)^\epsilon = \left(-\frac{\mu_R^2}{s_{12}} \right)^\epsilon, \quad \text{Re} \left(\frac{z}{1-z} \right)^\epsilon = \left(-\frac{z}{1-z} \right)^\epsilon \cos(\pi\epsilon). \quad (\text{C.44})$$

Also the the polylogarithms of $-z/(1-z) \in [1, +\infty[$ develop an imaginary part in this case. For the next-to-next-to-leading order calculation only the real parts are needed:

$$\begin{aligned} \text{Re}(\text{Li}_1(1/x)) &= -\text{Re}(\ln(1-1/x)) = -\ln(1-x) + \ln(x), \\ \text{Re}(\text{Li}_2(1/x)) &= \frac{\pi^2}{3} - \frac{\ln^2(x)}{2} - \text{Li}_2(x), \\ \text{Re}(\text{Li}_3(1/x)) &= -\frac{\pi^2}{3} \ln(x) + \frac{\ln^3(x)}{6} + \text{Li}_3(x), \\ \text{Re}(\text{Li}_4(1/x)) &= \frac{\pi^4}{45} + \frac{\pi^2}{6} \ln^2(x) - \frac{\ln^4(x)}{24} - \text{Li}_4(x), \end{aligned} \quad (\text{C.45})$$

with $x = -(1-z)/z \in [0, 1]$.

C.2.2. Soft limit

In the soft limit, the coefficients of the function

$$g_{ij}^{(1)} = -\frac{1}{2} a_S^b \left(\frac{2(p_I \cdot p_J) \mu^2}{2(p_I \cdot q) 2(p_J \cdot q)} \right)^\epsilon \left[\frac{1}{\epsilon^2} + \sum_{n=-1}^1 \epsilon^n \left(R_{ij}^{(n)} + i\pi I_{ij}^{(n)} \right) \right], \quad (\text{C.46})$$

appear. The results have been originally obtained in [240] and reformulated in [241]. The coefficients are given in the timelike (TL) case where both momenta p_i and p_j are in- or outgoing (the incoming case has an additional minus sign in front of the imaginary part

C. Factorization Formula

(I_{ij}) and the spacelike (SL) case were p_i is outgoing and p_j is incoming.

$$\begin{aligned}
R_{ij}^{(-1)[SL]} &= R_{ij}^{(-1)[TL]} , \\
R_{ij}^{(0)[SL]} &= R_{ij}^{(0)[TL]} - 12\zeta_2 \frac{v_-}{v} , \\
R_{ij}^{(1)[SL]} &= R_{ij}^{(1)[TL]} + 12\zeta_2 \frac{1}{v} \left[\frac{2}{(d_i + d_j)} (\alpha_J v_+ - \alpha_I v_-) \ln \left(\frac{\alpha_J}{v_+} \right) + (v_+ \ln(v_+) - \ln(v)) \right] ,
\end{aligned} \tag{C.47}$$

with the imaginary part

$$\begin{aligned}
I_{ij}^{(-1)[SL]} &= 1 , \\
I_{ij}^{(0)[SL]} &= \frac{2}{v(d_i + d_j)} \left((\alpha_I - v_-) \ln \left(\frac{\alpha_I}{v_+} \right) - (d_i v_- + \alpha_J v) \ln \left(\frac{\alpha_J}{v_+} \right) \right) + \ln(v_+) , \\
I_{ij}^{(1)[SL]} &= \frac{1}{(d_i + d_j)} \left\{ (1 - (d_i + d_j)) \right. \\
&\quad \left[2 \ln \left(\frac{\alpha_I}{v_+} \right) \ln \left(1 - \frac{\alpha_I}{v_+} \right) - \ln \left(\frac{\alpha_J}{v_+} \right) \left(2 \ln \left(1 - \frac{\alpha_J}{v_+} \right) + \ln(v_+) \right) \right. \\
&\quad \left. - 2\text{Li}_2 \left(\frac{\alpha_J}{v_+} \right) + 2\text{Li}_2 \left(\frac{\alpha_I}{v_+} \right) \right] + \frac{1}{v} \left[(\alpha_I - v_-) \ln^2 \left(\frac{\alpha_I}{v_+} \right) + (d_i v_- + \alpha_J v) \ln^2 \left(\frac{\alpha_J}{v_+} \right) \right. \\
&\quad \left. + 2 \ln \left(\frac{\alpha_I}{v_+} \right) \left((v_+ - \alpha_I) \ln(v_+) - d_i \ln(v) \right) + d_i \ln \left(\frac{\alpha_J}{v_+} \right) \left(\ln(v_+) - 2 \ln(v) \right) \right. \\
&\quad \left. \left. - 2d_i \text{Li}_2(x) - 2\zeta_2 d_j \right] \right\} + \frac{1}{2} \ln^2(v_+) - \zeta_2 \left(\frac{3}{2} - \frac{2}{v} \right) .
\end{aligned}$$

And the time-like results read:

$$\begin{aligned}
 R_{ij}^{(-1)[TL]} &= \ln(v_+) - \frac{v_-}{v} \left(\ln\left(\frac{\alpha_I}{v_+}\right) + \ln\left(\frac{\alpha_J}{v_+}\right) \right), \\
 R_{ij}^{(0)[TL]} &= \frac{1}{v} \left[\frac{1}{(d_i + d_j)} \left((\alpha_I v_+ - \alpha_J v_-) \ln^2\left(\frac{\alpha_I}{v_+}\right) + (\alpha_J v_+ - \alpha_I v_-) \ln^2\left(\frac{\alpha_J}{v_+}\right) \right) \right. \\
 &\quad \left. + \left(\ln\left(\frac{\alpha_I}{v_+}\right) + \ln\left(\frac{\alpha_J}{v_+}\right) \right) (v_+ \ln(v_+) - \ln(v)) - \text{Li}_2(x) \right] + \frac{1}{2} \ln^2(v_+) \\
 &\quad + \zeta_2 \left(\frac{7}{v} - \frac{19}{2} \right), \\
 R_{ij}^{(1)[TL]} &= \frac{1}{(d_i + d_j)} \left\{ (1 - (d_i + d_j)) \left[\ln\left(1 - \frac{\alpha_I}{v_+}\right) \ln^2\left(\frac{\alpha_I}{v_+}\right) + \ln\left(1 - \frac{\alpha_J}{v_+}\right) \ln^2\left(\frac{\alpha_J}{v_+}\right) \right. \right. \\
 &\quad \left. \left. + 2 \left(\ln\left(\frac{\alpha_I}{v_+}\right) \text{Li}_2\left(\frac{\alpha_I}{v_+}\right) + \ln\left(\frac{\alpha_J}{v_+}\right) \text{Li}_2\left(\frac{\alpha_J}{v_+}\right) \right) - \text{Li}_2(x) \left(\ln\left(\frac{\alpha_I}{v_+}\right) + \ln\left(\frac{\alpha_J}{v_+}\right) \right) \right. \right. \\
 &\quad \left. \left. + 2 \left(\text{Li}_3(x) - \text{Li}_3\left(\frac{\alpha_I}{v_+}\right) - \text{Li}_3\left(\frac{\alpha_J}{v_+}\right) + \zeta_3 \right) \right] - 7\zeta_2 \left(\ln\left(\frac{\alpha_I}{v_+}\right) + \ln\left(\frac{\alpha_J}{v_+}\right) \right) \right. \\
 &\quad \left. + \frac{1}{v} \left[\left((\alpha_J v_+ - \alpha_I v_-) \ln^2\left(\frac{\alpha_I}{v_+}\right) + (\alpha_I v_+ - \alpha_J v_-) \ln^2\left(\frac{\alpha_J}{v_+}\right) \right) \ln(v_+) \right. \right. \\
 &\quad \left. \left. + (\alpha_I - \alpha_J) \left(\ln^2\left(\frac{\alpha_I}{v_+}\right) - \ln^2\left(\frac{\alpha_J}{v_+}\right) \right) \ln(v) \right. \right. \\
 &\quad \left. \left. - \left(d_i \ln\left(\frac{\alpha_I}{v_+}\right) + d_j \ln\left(\frac{\alpha_J}{v_+}\right) \right) (\text{Li}_2(x) - 7\zeta_2) \right] \right\} \\
 &\quad + \frac{1}{v} \left\{ \left[\ln(v_+) \left(\frac{3+v}{4} \ln(v_+) - \ln(v) \right) - \frac{9v_-}{2} \zeta_2 \right] \left(\ln\left(\frac{\alpha_I}{v_+}\right) + \ln\left(\frac{\alpha_J}{v_+}\right) \right) \right. \\
 &\quad \left. - \frac{v_-}{6} \left(\ln^3\left(\frac{\alpha_I}{v_+}\right) + \ln^3\left(\frac{\alpha_J}{v_+}\right) \right) + 2\text{Li}_3(1-x) + \text{Li}_3(x) \right. \\
 &\quad \left. - \left[\text{Li}_2(x) + \zeta_2 \left(5 + \frac{19}{2} v \right) \right] \ln(v_+) \right. \\
 &\quad \left. + 12\zeta_2 \ln(v) \right\} + \frac{1}{6} \ln^3(v_+) - \left(\frac{7}{3} + \frac{1}{v} \right) \zeta_3,
 \end{aligned}$$

C. Factorization Formula

and

$$\begin{aligned}
I_{ij}^{(-1)[TL]} &= 2 - \frac{1}{v}, \\
I_{ij}^{(0)[TL]} &= \frac{2}{v} \left[\frac{1}{(d_i + d_j)} \left((\alpha_I - v_-) \ln \left(\frac{\alpha_I}{v_+} \right) + (\alpha_J - v_-) \ln \left(\frac{\alpha_J}{v_+} \right) \right) \right. \\
&\quad \left. + \left(\frac{1}{2} + v \right) \ln(v_+) - \ln(v) \right], \\
I_{ij}^{(1)[TL]} &= \frac{1}{(d_i + d_j)} \left\{ 2(1 - (d_i + d_j)) \left(\ln \left(\frac{\alpha_I}{v_+} \right) \ln \left(1 - \frac{\alpha_I}{v_+} \right) + \ln \left(\frac{\alpha_J}{v_+} \right) \ln \left(1 - \frac{\alpha_J}{v_+} \right) \right) \right. \\
&\quad + \text{Li}_2 \left(\frac{\alpha_I}{v_+} \right) + \text{Li}_2 \left(\frac{\alpha_J}{v_+} \right) + \left(\ln \left(\frac{\alpha_I}{v_+} \right) + \ln \left(\frac{\alpha_J}{v_+} \right) \right) \ln(v_+) - 2(\text{Li}_2(x) + \zeta_2) \\
&\quad + \frac{1}{v} \left[\left((\alpha_I - v_-) \ln^2 \left(\frac{\alpha_I}{v_+} \right) \right) \right. \\
&\quad \left. + (\alpha_J - v_-) \ln^2 \left(\frac{\alpha_J}{v_+} \right) + \left(d_i \ln \left(\frac{\alpha_I}{v_+} \right) + d_j \ln \left(\frac{\alpha_J}{v_+} \right) \right) (\ln(v_+) - 2 \ln(v)) \right] \left. \right\} \\
&\quad - \frac{1}{v} \left(4v_- \text{Li}_2(x) + \frac{1}{2} (\ln(v_+) - 2 \ln(v))^2 \right) + \ln^2(v_+) - \zeta_2 \left(1 - \frac{3}{2v} \right). \tag{C.48}
\end{aligned}$$

The appearing variables are defined as

$$\begin{aligned}
\alpha_I &\equiv \frac{m_i^2 2(p_J \cdot q)}{2(p_I \cdot p_J) 2(p_I \cdot q)}, \quad \alpha_J \equiv \frac{m_j^2 2(p_I \cdot q)}{2(p_I \cdot p_J) 2(p_J \cdot q)}, \quad d_i \equiv 1 - 2\alpha_I, \quad d_j \equiv 1 - 2\alpha_J, \\
v &\equiv \sqrt{1 - 4\alpha_I \alpha_J}, \quad v_{\pm} \equiv \frac{1 \pm v}{2}, \quad x \equiv \frac{v_-}{v_+}, \tag{C.49}
\end{aligned}$$

This results are not UV renormalized, the prescription to do so can be found in [240].

C.2.3. Limits of matrix elements of $Z^{(1)}$

The solution of the RGE equation for $Z^{(1)}$ 2.29 sandwiched between tree-level amplitudes read

$$\begin{aligned}
 2\text{Re} \langle \mathcal{M}_{n+1}^{(0)} | Z^{(1)} | \mathcal{M}_{n+1}^{(0)} \rangle = & \\
 \frac{\alpha_s}{4\pi} \frac{1}{\epsilon} \left[\left(-\frac{2}{\epsilon} \sum_{i_0} C_{i_0} + \sum_i \gamma_0^i \right) |\mathcal{M}_{n+1}^{(0)}|^2 \right. & \\
 + 2 \sum_{(i_0, j_0)} \ln \left| \frac{\mu_R^2}{s_{i_0 j_0}} \right| \langle \mathcal{M}_{n+1}^{(0)} | \mathbf{T}_{i_0} \cdot \mathbf{T}_{j_0} | \mathcal{M}_{n+1}^{(0)} \rangle & \\
 - \sum_{(I, J)} \frac{1}{v_{IJ}} \ln \left(\frac{1 + v_{IJ}}{1 - v_{IJ}} \right) \langle \mathcal{M}_{n+1}^{(0)} | \mathbf{T}_I \cdot \mathbf{T}_J | \mathcal{M}_{n+1}^{(0)} \rangle & \\
 \left. + 4 \sum_{I, j_0} \ln \left| \frac{m_I \mu_R}{s_{I j_0}} \right| \langle \mathcal{M}_{n+1}^{(0)} | \mathbf{T}_I \cdot \mathbf{T}_{j_0} | \mathcal{M}_{n+1}^{(0)} \rangle \right]. & \quad (\text{C.50})
 \end{aligned}$$

This matrix element factorizes in the collinear limit as

$$\begin{aligned}
 2\text{Re} \langle \mathcal{M}_{a_1, a_2, \dots}^{(0)}(p_1, p_2, \dots) | Z^{(1)} | \mathcal{M}_{a_1, a_2, \dots}^{(0)}(p_1, p_2, \dots) \rangle \simeq & \\
 4\pi\alpha_s \frac{2}{s_{12}} \left\{ 2\text{Re} \langle \mathcal{M}_{a, \dots}^{(0)}(p, \dots) | \hat{\mathbf{P}}_{a_1 a_2}^{(0)}(z, k_\perp; \epsilon) Z^{(1)} | \mathcal{M}_{a, \dots}^{(0)}(p, \dots) \rangle \right. & \\
 + \frac{\alpha_s}{4\pi} \frac{1}{\epsilon} \left[2(C_a - C_{a_1} - C_{a_2}) \left(\frac{1}{\epsilon} + \ln \left| \frac{\mu_R^2}{s_{12}} \right| \right) - (\gamma_0^a - \gamma_0^{a_1} - \gamma_0^{a_2}) \right. & \\
 + 2C_a \ln |z(1-z)| + 2(C_{a_1} - C_{a_2}) \ln \left| \frac{z}{1-z} \right| & \\
 \left. \left. \times \langle \mathcal{M}_{a, \dots}^{(0)}(p, \dots) | \hat{\mathbf{P}}_{a_1 a_2}^{(0)}(z, k_\perp; \epsilon) | \mathcal{M}_{a, \dots}^{(0)}(p, \dots) \rangle \right\}. & \quad (\text{C.51})
 \end{aligned}$$

The initial state case is again obtained by crossing (C.12)

C. Factorization Formula

The soft limit of Eq. (C.50), $q \rightarrow 0$, reads

$$\begin{aligned}
2\text{Re} \langle \mathcal{M}_{g,a_1,\dots}^{(0)}(q, p_1, \dots) | \mathbf{Z}^{(1)} | \mathcal{M}_{g,a_1,\dots}^{(0)}(q, p_1, \dots) \rangle \simeq \\
-4\pi\alpha_s \left\{ \sum_{(i,j)} \left(\mathcal{S}_{ij}(q) - \mathcal{S}_{ii}(q) \right) 2\text{Re} \langle \mathcal{M}_{a_1,\dots}^{(0)}(p_1, \dots) | \mathbf{T}_i \cdot \mathbf{T}_j \mathbf{Z}^{(1)} | \mathcal{M}_{a_1,\dots}^{(0)}(p_1, \dots) \rangle \right. \\
+ \frac{\alpha_s}{4\pi} \frac{1}{\epsilon} \left[\sum_{(i,j)} \left(\mathcal{S}_{ij}(q) - \mathcal{S}_{ii}(q) \right) \right. \\
\cdot \left(-2C_A \left(\frac{1}{\epsilon} + \ln\left(\frac{1}{2}\mu_R^2 \mathcal{S}_{ij}(q)\right) \right) + \gamma_0^g \right) \langle \mathcal{M}_{a_1,\dots}^{(0)}(p_1, \dots) | \mathbf{T}_i \cdot \mathbf{T}_j | \mathcal{M}_{a_1,\dots}^{(0)}(p_1, \dots) \rangle \\
- C_A \sum_{(I,J)} \left(\mathcal{S}_{IJ}(q) - \mathcal{S}_{II}(q) \right) \left(\frac{1}{v_{IJ}} \ln\left(\frac{1+v_{IJ}}{1-v_{IJ}}\right) + 2 \ln\left(\frac{m_I m_J}{s_{IJ}}\right) \right) \\
\cdot \langle \mathcal{M}_{a_1,\dots}^{(0)}(p_1, \dots) | \mathbf{T}_I \cdot \mathbf{T}_J | \mathcal{M}_{a_1,\dots}^{(0)}(p_1, \dots) \rangle \\
- 4\pi \sum_{(i,j,k)} \mathcal{S}_{ik}(q) \left(\frac{1}{v_{ij}} \theta(\sigma_{ij}) - \theta(\sigma_{iq}) - \theta(\sigma_{jq}) \right) \\
\left. \left. \langle \mathcal{M}_{a_1,\dots}^{(0)}(p_1, \dots) | f^{abc} T_i^a T_j^b T_k^c | \mathcal{M}_{a_1,\dots}^{(0)}(p_1, \dots) \rangle \right] \right\}. \tag{C.52}
\end{aligned}$$

C.2.4. Limits of the finite remainder

Finally the collinear limit of the finite remainder:

$$\begin{aligned}
2\text{Re} \langle \mathcal{M}_{a_1,a_2,\dots}^{(0)}(p_1, p_2, \dots) | \mathcal{F}_{a_1,a_2,\dots}^{(1)}(p_1, p_2, \dots) \rangle \simeq \\
4\pi\alpha_s \frac{2}{s_{12}} \left[2\text{Re} \langle \mathcal{M}_{a,\dots}^{(0)}(p, \dots) | \hat{\mathbf{P}}_{a_1 a_2}^{(0)}(z, k_\perp; \epsilon = 0) | \mathcal{F}_{a,\dots}^{(1)}(p, \dots) \rangle \right. \\
\left. + \frac{\alpha_s}{4\pi} \langle \mathcal{M}_{a,\dots}^{(0)}(p, \dots) | \hat{\mathbf{P}}_{F a_1 a_2}^{(1)}(z, k_\perp) | \mathcal{M}_{a,\dots}^{(0)}(p, \dots) \rangle \right]. \tag{C.53}
\end{aligned}$$

The finite one-loop splitting functions, $\hat{\mathbf{P}}_{F a_1 a_2}^{(1)}(z, k_\perp)$ operate on spin space as their tree-level counterparts

$$\langle s | \hat{\mathbf{P}}_{F a_1 a_2}^{(1)}(z, k_\perp) | s' \rangle = \hat{P}_{F a_1 a_2}^{(1), ss'}(z, k_\perp), \tag{C.54}$$

with

$$\begin{aligned}
\hat{P}_{F gg}^{(1), \mu\nu}(z, k_\perp) &= r_{SF}^{gg}(z) \hat{P}_{gg}^{(0), \mu\nu}(z, k_\perp; \epsilon = 0) - \frac{4}{3} C_A (C_A - 2T_F n_l) \frac{k_\perp^\mu k_\perp^\nu}{k_\perp^2}, \\
\hat{P}_{F q\bar{q}}^{(1), \mu\nu}(z, k_\perp) &= \hat{P}_{F q\bar{q}}^{(1), \mu\nu}(z, k_\perp) = r_{SF}^{q\bar{q}}(z) \hat{P}_{q\bar{q}}^{(0), \mu\nu}(z, k_\perp; \epsilon = 0), \\
\hat{P}_{F qg}^{(1), ss'}(z, k_\perp) &= \hat{P}_{F q\bar{q}}^{(1), ss'}(z, k_\perp) = r_{SF}^{qg}(z) \hat{P}_{qg}^{(0), ss'}(z, k_\perp; \epsilon = 0) + 2C_F (C_A - C_F) \delta^{ss'}, \\
\hat{P}_{F gq}^{(1), ss'}(z, k_\perp) &= \hat{P}_{F g\bar{q}}^{(1), ss'}(z, k_\perp) = \hat{P}_{F qg}^{(1), ss'}(1-z, k_\perp). \tag{C.55}
\end{aligned}$$

The finite coefficients $r_{SF}^{a_1 a_2}(z)$ are given by

$$r_{SF}^{gg}(z) = C_A \left(\frac{5\pi^2}{6} - \ln^2 \left| \frac{z}{1-z} \right| + 2 \ln |z(1-z)| \ln \left| \frac{\mu_R^2}{s_{12}} \right| - \ln^2 \left| \frac{\mu_R^2}{s_{12}} \right| \right), \quad (\text{C.56})$$

$$r_{SF}^{\bar{q}q}(z) = C_A \left(\frac{152}{9} - \frac{3\pi^2}{2} \right) + C_F \left(\frac{7\pi^2}{3} - 16 \right) - \frac{40}{9} T_F n_l - C_A \ln^2 \left| \frac{z}{1-z} \right| + 2 \left(\beta_0 - 3C_F + C_A \ln |z(1-z)| \right) \ln \left| \frac{\mu_R^2}{s_{12}} \right| + (C_A - 2C_F) \ln^2 \left| \frac{\mu_R^2}{s_{12}} \right| \quad (\text{C.57})$$

$$+ 2(C_A - C_F) \pi^2 \theta(-s_{12}), \quad (\text{C.58})$$

$$r_{SF}^{qq}(z) = \frac{5\pi^2}{6} C_A + 4C_F \ln |z| \ln \left| \frac{\mu_R^2}{s_{12}} \right| - C_A \left(\ln \left| \frac{z}{1-z} \right| + \ln \left| \frac{\mu_R^2}{s_{12}} \right| \right)^2 \quad (\text{C.59})$$

$$+ 4(C_F - C_A) \text{Re Li}_2 \left(-\frac{1-z}{z} \right). \quad (\text{C.60})$$

Again the crossing relation (C.12) can be used to obtain the initial state case. Additionally the analytic continuation in Eq. (C.45) needs to be employed.

The soft limit of the finite remainder function is given by

$$\begin{aligned} & 2\text{Re} \langle \mathcal{M}_{g,a_1,\dots}^{(0)}(q, p_1, \dots) | \mathcal{F}_{g,a_1,\dots}^{(1)}(q, p_1, \dots) \rangle \simeq \\ & -4\pi\alpha_s \left\{ \sum_{(i,j)} \left(\mathcal{S}_{ij}(q) - \mathcal{S}_{ii}(q) \right) 2\text{Re} \langle \mathcal{M}_{a_1,\dots}^{(0)}(p_1, \dots) | \mathbf{T}_i \cdot \mathbf{T}_j | \mathcal{F}_{a_1,\dots}^{(1)}(p_1, \dots) \rangle \right. \\ & + \frac{\alpha_s}{4\pi} \left[\sum_{(i,j)} \left(\mathcal{S}_{ij}(q) - \mathcal{S}_{ii}(q) \right) R_{ij}^F \langle \mathcal{M}_{a_1,\dots}^{(0)}(p_1, \dots) | \mathbf{T}_i \cdot \mathbf{T}_j | \mathcal{M}_{a_1,\dots}^{(0)}(p_1, \dots) \rangle \right. \\ & \left. \left. - 4\pi \sum_{(i,j,k)} \mathcal{S}_{ik}(q) I_{ij}^F \langle \mathcal{M}_{a_1,\dots}^{(0)}(p_1, \dots) | f^{abc} T_i^a T_j^b T_k^c | \mathcal{M}_{a_1,\dots}^{(0)}(p_1, \dots) \rangle \right] \right\}, \quad (\text{C.61}) \end{aligned}$$

The the functions R_{ij}^F and I_{ij}^F are the $\mathcal{O}(\epsilon^0)$ coefficients discussed in (C.2.2) after expansion in ϵ

C.3. Splitting functions

The collinear factorization contributions require the splitting functions up to $\mathcal{O}(\alpha_s)$ [242]

$$P_{q_i q_j}(x, \alpha_s) = \delta_{ij} P_{qq}^{(0)}(x) + \frac{\alpha_s}{2\pi} P_{q_i q_j}^{(1)}(x) + \dots, \quad (\text{C.62})$$

$$P_{gg}(x, \alpha_s) = P_{gg}^{(0)}(x) + \frac{\alpha_s}{2\pi} P_{gg}^{(1)}(x) + \dots, \quad (\text{C.63})$$

$$P_{gq}(x, \alpha_s) = P_{gq}^{(0)}(x) + \frac{\alpha_s}{2\pi} P_{gq}^{(1)}(x) + \dots, \quad (\text{C.64})$$

$$P_{qq}(x, \alpha_s) = P_{qq}^{(0)}(x) + \frac{\alpha_s}{2\pi} P_{qq}^{(1)}(x) + \dots. \quad (\text{C.65})$$

C. Factorization Formula

The leading order contributions are

$$P_{qq}^{(0)}(x) = C_F \left[\frac{1+x^2}{(1-x)_+} + \frac{3}{2} \delta(1-x) \right], \quad (\text{C.66})$$

$$P_{qg}^{(0)}(x) = T_F [x^2 + (1-x)^2], \quad (\text{C.67})$$

$$P_{gq}^{(0)}(x) = C_F \left[\frac{1+(1-x)^2}{x} \right], \quad (\text{C.68})$$

$$P_{gg}^{(0)}(x) = 2C_A \left[\frac{x}{(1-x)_+} + \frac{1-x}{x} + x(1-x) \right] + \delta(1-x) \frac{11C_A - 4T_F n_l}{6}. \quad (\text{C.69})$$

The splitting functions $P_{q_i q_j}$ are written terms of a flavor singlet (S) and non-singlet (V) contribution starting at NLO

$$P_{q_i q_j}(x, \alpha_s) = \delta_{ij} P_{qq}^V(x, \alpha_s) + P_{qq}^S(x, \alpha_s), \quad (\text{C.70})$$

$$P_{q_i \bar{q}_j}(x, \alpha_s) = \delta_{ij} P_{q\bar{q}}^V(x, \alpha_s) + P_{q\bar{q}}^S(x, \alpha_s). \quad (\text{C.71})$$

The NLO part of the splitting functions is given by

$$\begin{aligned} P_{qq}^{V(1)}(x) &= C_F^2 \left\{ - \left[2 \ln x \ln(1-x) + \frac{3}{2} \ln x \right] p_{qq}(x) - \left(\frac{3}{2} + \frac{7}{2} x \right) \ln x \right. \\ &\quad \left. - \frac{1}{2} (1+x) \ln^2 x - 5(1-x) \right\} \\ &\quad + C_F C_A \left\{ \left[\frac{1}{2} \ln^2 x + \frac{11}{6} \ln x + \frac{67}{18} - \frac{\pi^2}{6} \right] p_{qq}(x) + (1+x) \ln x + \frac{20}{3} (1-x) \right\} \\ &\quad + C_F T_F n_l \left\{ - \left[\frac{2}{3} \ln x + \frac{10}{9} \right] p_{qq}(x) - \frac{4}{3} (1-x) \right\} + \delta P_{qq}^{(1)}(x), \end{aligned} \quad (\text{C.72})$$

$$P_{q\bar{q}}^{V(1)}(x) = C_F \left(C_F - \frac{C_A}{2} \right) \{ 2p_{qq}(-x) S_2(x) + 2(1+x) \ln x + 4(1-x) \}, \quad (\text{C.73})$$

$$\begin{aligned} P_{qq}^{S(1)}(x) &= P_{q\bar{q}}^{S(1)}(x) = C_F T_F \left[-2 + \frac{20}{9x} + 6x - \frac{56}{9} x^2 + \left(1 + 5x + \frac{8}{3} x^2 \right) \ln x \right. \\ &\quad \left. - (1+x) \ln^2 x \right], \end{aligned} \quad (\text{C.74})$$

$$(\text{C.75})$$

$$\begin{aligned} P_{qg}^{(1)}(x) &= \frac{C_F T_F}{2} \left\{ 4 - 9x - (1-4x) \ln x - (1-2x) \ln^2 x + 4 \ln(1-x) \right. \\ &\quad \left. + \left[2 \ln^2 \left(\frac{1-x}{x} \right) - 4 \ln \left(\frac{1-x}{x} \right) - \frac{2}{3} \pi^2 + 10 \right] p_{qg}(x) \right\} \\ &\quad + \frac{C_A T_F}{2} \left\{ \frac{182}{9} + \frac{14}{9} x + \frac{40}{9x} + \left(\frac{136}{3} x - \frac{38}{3} \right) \ln x - 4 \ln(1-x) \right. \\ &\quad \left. - (2+8x) \ln^2 x + 2p_{qg}(-x) S_2(x) \right\} \end{aligned}$$

C.3. Splitting functions

$$+ \left[-\ln^2 x + \frac{44}{3} \ln x - 2 \ln^2(1-x) + 4 \ln(1-x) + \frac{\pi^2}{3} - \frac{218}{9} \right] p_{qg}(x) \} \quad (\text{C.76})$$

$$\begin{aligned} P_{gq}^{(1)}(x) &= C_F^2 \left\{ -\frac{5}{2} - \frac{7x}{2} + \left(2 + \frac{7}{2}x\right) \ln x - \left(1 - \frac{1}{2}x\right) \ln^2 x - 2x \ln(1-x) \right. \\ &\quad \left. - [3 \ln(1-x) + \ln^2(1-x)] p_{gq}(x) \right\} \\ &\quad + C_F C_A \left\{ \frac{28}{9} + \frac{65}{18}x + \frac{44}{9}x^2 - \left(12 + 5x + \frac{8}{3}x^2\right) \ln x + (4+x) \ln^2 x \right. \\ &\quad \left. + 2x \ln(1-x) + S_2(x) p_{gq}(-x) \right. \\ &\quad \left. + \left[\frac{1}{2} - 2 \ln x \ln(1-x) + \frac{1}{2} \ln^2 x + \frac{11}{3} \ln(1-x) + \ln^2(1-x) - \frac{\pi^2}{6} \right] p_{gq}(x) \right\} \\ &\quad + C_F T_F n_l \left\{ -\frac{4}{3}x - \left[\frac{20}{9} + \frac{4}{3} \ln(1-x) \right] p_{gq}(x) \right\}, \quad (\text{C.77}) \end{aligned}$$

$$\begin{aligned} P_{gg}^{(1)}(x) &= C_F T_F n_l \left\{ -16 + 8x + \frac{20}{3}x^2 + \frac{4}{3x} - (6 + 10x) \ln x - (2 + 2x) \ln^2 x \right\} \\ &\quad + C_A T_F n_l \left\{ 2 - 2x + \frac{26}{9} \left(x^2 - \frac{1}{x}\right) - \frac{4}{3}(1+x) \ln x - \frac{20}{9} p_{gg}(x) \right\} \\ &\quad + C_A^2 \left\{ \frac{27}{2}(1-x) + \frac{67}{9} \left(x^2 - \frac{1}{x}\right) - \left(\frac{25}{3} - \frac{11}{3}x + \frac{44}{3}x^2\right) \ln x \right. \\ &\quad \left. + 4(1+x) \ln^2 x + 2 p_{gg}(-x) S_2(x) + \right. \\ &\quad \left. \left[\frac{67}{9} - 4 \ln x \ln(1-x) + \ln^2 x - \frac{\pi^2}{3} \right] p_{gg}(x) \right\} + \delta P_{gg}^{(1)}(x), \quad (\text{C.78}) \end{aligned}$$

where

$$S_2(x) = -2\text{Li}_2(-x) + \frac{1}{2} \ln^2 x - 2 \ln x \ln(1+x) - \frac{\pi^2}{6}. \quad (\text{C.79})$$

The functions p_{qq} , p_{qg} , p_{gq} and p_{gg} read

$$p_{qg}(x) = x^2 + (1-x)^2, \quad p_{gq}(x) = \frac{1 + (1-x^2)}{x}, \quad (\text{C.80})$$

$$p_{qq}(x) = \frac{2}{(1-x)_+} - 1 - x, \quad p_{qq}(-x) = \frac{2}{1+x} - 1 + x, \quad (\text{C.81})$$

$$p_{gg}(x) = \frac{1}{(1-x)_+} + \frac{1}{x} - 2 + x(1-x), \quad p_{gg}(-x) = \frac{1}{(1+x)} - \frac{1}{x} - 2 - x(1+x). \quad (\text{C.82})$$

The terms proportional to the δ -functions are

$$\delta P_{qq}^{(1)}(x) = \left[C_F^2 \left\{ \frac{3}{8} - \frac{\pi^2}{2} + 6\zeta_3 \right\} + C_F C_A \left\{ \frac{17}{24} + \frac{11\pi^2}{18} - 3\zeta_3 \right\} - C_F T_F n_l \left\{ \frac{1}{6} + \frac{2\pi^2}{9} \right\} \right] \delta(\mathbb{1}(\text{C.83}))$$

C. Factorization Formula

and

$$\delta P_{gg}^{(1)}(x) = \left[C_A^2 \left\{ \frac{8}{3} + 3\zeta_3 \right\} - C_{FT_{Fn_l}} - \frac{4}{3} C_{AT_{Fn_l}} \right] \delta(1-x). \quad (\text{C.84})$$

D. $t\bar{t}$ amplitude supplements

D.1. Projectors

The in section 3.1 constructed projectors read in the gg -channel:

$$\begin{aligned} \langle P_1 | &= \frac{(m_s - x - 1)(m_s - x)}{4(2\epsilon - 1)((m_s - x)^2 + x)^2} \langle S_1 | + \frac{m_s(-2m_s + 2x + 1)}{2(2\epsilon - 1)((m_s - x)^2 + x)^2} \langle S_4 | \\ &+ \frac{m_s}{4(2\epsilon - 1)((m_s - x)^2 + x)^2} \langle S_6 | \end{aligned} \quad (D.1)$$

$$\begin{aligned} \langle P_2 | &= -\frac{(m_s - x - 1)(m_s - x)}{2(2\epsilon - 1)m_s((m_s - x)^2 + x)} \langle S_2 | + \frac{(m_s - x - 1)(m_s - x)}{2(2\epsilon - 1)((m_s - x)^2 + x)^2} \langle S_3 | \\ &+ \frac{m_s(-2m_s + 2x + 1)}{2(2\epsilon - 1)((m_s - x)^2 + x)^2} \langle S_4 | + \frac{2m_s - 2x - 1}{2(2\epsilon - 1)((m_s - x)^2 + x)} \langle S_5 | \end{aligned} \quad (D.2)$$

$$\begin{aligned} \langle P_3 | &= \frac{(m_s - x - 1)(m_s - x)}{2(2\epsilon - 1)((m_s - x)^2 + x)^2} \langle S_2 | + \frac{(\epsilon - 2)m_s(m_s - x - 1)(m_s - x)}{(2\epsilon - 1)((m_s - x)^2 + x)^3} \langle S_3 | \\ &+ -\frac{(\epsilon - 2)m_s^2(2m_s - 2x - 1)}{(2\epsilon - 1)((m_s - x)^2 + x)^3} \langle S_4 | + \frac{m_s(-2m_s + 2x + 1)}{2(2\epsilon - 1)((m_s - x)^2 + x)^2} \langle S_5 | \\ &+ -\frac{m_s}{2(2\epsilon - 1)((m_s - x)^2 + x)^2} \langle S_6 | \end{aligned} \quad (D.3)$$

$$\begin{aligned} \langle P_4 | &= \frac{m_s(-2m_s + 2x + 1)}{2(2\epsilon - 1)((m_s - x)^2 + x)^2} \langle S_1 | + \frac{m_s(-2m_s + 2x + 1)}{2(2\epsilon - 1)((m_s - x)^2 + x)^2} \langle S_2 | \\ &+ -\frac{(\epsilon - 2)m_s^2(2m_s - 2x - 1)}{(2\epsilon - 1)((m_s - x)^2 + x)^3} \langle S_3 | \\ &+ \frac{m_s^2(4(m_s - x)^2 + \epsilon(4m_s - 1) - 8m_s + 4x + 2)}{(2\epsilon - 1)((m_s - x)^2 + x)^3} \langle S_4 | \\ &+ \frac{m_s(4m_s - 1)}{2(2\epsilon - 1)((m_s - x)^2 + x)^2} \langle S_5 | \end{aligned} \quad (D.4)$$

$$\begin{aligned} \langle P_5 | &= \frac{2m_s - 2x - 1}{2(2\epsilon - 1)((m_s - x)^2 + x)} \langle S_2 | + \frac{m_s(-2m_s + 2x + 1)}{2(2\epsilon - 1)((m_s - x)^2 + x)^2} \langle S_3 | \\ &+ \frac{m_s(4m_s - 1)}{2(2\epsilon - 1)((m_s - x)^2 + x)^2} \langle S_4 | + \frac{1 - 4m_s}{2(2\epsilon - 1)((m_s - x)^2 + x)} \langle S_5 | \end{aligned} \quad (D.5)$$

$$\begin{aligned} \langle P_6 | &= \frac{m_s}{4(2\epsilon - 1)((m_s - x)^2 + x)^2} \langle S_1 | + -\frac{m_s}{2(2\epsilon - 1)((m_s - x)^2 + x)^2} \langle S_3 | \\ &+ -\frac{m_s}{4(2\epsilon - 1)((m_s - x)^2 + x)^2} \langle S_6 | \end{aligned} \quad (D.6)$$

$$\begin{aligned} \langle P_7 | &= \frac{(\epsilon - 1)(m_s - x - 1)(m_s - x)}{4(2\epsilon - 1)((m_s - x)^2 + x)(-m_s(2x\epsilon + \epsilon - 1) + \epsilon m_s^2 + x(x + 1)\epsilon)} \langle S_7 | \\ &+ -\frac{1}{4(2\epsilon - 1)(-m_s(2x\epsilon + \epsilon - 1) + \epsilon m_s^2 + x(x + 1)\epsilon)} \langle S_8 | \end{aligned} \quad (D.7)$$

D. $t\bar{t}$ amplitude supplements

$$\begin{aligned} \langle P_8 | &= -\frac{1}{4(2\epsilon - 1)(-m_s(2x\epsilon + \epsilon - 1) + \epsilon m_s^2 + x(x + 1)\epsilon)} \langle S_7 | \\ &+ \frac{1}{4(2\epsilon - 1)(-m_s(2x\epsilon + \epsilon - 1) + \epsilon m_s^2 + x(x + 1)\epsilon)} \langle S_8 | \end{aligned} \quad (\text{D.8})$$

The following four projectors have been found for the $q\bar{q}$ channel:

$$\begin{aligned} \langle P_1 | &= -\frac{(\epsilon - 1)m_s(m_s - x - 1)(m_s - x)}{2(2\epsilon - 1)((m_s - x)^2 + x)^2} \langle S_1 | + \frac{(\epsilon - 1)m_s^2(2m_s - 2x - 1)}{2(2\epsilon - 1)((m_s - x)^2 + x)^2} \langle S_2 | \\ &+ \frac{m_s}{4(2\epsilon - 1)((m_s - x)^2 + x)} \langle S_4 | \\ \langle P_2 | &= \frac{(\epsilon - 1)m_s^2(2m_s - 2x - 1)}{2(2\epsilon - 1)((m_s - x)^2 + x)^2} \langle S_1 | \\ &+ \frac{m_s^2(-2(m_s - x)^2 - 4\epsilon m_s + 4m_s - 2x + \epsilon - 1)}{2(2\epsilon - 1)((m_s - x)^2 + x)^2} \langle S_2 | \end{aligned} \quad (\text{D.9})$$

$$+ \frac{m_s(2m_s - 2x - 1)}{4(2\epsilon - 1)((m_s - x)^2 + x)} \langle S_3 | \quad (\text{D.10})$$

$$\begin{aligned} \langle P_3 | &= \frac{m_s(2m_s - 2x - 1)}{4(2\epsilon - 1)((m_s - x)^2 + x)} \langle S_2 | + -\frac{(m_s - x - 1)(m_s - x)}{4(2\epsilon - 1)((m_s - x)^2 + x)} \langle S_3 | \\ &+ -\frac{m_s}{4(2\epsilon - 1)((m_s - x)^2 + x)} \langle S_4 | \end{aligned} \quad (\text{D.11})$$

$$\begin{aligned} \langle P_4 | &= \frac{m_s}{4(2\epsilon - 1)((m_s - x)^2 + x)} \langle S_1 | + -\frac{m_s}{4(2\epsilon - 1)((m_s - x)^2 + x)} \langle S_3 | \\ &+ \frac{m_s}{4(2\epsilon - 1)((m_s - x)^2 + x)} \langle S_4 | \end{aligned} \quad (\text{D.12})$$

The appearing $\langle S_i |$ and the kinematic variables have been defined in section 3.1.

Bibliography

- [1] L. Chen, M. Czakon, and R. Poncelet, “Polarized double-virtual amplitudes for heavy-quark pair production”, JHEP **03** (2018) 085, arXiv:1712.08075 [hep-ph].
- [2] F. Abe, et al., “Evidence for color coherence in $p\bar{p}$ collisions at $\sqrt{s} = 1.8$ TeV”, Phys. Rev. **D50** (1994) 5562.
- [3] S. Abachi, et al., “Observation of the top quark”, Phys. Rev. Lett. **74** (1995) 2632, arXiv:hep-ex/9503003 [hep-ex].
- [4] M. Kobayashi, and T. Maskawa, “CP Violation in the Renormalizable Theory of Weak Interaction”, Prog. Theor. Phys. **49** (1973) 652.
- [5] M. L. Perl, et al., “Evidence for Anomalous Lepton Production in e^+e^- Annihilation”, Phys. Rev. Lett. **35** (1975) 1489.
- [6] H. Harari, “A New Quark Model for Hadrons”, Phys. Lett. **57B** (1975) 265.
- [7] S. W. Herb, et al., “Observation of a Dimuon Resonance at 9.5-GeV in 400-GeV Proton-Nucleus Collisions”, Phys. Rev. Lett. **39** (1977) 252.
- [8] T. L. Collaborations, “A Combination of preliminary electroweak measurements and constraints on the standard model”, (2002), arXiv:hep-ex/0212036 [hep-ex].
- [9] M. Baak, and R. Kogler, “The global electroweak Standard Model fit after the Higgs discovery”, in Proceedings, 48th Rencontres de Moriond on Electroweak Interactions and Unified Theories: La Thuile, Italy, March 2-9, 2013 (2013), 349, arXiv:1306.0571 [hep-ph].
- [10] M. Baak, J. Cúth, J. Haller, A. Hoecker, R. Kogler, K. Mönig, M. Schott, and J. Stelzer, “The global electroweak fit at NNLO and prospects for the LHC and ILC”, Eur. Phys. J. **C74** (2014) 3046, arXiv:1407.3792 [hep-ph].
- [11] G. Degrandi, S. Di Vita, J. Elias-Miro, J. R. Espinosa, G. F. Giudice, G. Isidori, and A. Strumia, “Higgs mass and vacuum stability in the Standard Model at NNLO”, JHEP **08** (2012) 098, arXiv:1205.6497 [hep-ph].
- [12] “Projected Performance of an Upgraded CMS Detector at the LHC and HL-LHC: Contribution to the Snowmass Process”, in Proceedings, 2013 Community Summer Study on the Future of U.S. Particle Physics: Snowmass on the Mississippi (CSS2013): Minneapolis, MN, USA, July 29-August 6, 2013 (2013), arXiv:1307.7135 [hep-ex].
- [13] “Physics at a High-Luminosity LHC with ATLAS”, in Proceedings, 2013 Community Summer Study on the Future of U.S. Particle Physics: Snowmass on the Mississippi (CSS2013): Minneapolis, MN, USA, July 29-August 6, 2013 (2013), arXiv:1307.7292 [hep-ex].
- [14] CMS, *Luminosity*, (2018) <https://twiki.cern.ch/twiki/bin/view/CMSPublic/LumiPublicResults> (visited on 07/15/2018).

Bibliography

- [15] ATLAS, *Luminosity*, (2018) <https://twiki.cern.ch/twiki/bin/view/AtlasPublic/LuminosityPublicResultsRun2> (visited on 07/15/2018).
- [16] R. K. Ellis, W. J. Stirling, and B. R. Webber, *Qcd and collider physics*, Cambridge Monographs on Particle Physics, Nuclear Physics and Cosmology (Cambridge University Press, 1996).
- [17] CMS, *Physics results*, (2018) <https://twiki.cern.ch/twiki/bin/view/CMSPublic/PhysicsResultsCombined> (visited on 07/15/2018).
- [18] J. Alwall, R. Frederix, S. Frixione, V. Hirschi, F. Maltoni, O. Mattelaer, H. S. Shao, T. Stelzer, P. Torrielli, and M. Zaro, “The automated computation of tree-level and next-to-leading order differential cross sections, and their matching to parton shower simulations”, *JHEP* **07** (2014) 079, arXiv:1405.0301 [hep-ph].
- [19] A. Cafarella, C. G. Papadopoulos, and M. Worek, “Helac-Phegas: A Generator for all parton level processes”, *Comput. Phys. Commun.* **180** (2009) 1941, arXiv:0710.2427 [hep-ph].
- [20] F. Cascioli, P. Maierhofer, and S. Pozzorini, “Scattering Amplitudes with Open Loops”, *Phys. Rev. Lett.* **108** (2012) 111601, arXiv:1111.5206 [hep-ph].
- [21] S. Actis, A. Denner, L. Hofer, J.-N. Lang, A. Scharf, and S. Uccirati, “RECOLA: REcursive Computation of One-Loop Amplitudes”, *Comput. Phys. Commun.* **214** (2017) 140, arXiv:1605.01090 [hep-ph].
- [22] S. Catani, and M. H. Seymour, “A General algorithm for calculating jet cross-sections in NLO QCD”, *Nucl. Phys.* **B485** (1997) 291, arXiv:hep-ph/9605323 [hep-ph], [Erratum: *Nucl. Phys.* **B510** (1998) 503].
- [23] S. Frixione, Z. Kunszt, and A. Signer, “Three jet cross-sections to next-to-leading order”, *Nucl. Phys.* **B467** (1996) 399, arXiv:hep-ph/9512328 [hep-ph].
- [24] Z. Nagy, and D. E. Soper, “Parton showers with quantum interference”, *JHEP* **09** (2007) 114, arXiv:0706.0017 [hep-ph].
- [25] T. Gleisberg, S. Höche, F. Krauss, M. Schönherr, S. Schumann, F. Siegert, and J. Winter, “Event generation with Sherpa 1.1”, *JHEP* **02** (2009) 007, arXiv:0811.4622 [hep-ph].
- [26] G. Bevilacqua, M. Czakon, M. V. Garzelli, A. van Hameren, A. Kardos, C. G. Papadopoulos, R. Pittau, and M. Worek, “HELAC-NLO”, *Comput. Phys. Commun.* **184** (2013) 986, arXiv:1110.1499 [hep-ph].
- [27] T. Sjöstrand, S. Ask, J. R. Christiansen, R. Corke, N. Desai, P. Ilten, S. Mrenna, S. Prestel, C. O. Rasmussen, and P. Z. Skands, “An Introduction to PYTHIA 8.2”, *Comput. Phys. Commun.* **191** (2015) 159, arXiv:1410.3012 [hep-ph].
- [28] J. Bellm, et al., “Herwig 7.0/Herwig++ 3.0 release note”, *Eur. Phys. J.* **C76** (2016) 196, arXiv:1512.01178 [hep-ph].
- [29] S. Schumann, and F. Krauss, “A Parton shower algorithm based on Catani-Seymour dipole factorisation”, *JHEP* **03** (2008) 038, arXiv:0709.1027 [hep-ph].
- [30] A. Denner, S. Dittmaier, M. Hecht, and C. Pasold, “NLO QCD and electroweak corrections to $W + \gamma$ production with leptonic W-boson decays”, *JHEP* **04** (2015) 018, arXiv:1412.7421 [hep-ph].

- [31] M. Czakon, D. Heymes, A. Mitov, D. Pagani, I. Tsinikos, and M. Zaro, “The top-quark charge asymmetry at the LHC and Tevatron through NNLO QCD and NLO EW”, *Phys. Rev.* **D98** (2018) 014003, arXiv:1711.03945 [hep-ph].
- [32] M. Czakon, P. Fiedler, A. Mitov, and J. Rojo, “Further exploration of top pair hadroproduction at NNLO”, in *Proceedings, 27th Rencontres de Physique de La Vallée d’Aoste: La Thuile, Aosta, Italy, February 23-March 1, 2013* (2013), arXiv:1305.3892 [hep-ph].
- [33] LHCTOPWG, *Physics results*, (2018) <https://twiki.cern.ch/twiki/bin/view/LHCPhysics/LHCTopWGSummaryPlots> (visited on 07/15/2018).
- [34] G. Aad, et al., “Measurement of the top pair production cross section in 8 TeV proton-proton collisions using kinematic information in the lepton+jets final state with ATLAS”, *Phys. Rev.* **D91** (2015) 112013, arXiv:1504.04251 [hep-ex].
- [35] V. Khachatryan, et al., “Measurement of the $t\bar{t}$ production cross section in pp collisions at $\sqrt{s} = 8$ TeV in dilepton final states containing one τ lepton”, *Phys. Lett.* **B739** (2014) 23, arXiv:1407.6643 [hep-ex].
- [36] G. Aad, et al., “Measurement of the $t\bar{t}$ production cross-section using $e\mu$ events with b-tagged jets in pp collisions at $\sqrt{s} = 7$ and 8 TeV with the ATLAS detector”, *Eur. Phys. J.* **C74** (2014) 3109, arXiv:1406.5375 [hep-ex], [Addendum: *Eur. Phys. J.* **C76** (2016) 642].
- [37] S. Chatrchyan, et al., “Measurement of the $t\bar{t}$ production cross section in the dilepton channel in pp collisions at $\sqrt{s} = 8$ TeV”, *JHEP* **02** (2014) 024, arXiv:1312.7582 [hep-ex], [Erratum: *JHEP* **02** (2014) 102].
- [38] P. Nason, S. Dawson, and R. K. Ellis, “The Total Cross-Section for the Production of Heavy Quarks in Hadronic Collisions”, *Nucl. Phys.* **B303** (1988) 607.
- [39] W. Beenakker, H. Kuijf, W. L. van Neerven, and J. Smith, “QCD Corrections to Heavy Quark Production in p anti-p Collisions”, *Phys. Rev.* **D40** (1989) 54.
- [40] M. Czakon, and A. Mitov, “Inclusive Heavy Flavor Hadroproduction in NLO QCD: The Exact Analytic Result”, *Nucl. Phys.* **B824** (2010) 111, arXiv:0811.4119 [hep-ph].
- [41] S. Catani, M. L. Mangano, P. Nason, and L. Trentadue, “The Top cross-section in hadronic collisions”, *Phys. Lett.* **B378** (1996) 329, arXiv:hep-ph/9602208 [hep-ph].
- [42] R. Bonciani, S. Catani, M. L. Mangano, and P. Nason, “NLL resummation of the heavy quark hadroproduction cross-section”, *Nucl. Phys.* **B529** (1998) 424, arXiv:hep-ph/9801375 [hep-ph], [Erratum: *Nucl. Phys.* **B803** (2008) 234].
- [43] N. Kidonakis, E. Laenen, S. Moch, and R. Vogt, “Sudakov resummation and finite order expansions of heavy quark hadroproduction cross-sections”, *Phys. Rev.* **D64** (2001) 114001, arXiv:hep-ph/0105041 [hep-ph].
- [44] N. Kidonakis, and R. Vogt, “Next-to-next-to-leading order soft gluon corrections in top quark hadroproduction”, *Phys. Rev.* **D68** (2003) 114014, arXiv:hep-ph/0308222 [hep-ph].
- [45] S. Moch, and P. Uwer, “Theoretical status and prospects for top-quark pair production at hadron colliders”, *Phys. Rev.* **D78** (2008) 034003, arXiv:0804.1476 [hep-ph].

Bibliography

- [46] M. Czakon, and A. Mitov, “On the Soft-Gluon Resummation in Top Quark Pair Production at Hadron Colliders”, *Phys. Lett.* **B680** (2009) 154, arXiv:0812.0353 [hep-ph].
- [47] M. Cacciari, M. Czakon, M. Mangano, A. Mitov, and P. Nason, “Top-pair production at hadron colliders with next-to-next-to-leading logarithmic soft-gluon resummation”, *Phys. Lett.* **B710** (2012) 612, arXiv:1111.5869 [hep-ph].
- [48] M. Beneke, P. Falgari, S. Klein, and C. Schwinn, “Hadronic top-quark pair production with NNLL threshold resummation”, *Nucl. Phys.* **B855** (2012) 695, arXiv:1109.1536 [hep-ph].
- [49] M. Czakon, and A. Mitov, “NNLO corrections to top-pair production at hadron colliders: the all-fermionic scattering channels”, *JHEP* **12** (2012) 054, arXiv:1207.0236 [hep-ph].
- [50] M. Czakon, and A. Mitov, “NNLO corrections to top pair production at hadron colliders: the quark-gluon reaction”, *JHEP* **01** (2013) 080, arXiv:1210.6832 [hep-ph].
- [51] M. Czakon, P. Fiedler, and A. Mitov, “Total Top-Quark Pair-Production Cross Section at Hadron Colliders Through $O(\alpha_s^4)$ ”, *Phys. Rev. Lett.* **110** (2013) 252004, arXiv:1303.6254 [hep-ph].
- [52] M. Czakon, and A. Mitov, “Top++: A Program for the Calculation of the Top-Pair Cross-Section at Hadron Colliders”, *Comput. Phys. Commun.* **185** (2014) 2930, arXiv:1112.5675 [hep-ph].
- [53] M. Czakon, P. Fiedler, and A. Mitov, “Resolving the Tevatron Top Quark Forward-Backward Asymmetry Puzzle: Fully Differential Next-to-Next-to-Leading-Order Calculation”, *Phys. Rev. Lett.* **115** (2015) 052001, arXiv:1411.3007 [hep-ph].
- [54] M. Czakon, D. Heymes, and A. Mitov, “High-precision differential predictions for top-quark pairs at the LHC”, *Phys. Rev. Lett.* **116** (2016) 082003, arXiv:1511.00549 [hep-ph].
- [55] M. Czakon, P. Fiedler, D. Heymes, and A. Mitov, “NNLO QCD predictions for fully-differential top-quark pair production at the Tevatron”, *JHEP* **05** (2016) 034, arXiv:1601.05375 [hep-ph].
- [56] M. Czakon, D. Heymes, and A. Mitov, “Dynamical scales for multi-TeV top-pair production at the LHC”, *JHEP* **04** (2017) 071, arXiv:1606.03350 [hep-ph].
- [57] M. Czakon, D. Heymes, and A. Mitov, “Bump hunting in LHC $t\bar{t}$ events”, *Phys. Rev.* **D94** (2016) 114033, arXiv:1608.00765 [hep-ph].
- [58] M. Czakon, P. Fiedler, D. Heymes, and A. Mitov, “Measurement of the Pole Mass of the Top Quark using Differential $t\bar{t}$ Cross Sections in $p\bar{p}$ Collisions at $\sqrt{s} = 1.96$ TeV”, in (2016).
- [59] K. Melnikov, and M. Schulze, “NLO QCD corrections to top quark pair production and decay at hadron colliders”, *JHEP* **08** (2009) 049, arXiv:0907.3090 [hep-ph].
- [60] J. M. Campbell, and R. K. Ellis, “Top-Quark Processes at NLO in Production and Decay”, *J. Phys.* **G42** (2015) 015005, arXiv:1204.1513 [hep-ph].
- [61] A. Denner, S. Dittmaier, S. Kallweit, and S. Pozzorini, “NLO QCD corrections to WWbb production at hadron colliders”, *Phys. Rev. Lett.* **106** (2011) 052001, arXiv:1012.3975 [hep-ph].

- [62] G. Bevilacqua, M. Czakon, A. van Hameren, C. G. Papadopoulos, and M. Worek, “Complete off-shell effects in top quark pair hadroproduction with leptonic decay at next-to-leading order”, *JHEP* **02** (2011) 083, arXiv:1012.4230 [hep-ph].
- [63] A. Denner, S. Dittmaier, S. Kallweit, and S. Pozzorini, “NLO QCD corrections to off-shell top-antitop production with leptonic decays at hadron colliders”, *JHEP* **10** (2012) 110, arXiv:1207.5018 [hep-ph].
- [64] F. Cascioli, S. Kallweit, P. Maierhöfer, and S. Pozzorini, “A unified NLO description of top-pair and associated Wt production”, *Eur. Phys. J.* **C74** (2014) 2783, arXiv:1312.0546 [hep-ph].
- [65] R. Frederix, “Top Quark Induced Backgrounds to Higgs Production in the $WW^{(*)} \rightarrow ll\nu\nu$ Decay Channel at Next-to-Leading-Order in QCD”, *Phys. Rev. Lett.* **112** (2014) 082002, arXiv:1311.4893 [hep-ph].
- [66] G. Heinrich, A. Maier, R. Nisius, J. Schlenk, and J. Winter, “NLO QCD corrections to $W^+W^-b\bar{b}$ production with leptonic decays in the light of top quark mass and asymmetry measurements”, *JHEP* **06** (2014) 158, arXiv:1312.6659 [hep-ph].
- [67] S. Frixione, P. Nason, and G. Ridolfi, “A Positive-weight next-to-leading-order Monte Carlo for heavy flavour hadroproduction”, *JHEP* **09** (2007) 126, arXiv:0707.3088 [hep-ph].
- [68] S. Frixione, P. Nason, and B. R. Webber, “Matching NLO QCD and parton showers in heavy flavor production”, *JHEP* **08** (2003) 007, arXiv:hep-ph/0305252 [hep-ph].
- [69] J. M. Campbell, R. K. Ellis, P. Nason, and E. Re, “Top-Pair Production and Decay at NLO Matched with Parton Showers”, *JHEP* **04** (2015) 114, arXiv:1412.1828 [hep-ph].
- [70] M. Beneke, and V. M. Braun, “Heavy quark effective theory beyond perturbation theory: Renormalons, the pole mass and the residual mass term”, *Nucl. Phys.* **B426** (1994) 301, arXiv:hep-ph/9402364 [hep-ph].
- [71] I. I. Y. Bigi, M. A. Shifman, N. G. Uraltsev, and A. I. Vainshtein, “The Pole mass of the heavy quark. Perturbation theory and beyond”, *Phys. Rev.* **D50** (1994) 2234, arXiv:hep-ph/9402360 [hep-ph].
- [72] P. Ball, M. Beneke, and V. M. Braun, “Resummation of $(\beta_0\alpha_s)^n$ corrections in QCD: Techniques and applications to the tau hadronic width and the heavy quark pole mass”, *Nucl. Phys.* **B452** (1995) 563, arXiv:hep-ph/9502300 [hep-ph].
- [73] M. Beneke, P. Marquard, P. Nason, and M. Steinhauser, “On the ultimate uncertainty of the top quark pole mass”, *Phys. Lett.* **B775** (2017) 63, arXiv:1605.03609 [hep-ph].
- [74] A. H. Hoang, S. Plätzer, and D. Samitz, “On the Cutoff Dependence of the Quark Mass Parameter in Angular Ordered Parton Showers”, (2018), arXiv:1807.06617 [hep-ph].
- [75] P. A. Baikov, K. G. Chetyrkin, and J. H. Kühn, “Quark Mass and Field Anomalous Dimensions to $\mathcal{O}(\alpha_s^5)$ ”, *JHEP* **10** (2014) 076, arXiv:1402.6611 [hep-ph].
- [76] P. Marquard, A. V. Smirnov, V. A. Smirnov, and M. Steinhauser, “Quark Mass Relations to Four-Loop Order in Perturbative QCD”, *Phys. Rev. Lett.* **114** (2015) 142002, arXiv:1502.01030 [hep-ph].

Bibliography

- [77] P. Marquard, A. V. Smirnov, V. A. Smirnov, and M. Steinhauser, “Four-loop relation between the $\overline{\text{MS}}$ and on-shell quark mass”, PoS **RADCOR2015** (2016) 094, arXiv:1601.03748 [hep-ph].
- [78] A. H. Hoang, and T. Teubner, “Top quark pair production close to threshold: Top mass, width and momentum distribution”, Phys. Rev. **D60** (1999) 114027, arXiv:hep-ph/9904468 [hep-ph].
- [79] M. Beneke, A. Signer, and V. A. Smirnov, “Top quark production near threshold and the top quark mass”, Phys. Lett. **B454** (1999) 137, arXiv:hep-ph/9903260 [hep-ph].
- [80] S. Chatrchyan, et al., “Determination of the top-quark pole mass and strong coupling constant from the $t\bar{t}$ production cross section in pp collisions at $\sqrt{s} = 7$ TeV”, Phys. Lett. **B728** (2014) 496, arXiv:1307.1907 [hep-ex], [Erratum: Phys. Lett. **B738** (2014) 526].
- [81] V. Khachatryan, et al., “Measurement of the $t\bar{t}$ production cross section in the $e\mu$ channel in proton-proton collisions at $\sqrt{s} = 7$ and 8 TeV”, JHEP **08** (2016) 029, arXiv:1603.02303 [hep-ex].
- [82] V. Khachatryan, et al., “Measurement of the top quark mass using proton-proton data at $\sqrt{s} = 7$ and 8 TeV”, Phys. Rev. **D93** (2016) 072004, arXiv:1509.04044 [hep-ex].
- [83] W. Wagner, “Top quark physics in hadron collisions”, Rept. Prog. Phys. **68** (2005) 2409, arXiv:hep-ph/0507207 [hep-ph].
- [84] A. Quadt, “Top quark physics at hadron colliders”, Eur. Phys. J. **C48** (2006) 835.
- [85] W. Bernreuther, “Top quark physics at the LHC”, J. Phys. **G35** (2008) 083001, arXiv:0805.1333 [hep-ph].
- [86] F.-P. Schilling, “Top Quark Physics at the LHC: A Review of the First Two Years”, Int. J. Mod. Phys. **A27** (2012) 1230016, arXiv:1206.4484 [hep-ex].
- [87] S. Alioli, P. Fernandez, J. Fuster, A. Irlles, S.-O. Moch, P. Uwer, and M. Vos, “A new observable to measure the top-quark mass at hadron colliders”, Eur. Phys. J. **C73** (2013) 2438, arXiv:1303.6415 [hep-ph].
- [88] J. Fuster, A. Irlles, D. Melini, P. Uwer, and M. Vos, “Extracting the top-quark running mass using $t\bar{t} + 1$ -jet events produced at the Large Hadron Collider”, Eur. Phys. J. **C77** (2017) 794, arXiv:1704.00540 [hep-ph].
- [89] G. Aad, et al., “Determination of the top-quark pole mass using $t\bar{t} + 1$ -jet events collected with the ATLAS experiment in 7 TeV pp collisions”, JHEP **10** (2015) 121, arXiv:1507.01769 [hep-ex].
- [90] CMS Collaboration, “Determination of the normalised invariant mass distribution of $t\bar{t} + \text{jet}$ and extraction of the top quark mass”, CMS-PAS-TOP-13-006 (2016).
- [91] S. Chatrchyan, et al., “Measurement of masses in the $t\bar{t}$ system by kinematic endpoints in pp collisions at $\sqrt{s} = 7$ TeV”, Eur. Phys. J. **C73** (2013) 2494, arXiv:1304.5783 [hep-ex].
- [92] M. Jezabek, and J. H. Kühn, “QCD Corrections to Semileptonic Decays of Heavy Quarks”, Nucl. Phys. **B314** (1989) 1.

- [93] A. Denner, and T. Sack, “The Top width”, Nucl. Phys. **B358** (1991) 46.
- [94] A. Czarnecki, and K. Melnikov, “Two loop QCD corrections to top quark width”, Nucl. Phys. **B544** (1999) 520, arXiv:hep-ph/9806244 [hep-ph].
- [95] A. Czarnecki, S. Groote, J. G. Körner, and J. H. Piclum, “NNLO QCD corrections to the polarized top quark decay $t(\uparrow) \rightarrow X_b + W^+$ ”, Phys. Rev. **D97** (2018) 094008, arXiv:1803.03658 [hep-ph].
- [96] K. G. Chetyrkin, R. Harlander, T. Seidensticker, and M. Steinhauser, “Second order QCD corrections to $\Gamma(t \rightarrow Wb)$ ”, Phys. Rev. **D60** (1999) 114015, arXiv:hep-ph/9906273 [hep-ph].
- [97] J. Gao, C. S. Li, and H. X. Zhu, “Top Quark Decay at Next-to-Next-to Leading Order in QCD”, Phys. Rev. Lett. **110** (2013) 042001, arXiv:1210.2808 [hep-ph].
- [98] D. Wicke, “Properties of the Top Quark”, Eur. Phys. J. **C71** (2011) 1627, arXiv:1005.2460 [hep-ex].
- [99] G. Aad, et al., “Measurements of spin correlation in top-antitop quark events from proton-proton collisions at $\sqrt{s} = 7$ TeV using the ATLAS detector”, Phys. Rev. **D90** (2014) 112016, arXiv:1407.4314 [hep-ex].
- [100] L. Sonnenschein, “Analytical solution of ttbar dilepton equations”, Phys. Rev. **D73** (2006) [Erratum: Phys. Rev.D78,079902(2008)], 054015, arXiv:hep-ph/0603011 [hep-ph].
- [101] W. Bernreuther, and Z.-G. Si, “Distributions and correlations for top quark pair production and decay at the Tevatron and LHC.”, Nucl. Phys. **B837** (2010) 90, arXiv:1003.3926 [hep-ph].
- [102] J. C. Collins, D. E. Soper, and G. F. Sterman, “Factorization of Hard Processes in QCD”, Adv. Ser. Direct. High Energy Phys. **5** (1989) 1, arXiv:hep-ph/0409313 [hep-ph].
- [103] R. D. Ball, et al., “Parton distributions for the LHC Run II”, JHEP **04** (2015) 040, arXiv:1410.8849 [hep-ph].
- [104] A. D. Martin, W. J. Stirling, R. S. Thorne, and G. Watt, “Parton distributions for the LHC”, Eur. Phys. J. **C63** (2009) 189, arXiv:0901.0002 [hep-ph].
- [105] H.-L. Lai, M. Guzzi, J. Huston, Z. Li, P. M. Nadolsky, J. Pumplin, and C. -P. Yuan, “New parton distributions for collider physics”, Phys. Rev. **D82** (2010) 074024, arXiv:1007.2241 [hep-ph].
- [106] S. Dulat, T.-J. Hou, J. Gao, M. Guzzi, J. Huston, P. Nadolsky, J. Pumplin, C. Schmidt, D. Stump, and C. P. Yuan, “New parton distribution functions from a global analysis of quantum chromodynamics”, Phys. Rev. **D93** (2016) 033006, arXiv:1506.07443 [hep-ph].
- [107] T. Kinoshita, “Mass singularities of Feynman amplitudes”, J. Math. Phys. **3** (1962) 650.
- [108] T. D. Lee, and M. Nauenberg, “Degenerate Systems and Mass Singularities”, Phys. Rev. **133** (1964) B1549.
- [109] G. 't Hooft, and M. J. G. Veltman, “Regularization and Renormalization of Gauge Fields”, Nucl. Phys. **B44** (1972) 189.

Bibliography

- [110] J. F. Ashmore, “A Method of Gauge Invariant Regularization”, *Lett. Nuovo Cim.* **4** (1972) 289.
- [111] G. M. Cicuta, and E. Montaldi, “Analytic renormalization via continuous space dimension”, *Lett. Nuovo Cim.* **4** (1972) 329.
- [112] C. G. Bollini, and J. J. Giambiagi, “Dimensional Renormalization: The Number of Dimensions as a Regularizing Parameter”, *Nuovo Cim.* **B12** (1972) 20.
- [113] J. C. Collins, *Renormalization*, Vol. 26, Cambridge Monographs on Mathematical Physics (Cambridge University Press, Cambridge, 1986).
- [114] S. M. Aybat, L. J. Dixon, and G. F. Sterman, “The Two-loop soft anomalous dimension matrix and resummation at next-to-next-to leading pole”, *Phys. Rev.* **D74** (2006) 074004, arXiv:hep-ph/0607309 [hep-ph].
- [115] A. Mitov, G. F. Sterman, and I. Sung, “The Massive Soft Anomalous Dimension Matrix at Two Loops”, *Phys. Rev.* **D79** (2009) 094015, arXiv:0903.3241 [hep-ph].
- [116] T. Becher, and M. Neubert, “On the Structure of Infrared Singularities of Gauge-Theory Amplitudes”, *JHEP* **06** (2009) 081, arXiv:0903.1126 [hep-ph], [Erratum: *JHEP* **11** (2013) 024].
- [117] T. Becher, and M. Neubert, “Infrared singularities of QCD amplitudes with massive partons”, *Phys. Rev.* **D79** (2009) 125004, arXiv:0904.1021 [hep-ph], [Erratum: *Phys. Rev.* **D80** (2009) 109901].
- [118] A. Ferroglia, M. Neubert, B. D. Pecjak, and L. L. Yang, “Two-loop divergences of massive scattering amplitudes in non-abelian gauge theories”, *JHEP* **11** (2009) 062, arXiv:0908.3676 [hep-ph].
- [119] A. Mitov, G. F. Sterman, and I. Sung, “Computation of the Soft Anomalous Dimension Matrix in Coordinate Space”, *Phys. Rev.* **D82** (2010) 034020, arXiv:1005.4646 [hep-ph].
- [120] T. Becher, and M. Neubert, “Infrared singularities of scattering amplitudes in perturbative QCD”, *Phys. Rev. Lett.* **102** (2009) 162001, arXiv:0901.0722 [hep-ph], [Erratum: *Phys. Rev. Lett.* **111** (2013) 199905].
- [121] S. Catani, “The Singular behavior of QCD amplitudes at two loop order”, *Phys. Lett.* **B427** (1998) 161, arXiv:hep-ph/9802439 [hep-ph].
- [122] S. Catani, and M. Grazzini, “Infrared factorization of tree level QCD amplitudes at the next-to-next-to-leading order and beyond”, *Nucl. Phys.* **B570** (2000) 287, arXiv:hep-ph/9908523 [hep-ph].
- [123] A. Denner, S. Dittmaier, M. Roth, and D. Wackerroth, “Predictions for all processes $e^+e^- \rightarrow 4$ fermions + γ ”, *Nucl. Phys.* **B560** (1999) 33, arXiv:hep-ph/9904472 [hep-ph].
- [124] A. Denner, S. Dittmaier, M. Roth, and L. H. Wieders, “Electroweak corrections to charged-current $e^+e^- \rightarrow 4$ fermion processes: Technical details and further results”, *Nucl. Phys.* **B724** (2005) 247, arXiv:hep-ph/0505042 [hep-ph], [Erratum: *Nucl. Phys.* **B854** (2012) 504].
- [125] C. F. Uhlemann, and N. Kauer, “Narrow-width approximation accuracy”, *Nucl. Phys.* **B814** (2009) 195, arXiv:0807.4112 [hep-ph].

- [126] R. Kleiss, and W. J. Stirling, “Spinor Techniques for Calculating $p\bar{p} \rightarrow W^\pm/Z^0 + \text{jets}$ ”, Nucl. Phys. **B262** (1985) 235.
- [127] L. J. Dixon, “Calculating scattering amplitudes efficiently”, in QCD and beyond. Proceedings, Theoretical Advanced Study Institute in Elementary Particle Physics, TASI-95, Boulder, USA, June 4-30, 1995 (1996), 539, arXiv:hep-ph/9601359 [hep-ph].
- [128] S. Dittmaier, “Weyl-van der Waerden formalism for helicity amplitudes of massive particles”, Phys. Rev. **D59** (1998) 016007, arXiv:hep-ph/9805445 [hep-ph].
- [129] G. Luisoni, and S. Marzani, “QCD resummation for hadronic final states”, J. Phys. **G42** (2015) 103101, arXiv:1505.04084 [hep-ph].
- [130] R. D. Ball, V. Bertone, F. Cerutti, L. Del Debbio, S. Forte, A. Guffanti, J. I. Latorre, J. Rojo, and M. Ubiali, “Unbiased global determination of parton distributions and their uncertainties at NNLO and at LO”, Nucl. Phys. **B855** (2012) 153, arXiv:1107.2652 [hep-ph].
- [131] M. Czakon, “A novel subtraction scheme for double-real radiation at NNLO”, Phys. Lett. **B693** (2010) 259, arXiv:1005.0274 [hep-ph].
- [132] M. Czakon, “Double-real radiation in hadronic top quark pair production as a proof of a certain concept”, Nucl. Phys. **B849** (2011) 250, arXiv:1101.0642 [hep-ph].
- [133] P. Bärnreuther, M. Czakon, and P. Fiedler, “Virtual amplitudes and threshold behaviour of hadronic top-quark pair-production cross sections”, JHEP **02** (2014) 078, arXiv:1312.6279 [hep-ph].
- [134] V. M. Abazov, et al., “Measurement of differential $t\bar{t}$ production cross sections in $p\bar{p}$ collisions”, Phys. Rev. **D90** (2014) 092006, arXiv:1401.5785 [hep-ex].
- [135] V. Khachatryan, et al., “Measurement of the differential cross section for top quark pair production in pp collisions at $\sqrt{s} = 8 \text{ TeV}$ ”, Eur. Phys. J. **C75** (2015) 542, arXiv:1505.04480 [hep-ex].
- [136] M. Czakon, N. P. Hartland, A. Mitov, E. R. Nocera, and J. Rojo, “Pinning down the large-x gluon with NNLO top-quark pair differential distributions”, JHEP **04** (2017) 044, arXiv:1611.08609 [hep-ph].
- [137] R. Bonciani, and A. Ferroglia, “Two-Loop QCD Corrections to the Heavy-to-Light Quark Decay”, JHEP **11** (2008) 065, arXiv:0809.4687 [hep-ph].
- [138] H. M. Asatrian, C. Greub, and B. D. Pecjak, “NNLO corrections to $\bar{B} \rightarrow X_u \ell \bar{\nu}$ in the shape-function region”, Phys. Rev. **D78** (2008) 114028, arXiv:0810.0987 [hep-ph].
- [139] M. Beneke, T. Huber, and X.-Q. Li, “Two-loop QCD correction to differential semi-leptonic $b \rightarrow u$ decays in the shape-function region”, Nucl. Phys. **B811** (2009) 77, arXiv:0810.1230 [hep-ph].
- [140] B. W. Harris, E. Laenen, L. Phaf, Z. Sullivan, and S. Weinzierl, “The Fully differential single top quark cross-section in next to leading order QCD”, Phys. Rev. **D66** (2002) 054024, arXiv:hep-ph/0207055 [hep-ph].
- [141] I. R. Blokland, A. Czarnecki, M. Slusarczyk, and F. Tkachov, “Heavy to light decays with a two loop accuracy”, Phys. Rev. Lett. **93** (2004) 062001, arXiv:hep-ph/0403221 [hep-ph].

Bibliography

- [142] J. Alcaraz Maestre, et al., “The SM and NLO Multileg and SM MC Working Groups: Summary Report”, in Proceedings, 7th Les Houches Workshop on Physics at TeV Colliders: Les Houches, France, May 30-June 17, 2011 (2012), 1, arXiv:1203.6803 [hep-ph].
- [143] B. Page, S. Abreu, F. Febres Cordero, H. Ita, M. Jaquier, and M. Zeng, “First two-loop amplitudes with the numerical unitarity method”, PoS **RADCOR2017** (2018) 012.
- [144] S. Badger, C. Brønnum-Hansen, H. B. Hartanto, and T. Peraro, “First look at two-loop five-gluon scattering in QCD”, Phys. Rev. Lett. **120** (2018) 092001, arXiv:1712.02229 [hep-ph].
- [145] T. Gehrmann, and L. Tancredi, “Two-loop QCD helicity amplitudes for $q\bar{q} \rightarrow W^\pm\gamma$ and $q\bar{q} \rightarrow Z^0\gamma$ ”, JHEP **02** (2012) 004, arXiv:1112.1531 [hep-ph].
- [146] A. von Manteuffel, and L. Tancredi, “The two-loop helicity amplitudes for $gg \rightarrow V_1V_2 \rightarrow 4$ leptons”, JHEP **06** (2015) 197, arXiv:1503.08835 [hep-ph].
- [147] T. Gehrmann, A. von Manteuffel, and L. Tancredi, “The two-loop helicity amplitudes for $q\bar{q}' \rightarrow V_1V_2 \rightarrow 4$ leptons”, JHEP **09** (2015) 128, arXiv:1503.04812 [hep-ph].
- [148] J. Kuipers, T. Ueda, J. A. M. Vermaseren, and J. Vollinga, “FORM version 4.0”, Comput. Phys. Commun. **184** (2013) 1453, arXiv:1203.6543 [cs.SC].
- [149] K. G. Chetyrkin, and F. V. Tkachov, “Integration by Parts: The Algorithm to Calculate beta Functions in 4 Loops”, Nucl. Phys. **B192** (1981) 159.
- [150] S. Laporta, “High precision calculation of multiloop Feynman integrals by difference equations”, Int. J. Mod. Phys. **A15** (2000) 5087, arXiv:hep-ph/0102033 [hep-ph].
- [151] A. von Manteuffel, and C. Studerus, “Reduze 2 - Distributed Feynman Integral Reduction”, (2012), arXiv:1201.4330 [hep-ph].
- [152] A. V. Smirnov, “FIRE5: a C++ implementation of Feynman Integral REduction”, Comput. Phys. Commun. **189** (2015) 182, arXiv:1408.2372 [hep-ph].
- [153] P. Maierhöfer, J. Usovitsch, and P. Uwer, “Kira—A Feynman integral reduction program”, Comput. Phys. Commun. **230** (2018) 99, arXiv:1705.05610 [hep-ph].
- [154] R. Bonciani, A. Ferroglia, T. Gehrmann, D. Maitre, and C. Studerus, “Two-Loop Fermionic Corrections to Heavy-Quark Pair Production: The Quark-Antiquark Channel”, JHEP **07** (2008) 129, arXiv:0806.2301 [hep-ph].
- [155] R. Bonciani, A. Ferroglia, T. Gehrmann, and C. Studerus, “Two-Loop Planar Corrections to Heavy-Quark Pair Production in the Quark-Antiquark Channel”, JHEP **08** (2009) 067, arXiv:0906.3671 [hep-ph].
- [156] R. Bonciani, A. Ferroglia, T. Gehrmann, A. von Manteuffel, and C. Studerus, “Two-Loop Leading Color Corrections to Heavy-Quark Pair Production in the Gluon Fusion Channel”, JHEP **01** (2011) 102, arXiv:1011.6661 [hep-ph].
- [157] A. von Manteuffel, and C. Studerus, “Massive planar and non-planar double box integrals for light N_f contributions to $gg \rightarrow t\bar{t}$ ”, JHEP **10** (2013) 037, arXiv:1306.3504 [hep-ph].

- [158] R. Bonciani, A. Ferroglia, T. Gehrmann, A. von Manteuffel, and C. Studerus, “Light-quark two-loop corrections to heavy-quark pair production in the gluon fusion channel”, JHEP **12** (2013) 038, arXiv:1309.4450 [hep-ph].
- [159] J. M. Henn, “Multiloop integrals in dimensional regularization made simple”, Phys. Rev. Lett. **110** (2013) 251601, arXiv:1304.1806 [hep-th].
- [160] J. M. Henn, “Lectures on differential equations for Feynman integrals”, J. Phys. **A48** (2015) 153001, arXiv:1412.2296 [hep-ph].
- [161] L. Adams, E. Chaubey, and S. Weinzierl, “Simplifying Differential Equations for Multiscale Feynman Integrals beyond Multiple Polylogarithms”, Phys. Rev. Lett. **118** (2017) 141602, arXiv:1702.04279 [hep-ph].
- [162] R. N. Lee, and A. A. Pomeransky, “Normalized Fuchsian form on Riemann sphere and differential equations for multiloop integrals”, (2017), arXiv:1707.07856 [hep-th].
- [163] M. Caffo, H. Czyz, S. Laporta, and E. Remiddi, “The Master differential equations for the two loop sunrise selfmass amplitudes”, Nuovo Cim. **A111** (1998) 365, arXiv:hep-th/9805118 [hep-th].
- [164] S. Laporta, and E. Remiddi, “Analytic treatment of the two loop equal mass sunrise graph”, Nucl. Phys. **B704** (2005) 349, arXiv:hep-ph/0406160 [hep-ph].
- [165] C. Meyer, “Algorithmic transformation of multi-loop master integrals to a canonical basis with CANONICA”, Comput. Phys. Commun. **222** (2018) 295, arXiv:1705.06252 [hep-ph].
- [166] M. Czakon, “Automatized analytic continuation of Mellin-Barnes integrals”, Comput. Phys. Commun. **175** (2006) 559, arXiv:hep-ph/0511200 [hep-ph].
- [167] D. H. Bailey, and H. R. P. Ferguson, “Numerical results on relations between fundamental constants using a new algorithm”, Math. Comp. **53** (1989) 649.
- [168] S. Moch, and P. Uwer, “XSummer: Transcendental functions and symbolic summation in form”, Comput. Phys. Commun. **174** (2006) 759, arXiv:math-ph/0508008 [math-ph].
- [169] P. Brown, G. Byrne, and A. Hindmarsh, “Vode: a variable-coefficient ode solver”, SIAM Journal on Scientific and Statistical Computing **10** (1989) 1038.
- [170] D. H. Bailey, Y. Hida, and X. S. Li, *Quad-double/double-double computation package*, <http://crd-legacy.lbl.gov/~dhbailey/mpdist/> (visited on 07/15/2018).
- [171] Wolfram Research, *Wolfram Mathematica*, 2018.
- [172] M. Czakon, A. Mitov, and G. F. Sterman, “Threshold Resummation for Top-Pair Hadroproduction to Next-to-Next-to-Leading Log”, Phys. Rev. **D80** (2009) 074017, arXiv:0907.1790 [hep-ph].
- [173] M. Czakon, and P. Fiedler, “The soft function for color octet production at threshold”, Nucl. Phys. **B879** (2014) 236, arXiv:1311.2541 [hep-ph].
- [174] W. Bernreuther, and A. Brandenburg, “Tracing CP violation in the production of top quark pairs by multiple TeV proton proton collisions”, Phys. Rev. **D49** (1994) 4481, arXiv:hep-ph/9312210 [hep-ph].
- [175] S. Catani, and M. Grazzini, “An NNLO subtraction formalism in hadron collisions and its application to Higgs boson production at the LHC”, Phys. Rev. Lett. **98** (2007) 222002, arXiv:hep-ph/0703012 [hep-ph].

Bibliography

- [176] G. Ferrera, M. Grazzini, and F. Tramontano, “Associated WH production at hadron colliders: a fully exclusive QCD calculation at NNLO”, *Phys. Rev. Lett.* **107** (2011) 152003, arXiv:1107.1164 [hep-ph].
- [177] S. Catani, L. Cieri, D. de Florian, G. Ferrera, and M. Grazzini, “Vector boson production at hadron colliders: hard-collinear coefficients at the NNLO”, *Eur. Phys. J.* **C72** (2012) 2195, arXiv:1209.0158 [hep-ph].
- [178] T. Gehrmann, M. Grazzini, S. Kallweit, P. Maierhöfer, A. von Manteuffel, S. Pozzorini, D. Rathlev, and L. Tancredi, “ W^+W^- Production at Hadron Colliders in Next to Next to Leading Order QCD”, *Phys. Rev. Lett.* **113** (2014) 212001, arXiv:1408.5243 [hep-ph].
- [179] F. Cascioli, T. Gehrmann, M. Grazzini, S. Kallweit, P. Maierhöfer, A. von Manteuffel, S. Pozzorini, D. Rathlev, L. Tancredi, and E. Weihs, “ZZ production at hadron colliders in NNLO QCD”, *Phys. Lett.* **B735** (2014) 311, arXiv:1405.2219 [hep-ph].
- [180] M. Grazzini, S. Kallweit, and D. Rathlev, “ $W\gamma$ and $Z\gamma$ production at the LHC in NNLO QCD”, *JHEP* **07** (2015) 085, arXiv:1504.01330 [hep-ph].
- [181] M. Grazzini, S. Kallweit, and M. Wiesemann, “Fully differential NNLO computations with MATRIX”, *Eur. Phys. J.* **C78** (2018) 537, arXiv:1711.06631 [hep-ph].
- [182] R. Bonciani, S. Catani, M. Grazzini, H. Sargsyan, and A. Torre, “The q_T subtraction method for top quark production at hadron colliders”, *Eur. Phys. J.* **C75** (2015) 581, arXiv:1508.03585 [hep-ph].
- [183] J. Gaunt, M. Stahlhofen, F. J. Tackmann, and J. R. Walsh, “N-jettiness Subtractions for NNLO QCD Calculations”, *JHEP* **09** (2015) 058, arXiv:1505.04794 [hep-ph].
- [184] I. W. Stewart, F. J. Tackmann, and W. J. Waalewijn, “Dissecting Soft Radiation with Factorization”, *Phys. Rev. Lett.* **114** (2015) 092001, arXiv:1405.6722 [hep-ph].
- [185] R. Boughezal, C. Focke, W. Giele, X. Liu, and F. Petriello, “Higgs boson production in association with a jet at NNLO using jettiness subtraction”, *Phys. Lett.* **B748** (2015) 5, arXiv:1505.03893 [hep-ph].
- [186] R. Boughezal, C. Focke, X. Liu, and F. Petriello, “W-boson production in association with a jet at next-to-next-to-leading order in perturbative QCD”, *Phys. Rev. Lett.* **115** (2015) 062002, arXiv:1504.02131 [hep-ph].
- [187] R. Boughezal, J. M. Campbell, R. K. Ellis, C. Focke, W. T. Giele, X. Liu, and F. Petriello, “Z-boson production in association with a jet at next-to-next-to-leading order in perturbative QCD”, *Phys. Rev. Lett.* **116** (2016) 152001, arXiv:1512.01291 [hep-ph].
- [188] J. M. Campbell, R. K. Ellis, and C. Williams, “Direct Photon Production at Next-to-Next-to-Leading Order”, *Phys. Rev. Lett.* **118** (2017) 222001, arXiv:1612.04333 [hep-ph].
- [189] G. Somogyi, Z. Trocsanyi, and V. Del Duca, “Matching of singly- and doubly-unresolved limits of tree-level QCD squared matrix elements”, *JHEP* **06** (2005) 024, arXiv:hep-ph/0502226 [hep-ph].
- [190] G. Somogyi, and Z. Trocsanyi, “A Subtraction scheme for computing QCD jet cross sections at NNLO: Regularization of real-virtual emission”, *JHEP* **01** (2007) 052, arXiv:hep-ph/0609043 [hep-ph].

- [191] G. Somogyi, and Z. Trocsanyi, “A Subtraction scheme for computing QCD jet cross sections at NNLO: Integrating the subtraction terms. I.”, *JHEP* **08** (2008) 042, arXiv:0807.0509 [hep-ph].
- [192] U. Aglietti, V. Del Duca, C. Duhr, G. Somogyi, and Z. Trocsanyi, “Analytic integration of real-virtual counterterms in NNLO jet cross sections. I.”, *JHEP* **09** (2008) 107, arXiv:0807.0514 [hep-ph].
- [193] P. Bolzoni, S.-O. Moch, G. Somogyi, and Z. Trocsanyi, “Analytic integration of real-virtual counterterms in NNLO jet cross sections. II.”, *JHEP* **08** (2009) 079, arXiv:0905.4390 [hep-ph].
- [194] P. Bolzoni, G. Somogyi, and Z. Trocsanyi, “A subtraction scheme for computing QCD jet cross sections at NNLO: integrating the iterated singly-unresolved subtraction terms”, *JHEP* **01** (2011) 059, arXiv:1011.1909 [hep-ph].
- [195] G. Somogyi, “A subtraction scheme for computing QCD jet cross sections at NNLO: integrating the doubly unresolved subtraction terms”, *JHEP* **04** (2013) 010, arXiv:1301.3919 [hep-ph].
- [196] V. Del Duca, G. Somogyi, and Z. Trocsanyi, “Integration of collinear-type doubly unresolved counterterms in NNLO jet cross sections”, *JHEP* **06** (2013) 079, arXiv:1301.3504 [hep-ph].
- [197] V. Del Duca, C. Duhr, G. Somogyi, F. Tramontano, and Z. Trocsanyi, “Higgs boson decay into b-quarks at NNLO accuracy”, *JHEP* **04** (2015) 036, arXiv:1501.07226 [hep-ph].
- [198] G. Ferrera, G. Somogyi, and F. Tramontano, “Associated production of a Higgs boson decaying into bottom quarks at the LHC in full NNLO QCD”, *Phys. Lett.* **B780** (2018) 346, arXiv:1705.10304 [hep-ph].
- [199] V. Del Duca, C. Duhr, A. Kardos, G. Somogyi, Z. Szor, Z. Trocsanyi, and Z. Tulipánt, “Jet production in the CoLoRFulNNLO method: event shapes in electron-positron collisions”, *Phys. Rev.* **D94** (2016) 074019, arXiv:1606.03453 [hep-ph].
- [200] A. Kardos, G. Bevilacqua, G. Somogyi, Z. Trócsányi, and Z. Tulipánt, “CoLoR-FulNNLO for LHC processes”, in 14th DESY Workshop on Elementary Particle Physics: Loops and Legs in Quantum Field Theory 2018 (LL2018) St Goar, Germany, April 29-May 4, 2018 (2018), arXiv:1807.04976 [hep-ph].
- [201] D. A. Kosower, “Antenna factorization of gauge theory amplitudes”, *Phys. Rev.* **D57** (1998) 5410, arXiv:hep-ph/9710213 [hep-ph].
- [202] D. A. Kosower, “Antenna factorization in strongly ordered limits”, *Phys. Rev.* **D71** (2005) 045016, arXiv:hep-ph/0311272 [hep-ph].
- [203] A. Gehrmann-De Ridder, T. Gehrmann, and E. W. N. Glover, “Antenna subtraction at NNLO”, *JHEP* **09** (2005) 056, arXiv:hep-ph/0505111 [hep-ph].
- [204] A. Gehrmann-De Ridder, T. Gehrmann, E. W. N. Glover, and G. Heinrich, “NNLO corrections to event shapes in e+ e- annihilation”, *JHEP* **12** (2007) 094, arXiv:0711.4711 [hep-ph].
- [205] A. Gehrmann-De Ridder, T. Gehrmann, E. W. N. Glover, and G. Heinrich, “Jet rates in electron-positron annihilation at $O(\alpha_s^3)$ in QCD”, *Phys. Rev. Lett.* **100** (2008) 172001, arXiv:0802.0813 [hep-ph].

Bibliography

- [206] W. Bernreuther, C. Bogner, and O. Dekkers, “The real radiation antenna functions for $S \rightarrow Q\bar{Q}gg$ at NNLO QCD”, JHEP **10** (2013) 161, arXiv:1309.6887 [hep-ph].
- [207] W. Bernreuther, C. Bogner, and O. Dekkers, “The real radiation antenna function for $S \rightarrow Q\bar{Q}q\bar{q}$ at NNLO QCD”, JHEP **06** (2011) 032, arXiv:1105.0530 [hep-ph].
- [208] G. Abelof, A. Gehrmann-De Ridder, and I. Majer, “Top quark pair production at NNLO in the quark-antiquark channel”, JHEP **12** (2015) 074, arXiv:1506.04037 [hep-ph].
- [209] G. Abelof, and A. Gehrmann-De Ridder, “Antenna subtraction for the production of heavy particles at hadron colliders”, JHEP **04** (2011) 063, arXiv:1102.2443 [hep-ph].
- [210] G. Abelof, A. Gehrmann-De Ridder, P. Maierhofer, and S. Pozzorini, “NNLO QCD subtraction for top-antitop production in the $q\bar{q}$ channel”, JHEP **08** (2014) 035, arXiv:1404.6493 [hep-ph].
- [211] X. Chen, J. Cruz-Martinez, T. Gehrmann, E. W. N. Glover, and M. Jaquier, “NNLO QCD corrections to Higgs boson production at large transverse momentum”, JHEP **10** (2016) 066, arXiv:1607.08817 [hep-ph].
- [212] J. Currie, A. Gehrmann-De Ridder, T. Gehrmann, E. W. N. Glover, A. Huss, and J. Pires, “Precise predictions for dijet production at the LHC”, Phys. Rev. Lett. **119** (2017) 152001, arXiv:1705.10271 [hep-ph].
- [213] J. Currie, E. W. N. Glover, and J. Pires, “Next-to-Next-to Leading Order QCD Predictions for Single Jet Inclusive Production at the LHC”, Phys. Rev. Lett. **118** (2017) 072002, arXiv:1611.01460 [hep-ph].
- [214] T. Binoth, and G. Heinrich, “An automatized algorithm to compute infrared divergent multiloop integrals”, Nucl. Phys. **B585** (2000) 741, arXiv:hep-ph/0004013 [hep-ph].
- [215] C. Anastasiou, K. Melnikov, and F. Petriello, “A new method for real radiation at NNLO”, Phys. Rev. **D69** (2004) 076010, arXiv:hep-ph/0311311 [hep-ph].
- [216] T. Binoth, and G. Heinrich, “Numerical evaluation of phase space integrals by sector decomposition”, Nucl. Phys. **B693** (2004) 134, arXiv:hep-ph/0402265 [hep-ph].
- [217] M. Czakon, and D. Heymes, “Four-dimensional formulation of the sector-improved residue subtraction scheme”, Nucl. Phys. **B890** (2014) 152, arXiv:1408.2500 [hep-ph].
- [218] R. Boughezal, F. Caola, K. Melnikov, F. Petriello, and M. Schulze, “Higgs boson production in association with a jet at next-to-next-to-leading order”, Phys. Rev. Lett. **115** (2015) 082003, arXiv:1504.07922 [hep-ph].
- [219] F. Caola, K. Melnikov, and R. Röntsch, “Nested soft-collinear subtractions in NNLO QCD computations”, Eur. Phys. J. **C77** (2017) 248, arXiv:1702.01352 [hep-ph].
- [220] F. Caola, G. Luisoni, K. Melnikov, and R. Röntsch, “NNLO QCD corrections to associated WH production and $H \rightarrow b\bar{b}$ decay”, Phys. Rev. **D97** (2018) 074022, arXiv:1712.06954 [hep-ph].
- [221] S. Frixione, and B. R. Webber, “Matching NLO QCD computations and parton shower simulations”, JHEP **06** (2002) 029, arXiv:hep-ph/0204244 [hep-ph].

- [222] S. Frixione, P. Nason, and C. Oleari, “Matching NLO QCD computations with Parton Shower simulations: the POWHEG method”, *JHEP* **11** (2007) 070, arXiv:0709.2092 [hep-ph].
- [223] J. M. Campbell, R. K. Ellis, and F. Tramontano, “Single top production and decay at next-to-leading order”, *Phys. Rev.* **D70** (2004) 094012, arXiv:hep-ph/0408158 [hep-ph].
- [224] J. Gao, and A. S. Papanastasiou, “Top-quark pair-production and decay at high precision”, *Phys. Rev.* **D96** (2017) 051501, arXiv:1705.08903 [hep-ph].
- [225] ATLAS collaboration, “Measurements of top-quark pair spin correlations in the $e\mu$ channel at $\sqrt{s} = 13$ TeV using pp collisions in the ATLAS detector”, ATLAS-CONF-2018-027 (2018).
- [226] K. G. Chetyrkin, B. A. Kniehl, and M. Steinhauser, “Decoupling relations to $O(\alpha_s^3)$ and their connection to low-energy theorems”, *Nucl. Phys.* **B510** (1998) 61, arXiv:hep-ph/9708255 [hep-ph].
- [227] M. Czakon, A. Mitov, and S. Moch, “Heavy-quark production in massless quark scattering at two loops in QCD”, *Phys. Lett.* **B651** (2007) 147, arXiv:0705.1975 [hep-ph].
- [228] M. Czakon, A. Mitov, and S. Moch, “Heavy-quark production in gluon fusion at two loops in QCD”, *Nucl. Phys.* **B798** (2008) 210, arXiv:0707.4139 [hep-ph].
- [229] D. J. Broadhurst, N. Gray, and K. Schilcher, “Gauge invariant on-shell Z_2 in QED, QCD and the effective field theory of a static quark”, *Z. Phys.* **C52** (1991) 111.
- [230] W. Bernreuther, and W. Wetzel, “Decoupling of Heavy Quarks in the Minimal Subtraction Scheme”, *Nucl. Phys.* **B197** (1982) 228, [Erratum: *Nucl. Phys.* **B513** (1998) 758].
- [231] G. P. Korchemsky, and A. V. Radyushkin, “Renormalization of the Wilson Loops Beyond the Leading Order”, *Nucl. Phys.* **B283** (1987) 342.
- [232] N. Kidonakis, “Two-loop soft anomalous dimensions and NNLL resummation for heavy quark production”, *Phys. Rev. Lett.* **102** (2009) 232003, arXiv:0903.2561 [hep-ph].
- [233] J. M. Campbell, and E. W. N. Glover, “Double unresolved approximations to multiparton scattering amplitudes”, *Nucl. Phys.* **B527** (1998) 264, arXiv:hep-ph/9710255 [hep-ph].
- [234] S. Catani, and M. Grazzini, “Collinear factorization and splitting functions for next-to-next-to-leading order QCD calculations”, *Phys. Lett.* **B446** (1999) 143, arXiv:hep-ph/9810389 [hep-ph].
- [235] Z. Bern, L. J. Dixon, D. C. Dunbar, and D. A. Kosower, “One loop n point gauge theory amplitudes, unitarity and collinear limits”, *Nucl. Phys.* **B425** (1994) 217, arXiv:hep-ph/9403226 [hep-ph].
- [236] Z. Bern, V. Del Duca, and C. R. Schmidt, “The Infrared behavior of one loop gluon amplitudes at next-to-next-to-leading order”, *Phys. Lett.* **B445** (1998) 168, arXiv:hep-ph/9810409 [hep-ph].
- [237] D. A. Kosower, “All order collinear behavior in gauge theories”, *Nucl. Phys.* **B552** (1999) 319, arXiv:hep-ph/9901201 [hep-ph].

Bibliography

- [238] D. A. Kosower, and P. Uwer, “One loop splitting amplitudes in gauge theory”, Nucl. Phys. **B563** (1999) 477, arXiv:hep-ph/9903515 [hep-ph].
- [239] Z. Bern, V. Del Duca, W. B. Kilgore, and C. R. Schmidt, “The infrared behavior of one loop QCD amplitudes at next-to-next-to leading order”, Phys. Rev. **D60** (1999) 116001, arXiv:hep-ph/9903516 [hep-ph].
- [240] I. Bierenbaum, M. Czakon, and A. Mitov, “The singular behavior of one-loop massive QCD amplitudes with one external soft gluon”, Nucl. Phys. **B856** (2012) 228, arXiv:1107.4384 [hep-ph].
- [241] M. L. Czakon, and A. Mitov, “A simplified expression for the one-loop soft-gluon current with massive fermions”, (2018), arXiv:1804.02069 [hep-ph].
- [242] R. K. Ellis, W. J. Stirling, and B. R. Webber, “QCD and collider physics”, Camb. Monogr. Part. Phys. Nucl. Phys. Cosmol. **8** (1996) 1.

Acknowledgements

Firstly, I would like to thank my supervisor Prof. Dr. Michal Czakon for the great opportunity to come to Aachen and join his group. His knowledge, encouragement and guidance have had a major impact on my understanding of physics and on my professional development. The productive environment and challenging tasks he provided me with were very motivating, and I learned to appreciate his way of mentoring.

I express my gratitude to my second referee Prof. Dr. Robert Harlander.

I want to thank the DFG (Deutsche Forschungs Gesellschaft) for financing the GK “Teilchen- und Astroteilchenphysik in Lichte von LHC” and thus my position at the ITTK.

Special thanks go to Arnd Behring for all the extensive discussions and his motivating enthusiasm as well as for his tremendous technical knowledge which solved an uncountable amount of problems.

Further I want to thank Prof. Alexander Mitov for the access to the Cambridge High Performance Computing center and Andrew Papanastasiou for his support regarding the virtual decay matrix elements and discussions.

Also I want to thank all the (former) PhD and Master students at the ITTK for all the discussions and different perspectives. Especially I want to thank my former office mate Bayu Hartanto and my former PhD colleagues Manfred Krauss and Sebastian Kirchner for their warm welcome into the group and for sharing their experience with me. Special thanks go also to Long Chen for the productive collaboration.

Finally, I would like to thank my family for their support along my whole scientific career, as well as for providing a space of calmness when needed. Especially, I need to thank my wife Judith for her never-ending encouragement, support, and endurance during the “busy” times.